**Cellulose/Titanium Dioxide Nanocomposites and
Silicon Diimide Gel as a Stationary Phase for Chromatography**

Seyed Mani Sajedin

Department of Chemistry

University of Hull

February 2015

Acknowledgement

I would give huge thanks to my academic supervisors, Prof Stephen M Kelly and Dr Jay Wadhawan for their continued guidance, assistance, inspiring discussion and encouragement throughout the project. All the projects attempted during the program of study would be nothing without the enthusiasm and imagination of both of them from the initial to the final level.

I would also like to thank the other members of the projects team, Dr Fei Cheng and Dr Stuart Paul Kitney, for their guidance and for helping me to learn many synthetic and analytical techniques and how to develop a scientific approach to research.

Special thanks to my mum, dad, brother and best friend Dr Masoumeh Jahani for their bottomless love and supporting me spiritually through the many years spent in Higher Education and during the rest of my life so far.

Lastly, I offer my regards to all of those who supported me in any respect during the completion of the work for this thesis and its submission.

Abstract

There were two main aims of this thesis, both of which involved the synthesis, often using environmentally friendly (green) methods involving water as the solvent and reagent, and the analysis and determination of the physical properties of novel inorganic nanomaterials and nano-composites. The first part of this project was the study of the general methods for the preparation of titanium dioxide nanoparticles and the investigation of the most efficient ways of coating CP with these nanoparticles in order to improve UV-stability and also to increase the whiteness and reflectivity of the paper. The second part of this research involved investigation silicon diimide mesoporous gel as a basic stationary phase for thin film and column chromatography for acid-sensitive organic compounds.

A number of different methods have been investigated in order to improve the UV-stability and also to increase the whiteness and reflectivity of paper by using titanium dioxide nanoparticles to modify the optical properties of the surface of cellulose products and especially writing paper. The bleaching and yellowing of paper in visible light has been a common problem in the paper industry for very many years. A thin, but very efficient surface coating would allow a lighter paper with less standard stabilisers and whitening agents to be manufactured with enormous savings in terms of the processing and manufacture of paper. A higher brightness and whiteness of paper would also increase the optical contrast of writing paper, for example. The methods investigated in this project to attain these objectives include: preparation of bigger titanium dioxide nanoparticle powder for coating solutions with and without the formation of seeds, *in-situ* coating of titanium dioxide nanoparticles on CP, preparation of titanium dioxide nanoparticles as stable colloidal solutions, coating CP with core/shell TiO_2/SiO_2 nanoparticles and coating CP with TiO_2/APTES nanoparticles.

Two reaction approaches have been investigated to prepare titanium dioxide nanoparticles with a size of about 200 nm, i.e., preparation of titanium dioxide nanoparticles without seed formation and preparation of titanium dioxide nanoparticles with seed formation. In the preparation of the titanium dioxide nanoparticles without seed formation, different starting materials were used. The size of the secondary nanoparticles is about 120 nm for

TiOSO$_4$.xH$_2$SO$_4$.xH$_2$O, about 50 nm for TiOSO$_4$.xH$_2$O and about 100-300 nm when using TiOCl$_2$ as the source of titania. Titanium dioxide nanoparticles with a size of about 200 nm were obtained using the method involving the formation of seeds.

In *in-situ* coating about 200 nm of titanium dioxide were coated on CP surface in just 20 min by heating of the CPs in the TiOSO$_4$ solution at 110 ^{o}C. The results also show that the titanium dioxide particle size increase with increasing of reaction time. Stable titanium dioxide nanoparticle colloidal solutions have been prepared with TiOCl$_2$ as a starting material. Because of high photocatalyst activity of small titanium dioxide nanoparticle, the surface of TiO$_2$-RP and TiO$_2$-P25 nanoparticles were protected by APTES and silica to reduce the photocatalytic degradation of organic material support.

In order to inhibit the photocatalytic degradation of organic material supports induced by small titania (TiO$_2$) nanoparticles, four kinds of titanium dioxide nanoparticles, that is, commercial P25-TiO$_2$, commercial rutile phase titanium dioxide (RA), rutile titanium dioxide nanorods (RP) and rutile titanium dioxide spheres (RP500), prepared from TiCl$_4$. Small titanium dioxide nanoparticles were coated with a thin, but dense, coating of silica (SiO$_2$) using a conventional sol-gel technique to form TiO$_2$/SiO$_2$ core/shell nanoparticles. These core/shell nanoparticles were deposited and fixed as a very thin coating onto the surface of CP samples *via* a wet-chemistry polyelectrolyte layer-by-layer approach. The TiO$_2$/SiO$_2$ nano-coated paper samples exhibit higher whiteness and brightness and greater stability to UV-bleaching than comparable samples of blank paper. Comparison of the physical property of TiO$_2$/SiO$_2$ core/shell with the result presented in literature for bulk titanium dioxide evidenced UV-stability, whiteness and reflectivity were improved in these core/shell coatings.

Titanium dioxide nanoparticles have also successfully modified with (3-aminopropyl)triethoxysilane (APTES). Commercially available-P25-titanium dioxide nanoparticles and rutile titanium dioxide nanorods, prepared from TiCl$_4$, were first modified with a thin layer of APTES. These APTES-modified-P25 titanium dioxide nanoparticles and rutile titanium dioxide nanorods were then deposited *and* fixed onto the surface of paper samples *via* a simple, dip-coating process in water at room temperature. The resultant APTES-modified-P25 titanium dioxide nanoparticle-coated paper samples exhibit much greater stability to UV-illumination than uncoated blank reference paper and very little, or no, photo-degradation in terms of brightness and whiteness, respectively, of the-P25-TiO$_2$-

nanoparticle-treated paper is observed. There are many other potential applications for this Green Chemistry approach to protect cellulosic fibres from UV-bleaching in sunlight and to improve their whiteness and brightness.

In the second part of this thesis mesoporous silicon diimide gel was prepared and used for the first time as a basic stationary phase in thin layer and column chromatography. Silicon diimide gel, $Si(NH)_2$, is the basic equivalent of silica gel, SiO_2, whereby the oxygen atoms of silica have effectively been replaced by nitrogen. Silica gel is the most commonly used stationary phase for thin film and column chromatography. However, it is lightly acidic and this acidity can lead to the chemical decomposition of acid-sensitive compounds during chromatography. The mesoporous silicon diimide gel used here was prepared and optimised using a sol-gel process developed previously at the University of Hull. It exhibits a large specific surface area, a weakly basic surface and it is ideal for the characterisation, separation and purification of acid-sensitive compounds.

The nanoparticles and nanocomposite materials prepared in this thesis were characterized by appropriate combinations of analytical techniques, such as SEM, TEM, EDX, XPS, ICP, UV-Vis, ζ-potential, FT-IR, XRD, CHN and NTA. The BET surface area, whiteness, brightness and some of the nanocomposite materials were also determined and the values compared with standard materials.

Contents

List of Tables

XIII

List of Figures

XIX

XX

XXIII

List of Abbreviations

Some common abbreviations used in this report are given below:

APTES	3-Aminopropyltriethoxysilane
BET	Barrett-Emmett-Teller analysis
CMC	Carboxymethyl cellulose
CMS	Carboxymethyl starch
CP	Cellulosic paper
EDX	Energy-dispersive X-ray spectroscopy
FT-IR	Fourier transform infrared spectroscopy
ICP	Inductively coupled plasma
LBL	Layer by layer
NIRS	Near-infrared spectroscopy
NMR	Nuclear magnetic resonance
NP	Nanoparticles
NTA	Nanoparticle tracking analysis
PDDA	Poly(diallyldimethylammonium chloride)
PSS	Poly(sodium 4-styrene-sulfonate)
RA	Commercial titanium dioxide Rutile from Sigma Aldrich
RP	Titanium dioxide Rutile prepared in experiment
RP-500	Titanium dioxide Rutile prepared in experiment after heating in 500 $^{\circ}$C

rpm	Rotations per minute
r.t	Room temperature
SD	Standard deviation
SEM	Scanning electron microscopy
TEM	Transmission electron microscopy
TEOS	Tetraethylorthosilicate
TLC	Thin layer chromatography
UV-vis	Ultraviolet-visible
VHN	Vickers hardness number
XPS	X-ray photoelectron spectroscopy
XRD	X-ray diffractometer
ζ-potential	Zeta potential

Part 1. Cellulose Surface Modification with Titanium Dioxide Nanocomposites and Novel Chromatographic materials.

1 Introduction

1.1 Overview of Research Area

Cellulose Surface Modification:

In recent years, various industrial and academic research groups have investigated the value and utility of paper quality, such as improving the brightness and whiteness. The properties of nanoparticles and control of their structure has also been a fast growing research topic in recent years.[1, 2] Many investigations have now focused on using nanoparticles as surface modifiers to apply to different kinds of paper to improve their surface and optical properties, such as higher UV-resistance, higher whiteness and less yellowing for various industrial and commercial applications.[3] The results of these studies, and the work described here, will lead to the production of lower base-weight paper and the production of higher quality paper.[4, 5] It should not only have a remarkable effect in the saving of natural resources and energy, but also have an influence on using less bleaching chemicals and therefore have beneficial environmental consequences.[6]

Novel Chromatographic Materials:

One of the first steps in scale-up of preparative liquid chromatography separations is selection of an appropriate mobile phase. Two methods are commonly used to determine the proper mobile phase composition: Thin layer chromatography (TLC) or high performance liquid chromatography (HPLC). In this research silicon diimide mesoporous gel was used as a pH-basic stationary phase for TLC plates, which were successfully used to isolate acid-sensitive organic compounds.

1.2 Nanoparticles

Nanoparticles have historically been exploited, even before being identified as such, with one of the earliest uses is the incorporation of nanoparticles in glazes for early-dynasty Chinese porcelain.[7] In the 9th century artisans used nanoparticles to generate glittering effects on the surface of pots.[8] Gold nanoparticles have also been extensively used in the glass industry to provide coloured glasses, most notably the red stars that crown buildings in the Kremlin region of Moscow.[9]

The first reported description of the optical properties of nanometer-scale materials, in scientific terms, that we are aware of, was provided by Michael Faraday in 1857.[10] The use of nanoparticles in drug delivery was introduced in 1960 by Professor Peter Speiser and his research group.[11] In 1981 the popular nano-revolution was started and the first paper on nanotechnology was published by K. Eric Drexler.[12]

Nanoparticles are very small particles with a diameter of between 1 and 100 nanometers. As these particles are intermediate in size between lone molecules and bulk materials, their chemical and physical properties are not the same as either and are therefore of particular interest. It has been shown that nanoparticles have a larger surface area per weight in comparison with that of bulk materials and this typically causes them to be more reactive.[13] The large surface area of nanoparticles as compared with bulk materials results in an increasing the interaction between the nanoparticle and the host materials in nano-composites, which can lead to unique properties. For certain nano-composites that have diameters below the critical wavelength of light, the nano-particles are rendered transparent to visible light. This property makes these nanoparticles useful in different applications such as coating, cosmetics and packaging. Nanoparticle research is currently an area of intense scientific interest, due in part to the wide variety of potential applications in biomedical, optical and electronic fields.[14]
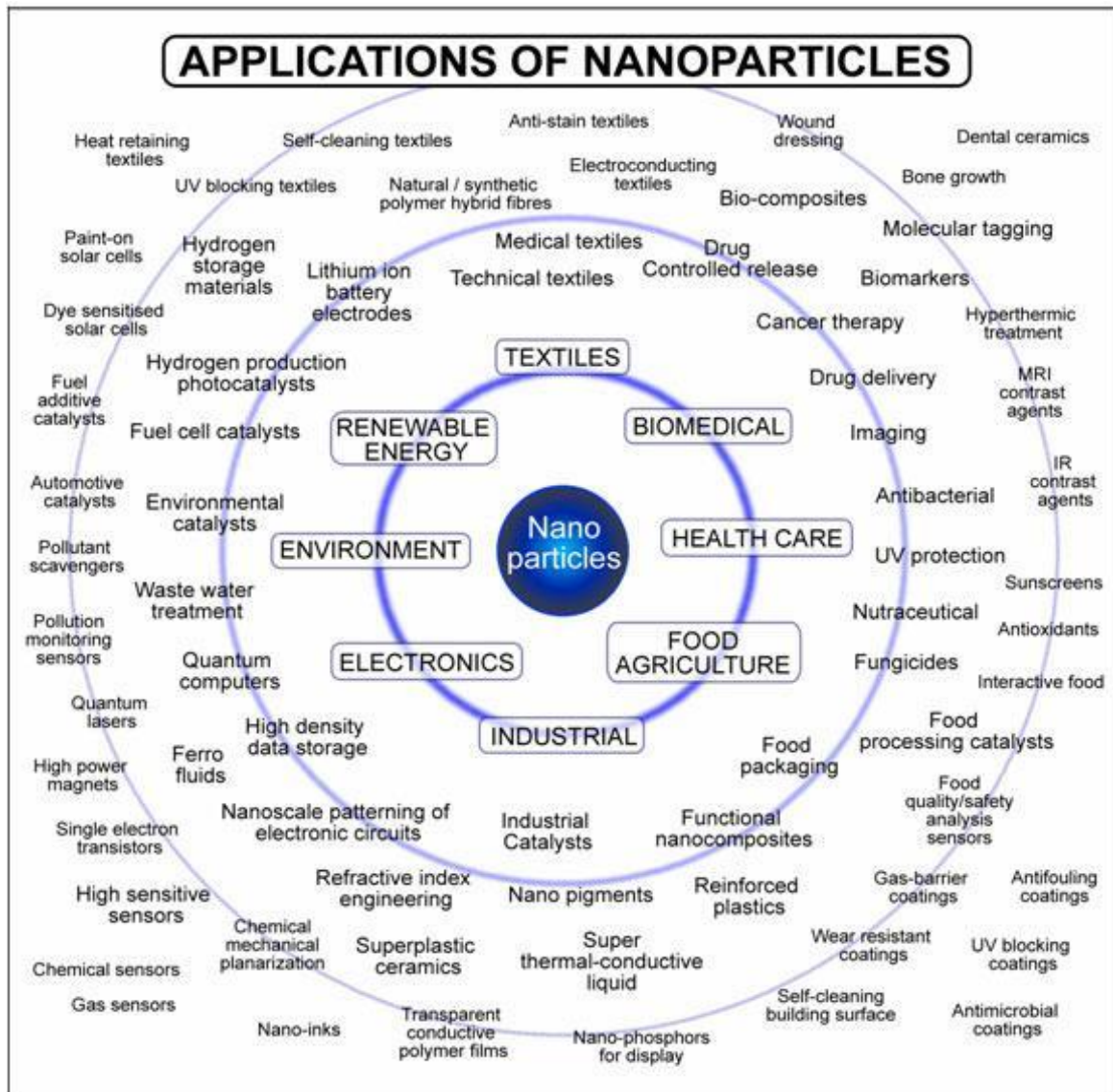
Figure 1-1: Commercial scale production of inorganic nanoparticles.[15]

This nanotechnology field that most people know nothing about is going to change how the world develops in ways completely unimaginative to most, as seen in the incomplete chart above, i.e. flexible solar cells with up to 65% efficiency, selective cell isolation to eradicate cancers, tissue welding with lasers during surgery, 3D TV's that could go into the realm of holographic realism, power consumption 50% less than existing means, displays that pop with vibrant colours, clothing and paints that change colour with the whim of desires, waste heat recovery not addressed.

1.2.1 Properties of nanoparticles

As the size of the nanoparticles in a system decreases, several physical properties change their magnitude and this become much more evident on the nano scale, e.g., the mechanical, catalytic and thermal properties of the material can change significantly with an increase in the surface-area-to-volume ratio. With this change, atoms behave differently on the surface of the nanoparticles in comparison with those in the interior region, which leads to different properties for the nano-system. These properties are completely different from the properties of the component in the bulk system. The size-dependent properties of nanoparticles, *i.e.*, quantum confinement, include surface plasmon resonance and paramagnetism.[16,17]

1.2.2 Different techniques for nanoparticle synthesis

There are very many physical and chemical methods for the preparation of a wide range of metallic and inorganic nanoparticles. Some of the most common and widely used synthetic methods for nanoparticles include:[18]

- Sol-gel technique
- Chemical reduction
- Inert gas condensation
- Solvothermal synthesis

1.2.2.1 Sol-gel technique

One of the most commonly used approaches in the field of material science is the sol-gel technique, which is a wet-chemical process. The sol-gel technique is based on the hydrolysis of different precursors, such as metal chlorides and metal alkoxides, to form colloidal sols.[19] The precursor sol can be used to synthesize powders of nanoparticles. These colloidal solutions can be deposited on a substrate surface in order to form a thin film or surface coating in practical applications of novel nanocomposites.[20] Sol–gel processing has the advantages of synthetic flexibility, high product purity and material homogeneity. It is a very

well established and important route to prepare shapeable, as well as size-selective, microporous and mesoporous metal oxide materials.[21, 22]

1.2.2.2 Chemical reduction

The simplest method for the synthesis of metal nanoparticles is the chemical reduction at relatively low temperatures of metal salts in an appropriate solvent. In this method, an ionic salt is usually reduced in the presence of an appropriate surfactant using a reducing agent to synthesise stable, colloidal solutions of surface-stabilised nanoparticles of metals and metal oxides, for example, in an appropriate solvent, preferentially simple alcohols and/or water.[23]

1.2.2.3 Inert gas condensation

Inert gas condensation is a method, which is used to make metallic nanoparticles from metals with a low melting point. In this method materials are vaporized inside an especially high vacuum chamber and then cooled with an inert gas. As a result of this process the evaporated metal condenses into nanometer-sized metallic nanoparticles.[24] If this reaction is carried out in the presence of a reactive chemical, which can bind to the surface of the nanoparticles, then surface nanoparticles can be prepared as powders that can be dissolved in appropriate solvents to prepare stable colloidal solutions.

1.2.2.4 Solvothermal synthesis

The solvothermal method is another general approach to produce chemical compounds. This technique involves the use of a solvent under moderate-to-high pressure and temperature, which increases the interaction of precursors during synthesis. Under solvothermal conditions, solubility of reactants increase and reaction occurs at lower temperature.[25]

These approaches are of relevance to this thesis as they are very important synthetic methods for nanoparticles intended for use in practical applications as these colloidal solutions can be used to coat the surface of absorbent materials to create novel nanocomposite materials whereby the mechanical properties of the original bulk product are not changed due to the presence of a very thin coating of nanoparticles on the substrate surface. It is common practice to mix commercially available nanoparticles into mixtures of raw materials, usually in the presence of a solvent, to create nanocomposite materials. The nanoparticles are distributed throughout the bulk of the resultant nanocomposite product as well as being present on the surface of the nanocomposite, which may lead to the desired modification of the surface properties of the substrate, but also to inferior values of the bulk mechanical properties of the substrate due to interactions between the nanoparticles and the bulk material.

1.3   Titanium dioxide (TiO$_2$)

1.3.1   Bulk Titanium Dioxide

Titanium dioxide (titania), as a semiconductor inorganic material, is one of the most important materials used extensively for optical coatings due to its properties of chemical and photochemical stability, *i.e.*, inertness, and its combination of high values for its dielectric constant, refractive index and brightness. As a light powder bulk titanium dioxide is white, opaque and bright, which has led to its two main industrial applications, i.e., as a white pigment in paints and as UV absorber to protect materials from bleaching and degradation through UV-induced photochemical degradation. Bulk titanium dioxide (TiO$_2$), as a powder, is a very important industrial material and has been widely used in pigments because of its combination of very high refractive index and brightness. In metal surface science it is the most investigated single crystalline system. Nearly four million tons of titanium dioxide pigments are used annually worldwide.[26, 27] Titanium dioxide is often used to whiten and improve the palatability of skimmed milk.[28] It is used to draw the white lines on croquet and tennis courts[29] and also it used for coating paper products to improve whiteness and opacity.[30] It is very important in earth science research and in the biocompatibility of bone implants.[31, 32] Titanium dioxide is used in ceramic glazes and also acts as an opacifier in very many industrials products for various applications.[33, 34] Titanium dioxide is non-toxic and safe for

use as an additive to inks, foods, toothpaste, plastics, medicines, i.e., tablets and pills, cosmetics and coatings.[35-37, 38] It has also been used for anti-reflection coatings, optical coatings and beam splitters due to its high dielectric constant and reflection index.[39]

Titanium dioxide naturally exists in three crystalline polymorphs: anatase, rutile and brookite. The most commonly used forms of titanium dioxide are the anatase and rutile polymorphs[40, 41] and are manufactured in large amounts by the chemical industry as microcrystalline materials.[36] The brookite polymorph of titania is still more of a curiosity mineral. Both anatase and rutile titanium dioxide is a thermodynamically stable phase, and has smaller band gap, i.e., Eg = 3.0 eV.[42] The anatase and brookite forms of titanium dioxide are typical of retrogression of metamorphic rutile titanium dioxide to another polymorph.[43] Both of the anatase and rutile polymorphs of titanium dioxide nanoparticles are commonly used in photocatalysis, with the anatase polymorph of titanium dioxide nanoparticles showing higher photocatalytic activity, see the next section.

Anatase titanium dioxide has nearly the same properties as rutile titanium dioxide such as the density, luster and hardness. The colour of anatase mineral is brown, indigo, pale yellow or reddish brown, black, pale green, grey and pale lilac and also rarely nearly colourless; pale green, brown, yellow-brown, blue in transmitted light and white to pale yellow streak. The micro-hardness value of mineral is $VHN_{100} = 616 - 698$ kg/mm^2 and density is 3.79 - 3.97 g/cm^3.
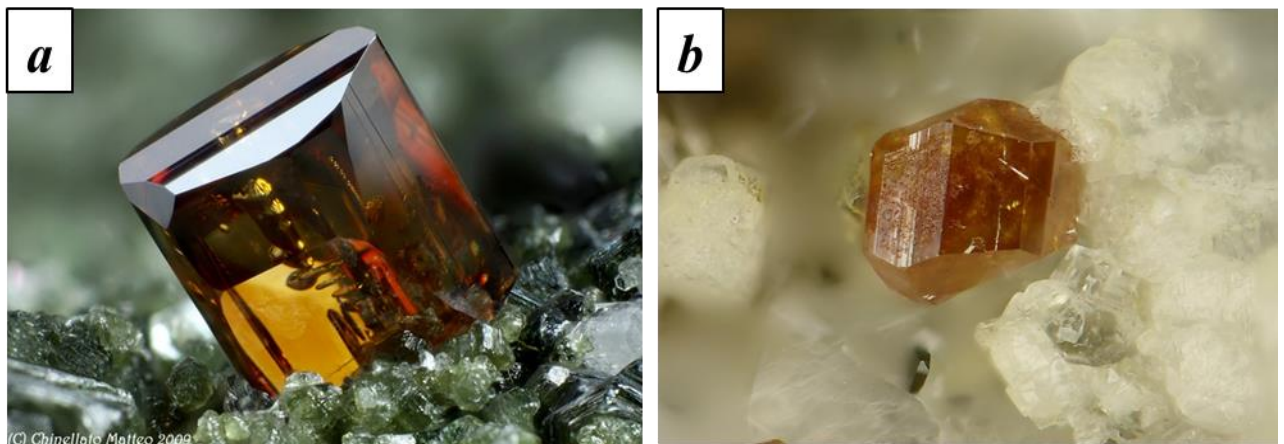
Figure 1-2: Photos of mineral of (a) anatase titanium dioxide, (b) rutile titanium dioxide.

Rutile mineral colour is blood red, yellow, brown-red, brown, black, greyish-black, brownish yellow, bluish or violet and it has light yellow, greyish black and pale brown streak. The micro-hardness value of mineral is VHN_{100}=894 - 974 kg/mm^2 and density is 4.23 g/cm^3.[44]
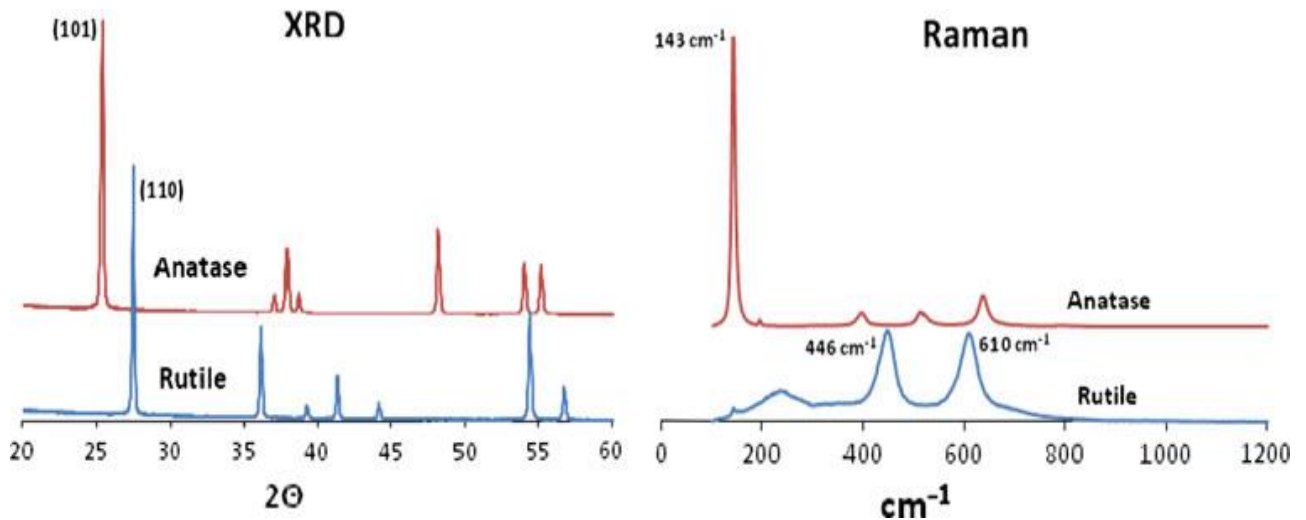
Figure 1-3: Left; Powder X-ray diffraction (XRD) pattern of anatase (red) and rutile (blue) titanium dioxide polymorphs. Right; raman spectroscopy of anatase (red) and rutile (blue) titanium dioxide polymorphs. [45, 46]

At 915 °C and higher temperatures, the anatase titanium dioxide automatically changes to the rutile structure.[47] Crystals of anatase are very distinctive and are not easily confused with any other mineral. The different between the structures of anatase and rutile in XRD and Raman spectroscopy are shown in Figure 1-3. The XRD pattern for anatase and rutile peaks shows titanium dioxide different crystal faces. The Raman spectrum presents peaks with wave numbers of about 144, 196, 387, 514 and 633 cm^{-1}, which can be all assigned to the anatase phase and the typical peaks of the rutile phase are 138, 230, 443, 606 cm^{-1}.

1.3.2 Titanium Dioxide Nanoparticles

The first observation of the photo-catalytic properties of nanoparticles of titanium dioxide was by Akira Fujishima in 1967,[48] which were only published in 1972. In the intervening decades the growth of research activities in nanotechnology and nanoscience has been nothing short of enormous.[49-51] This rapid and extensive growth in research activity may be attributable to the fact that new chemical and physical properties appear when the size of a

given material becomes smaller and smaller, and finally reaches the nanometre scale.[52, 53] The very large surface area resulting from the very small diameter of nanoparticles is advantageous in many titanium dioxide -based devices, as it facilitates reaction/interaction between the devices and the interacting media, which mainly happen at the interface or on the surface and which depend on the size and nature of the surface area of the material. Therefore, the size, shape and morphology of titanium dioxide nanoparticles have a strong effect on the performance of titanium dioxide -based devices.[54-57]
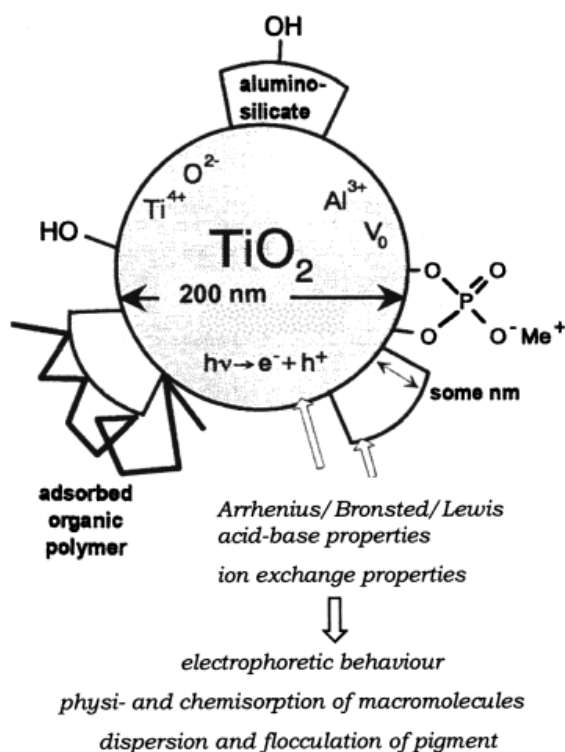
Figure 1-4: Typical structure of a TiO₂ white pigment.[58]

Due to their very small diameter, titania nanoparticles have a very large, active and reactive surface area. They are used, for example, as using as self-cleaning coating on windows and car windshields.[59-62] The excited state of the titania nanoparticles, produced by then absorption of UV-light, oxidizes organic compounds, perceived as dirt on transparent surfaces, to smaller non visible molecules and, especially, carbon dioxide. Titania nanoparticles are also used in the operating rooms in hospitals as disinfectants based on their bactericidal properties associated with the active surface of the nanoparticles.[63] The surface properties of titanium dioxide nanoparticles are also responsible for the use of titania nanoparticles as catalysts in heterogeneous catalysis, coatings in corrosion protective, in gas

sensor technology, as a photocatalyst in solar cells for the production of hydrogen. The quantum yield of titanium dioxide for the photochemical discussion of solar energy is low, but with the addition of dye molecules the colloidal suspension shows to improve efficiency of solar cell,[64] and titanium dioxide -based photo-electrochemical converters moved into the realm of economic competitiveness.[65] However, the most actively pursued applied research on titania is its use for photo-assisted degradation of organic molecules, usually on transparent surfaces, such as glass windows.

As the shape, crystal structure, and size of titanium dioxide nanomaterials change, then not only does surface stability change, but also the transitions between different phases of titanium dioxide under heat or pressure is dependent on those factors. The dependence of X-ray diffraction patterns and Raman vibrational spectra results on the size of titanium dioxide nanoparticles is also summarized. titanium dioxide nanoparticles normally are transparent in the visible light region. By doping or sensitization, it is possible to improve the optical sensitivity and activity of titanium dioxide nanomaterials in the visible light region. Many excellent reports and reviews on the structural, electronic, optical, and thermal properties and the preparation of nanomaterials have been published recently.[45, 54, 66, 67]

Titanium dioxide can be used in energy production, as a photocatalyst.[68] Titanium dioxide can catalyse hydrolysis, i.e., break up water to its constituent oxygen and hydrogen molecules. The hydrogen released could be used as a clean fuel. Sunscreens designed for people with sensitive skin are often based on nanoparticles of zinc oxide and titanium dioxide. titanium dioxide is also used in UV-resistant products such as cosmetics, thickeners, tattoos, styptic pencils and skin-care products. In industrial technology titanium dioxide has great potential for the detoxification of wastewater due to several factors.[69] Titanium dioxide nanoparticles are also used in water treatment for the removal of arsenic. It is also used for cancer treatments, noise absorption, dye-sensitised solar cells, Li-based batteries and electrochromic devices. The first synthesis of the rutile nanostructure of titanium dioxide, first reported by Zhang et al, used a low temperature method and hydrolysis of a $TiOCl_2$ solution to prevent nanoparticle aggregation.[70]
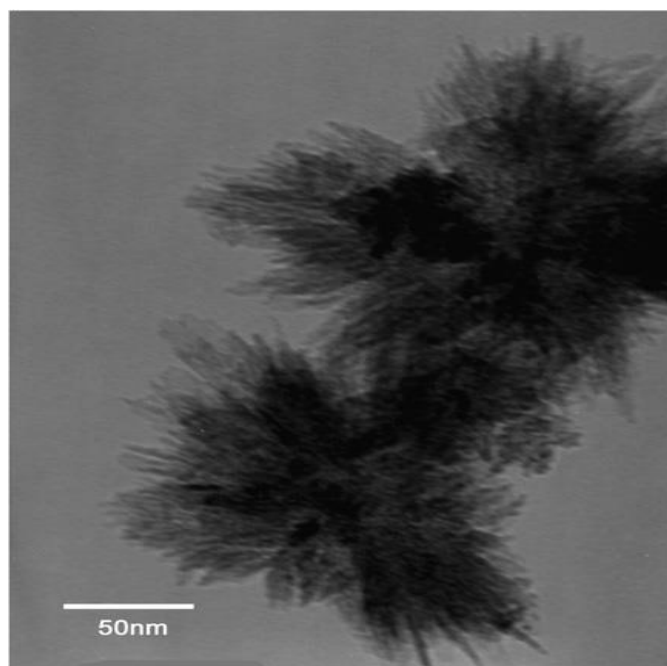
Figure 1-5: Transmission Electron Microscopy (TEM) image of the as-prepared titanium dioxide.[70]

Different methods have been investigated for the preparation of nanostructured semiconductors, due to their unique photochemical characteristics. Samuel et al. reported the preparation of titanium dioxide by the citrate gel and digestion technique.[71] They also employed urea in a homogeneous precipitation method to provide ultrafine rutile powders[39]. Controlling the photocatalytic properties of titanium dioxide nanoparticles is a topic of high interest at the moment. Optimizing the photocatalytic properties of titanium dioxide as a function of the method of synthesis has been examined by Testino and co-workers. They have investigated the influence of different synthesis parameters such as pH, temperature and duration of the hydrothermal technique on the nanoparticles size and shape and also the phase composition.[72]

P25 titanium dioxide from EVONIK has become one of the standard materials used for photo-catalytic studies. It is a commercial titanium dioxide powder consisting of 80% of the anatase phase and 20% of the rutile phase of the crystal forms (polymorphs) of titanium dioxide and was prepared by fuming titanium tetrachloride ($TiCl_4$).[47] $TiOCl_2$, $TiCl_4$ was diluted with ice-cold distilled water, because $TiCl_4$ is sensitive to air.[73, 74] It has been widely applied in the field of photo-catalytic reactions due to its high photo-catalytic activity.[75,76]

6

P25 titanium dioxide nano-powder is made up of 0.1 μm agglomerates comprised of 30 nm primary nanoparticles. P25 titanium dioxide is a nonporous solid with a specific surface area of 55 ± 15 m^2g^{-1}. If agglomerated titanium dioxide nanoparticles are separated into smaller nanoparticles in order to generate a larger surface area, these dispersions are found to be intrinsically unstable.[77] The size of the agglomerates can be reduced by controlling the reaction ionic strength, temperature and changes in pH during the synthesis of this material.[78] Different types of starting material used to prepare titanium dioxide nanoparticles also include $TiOSO_4$, $TiOCl_2$ and $Ti(OBu)_4$. $TiOSO_4$ is available in several different forms, such as $TiOSO_4.xH_2SO_4.H_2O$, $TiOSO_4.xH_2SO_4.xH_2O$ and $TiOSO_4.xH_2O$ solution (15 Wt%).

Recently, significant effort has been focused on developing innovative synthetic approaches to control the morphology and structures of titanium dioxide nanoparticles and its subsequent combination with organic materials to produce novel hybrid nanocomposite materials with an improved combination of mechanical, chemical and optical properties.[66, 79] Inorganic/organic hybrid materials are generating many novel exciting properties which not only depend on the properties of their individual component but also the characteristics of their inner interfaces.[80, 81] For example, a new type of polysaccharide/titanium oxide colloid has been prepared from surfactant-modified carboxymethyl starch and butyl tetratitanate [$Ti(OBu)_4$] by an *in-situ* sol-gel technique.[82] Monreal *et al.* have also reported the preparation of titanium dioxide nanoparticles by hydrolysis of titanium alkoxide in the presence of a linear polysaccharide, *i.e.*, 1,3-linked *beta*-D-galactapyranose and 1,4-linked 3,6-anyhdro-*alpha*-L-galactopyranose, whereby spherical, crystalline, surface-stabilised titania nanoparticles with a diameter of about 5-60 nm were obtained.[83]

Unfortunately, the high redox activity of titanium dioxide can lead to photo-degradation of any organic substrate, support, functional material, *etc.*, which will limit its applications in paper, textile, paint and plastic film industries. Selecting large particle size titania (particle size larger 200 nm), using rutile titania and passivated titania nanoparticles with inert shells, such as silica (SiO_2), to form core/shell TiO_2/SiO_2 nanoparticles are the most common method used in attempts to inhibit the photo-catalytic effect of titanium dioxide and inhibit degradation of the supports.[84] The performance of titanium dioxide is strongly depended on the preparation method which influences the polymorphs, the morphology and the particle size.

Several techniques such as gaseous phase process, sol-gel process, chemical vapour deposition and direct hydrolysis of titanium slat can be used to prepare titanium dioxide powders or films. [85-89] Among these preparation techniques, direct hydrolysis of $TiOSO_4$, a technique called sulfate process, is a well-known reaction for preparation pigment and catalysis titanium dioxide. The first stage of the hydrolysis is the formation of a phase with a composition of $3TiO_2 \cdot 4H_2O$. Further thermal treatment results in the loose of water to produce anatase titanium dioxide, which is transformed into rutile phase at temperature higher than 450 °C.[90] This well-established process has been applied in the large-scale production of titanium dioxide for many years.[91, 92]

$TiCl_4$ is another common starting material for the preparation of titanium dioxide nanoparticles. Since $TiCl_4$ is very sensitive to moisture, it is generally converted to stable $TiOCl_2$ solution before the reactions. Nanocrystalline titanium dioxide in the rutile phase has been obtained by homogeneous precipitation using urea and $TiOCl_2$.[39] Kim et al reported that heating an aqueous $TiOCl_2$ solution at room temperature to 65°C gave pure rutile phase crystalline titanium dioxide with spherical shapes 200–400 nm in diameter, whereas titanium dioxide crystalline precipitates with anatase phase started to form at temperatures >65°C.[93] A hair-like titanium dioxide powder has also been prepared from $TiOCl_2$ in a carboxy-containing ionic liquid solution.[94]

A sol-gel technique using tetraethoxysilane [TEOS: $Si(OC_2H_5)_4$ as a starting material] is generally applied to deposit a silica film ca the titanium oxide nanoparticles. Two kinds of silica film, dense film and porous sponge film, can be obtained at different conditions.[95] The dense film has a uniform thickness and condensed structure so that the photocatalysis of titanium dioxide can be sealed completely, by which the durability of the organic support can be remarkable increased.[84]

Eccentric TiO_2/SiO_2 core/shell nanoparticles were synthesized by taking advantage of porous titania nanoparticles that upon sintering shrink much more than the silica shell enclosing them.[75] A novel core–shell composite photocatalyst, titanium dioxide nanoparticles directly incorporated into a hollow amorphous silica shell, was fabricated by successive coating of titanium dioxide with a carbon layer and a silica layer followed by heat treatment to remove the carbon layer.[96-98] Rattle-type TiO_2/SiO_2 nanoparticles, with commercial titanium dioxide

nanoparticles encapsulated into hollow SiO_2 shell, were also fabricated by successive coating of multilayer polyelectrolytes and SiO_2 shell onto titanium dioxide nanoparticles and then treatment by UV irradiation to remove the polyelectrolyte layers.[99]

In this research, different kinds of titanium dioxide nanoparticles, such as commercial-P25 titanium dioxide, commercial rutile phase titanium dioxide and self-prepared rutile nanorod, have been chosen to modify CP surfaces. They were coated with silica by a conventional sol-gel process to form TiO_2/SiO_2 core/shell nanoparticles which were then attached on the CP surfaces *via* a polyelectrolytes lay-by-lay approach. The modified cellulosic papers *via* this process are expected to improve their optical properties and increase their brightness and stability to UV-bleaching.

3-Aminopropyltriethoxysilane (APTES) is frequently used as a coupling agent for attaching organic molecules to hydroxylated silicon oxide or metal oxide substrates due to the presence of terminal amine groups.[100, 101] For example, APTES has been applied to link proteins or to promote cell adhesion on titanium dioxide surfaces.[102, 103] Adsorption of organic dyes on titanium dioxide surfaces has also been reported using APTES as a coupling agent.[104] Although in many cases APTES has been applied for specific purposes, disagreements often occur on which is the dominant conformation or chemical form of APTES at interfaces because they not only depend on the reaction conditions but also on the crystal structures of titanium dioxide substrate. [102, 105, 106]

1.4   Cellulose as a Substrate for Titania Nanocomposites

Plants and trees have been a major source of raw materials and products for humankind for many millennia. For example, products derived from trees have been with us so long and are used so widely even in highly advanced societies that they are largely taken for granted as part of traditional industries and apparently, with no new science to investigate or understand. However, in fact, the opposite is true. Most of the technologies used in the forest products industry were first developed through trial and experiment due to the complex cascading hierarchical structure of wood. However, the complexities of the composition, structure and

nature of wood are now yielding to newer and more robust qualitative and quantitative analytical tools.

Cellulose is a naturally occurring polysaccharide, i.e., an straight-chain organic polymer.[107] It is the most important skeletal structure in plants, and is usually present in the amorphous form.[108] Cellulose is a carbohydrate and the most abundant and widespread, naturally occurring biopolymer in the world, representing about 1.5×10^{12} tons of total annual biomass production. Alongside its traditional applications in paper making and cotton textiles, cellulose is also a very important resource for the development of novel functional materials, since it is an environmentally friendly, biocompatible and cost-effective renewable resource.[67]

The use of cellulose-based materials to produce products in a sustainable and ecologically preferable manner is furthered by the need to adhere to the principles of Green Chemistry and Green Engineering. "Green" generally refers to materials, technologies and products that have less impact on the environment and/or are less detrimental to human health than traditional equivalents. The forest products industry has substantial infrastructure already in place to harvest sustainably grown trees and transport them to centres for debarking, chipping, and pulping. Such a sustainable supply base will enable the rapid scale up of nano-cellulosic materials based on this existing platform. It is a very widely spread and commonly used raw material with various properties and structures.[109] The term cellulose was first characterised in 1838 by the French chemist Anselme Payen, who isolated it from plant matter and determined its chemical formula.[110] In recent years, this material has received a great deal of attention due to its very useful physical and chemical properties. In general, cellulose is a water-insoluble, fibrous compound, which is an essential property for the structure of plant cell walls.[111] Figure 1-6 shows the general molecular structure of cellulose.
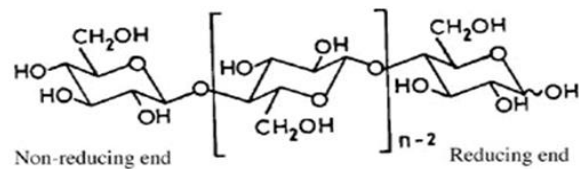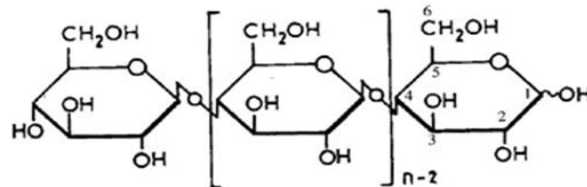
Figure 1-6: general molecular structure of cellulose.

Cellulose is a carbohydrate polymer consisting of repeating glucose units joined through covalent 1,4-β-glycosidic bonds through acetal functions between the equatorial OH groups, [112] compared to starch with 1,4-α-bonds and a non-linear structure. Different crystalline structures of carbohydrates are observed depending on the location of hydrogen bonds within and between the cellulose molecules. The physical properties of cellulose depend on the chain length of the carbohydrate chain, for example, plant fibres have a chain length ranging from 800 to 10,000 units, in contrast to the much longer chain lengths of cellulose extracted from wood pulp. The cellulose enzymes and the amylase enzymes, which naturally degrade cellulose, cannot break down starch due to the difference in the inter-sugar bond.[113]
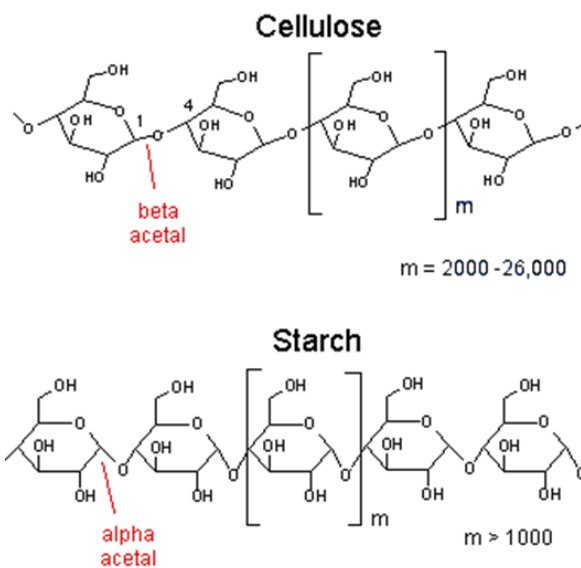
Figure 1-7: Different structure between cellulose and starch.

11

Cellulose acetate and triacetate are the most important forms of cellulose and are used in many different industries to form a variety of fibres and films for broad spectrum of industrial and commercial applications and products. Many recent investigations have focused on the application of the enzymes to modify the physical properties of cellulose fibres in order to provide environmentally friendly processes and products. Recently, Spiridonava *et al.,* used the addition of a mixture of oxidized enzymes to various wood pulps, after chemical and mechanical pre-treatments, to investigate and improve the optical, physical and mechanical properties of the final products.[114] In another study carried out by Pere and co-workers, to improve pulp strength, it was observed that the amount of enzyme added to the system had a great effect on the pulp viscosity. [115]

Standard paper, which has been traditionally produced from fibres of cellulose derived primarily from wood pulp from trees classified as softwoods,[116] is commonly used for a large range of purposes, such as writing, printing, wrapping and packaging applications. Paper materials have exceptional practical utility, due to the fact that they are lightweight, flexible, easy to handle, recyclable to some degree and, of course, biodegradable. The first true paper was appears to have been produced by Chinese ca the year 100 A.D. Since then paper has also been made from grass, rags and other plants.[117] Nowadays, many different industries produce paper from cellulose fibres for a very wide spectrum of products and applications. The first step of making paper is converting the cellulosic raw material to pulp, which is a concentrated mixture of fibres that are suspended in a liquid, usually water. Then the pulp is further broken down through either mechanical and/or chemical processes or a combination of both. After the extraction of the fibre, additional ingredients are added to bleach and change the appearance of the (yellowish) pulp before it is converted to (white/colourless) paper. The pulp mixture is then diluted further with more water to enable the pulp to be converted to sheets of paper.[118]

The reason why cellulose molecules in paper stick together when they are wet is that they are made of long strings of glucose moieties. A moving screen made of fine mesh is used to strain the mixture in order to prepare a fibrous web. The moving web of the mixture is then pressed to squeeze out most of the water. Then the paper sheet is removed from the mesh screen. The final stage of this process is drying. In the paper making process and during the drying the main aim is to increase fibre-to-fibre bonding to improve the mechanical strength

of the sheet of paper. There are several different methods for drying the paper using either force, air or heat to remove the water. One of the common methods is a heating drying mechanism, which is capable if drying paper to less than 6% moisture content.[119, 120]

Cellulose is an extensive, linear-chain polymer with a large number of hydroxyl groups.[109, 121] The presence of these hydrophilic groups can promote the nucleation and growth of inorganic phases at the fibre surface and thus facilitating the production of nanocomposites.[122-124]

Protection of textiles against photodegradation and the creation of new advantageous functions can be realised by coating of the textiles with silica nanoparticles, for example, with a diameters smaller than 50 nm using the corresponding silica sols.[125] Vegetable cellulose fibres have been surface-modified using the hydrolysis of tetraethoxysilane (TEOS), octyltrimethoxysilane (OTMS) or (PTMS), followed by the layer-by-layer deposition of previously synthesized titanium dioxide nanoparticles.[66] Morphological well-defined silica nanoparticles have been successfully deposited at cellulose fibre surfaces *via* a polyelectrolytes layer-by-layer approach.[122]

1.5 Titania/Cellulose Nanocomposites

1.5.1 Coating titanium dioxide on cellulosic paper

The photo-catalytic properties of paper coated with nanoparticles of titanium dioxide was demonstrated for the first time by Matsubara *et al.* in 1995.[126] The unique properties of nanoparticles render them of interest as property modifiers for paper due to their quantum-confined properties. Simon and co-workers have investigated paper functionalized by gold, silver and titania nanoparticles, which modify or induce the electronic, optical and catalytic properties of paper.[127] A very low concentration of nanoparticles can result in an excellent photo-catalytic performance. In this work different methods based on their ability to control the structure of paper have been reviewed for the preparation of the nanoparticle-functionalized paper.[128]
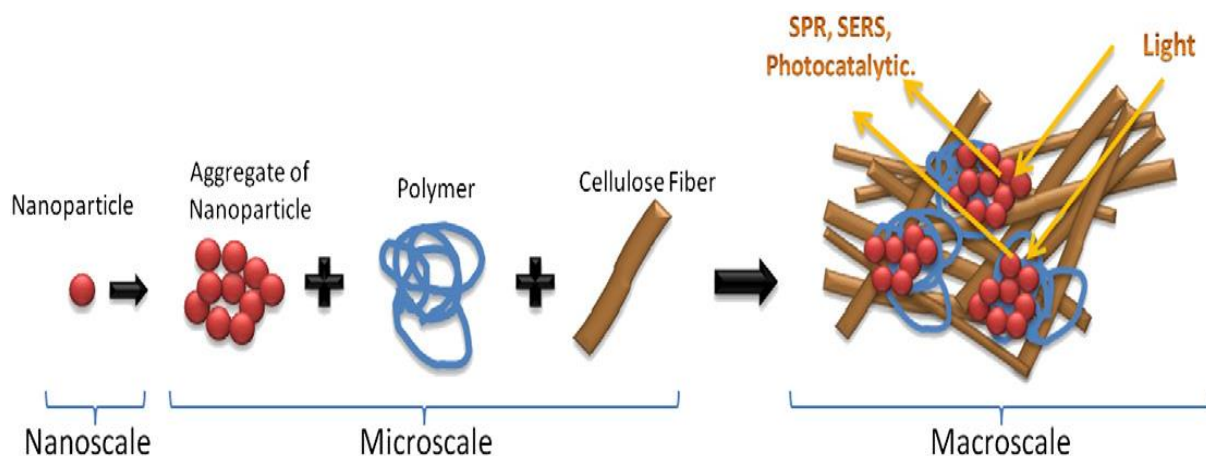
Figure 1-8: Different length scales of the constituents of nano-modified paper.[128]

In 2005 Koskinen *et al.* proposed a method to modify the wetting properties of cellulose surfaces by depositing plasma-polymerized fluorocarbon films on paper to achieve hydrophobic surfaces. They investigated the moisture-absorption features of fluorocarbon films deposited on cellulose and paper and also their resistance to lipophilic components.[129] The role titanium dioxide in the protection of paper works of art has been investigated as a protective coating against bacteria, pollutant gasses and the damaging effect of ultraviolet radiation by Afsharpour and co-workers. They have demonstrated the influence of this nanocomposite on the light stability of the paper component, as well as the preventive effect of paper, coated by titanium dioxide nanoparticles against moulds. They also studied the effect of heat and light as a common cause of damage in this kind of nano-treated paper.[130]
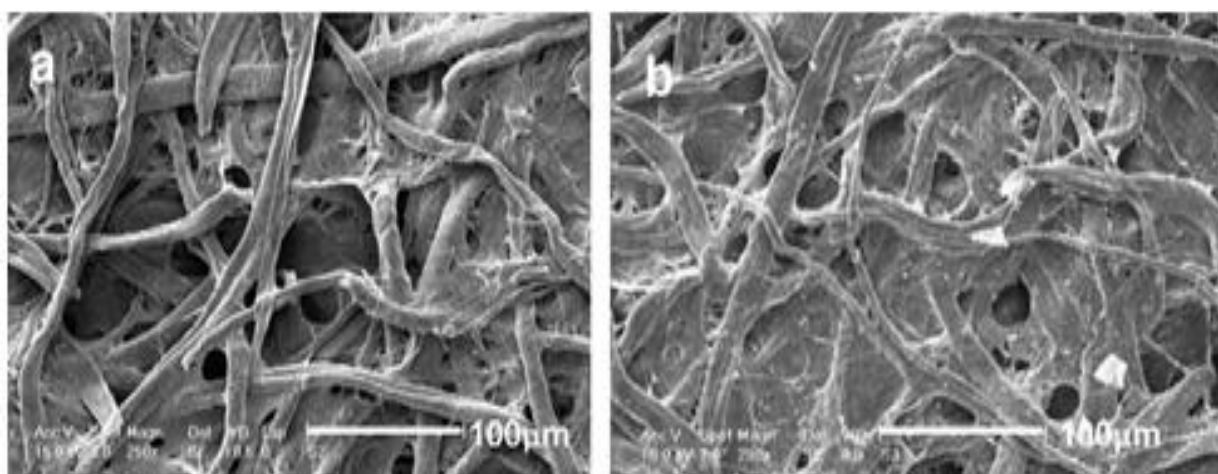
Figure 1-9: SEM images of (a) uncoated paper, (b) coated paper by titanium dioxide nanoparticles.[130]

14

On the production site, it is important to monitor and control the nature of the paper surface as this monitoring provides insight on how to improve the surface properties.[131] Samyn *et al.* have applied two techniques, i.e., non-contact profilometry and atomic force microscopy (AFM), to demonstrate and analyse the difference of surface roughness parameters for a range of sampling areas. The results obtained from these investigations allow a description of the multi-level roughness of nanoparticle paper coatings. The micro-to-nanoscale topography of the paper coating can be estimated from analysis of the results from these measurements.[132] Also Deumié *et al.*, illustrated (on a logarithmic scale) a linear relationship between the roughness spectrum of uncoated silicon wafer surface with the spatial frequencies.[133]
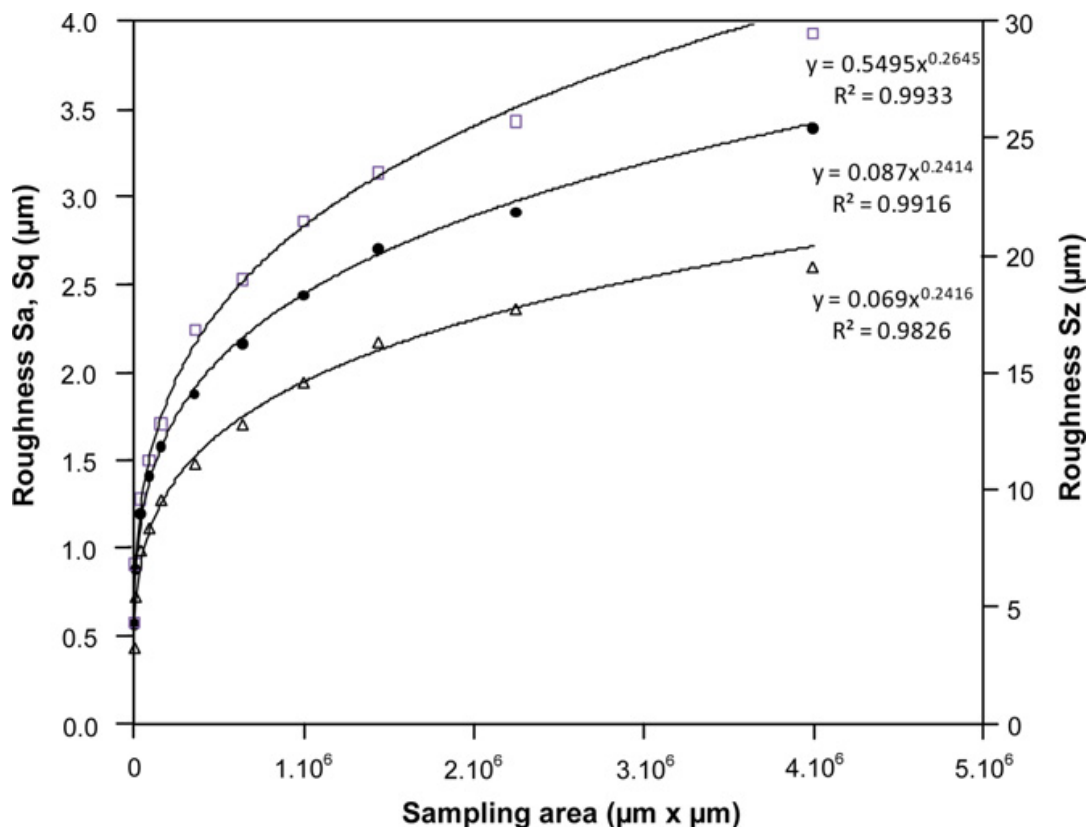
Figure 1-10: The average roughness as a function of the sampling area for NCP.[132]

Modification of the paper surface through the interaction between the nanoparticles and cellulose fibres has been investigated by Vonck and co-workers. The relationship between the physical properties of the nanoparticle-coated paper and control of surface hydrophobicity were investigated in this research.[134]
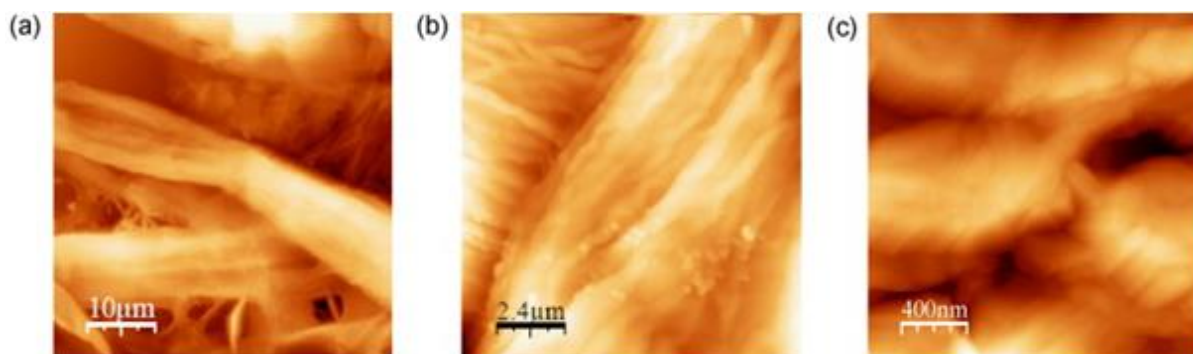
Figure 1-11: Atomic force microscopy of uncoated paper at different differential signal: (a) paper 50 µm × 50 µm, (b) paper 12 µm × 12 µm, (c) paper 2 µm × 2 µm.[134]

Abidi *et al.* reported the successful modification of cotton fabric by titanium dioxide nanosols prepared by means of the sol-gel process with tetrabutyl orthotitanate [Ti(OC$_4$H$_9$)$_4$] as the active ingredient.[135] The titania-nanosol treatment imparted to the cotton fabric a very good protection against UV radiation and self-cleaning properties. Self-cleaning cotton also has been reported by hydrolysis of titanium tetraisopropoxide in an acidic aqueous solution at room temperature.[136] Nishibori's patent describes the preparation of photo-catalytic fibres from waste paper using thermoplastic binders in a dry forming process.[137] The treated fibres can then be used in papermaking or nonwoven manufacture.

Vegetable cellulose fibres have been surface modified using the hydrolysis of tetraethoxysilane (TEOS), octyltrimethoxysilane (OTMS) or (PTMS), followed by the layer-by-layer deposition of previously synthesized titanium dioxide nanoparticles. A cellulose–titanium(IV) oxide nanocomposite modified with organosilicone (CTSN) was prepared by a reaction of cellulose powder with titanic chloride, followed by a reaction with 4-aza-6-aminohexyl triethoxysilane.[138] Neto et al. reported the preparation of TiO$_2$/cellulose nanocomposites through the titanyl sulphate hydrolysis in acidic medium in the presence of cellulosic fibres.[139]

Recently, Koga and his co-workers introduced amino groups onto the surface of CP through a silane-coupling technique using APTES to modify the cellulose surface. They then investigated the mechanical strength and hydrophobicity of the amino-modified paper.[140] They found that this paper modified with amino groups has great potential to be used in the chemical industry as a base catalyst.
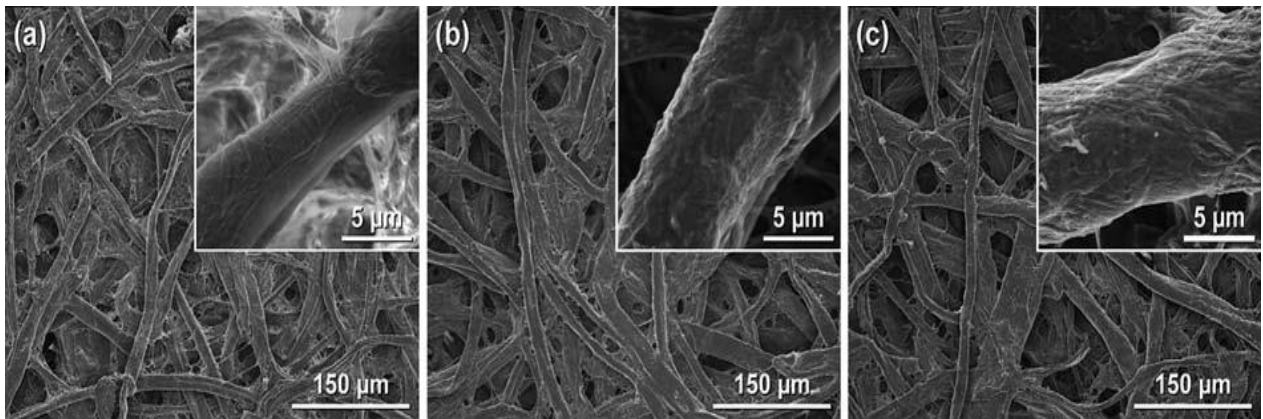
Figure 1-12: SEM images of (a) untreated paper, (b) NH$_2$-modified paper, and (c) PEI-modified paper investigated in Koga's work.[140]

In 2003, Atou *et al.* used spray coating of stable metal oxide nanoparticles, such as alumina or silica, onto the surface of titanium dioxide nanoparticles layers to inhibit or at least substantially reduce the photo-catalytic activity of titania nanoparticles.[141] Toni *et al.*, in 2006, protected photo-chemically active titanium dioxide nanoparticles with a chemically and photo-inactive silica shell, to produce photo-chemically inactive, but UV-light absorbing, TiO$_2$/SiO$_2$ core/shell nanoparticles by a seeded sol-gel process using tetraethyl ortho-silicate (TEOS) in ethanol.[142] Several researchers had investigated the synthesis of silica-coated core-shell titania nanoparticles with hydrophilic and insulating properties under mild fabrication conditions and at low cost.[99, 143]

17

1.6 Aims of project

There were two main aims for this thesis, both of which involved the synthesis, typically through environmentally friendly (green) methods, and the analysis and determination of the physical properties of novel inorganic nanomaterials and nano-composites. The first aim of this research was to prepare and then deposit a coating of titanium dioxide nanoparticles on the surface of CP in order to improve the UV-stability and improve the whiteness, brightness and reflectivity of commercial paper. Therefore, a number of different methods would be investigated, including the preparation and coating of large titanium dioxide nanoparticles, rutile hair-shaped titanium dioxide nanoparticles, TiO_2/APTES nanoparticles and TiO_2/SiO_2 core/shell nanoparticles. In order to prepare large nanoparticles, *i.e.*, with a diameter of about 200 nm, two different methods will be used, *i.e.*, preparation of titanium dioxide with formation of seed and *in-situ* coating, of CP can improve the UV-stability and increase the whiteness and brightness of the paper by attaching the nanoparticles directly to the surface of the cellulose and not by dispersing the nanoparticles throughout the bulk of the cellulose, e.g., in the pulp. In this work different reaction conditions are to be investigated, such as pH, reagent concentration and temperature in order to optimise the titanium dioxide coating. The investigation addresses the role of titanium dioxide metal oxide nanoparticles prepared *in-situ* on CP or pulp to generate the desired properties of the nanoparticle-coated fibres. Different experimental techniques will be used to study the minimum reaction time and to monitor the reaction conditions. Attempts to optimise the preparation of large titanium dioxide nanoparticles on the surface of the CP by acid-catalysed hydrolysis will also be made.

Another method to be investigated is the preparation of small rutile titanium dioxide nanoparticles as a powder (<200 nm) and also stable colloidal solutions of titanium dioxide nanoparticles stabilised and fixed on the surface of soluble cellulose derivatives, such as CMC, CL4, CMS and industrial starch. These stable aqueous colloidal solutions can be stored and used later to coat the cellulose surface. Alternatively, the solution can be dried and then reconstituted by the simple addition of water.

In order to eliminate the high photo-catalytic properties of small nanoparticles of titanium dioxide, we will also protected the nanoparticle's titanium dioxide surface with a SiO_2 layer or by modification with APTES. Stable colloidal solutions of core/shell TiO_2/SiO_2

nanoparticles were prepared to prevent creation of radicals on the surface of the titanium dioxide nanoparticles.[144] This approach may also generate a more hydrophilic surface in polysaccharide derivatives as well as inhibit the photo-catalysed decomposition of the polysaccharide fibre. The aim of this part of the work for this thesis was to inhibit this photo-degradation effect by adding a coating of SiO_2 to form stable core/shell TiO_2/SiO_2 nanoparticles with a high refractive index that could be attached to the cellulose surface to improve its optical properties and increase its brightness and stability to UV-bleaching.

One of the main aims of surface modification of paper is to ensure that the surface modification through the use of nanoparticles works for all kind of cellulose fibres and not only for a special type.

Finally the brightness and UV stability will be monitored of the CP coated with titanium dioxide nanoparticles prepared using different methods of described above.

The second primary aim of this research is to prepare and coat silicon diimide gel for use for the first time as a basic stationary phase on glass substrate surface to improve the efficiency of TLC for acid-sensitive organic compounds. Silicon diimide gel, $Si(NH)_2$, is the basic equivalent of silica gel, SiO_2, in which the oxygen atoms of silica have effectively been replaced by nitrogen atoms. Silica gel is the standard stationary phase for thin film chromatography (TLC) and column chromatography. However, silica gel is lightly acidic, which can lead to the chemical decomposition of acid-sensitive compounds during either thin layer or column chromatography. The mesoporous silicon diimide gel will be prepared and optimised using a sol-gel process originally developed previously at the University of Hull. It exhibits a large specific surface area, a weakly basic surface and it is ideal for the characterisation, separation and purification of acid-sensitive compounds.

1.7   Analytical methods used in this research

1.7.1   Transmission Electron Microscopy (TEM)

TEM is an imaging technique with much higher resolution than light microscopy. It is able to examine, in detail, a single column of atoms, which is 10,000 times smaller than the smallest resolvable object in optical microscopy using visible light to produce an image of the object. TEM provides valid information on the size of nanoparticles and has already been widely used to determine the shape of titanium dioxide nanoparticles.[145] Each basic TEM instrument has five main parts: a vacuum system, a specimen stage, an electron gun, an electron lens and apertures.

1.7.2   Scanning Electron Microscopy (SEM)

SEM is a type of electron microscope with the capability to image surfaces, with a magnification of 10 to 100,000 times and the resolution limit of 3 to 100 nm (depending on the sample). SEM scans the sample by a high-energy beam of electrons in a raster scan pattern. The intensity of the electron beam is much less than that of TEM and so is often used for the analysis of soft tissue, such as biological samples, which would be destroyed by a TEM beam of electrons. The atoms and electrons interact, which gives information about the sample composition, the sample's surface topography and occasionally other properties, such as electrical conductivity.[146] Each basic SEM apparatus has an electron gun, an X-ray detector, an electron detector, a focusing electromagnetic lens and a vacuum pump.

1.7.3   Energy-Dispersive X-ray Spectroscopy (EDX or EDS)

EDX is an additional analytical technique that is used for the chemical characterization or elemental analysis of a sample. It is a variant of X-ray fluorescence spectroscopy, which depends on interactions between electromagnetic radiation and matter. It analyses the X-rays emitted by the sample in response to being hit with highly charged nanoparticles.

1.7.4   Inductively Coupled Plasma (ICP)

ICP is designed to generate plasma, which is a gas of atoms present in an ionized state and then provide information on the chemical composition of the plasma sample. The basic set up of an ICP consists of three concentric tubes, usually made of silica. The basic ICP set-up consists of an ICP torch, a nebulizer (sample introduction system), a computer interface, transfer optics, a spectrometer and a high-frequency generator.

1.7.5   X-Ray Diffraction

The X-ray diffraction technique is an analytical technique for studying the structure of crystalline materials, usually at a wavelength of about 0.5 to 2.5 Å. This method is based on the diffraction of X-rays by crystal lattices. It can monitor the distance between crystal plates as well as the size and type of the unit cell.[147] Each basic XRD machine has a detector, an X-ray tube and a monochromator shutter. When a X-ray incident upon the sample, the X-rays are reflected according to the Bragg condition: $n\lambda = 2d\sin\theta$

Where (n) is an integer, (λ) is the wavelength of the X-rays, (d) is the layer spacing (separation of the reflecting planes), (θ) is the angle of incidence.

1.7.6   Infra-Red Spectroscopy (IR spectroscopy)

Infra-red spectroscopy is used to analyse the chemical composition of organic matter by absorption of infra-red radiation. In the electromagnetic spectrum, infrared radiation is divided into three parts: the far-infrared, 400–10 cm^{-1} (25–1000 μm), which has low energy and is used for rotational spectroscopy; the mid-infrared, 4000–400 cm^{-1} (2.5–25 μm), which is used to study associated rotational-vibrational structure and fundamental molecular vibrations. The higher-energy near-IR, 14000–4000 cm^{-1} (0.8–2.5 μm wavelength), which can excite overtone or harmonic vibrations. Each commercial IR spectrometer has a splitter, a detector, a sample tube and a reference tube.

1.7.7   Ultraviolet-Visible Spectroscopy (UV-Vis)

An UV-Vis spectrometer uses light in the visible, near-infrared (NIR) and near-UV electromagnetic spectrum in order to determine the nature the absorption of this radiation by molecules, which gives information about the molecular structure, particularly of highly-conjugated or aromatic species. The sample molecules undergo electronic transitions upon absorption of the appropriate part of the incident electromagnetic radiation.[148]

1.7.8   Near-Infrared Spectroscopy (NIRS)

This method measures the absorption of near-infrared region of the electromagnetic spectrum, from about 200 nm to 3300 nm wavelength, by organic molecules. Typical applications include food quality control, medical diagnostics, pharmaceutical, and combustion research and science. The instrumentation required for near-IR (NIR) spectroscopy is similar to that used in the UV-vis spectroscopy, *i.e.*, there is a detector, a source of near IR radiation, and a dispersive element to record the intensity of transmission of different wavelengths.

1.7.9   UV light 1

The compact and handheld ultraviolet lamps use UV wavelengths which are an essential multipurpose tool for laboratory applications. Shortwave (254nm - UVC) can be used for DNA/RNA fluorescence, sterilization/germicidal, analysis, photochemistry and more. Longwave (365nm - UVA) can be used for bacterial identification, inspection, specimen staining and titration processes, thin layer chromatography, gel electrophoresis, visualization of DNA and RNA and fluorescence of other materials are among the applications.

1.7.10 UV light 2

The Omni Cure Series 1000 is a highly versatile spot UV curing system with stable UV output. It is comprises a high pressure 100 watt mercury vapour short arc lamp, 250-450 nm, 365nm, 320-390nm, 400-500 nm optical filter, protective eyewear, grounded and shielded power cord, foot pedal.

1.7.11 Nanoparticle Tracking Analysis (NTA)

Nanoparticle tracking analysis comprises a microscope,[149] a scientific camera and a sample viewing unit. A laser diode is used for the viewing unit to illuminate nanoparticles in a liquid suspension. The laser light source uses a wavelength of 405 nm (blue), 532 nm (green), or 638 nm (red). NTA analyses videos captured using the instrument and measure a particle size distribution of typically 10 nm - 1000 nm. Tracking is carried out for all nanoparticles in the laser scattering volume to produce a particle size distribution using the Stokes-Einstein equation, relating the Brownian motion of a particle to a sphere-equivalent hydrodynamic radius.[150]

1.7.12 Barrett Emmett Teller analysis (BET)

In this method a fully automated analyser is used to determine the adsorption of a porous sample of nitrogen on the sample surface as a function of the nitrogen relative pressure. This approach provides useful data for the determination of the specific surface area of a porous material as well as to calculate the average size of the pores.

1.7.13 Electroacoustic Determination of Zeta Potential (ζ-potential)

The zeta potential is a scientific term for electro-kinetic potential in colloidal systems. It is a measure of the magnitude of the repulsive or attractive forces between neighbouring nanoparticles in a colloidal solution or suspension.[151]

1.7.14 Combustion analysis (CHN)

The amount of carbon (C), hydrogen (H), nitrogen (N) and sulphur (S) in an organic compound can be measured with this analytical technique. The analyser uses a combustion process to oxidise organic substances into simple decomposition products, which are then detected, identified and their concentration measured. The CHN analysers components are an ignition chamber, a pre-packed column, a TCD detector and spectrum analysers.

1.7.15 X-ray Photoelectron Spectroscopy (XPS)

X-ray photoelectron spectroscopy is a surface-sensitive quantitative spectroscopic analytical technique for measuring the elemental composition in the parts-per-thousand range, chemical and electronic state of the elements present on the surface of a material and their empirical formula. A beam of X-ray is focussed at an incidental angle on the test material and the number of electrons and their kinetic energy is measured at the time for electron escape from the The top 0 to 10 nm layer of the material surface. A high vacuum (P ~ 10-8 millibar) or an ultra-high vacuum (UHV; P < 10-9 millibar) are required for this analytical technique.

1.7.16 Nuclear Magnetic Resonance (NMR)

Nuclear magnetic resonance spectroscopy is a useful, versatile technique for the determination of the molecular structure and composition that relies on measuring the interactions of nuclear magnetic fields with an applied magnetic field. NMR uses a large magnet to probe the intrinsic spin properties of atomic nuclei. Like all spectroscopic techniques, NMR uses a component of electromagnetic radiation (radio frequency waves) to promote and measure transitions between quantised nuclear energy levels. It can be used with liquid, solid or gas samples, with compounds of various masses and compositions, and can be used to detect a wide range of nuclides depending on instrumentation. It has been used in a diverse range of research areas, including organic, inorganic, and physical chemistry, medicine, biochemistry, protein science, and the food industry. Solid-state NMR (SSNMR) spectroscopy is a kind of NMR spectroscopy, characterized by the presence of anisotropic

interactions. Solid-state NMR can offer information of dynamics and structure in solid materials and also for the characterisation of crystalline solids, it is often an invaluable complement to diffraction-based methods. In pharmaceutical systems, it is important to understand transformations between the different forms of a solid (polymorphs).

1.7.17 Whiteness

In colourimetry, whiteness is the grade to which surface is more white. For example it is used to compare quantitatively two pieces of A4 paper which appear white viewed individually, but not when juxtaposed.

1.7.18 Brightness

Brightness describes the luminance of a visual target. This is sometimes a subjective attribute of an object being observed. In other words, brightness is an attribute of visual realization in which a source appears to be radiating or reflecting light.

1.7.19 Centrifuge

A centrifuge rotates samples at high speed driven by an electric motor. Objects are rotated very quickly about a fixed axis, thereby applying a force perpendicular to the axis. A sedimentation principle is the basis of each the many types of centrifuge. This causes more dense substances to separate out in the bottom of the tube of a liquid sample.

1.7.20 Ultrapure water

Ultrapure water with the specific resistance of 18.2 MΩ.cm was obtained by using a reversed osmosis purification process followed by ion-exchange and filtration. [105]

1.8 Organisation of the thesis

The thesis is divided in to two parts, *i.e.*, Part 1 – Cellulose/Titanium Oxide nano-composites and Part 2 Silicon Diimide Gel as a Stationary Phase for Chromatography.

The first chapter of Part 1 of this thesis describes the thinking behind this research and introduces the synthetic and analytical methods used, as well as the target products. It includes the aims of this section of the thesis and includes a summary of the research literature, which informed the work presented in this dissertation.

Chapter two describes experiments, synthetic methods, reagents and chemicals used in this research and also equipment and characterization methods.

Chapter three contains results and discussion of the initial work of this research into making large nanoparticles with a diameter of *ca.* 200 nm. These particles were of particular interest as they exhibit much less photo-catalytic activity in comparison with that of much smaller nanoparticles. The *in-situ* deposition of the titanium dioxide nanoparticles prepared in this thesis onto the surface of CP is also discussed in this chapter.

Chapter four describes the results of making the titanium dioxide nanoparticles smaller than 200 nm. The complications that arise from coating CP with smaller titanium dioxide particles are described: in particular those of photo-catalytic activity.

Chapter five and six describe the use of passivating layers of SiO_2 and APTES treatments of small titanium dioxide nanoparticles in order to improve the UV stability of the titania/CP nano-composites and to reduce photochemical activity of the titanium dioxide nanoparticles.

Part 2 is just one chapter and it shows the methods used for making silicon diimide gel and it use as a basic stationary phase in thin film chromatography for acid-sensitive organic compounds.

2 Experimental

Reagents and Chemicals

All the starting materials were obtained from commercial suppliers and used without further purification. 18.2 MΩ deionised water was used for all the reactions requiring water.

2.1 Chemicals

suppliers	Reagents
Sigma Aldrich	Titanium (IV) oxysulfate (TiOSO$_4$.xH$_2$SO$_4$. H$_2$O)/99.99%, Titanium oxysulfate-sulfuric acid complex hydrate (TiOSO$_4$. xH$_2$SO$_4$.xH$_2$O), Titanium (IV) oxysulfate hydrate (TiOSO$_4$.xH$_2$O), Titanium (IV) choloride (TiCl$_4$), Titanium (IV) oxide (TiO$_2$)/99.5%, Titanium tetrachloride (TiCl$_4$), Urea (CH$_4$N$_2$O), APTES (3-aminopropyltriethoxysilane)(H$_2$NC$_6$H$_6$)(C$_2$H$_5$O)$_3$Si, Potato starch, PDDA [poly(diallyldimethylammonium chloride)] (C$_8$H$_{16}$ClN)$_n$/20 wt% in H$_2$O, PSS [poly(sodium 4-styrene-sulfonate)] [-CH$_2$CH(C$_6$H$_4$SO$_3$Na)-]$_n$, TEOS(Tetraethyl orthosilicate)(Si(OC$_2$H$_5$)$_4$), Rhodamine B (C$_{28}$H$_{31}$ClN$_2$O$_3$), Sodium, DCM (dichloromethane)(CH$_2$Cl$_2$), Palladium(II) acetate (Pd(OCOCH$_3$)$_2$), Benzophenone (C$_6$H$_5$)$_2$CO, Tris(dimethylamino)chlorosilane (ClSi(N(CH$_3$)$_2$)$_3$), Dimethylamine (CH$_3$)$_2$NH, Trifluoromethanesulfonic acid (CF$_3$SO$_3$H), Alumina (Al$_2$O$_3$), THF (tetrahydrofuran)(C$_4$H$_8$O), Potassium carbonate (K$_2$CO$_3$)/99%, Phenol (C$_6$H$_5$OH) /99.5%, Sulfuric acid(H$_2$SO$_4$)/99.99%, Diethyl ether (CH$_3$CH$_2$)$_2$O/99.7%.
Fisher Scientific	Sodium chloride (NaCl), Nitric acid (HNO$_3$)/70%, Hydrochloric acid (HCl)/36%, Ammonia (NH$_4$OH)/35%NH$_3$, Hexane (C$_6$H$_{14}$), Acetone, Xylene [C$_6$H$_4$(CH$_3$)$_2$], *iso*-Propanol [(CH$_3$)$_2$CHOH], Methanol (CH$_3$OH) and Ethanol (CH$_3$CH$_2$OH).

Acros	Sulphuric acid (H_2SO_4)/96%, 2,2'-Bithiophene ($C_8H_6S_2$)/97%, 3,4-Dihydro-2H-pyran (C_5H_8O)/99%, N,N-Dimethylformamide (DMF)(C_3H_7NO)/99.8%.
Schmincke	Anylate bindemittel.
Edonik	Hydrophilic fumed metal oxides (TiO_2-P25).
Titk	CMC (carboxymethyl cellulose), CMS (carboxymethyl starch).
BDH	Sodium hydroxide (NaOH).
Mondi	Bulk CP.

2.2 Equipment and characterization methods

Transmission electron microscopy (TEM) spectra were obtained using a Jeol 2010 TEM running at 200kV. Images were obtained with a Gatan Ultrascan 4000 digital camera. Solid samples were prepared by suspension in distilled water and 5 µl aliquots of a suitable dilution dropped onto carbon coated copper grids. EDX data were obtained using an Oxford Instruments 'INCA' Energy Dispersive X-ray Spectrometer.

Scanning electron microscopy (SEM) images were obtained using Carl Zeiss SMT 'EVO60' SEM microscope operating at 20 kV and EDX data were obtained using an Oxford Instruments 'INCA' Energy Dispersive X-ray Spectrometer.

The amount of metal in the nanocomposites was determined by an inductively coupled plasma Perkin Elmer 40 emission ICP instrument.

X-ray powder diffraction (XRD) analysis was carried out using a SIEMENS D5000 instrument and an X-ray wave length range of 0.5 Å to 2.5 Å.

Fourier transform infrared spectra were recorded on a Nicolet Magna-500 FTIR spectrometer.

The UV-Vis absorption spectra of the particle dispersions were measured using a Perkin Elmer Lambda 25 Scan UV-Vis spectrometer using a quartz cell of 1 cm path length.

Two-beam NIR spectrophotometer cary 5E, 200 – 3300 nm spectral range and 0,05 nm resolution.

The ultra-violet (UV) light, model UVGL-58. Mineralight lamp, multiband UV 254/365 nm.

Omni Cure spot UV curing system, series 1000 with high pressure 100 watt mercury vapour short arc lamp and 250-450 nm, 365nm, 320-390nm, 400-500 nm optical filters.

Nanoparticle Tracking Analysis (NTA) by LM10 NanoSight, Version 2.2 Build 0377.

The BET surface area and pore size diameter of powders was calculated from nitrogen adsorption/desorption isotherms at 77 K using a Micromeritics three-star 3000 instrument.

Zeta potential analysis was carried out using a Malvern 3000 instrument (Brookhaven Instruments Inc). The laser specification in this machine is 10 mW. The pH values were adjusted by the addition of 0.1 M HCl or 0.1 M NaOH aqueous solutions.

A Fisons EA 1108 CHN analyzer was used by Carol Kennedy to provide the CHN data.

XPS was performed on a Kratos Axis HSi X-ray photoelectron spectrometer fitted with a charge neutraliser and magnetic focusing lens employing Al K_α monochromated radiation (1486.7 eV) by Professor Adam Lee of Warwick University. Surface elemental analysis was undertaken on Shirley background-subtracted spectra applying the appropriate instrument and element specific response factors. Spectral fitting was conducted using CasaXPS version 2.3.14, with binding energies corrected to the C 1s peak at 284.5 eV and high-resolution C 1s, O 1s, N 1s, Si 2p and Ti 2p XP spectra fitted using a common Gaussian/Lorentzian peak shape. Errors were estimated by varying the Shirley background subtraction procedure across reasonable limits and re-calculating fits.

The solution NMR spectroscopy was carried out using a JEOL, JNM-ECP FT NMR spectrometer (400 MHz). Tetramethylsilane (TMS) was used as an internal standard.

Solid state NMR was carried out by Dr. Mark Lorch using a Bruker 500 MHz NMR instrument.

The whiteness of paper samples was measured using a standard whiteness tester (Lorentzen&Wettre, Elrepho).

The brightness of the paper samples was determined before and after the suntest (Suntest XLS$_+$; ATLAS Material Testing Solutions). The suntester allows irradiation of paper samples using a xenon lamp under reproducible conditions (i.e. 90 min, 500 W, and 2700 kJ/m^2).

Isolating and separating suspensions and also separation of final products with different shapes was accomplished by centrifugation at 10000 rpm for 10-15 min by using the Sigma centrifuge 2-15 Howe.

Ultrapure water with the specific resistance of 18.2 MΩ.cm was supplied by UPQ PS system, ELGA, USA.

The progress of many reactions was monitored by using thin layer chromatography (TLC). The TLC plates used had an aluminium backing, which was coated with silica gel type 60 F254 from Merck. It was used as reference silica gel TLC plate and compared with the performance of a silicon diimide gel TLC plate made in this research.

2.3 Synthetic Methods

2.3.1 Preparation of large titanium dioxide nanoparticles

2.3.1.1 Preparation titanium dioxide nanoparticles without seed formation

Method 1

Two different approaches were used in method 1. A $TiOSO_4$ solution was prepared from a mixture consisting of 33 mL of distilled water and 17 mL of $TiOSO_4 \cdot xH_2SO_4 \cdot xH_2O$ (0.34 M), while another solution was prepared from 5 g $TiOSO_4 \cdot xH_2O$ and a mixture of 2.8 mL H_2SO_4 and 100 mL water. The solutions were heated at 110 °C for 5 h. The white products obtained after centrifugation at 10,000 rpm for 15 minutes, were washed with water and then dried overnight under the vacuum (SMS029 and SMS035, respectively).

Method 2

5 g $TiOSO_4 \cdot XH_2O$ was dissolved in a solution of 100 mL distilled water and 2.8 mL H_2SO_4. The resultant solution was lowered into a pre-heated oil bath, at 120 °C. The reaction time is shown in Table 2-1. The precipitate obtained after centrifugation, was washed with water at least 5 times and until all the SO_4^{2-} ions were removed from the supernatant. After removal of the SO_4^{2-}, 100 mL distilled water was added to the precipitate obtained and the resultant solution was heated again at 120 °C for 5, 12 and 20 hours (Table 2-1). The product obtained after centrifugation at 10,000 rpm for 15 minutes was washed and then dried under vacuum.

Table 2-1: Preparation titanium dioxide nanoparticles without seed formation

Sample	$TiOSO_4 \cdot xH_2O$ (g)	H_2SO_4 solution (96%)	First heating (hour)	Second heating (hour)
SMS039A	5	2.8	5	5
SMS040	5	2.8	12	12
SMS039B	5	2.8	22	20

Aqueous Colloid Stability Tests

The stability of the solutions prepared in two methods was investigated using different concentrations of CMC, CMS, AVEBE and starch and a range of pH values.

2.3.1.2 Preparation of titanium dioxide nanoparticles with the formation of seeds

Luigi Piccolo and his colleagues published a process for the hydrolysis of titanium sulphate solution. In this thesis their method was used in the hydrolysis of a titanium sulphate solution to control the nanoparticle size for coating CP floating in the titanium dioxide solutions.[152]

2.3.1.2.1 *Preparation of titanium dioxide nanoparticles using TiOSO4·xH₂SO₄·H₂O as starting reagent*

Solution A: 45.2 g of $TiOSO_4.xH_2SO_4.H_2O$ (15 Wt%) was dissolved in 53 mL water and then 4.90 mL ammonia solution (35% NH_3) was added to the resultant solution to prepare a final solution with $TiOSO_4$ 416.0 g L^{-1}. The concentration of the H_2SO_4 acid was approximately 361.8 g L^{-1} as determined by titration.

Solution B: 2.6 mL of H_2SO_4 (18 M) was added to 58.2 mL of solution A to prepare a solution with a concentration of $TiOSO_4$ 402.2 gL^{-1} and H_2SO_4 426.0 gL^{-1}.

First, 1.8 mL of solution A, 58.2 mL of solution B and 15 mL water were heated separately to 95 °C. The solution A was added to the pre-heated water (15 mL) under stirring. Initially, a colloidal solution formed on the addition of solution A and then disappeared with addition of the remainder of solution A. Immediately after completion of this operation, solution B was added at a constant rate over 6 minutes to the reaction solution, which was then brought to reflux. Both the heating and stirring were stopped when a white precipitate was observed, indicating the beginning of hydrolysis. After 20 minutes the heating and stirring were started again and the reaction solution was heated under reflux for a further 2 hours. 7.5 mL of water, which had been pre-heated to 95 °C, was then added to the reaction solution and the resultant

solution was heated under reflux for a further 2 h. A white product was recovered after centrifugation, which was washed with water and dried under vacuum overnight.

2.3.1.2.2 Preparation of titanium dioxide nanoparticles using $TiOSO_4.xH_2O$ as a starting the reagent

One-solution approach

Solution A: A solution was prepared by adding 6.79 mL of H_2SO_4 (18 M) and 21 g of $TiOSO_4 \cdot xH_2O$ to 60 mL distilled water and then warming the reaction solution to 50 °C. ($TiOSO_4$:350 gL^{-1}; Free H_2SO_4: 200 gL^{-1}). The reaction time was either 1 hour or 2 hours. Firstly 60 mL of solution A and 15 mL water were heated to 95 °C. The solution A was then added to the pre-heated water under stirring and at a constant rate over 6 min. The resultant solution was then brought to 100 °C. The heating and stirring were stopped on the first appearance of a white precipitate indicating the beginning of the hydrolysis. After 20 minutes the heating and stirring were started again and the solution was heated under reflux for 2 h. A white product was recovered after centrifugation, washed with water and then dried under vacuum overnight (SMS061). The second reaction was stopped after heating under reflux for 1 hour followed by centrifugation, washing with water and drying overnight under vacuum (SMS062).

Two-solution approach

Solution A: was prepared by adding 1.6 mL of H_2SO_4 (18 M) and 9.89 g of $TiOSO_4 \cdot xH_2O$ to 20 mL distilled water and dissolving at 50 °C ($TiOSO_4$:494.7 gL^{-1}; Free H_2SO_4:141.5 gL^{-1}).

Solution B: was prepared by adding 7.51 mL of H_2SO_4 (18 M) and 29.68 g of $TiOSO_4 \cdot xH_2O$ to 60 mL distilled water and dissolving at 50 °C ($TiOSO_4$:494.7 gL^{-1}; Free H_2SO_4:221 gL^{-1}).

Solution C: was prepared by adding 5.65 mL of H_2SO_4 (18 M) and 29.68 g of $TiOSO_4 \cdot xH_2O$ to 60 mL distilled water and dissolving at 50 °C ($TiOSO_4$:494.7 gL^{-1}; Free H_2SO_4:166 gL^{-1}).

In this method four reactions were carried out: two reactions are the same and just differ in reaction time, i.e., either 4 h or 2 h, and in the other two reactions the pH was varied. In the first reaction (SMS036), 1.8 mL of solution A, 58.2 mL of solution B and 15 mL water were heated individually to 95 °C. Solution A was added to the pre-heated water (15 mL) under stirring. A colloidal solution formed at beginning of the addition and disappeared after completion of the addition of all of the solution A. Solution B was then added at a constant rate in 6 min to the reaction solution and the solution then brought to reflux. The heating and stirring were stopped upon the first appearance of a white precipitate, indicating the beginning of the hydrolysis. After 20 minutes the heating and stirring were started again and the solution was heated under reflux for 2 h. 7.5 mL of water, which had been pre-heated to 95 °C, was then added to the previous reaction solution and then solution heated in an oil bath for a further 2 hours. A white product was recovered after centrifugation, which was washed with water and dried under vacuum overnight, see Figure 2-1.
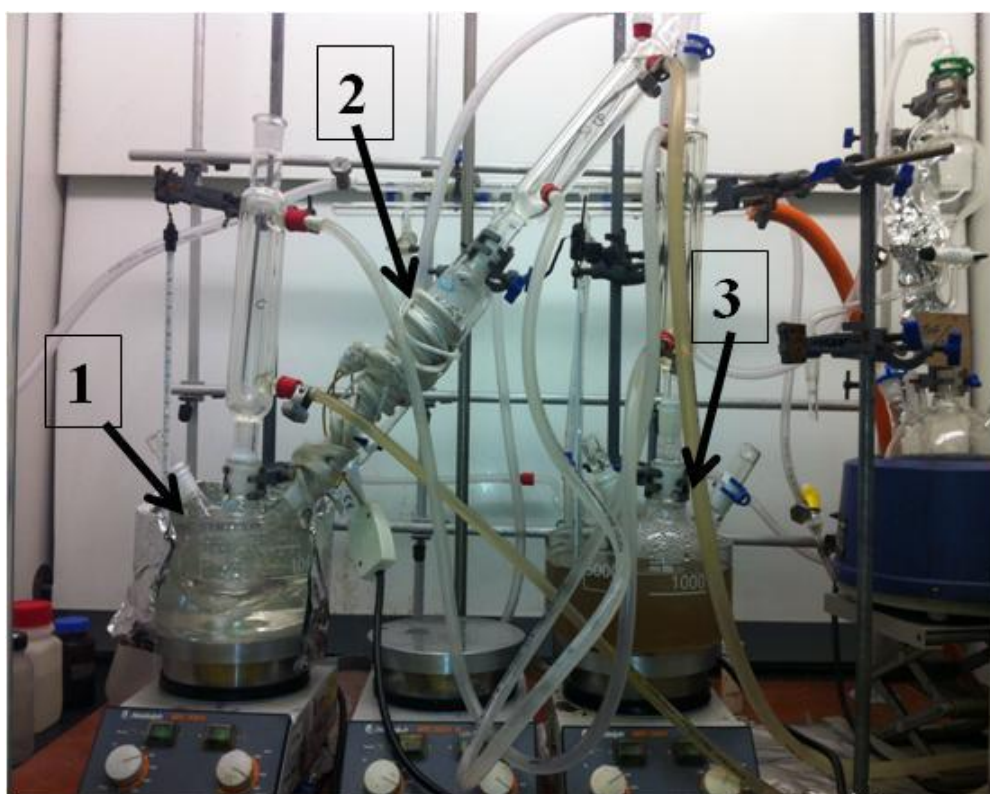
Figure 2-1: photo of using two solutions (1) water, (2) solution B, (3) solution A.

In the second reaction (SMS063), heating was stopped after first 2 h boiling then the section product was centrifuged, washed and dried under vacuum overnight.

In the third reaction (SMS057), 1.8 mL of solution A, 58.2 mL of solution C and 15 mL water were heated separately to 95 °C. All the reaction conditions were the same as those of first reaction (4 hour) except, that solution B was exchanged for solution C, whose acidity was reduced from 221 gL^{-1} to 166.3 gL^{-1}.

The fourth reaction (SMS047) is same as the first reaction (SMS036), except that 3.8 mL of solution A, 167 mL of solution B and 30 mL of water were used and also in second addition after 2 hour, 15 mL water was added to the solution.

Table 2-2: Preparation of titanium dioxide nanoparticles using TiOSO4.xH2O as a starting reagent

Sample	Solution A (mL)	Solution B (mL)	Solution C (mL)	Reaction time (h)
SMS061	60	-	-	2
SMS062	60	-	-	1
SMS036	1.8	58.2	-	4
SMS063	1.8	58.2	-	2
SMS057	1.8	-	58.2	4
SMS047	3.8	167	-	4

2.3.1.2.3 **Stability**

The stability of solutions prepared by these methods was investigated using different concentrations of CMC, CMS, AVEBE and starch with different range of various pH values. 10 mg of each samples after dry white powder mixed with 10 mL of CMC, CMS, AVEBE and starch solutions with different concentrations.

2.3.1.3 In-situ coating of titanium dioxide nanoparticles on cellulosic paper

2.3.1.3.1 **Coating of titanium dioxide nanoparticles on CP with TiOSO$_4$.xH$_2$SO$_4$.H$_2$O**

Method 1: Coating of titanium dioxide nanoparticles on CP at 95 ºC for 60 min

2.40 g TiOSO$_4$·xH$_2$SO$_4$·H$_2$O solution (15 w%) was added to 150 mL of an aqueos H$_2$SO$_4$ solution (0.25 M). The oil bath was first pre-heated to 95 °C and then the flask containing the CP and the TiOSO$_4$ solution was lowered into the pre-heated oil bath. The hydrolysis reaction started after about 10 minutes. After another 60 minutes the papers were removed and washed with distilled water and then dried overnight under vacuum at room temperature.

Method2: Coating of titanium dioxide nanoparticles on CP at 110 ºC for 20 min

The synthetic conditions used for the coating of titanium dioxide nanoparticles on CPs are set on Table 2-3. About 0.7 g of CP was used for this synthesis. Generally, TiOSO$_4$.xH$_2$SO$_4$.xH$_2$O solution (15 wt. % in dilute sulphuric acid) was first dissolved in 50 mL of 0.25 M H$_2$SO$_4$ solution in a 100 ml reaction flask and placed in a 110 °C thermostatised oil bath. CPs were then added to the Ti(IV) acidic aqueous solution and the mixture was stirred at the desired temperature for 20 minutes. The hydrolysis reaction started after about 8 minutes. The nanocomposite papers were then collected by filtering followed thoroughly washing with distilled water and finally dried under vacuum at room temperature overnight.

Table 2-3: Coating of titanium dioxide nanoparticles on CP at 110 ºC for 20 min.

Sample	TiOSO₄ solution (g)	H₂SO₄ solution (0.25 M) (mL)	Cellulosic paper (g)	Temperature (° C)	Time (min)
SMS021	0.80	50	0.70	110	20
SMS022A	1.67	50	0.78	110	20
SMS022B	3.30	50	0.70	110	20
SMS030	1.67	50	2.15	110	20

2.3.1.3.2   **Coating of titanium dioxide nanoparticles on CP with TiOSO₄.xH₂O**

0.25 g TiOSO₄.xH₂O was added to a number of 50 mL H₂SO₄ solutions with different concentrations. The oil bath was first heated to 110 °C and the flask containing CP and TiOSO₄ solution was lowered into oil bath. The hydrolysis reactions started after about 8 minutes. After heating for a further 12 minutes the papers were removed washed with distilled water and then dried overnight under vacuum at room temperature.

Table 2-4: Coating of titanium dioxide nanoparticles on CP with TiOSO₄· xH₂O.

Sample	TiOSO₄.xH₂O (g)	H₂SO₄ solution (50 mL) (M)	Cellulosic paper (g)	Temperature (° C)	Time (min)
SMS079 A	0.25	0.250	0.73	110	20
SMS079 B	0.25	0.275	0.75	110	20
SMS079C	0.25	0.300	0.75	110	20

2.3.2 Preparation of small titanium dioxide nanoparticles.

2.3.2.1 Preparation of stable rutile titanium dioxide NPs solution from $TiOCl_2$ at 50 °C.

Transparent titanium tetrachloride ($TiCl_4$, Aldrich Chemical) was used as a starting material to fabricate TiO_2 powder using the homogeneous precipitation method. $TiCl_4$ is another important precursor for preparation of titanium dioxide nanoparticles.

Since $TiCl_4$ is sensitive to air-moisture, it is generally converted to $TiOCl_2$ by diluting with ice-cold distilled water. To prepare an aqueous $TiOCl_2$ stock solution, $TiCl_4$ that had been cooled below 0 °C was placed in a constant-temperature (0 °C) reaction container, then distilled water ice was added to the container for the hydrolysis reaction. $TiOCl_2$ (0.79 M, 110 mL) was prepared by dropping $TiCl_4$ (17.1 g) into 35 mL ice-cold water under stirring. During the reaction, yellow cakes, such as an unstable $TiO(OH)_2$ intermediate product, were formed at first with the slow melting of ice pieces and then dissolved with the continuous addition of ice pieces to form a yellow, aqueous $TiOCl_2$ solution. The ice pieces cooled the reaction heat of the $TiCl_4$ solution, which occurred from the reaction with water and moisture from the air, and also helped the following reaction via the formation of yellow $TiO(OH)_2$ cake.[153]

$$TiCl_4 + H_2O \longrightarrow TiOCl_2 + 2HCl$$

The aqueous $TiOCl_2$ solution was kept in a stable state without precipitation, even after one year at room temperature. Finally, 75 mL distilled water was added to this stock solution to obtain a transparent aqueous $TiOCl_2$ solution and stirring at room temperature for 4 hrs. On the other hand, direct addition of a large amount of water to $TiCl_4$ easily made it white and turbid with formation of $Ti(OH)_4$ by the hydrolysis of the $TiCl_4$ solution[154] and without formation of a yellow aqueous $TiOCl_2$ solution. Crystalline TiO_2 powder was not precipitated during the process.[155]
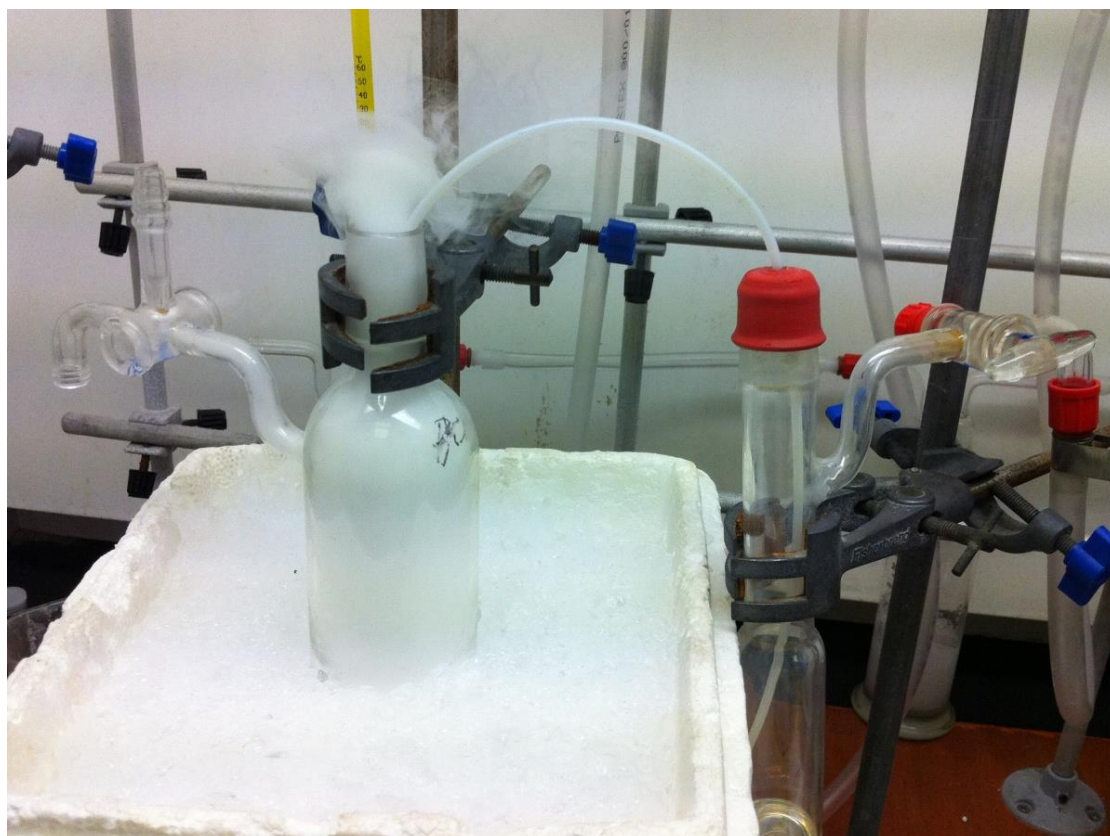
Figure 2-2. Photo of mixing TiCl₄ with cold water for prepare TiOCl₂ in presence of ice.

2.3.2.1.1 **Preparation of rutile titanium dioxide nanoparticles in water**

Preparation method 1

27 mL TiOCl$_2$ (0.79M) was mixed with 14 mL distilled water and then heated at 50 ^{o}C in an oil bath. This procedure was carried out with four different heating times.

$$TiOCl_2 + 2H_2O \rightarrow TiO(OH)_2 + 2HCl \rightarrow TiO_2.xH_2O + 2HCl$$
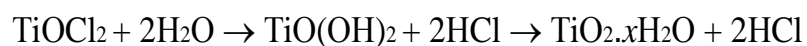
All the solutions were centrifuged at 10000 rpm for 15 minutes and the resultant precipitate was separated from the supernatant. The precipitate was then washed with distilled water and centrifuged at 10000 rpm for 30 minutes. The supernatant colloid solution was stored at room temperature. The precipitate was washed and dried under vacuum. The reactions were carried out for 6, 12, 24 and 48 hours (TiO$_2$ RP).

Preparation method 2

The initial steps to preparing TiO_2 in its rutile phase are exactly same as those described in method 1. After washing and drying the precipitate formed by method 1, the powder was heated in a Furnace at 500 $^\circ$C for 3 hours (TiO_2RP-500).

Preparation method 3

27 mL of $TiOCl_2$ (0.79 M) was mixed with 14 mL distilled water. This reaction was carried out at 50 $^\circ$C for 24 h. The reaction solution was centrifuged at 10000 rpm for 15 min. and the precipitate produced was then separated from the supernatant. The separated precipitate was washed with distilled water and centrifuged at 10000 rpm for 30 min. The supernatant colloidal solution was stored at room temperature. The main difference between this method and method 1 is that the washed precipitate was not dried and was directly mixed with 50 mL water in order to make an aqueous colloidal solution.

Stability

The stability of the titanium dioxide nanoparticles prepared in different solutions was checked as shown in Table 2-5. In order to prepare 10 mL of solutions to check the stability of the products prepared using methods 1 and 2, 10 mg of the relevant product was mixed with 10 mL of distilled water or 1% CMC, CMS and starch solution. However, for method 3 because of the product is a solution, 5 mL of product was mixed with 5 mL of 1% CMC, CMS and starch solution.

Table 2-5: Methods of preparation of colloidal solutions of titanium dioxide nanoparticles for stability tests.

Product Name	Methods name	Preparation Solution	Product Type	Product mg or mL	Mixture solutions for check stability	mL
SMS088C	Method1	Water	Powder	10 mg	Starch 1%	10 mL
SMS088C	Method 1	Water	Powder	10 mg	CMC 1%	10 mL
SMS088C	Method 1	Water	Powder	10 mg	CMS 1%	10 mL
SMS088C	Method1	Water	Powder	10 mg	Starch 1%, pH = 2	10 mL
SMS088C	Method 1	Water	Powder	10 mg	CMC 1%, pH = 2	10 mL
SMS088C	Method 1	Water	Powder	10 mg	CMS 1%, pH = 2	10 mL
SMS104C	Method 2	Water	Powder	10 mg	water	10 mL
SMS091B	Method 3	Water	Solution	5 mL	Starch 1%	5 mL
SMS091B	Method 3	Water	Solution	5 mL	CMC 1%	5 mL
SMS091B	Method 3	Water	Solution	5 mL	CMS 1%	5 mL

Coating cellulosic paper

In order to prepare the coating solutions of the powder products (TiO_2-RP and titanium dioxide RP-500), 0.07 g TiO_2 powder was added to 20 mL distilled water and for the colloidal solution of TiO_2 (method 3), 4.12 mL titanium dioxide solution was mixed with

15.88 mL water. The coating solutions were sonicated for 15 min. and then the CP was immersed in the solution and sonicated again for 15 min. After that the CP was washed with water and dried under vacuum.

2.3.2.1.2 Preparation of cellulose-stabilised titanium dioxide nanoparticles in starch, CMC and CMS solutions.

Preparation Method 4

27 mL $TiOCl_2$ (0.79M) was mixed with 25 mL starch 1% solution. The mixture was incubated at 50 °C for 24 h in an oil bath. The solution was then centrifuged at 10000 rpm for 15 min and washed three times with distilled water. The precipitate was dried under vacuum and 1.77 g of white powder was obtained. Similar reactions were carried out in 1 % CMC and 1 % CMS solutions to obtain 1.52 g and 1.67 g white powders for CMC and CMS respectively.

Preparation Method 5

27 mL $TiOCl_2$ 0.79 M was mixed with 25 mL starch 1%. The mixture was incubated at 50 °C for 24 hrs in an oil bath. The solution was centrifuged at 10000 rpm for 15 min, the resultant precipitate was separated off from the supernatant, washed with distilled water and then centrifuged at 10000 rpm for 30 min. The supernatant colloidal solution was stored at room temperature. The precipitate was washed and was mixed with 150 mL distilled water without being dried.

Stability

The stability of prepared titanium dioxide nano particle powder and also solution were checked as shown on Table 2-6.

Table 2-6: Stability test for the solutions prepared by methods 4 and 5.

Product Name	Methods name	Preparation Solution	Product Type	Product mg or mL	Mixture solution for check stability	mL
SMS090A	Method 4	Starch 1%	Powder	10 mg	Water	10 mL
SMS090B	Method 4	CMC 1%	Powder	10 mg	Water	10 mL
SMS090C	Method 4	CMS 1%	Powder	10 mg	Water	10 mL
SMS125A	Method 5	Starch 1%	Solution	5 mL	Starch 1%	5 mL
SMS125B	Method 5	CMC 1%	Solution	5 mL	CMC 1%	5 mL
SMS125C	Method 5	CMS 1%	Solution	5 mL	CMS 1%	5 mL

Coating cellulosic paper

In order to prepare the coating solution of the powder products (SMS090), 0.07 g of rutile titanium dioxide was added to 20 mL distilled water and for the product (SMS125) 4.12 mL titanium dioxide solution was mixed with 15.9 mL water. The coating solution was sonicated for 15 min. The CP was then immersed in the solution followed by further 15 minutes sonication. After that the CP was washed and dried under vacuum.

Coating LBL cellulosic paper

In the layer-by-layer method, two aqueous solutions of polyelectrolytes, 1% (wt/v) of PDDA in 0.5 M NaCl and 1% (wt/v) of PSS in 0.5 M NaCl solution, were prepared first. The CP samples were immersed alternately in then PDDA, PSS and again in the PDDA solution. After each immersion step (for 10 min.), the CP samples were washed carefully with water

and dried under vacuum overnight. The procedure is same as the last approach, which was used for coating blank CP.

Coating LBL cellulosic paper after change pH

After addition of titanium dioxide to starch, CMC and CMC 1% solution, observed solutions pH were reduced to 3.5. In these methods solution pH was first increase to pH = 7 and then coating on LBL paper was done (using same method as coating LBL).

2.3.2.2 Preparation of stable titanium dioxide nanoparticle solutions from TiOCl$_2$ at 95 ^{o}C

50 mL of an aqueous starch solution (0.5%) was added to an aqueous 25 mL TiOCl$_2$ (0.53 M) solution, which was made from TiCl$_4$ and cold water as previously described. Afterwards 11.84 g of urea was added to the reaction solution, which was then heated at 95 ^{o}C for 6 h, allowed to cool and then left over-night at room temperature. A clear layer was observed at the top of the reaction solution and a colloidal solution including precipitate was obtained at the bottom of the reaction mixture. All the solutions were centrifuged at 10000 rpm for 15 min. and the resultant precipitate separated off from the clear yellow solution. The solid was washed with distilled water and shaken with water to form a colloidal solution and then centrifuged at 10000 rpm for 30 min. After the centrifugation the solution was still colloidal. This colloidal solution was separated off (SMS003C). The precipitate was washed and dried under vacuum.

2.3.3 Surface modification of titanium dioxide nanoparticles to form silica-coated core/shell nanoparticles and their deposition on CP

2.3.3.1 Coating CP with inert shells passivated titanium dioxide nanoparticles

Four types of titanium oxide were used as the core of the composites. One is TiO$_2$-P25 from EVONIK with approximately 80/20 of anatase and rutile titanium dioxide, the second one is commercial TiO$_2$-RA from Sigma Aldrich (RA), the third one is rutile titanium dioxide

(TiO$_2$-RP) prepared from TiCl$_4$ (RP) with a size below 100 nm and the fourth one is TiO$_2$-RP500 after heating at 500 ^{o}C (RP 500 ^{o}C). Preparation of TiO$_2$-RP from TiCl$_4$ was explained in preparation of TiO2-RP in water in 24 hours, method 1.

2.3.3.1.1 Preparation of TiO$_2$/SiO$_2$ core/shell nanoparticles

In order to prepare TiO$_2$/SiO$_2$ core/shell nanoparticles, 10 mL ethanol was added to a 1.25 g titanium dioxide and sonicated for 15 min. The resultant solution was further diluted with a NH$_3$ solution (pH = 12) with strong stirring. 1.25 g TEOS was dissolved in 100 mL ethanol and then mixed with the previous solution. The resultant reaction solution was stirred for 6 hours and then centrifuged at 10000 rpm for 15 min. The resultant precipitate was separated off and washed once with water, twice with ethanol and then dried under vacuum.

2.3.3.1.2 Coating LBL modified core/shell TiO$_2$-P25/SiO$_2$ nanoparticles on CP

PDDA: Poly(diallydimethylammonium chloride), 20 wt% in water, M$_W$ 100,000 – 200,000

PSS: Poly(sodium 4-styrenesulfonate), M$_W$ 70,000.

The following aqueous solutions of polyelectrolytes have been previously prepared: 1% (wt/v) of PDDA in 0.5 M NaCl and 1% (wt/v) of PSS in 0.5 M NaCl.

The LBL technique was applied first to coat TiO$_2$/SiO$_2$ core/shell surfaces by alternate sonicating of TiO$_2$-P25/SiO$_2$ in PDDA, PSS and again PDDA solutions. After each sonication step (15 min), the products were collected by centrifugation (10,000 rpm, 15 min), washed with water and then dried under vacuum overnight at room temperature. The TiO$_2$/SiO$_2$ nanoparticles coated with PDDA (+)/PSS (-)/PDDA (+), were them added to distilled water and sonicated for 15 min. Finally the CP was immersed in the aqueous colloidal solution and sonicated for a further 10 min. The CP was washed with water and then dried under vacuum overnight.

2.3.3.1.3 Coating of TiO$_2$-P25/SiO$_2$ and TiO$_2$-RA/SiO$_2$ on LBL modified CPs

TiO$_2$/SiO$_2$ nanoparticles were deposited on CPs using a layer-by-layer method. Two aqueous solutions of polyelectrolytes, 1% (wt/v) of PDDA in 0.5 M NaCl and 1% (wt/v) of PSS in 0.5 M NaCl, were prepared first. The CPs were immersed alternately in the PDDA, PSS and again in the PDDA solution. After each immersion step (for 10 min), the CPs were washed carefully with water and dried under vacuum overnight. 0.07 g TiO$_2$/SiO$_2$ powder was added to 20 mL distilled water and sonicated for 15 min. 0.7 g CPs coated PDDA/PSS/PDDA were submersed in the colloidal solution and then sonicated for 10 min. The CP was washed with water and then dried under vacuum overnight.

2.3.3.1.4 Coating LBL modified core/shell TiO$_2$-RA/SiO$_2$ nanoparticles on CP

The general method is the same as the method used for coating LBL modified core/shell TiO$_2$-P25/SiO$_2$ nanoparticles on CP, TiO$_2$-RA/SiO$_2$ modified with PDDA, PSS and again PDDA solutions. After each sonication step (15 min), the products were collected by centrifugation (10,000 rpm, 15 min), washed with water and then dried under vacuum overnight at room temperature. 0.07 g of modified TiO$_2$/SiO$_2$ was added to 20 mL distilled water and sonicated for 15 min. Finally the CP was immersed in the colloidal solution and sonicated for a farther 10 min. The CP was washed with water and then dried under vacuum overnight.

2.3.3.1.5 Coating TiO$_2$-RP/SiO$_2$ on LBL modified cellulosic papers

0.07 g TiO$_2$/SiO$_2$ powder was added to 20 mL distilled water and sonicated for 15 min. 0.7 g PDDA/PSS/PDDA treated CPs were put into the colloidal solution and then sonicated for 10 min. The CP was washed with water and then dried under vacuum overnight.
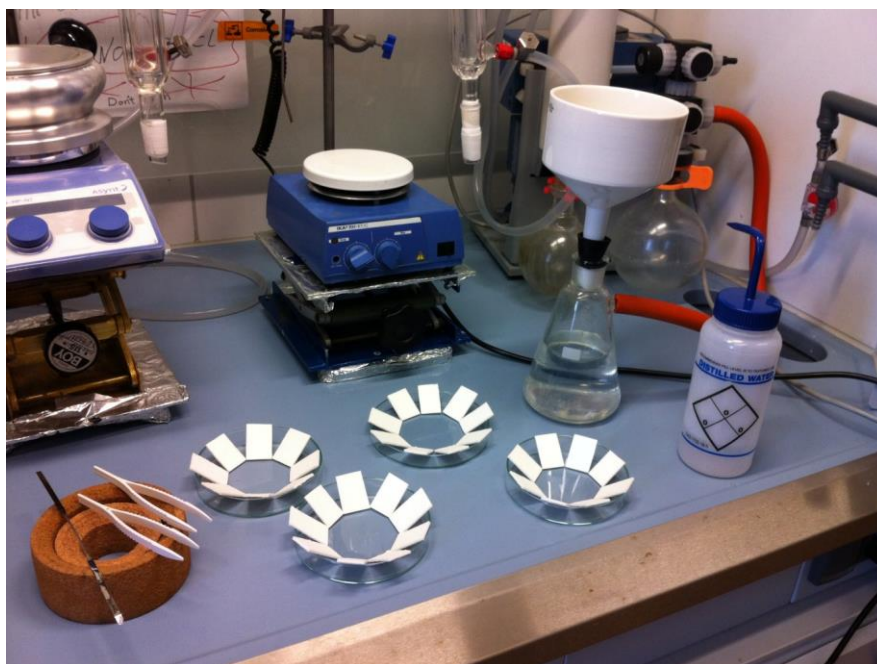
Figure 2-3: photo of washing processes of CP after coating and before drying.

2.3.4 Preparation of TiO$_2$-P25 - APTES nanoparticles

2.3.4.1 Preparation of TiO$_2$ P25– APTES in HCl solution

2.3.4.1.1 **Preparation of TiO2-P25 with APTES**

1 mL APTES was added to 50 mL distilled water and then 0.5 g P25 was added to the APTES solution under string. Next 0.5 mL HCl was added slowly to the reaction solution. The resultant suspension was incubated in an oil bath at 110 ^{o} C for 6 hrs. The resultant precipitate was centrifuged off and washed with ethanol and water alternatively for at least 2 cycles to remove excessive, unreacted APTES. The precipitate obtained was dried under vacuum. This reaction also was repeated with a heating time of 22 hrs.

2.3.4.1.2 **Stability**

The stability of the TiO$_2$-P25 nanoparticles in water, in a NaOH solution with pH = 12 and also in 1% CMC solution, with pH = 3-4 and pH = 2, has been evaluated. 10 mg of TiO$_2$-P25 powder was mixed with 10 mL of each solution.

2.3.4.1.3 **Coating**

0.07 g TiO$_2$-P25/APTES, which was prepared with 22 hrs heating, was mixed with 20 mL distilled water. Afterwards, the suspension was sonicated for 15 minutes at room temperature. The CP was then immersed in the coating solution and sonicated for further 15 minutes at room temperature. Finally, the CP sample was washed with water and dried under vacuum.

2.3.4.2 Preparation of TiO$_2$-P25-APTES in xylene solution

0.5 g of TiO$_2$-P25 was added to 50 mL xylene. Afterwards, different concentrations of APTES were added to the reaction solution. After heating at 50 °C for 10 h and then cooling to room temperature, the solutions were centrifuged at 10000 rpm for 15 min. The solid residue was washed once with xylene, then twice with acetone and then dried under the vacuum.

Table 2-7: Preparation of TiO$_2$-P25 – APTES in xylene solution.

Sample	APTES (mL)	TiO$_2$	Temperature (°C)	Time (h)
SMS053A	0.04	P25	50	10
SMS055	0.1	P25	50	10
SMS046B	0.25	P25	50	10
SMS043A	1.0	P25	50	10
SMS071	1.5	P25	50	10
SMS080	3.0	P25	50	10

2.3.4.2.1 Photocatalytic activity test

The photocatalytic activity of each-P25 TiO2/APTES powder was evaluated in terms of the degradation of Rhodamine B. 10 mg of TiO2/APTES powder was suspended in 10 mL of water and then 10 mL of Rhodamine B solution (20 mg/L) was added to the suspension solution. The UV irradiation was carried out under a UV light at 365 nm for 30 min. The suspension was centrifuged at 10000 rpm for 15 minutes and the clear solution was then covered with aluminium film until it was used for UV-Vis measurement. The concentration of the Rhodamine B in the solution was determined by UV-Vis analysis.

2.3.4.2.2 Coating with heating

0.07 g of TiO2-P25-APTES was mixed with 20mL distilled water and sonicated for 15 min. Then the CP was immersed into the solution and reaction flask was placed into the oil bath on 50 °C for 5 h. The CP was then washed and dried under vacuum.

2.3.4.2.3 Coating with sonicating

20 mL distilled water was added to 0.07 g TiO2-P25-APTES and the resultant solution was then sonicated for 15 min. The CP was immersed in the sonicated solution followed by further 15 min. sonication. After that the cellulosic paper was washed and dried under vacuum. This procedure was carried out for various concentrations of APTES, which are shown in Table 2-7.

2.3.4.2.4 Coating with immersing

20 mL distilled water was added to 0.07 g TiO2-P25 - APTES and the resultant solution was sonicated for 15 min. The cellulosic paper was immersed in the sonicated solution for 15 min. It was then washed and dried under vacuum.

Table 2-8: Coating of TiO₂-P25-APTES on cellulosic paper.

Sample	Concentrations of APTES	APTES [mL]	Method	Temperature (°C)	Time [min.]
SMS060	0.25 mL	0.25	heating	50	300
SMS072A	1 mL	1.0	heating	50	300
SMS072B	1 mL	1.0	sonicating	25	15
SMS076B	1 mL	1.0	Immerse	25	15
SMS086B	3 mL	3.0	sonicating	25	15
SMS086C	1 mL	1.0	sonicating	25	15
SMS086D	0.1 mL	0.1	sonicating	25	15
SMS086E	0.04 mL	0.04	sonicating	25	15
SMS086F	0.25 mL	0.25	sonicating	25	15
SMS086H	1.5 mL	1.5	sonicating	25	15

2.3.4.3 Preparation of TiO₂-RP/APTES nano nanoparticles in xylene solution

50 mL xylene was added to 0.5 g of TiO₂-RP, which was available from the hydrolysis of TiOCl₂. Different concentrations of APTES were added to the reaction solutions, which were then heated at 50 °C for 10 h. The reaction solutions were allowed to cool and then incubated over-night at room temperature. All solutions were centrifuged at 10000 rpm for 15 min. and the resultant precipitates were separated off. The solid residue was washed once with xylene and twice with acetone and then dried under vacuum.

Table 2-9: Preparation of TiO$_2$-RP / APTES in xylene solution.

Sample	APTES (mL)	TiO$_2$	Temperature (° C)	Time (h)
SMS105A	1.0	rutile	50	10
SMS105B	1.5	rutile	50	10
SMS105C	3.0	rutile	50	10

2.3.4.3.1 **Stability**

10 mg of TiO$_2$-RP powder was mixed with 10 mL of distilled water to test the stability.

2.3.4.3.2 **Photocatalytic activity test**

The photocatalytic activity of each rutile TiO$_2$/APTES powder was evaluated in terms of the degradation of Rhodamine B. 10 mg of TiO$_2$/APTES powder was suspended in 10 mL of distilled water and then 10 mL of Rhodamine B solution (20 mg/L) was added to the suspension. The UV irradiation was carried out under a UV light at 365 nm for 30 min. After centrifugation at 10000 rpm for 15 min., the clear solution covered with aluminium film until were used for analysed using UV/Vis analysis to determine the Rhodamine B concentration.

2.3.4.3.3 **Coating cellulosic paper**

20 mL distilled water was added to 0.07 g TiO$_2$-RP which was covered with APTES and the resultant mixture was sonicated for 15 min. The CP was immersed in the suspension solution and sonicated for another 15 min. The CP was then washed and dried under vacuum. This procedure was carried out for various concentrations of APTES, which are shown Table 2-9.

3 Preparation of large titanium dioxide nanoparticles

3.1 Introduction

Nanoparticles of titanium dioxide are widely used in many advanced functional materials,[156] such as cosmetics, catalysts, gas sensors, selective adsorbents, etc., because of their thermal, photochemical, electrochemical and chemical stability, combined with their advantageous spectrum of electronic, optical and mechanical properties.[157, 158]

In the paper industry titanium dioxide is sometimes used as a surface-coating on paper, based primarily on pulp consisting of derivatives of cellulose obtained from a very wide range of sources, in order to induce higher degrees of whiteness and brightness and also to protect the constituent fibres of cellulose from UV-induced photochemical degradation and damage less reflected in a clearly apparent yellowing of the paper surface. However, the main problem for using titanium dioxide as a coating of CP is that its addition to the pulp, before processing to form paper sheets, results in inferior mechanical properties of the modified paper due to the physical disruption of the fibre network by the presence of the relatively large titanium dioxide nanoparticles.[159]

In this Chapter, the preparation of relatively large titanium dioxide nanoparticles with a diameter of about 200 nm is reported. It was postulated that such nanoparticles might be small enough to absorb UV-radiation present in sunlight, but be large enough not to photo-chemically degrade the paper substrate on which the nanoparticles are distributed in order to protect it. However, a major challenge was to prepare stable, aqueous solutions of larger titanium dioxide nanoparticles in order to coat the surface of the cellulose fibres of paper.

This approach would allow the surface properties of the paper to be modified in order to provide a protection against photo-bleaching and photo-degradation, but also to provide paper with a higher degree of brightness and whiteness, which would in turn improve the optical contrast of the paper. It should also limit any negative impact on the mechanical properties of the paper as it would just be a surface coating, which would not interact with and so disrupt the organisation and structure of the polysaccharide chains of cellulose within the core of fibres responsible for the physical properties of the paper itself.

The main aim of this Chapter was to find a new and economical way for making titanium dioxide nanoparticles with a controlled size and shape with the desired spectrum of physical properties. The titanium dioxide nanoparticles should also be water soluble so that stable aqueous solutions could be prepared containing them that could then be used to coat the surface of cellulose fibres, in a cost-effective and environmentally friendly way, in order to manufacture paper on an industrial scale.

3.2 Preparation of titanium dioxide NPs and their deposition on CP.

The main methods for preparing nanosized titanium dioxide nanoparticles until now have been the sol-gel process, the gaseous phase process and the direct hydrolysis of a titanium salt.[160, 161] The direct hydrolysis of a titanium salt in homogeneous solution is simple in terms of processing equipment, with the size and shape of the titanium dioxide nanoparticles being controllable.[162]

3.2.1 Preparation titanium dioxide nanoparticles without seed formation

Two approaches were studied for the synthesis of titanium dioxide nanoparticles without seed formation. In the first method SMS029 was prepared using $TiOSO_4.xH_2SO_4.xH_2O$, which is more economical than either $TiOSO_4.xH_2SO_4.H_2O$ solution (15 wt%) or $TiOSO_4.xH_2O$. Unfortunately the molar ratio of H_2SO_4 and H_2O are both unknown and this starting material appears to contain some unknown and undefined impurities, which, fortunately, could be removed by filtration after the solution was made up. SMS035 was made up in the same way, except that the $TiOSO_4.xH_2SO_4.xH_2O$ was replaced with $TiOSO_4.xH_2O$ and H_2SO_4 was then added to this solution. The concentration of H_2SO_4 in SMS029 is 0.34 M and that in SMS035 is 0.5 M.
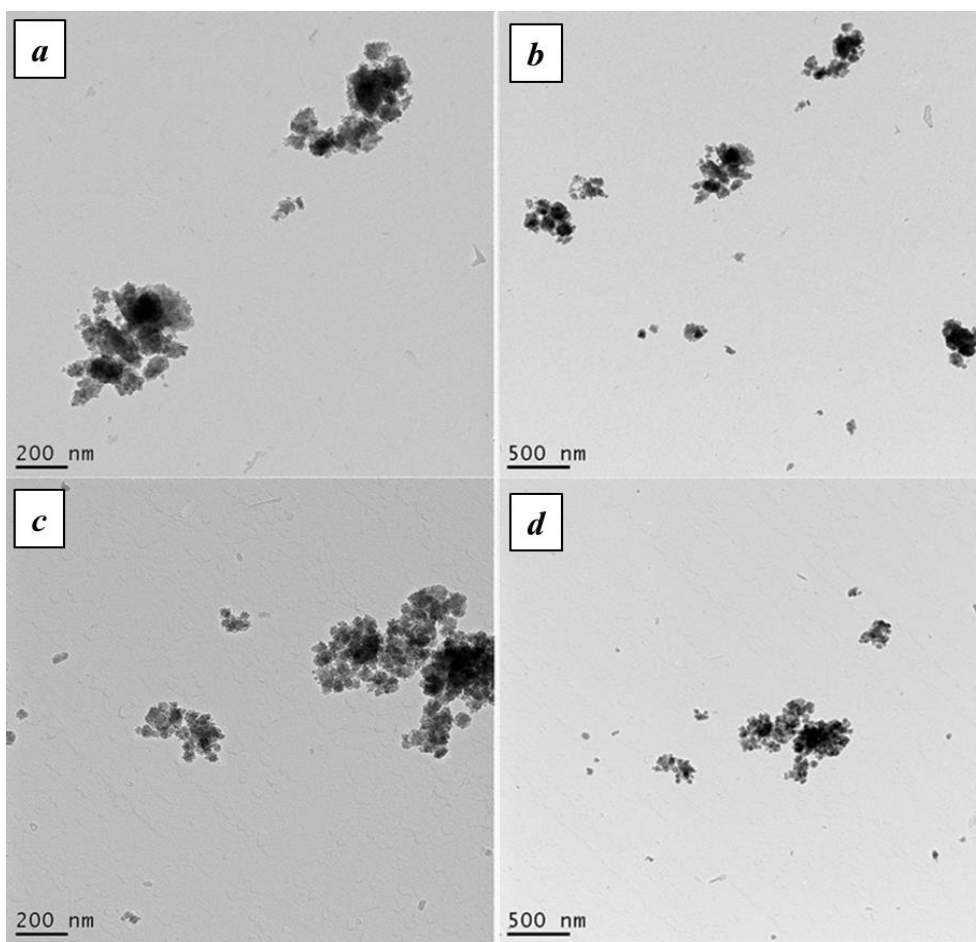
Figure 3-1: TEM images of titanium dioxide prepared from hydrolysis of TiOSO₄ without seed formation SMS029 (a & b) and SMS035 (c & d).

Analysis using TEM shows that for both samples, small nanoparticles aggregate to form much larger secondary nanoparticles. The diameters of the secondary nanoparticles are about 120 nm and 50 nm for the reactions using both 0.34 M and 0.5 M H_2SO_4 solutions, respectively (Figure 3-1). It was decided not to use $TiOSO_4 \cdot xH_2SO_4 \cdot xH_2O$ for the subsequent reactions, due to the presence of impurities.

The values for the stability over time of the aqueous colloidal solutions of SMS029 and SMS035 stabilised using different amounts of either CMC, CMS, AVEBE or starch at different pH values are shown in Table 3-1. The solutions of sample SMS035 in water and either 0.5% starch or 0.5% AVEBE at pH = 12 are not stable. After one hour the top of the solution became clear, while many precipitates were formed in the bottom of the tubes. Adjusting the acidity to pH = 2 can extend the stability for approximately another hour.

However, the stabilities of the colloidal solution with 0.5% CMS, 0.5 or 1% starch are much better. The nanoparticle aqueous colloidal solutions incorporating 0.5% CMS and 1% CMC can be stable for more than four hours, although a small amount of precipitate can be observed in the test samples. The aqueous colloidal solutions of CMC-stabilised titanium dioxide nanoparticles prepared in this way can be stable for nearly two weeks without precipitation after the pH was adjusted to about pH = 2. The greater stability of these colloidal solutions is probably due to the increase of the viscosity of the CMC solutions on the reduction of the pH value.

The stability of aqueous colloidal solutions of SMS035 in starch, 0.5% AVEBE, 0.5% CMS and also CMC at pH = 2 is found to be better than that of the corresponding solutions of SMS029, due to the smaller size of the titanium dioxide nanoparticles making up the SMS035 product compared to that of the SMS029 sample.

In the second method studied in this Chapter, the precipitate was washed with water after the hydrolysis reaction until all of the SO_4^{2-} ions had been removed. The presence of SO_4^{2-} ions can be tested with $BaCl_2$. Distilled water (100 mL) was added to the precipitate, after removal of the SO_4^{2-}, and the resultant solution was heated for a different length of time, see Table 3-1.

Table 3-1: The stability of aqueous colloidal solutions of titanium dioxide nanoparticles in the presence of CMC, CMS, AVEBE and starch stabilisers.

Time	SMS029 (10mg) CMC 1.5% (10 mL)	SMS029 (10mg) CMS 0.5% (10 mL)	SMS035 (10mg) CMC 1.5% (10 mL)	SMS035 (10mg) CMS 0.5% (10 mL)	SMS035 (10mg) AVEBE 0.5% (10mL)	SMS035 (10mg) Starch 0.5% (10 mL)	SMS035 (10mg) pH = 12 (10 mL)
60 min.	milky white colloid, Precipitate	milky white colloid, little precipitate	milky white colloid, precipitate	milky white colloid, little precipitate	milky white colloid, precipitate	colloid, precipitate	colloid, precipitate
120 min.	top little clear, middle colloid, precipitate	colloid, precipitate	colloid, precipitate	colloid, precipitate	top little clear, precipitate	top little clear, precipitate	top little clear, precipitate
180 min.	top little clear, middle colloid, precipitate	colloid, precipitate	colloid, precipitate	colloid, precipitate	top clear, precipitate	top clear, precipitate	top clear, precipitate
270 min.	top clear, middle colloid, precipitate	top little clear, middle colloid, precipitate	colloid, precipitate	top little clear, middle colloid, precipitate	top clear, precipitate	top clear, precipitate	top clear, precipitate
24 h	Near to clear solution, Precipitate	top clear, middle colloid, precipitate	top little clear, middle colloid, precipitate	top little clear, middle colloid, precipitate	top clear, middle colloid, precipitate	top clear, precipitate	top clear, precipitate
2 days	clear solution, precipitate	Near to clear solution, precipitate	top clear, middle colloid, precipitate	top clear, middle colloid, precipitate	Near to clear solution, Precipitate	top clear, precipitate	top clear, precipitate

Figure 3-2: SEM images of titanium dioxide nanoparticles prepared from hydrolysis of TiOSO₄ without seed formation of samples SMS035 (a & c) and SMS039B (b & d).

SEM images show that the titanium dioxide nanoparticles with a size greater than 200 nm are aggregated to form larger nanoparticles. XRD analysis of the white powders produced confirms the formation of anatase titanium dioxide, see Figure 3-2.

Table 3-2: Titanium dioxide nanoparticle size

Sample	SMS029	SMS035	SMS039A	SMS039B	SMS040
Crystallite size (nm)	6.71	8.63	11.44	12.73	12.33

The SEM results show that with increased reaction time, the size of the titanium dioxide nanoparticles formed increases and that the nanoparticles size arising from the second method is greater than that obtained using the first method. The titanium dioxide nanoparticle diameter was found to be between d = 6.7 - 12.3 nm. These nanoparticles were then found to aggregate to form titanium dioxide nanoparticle agglomerates with a size about 200 nm. XRD analysis of the white powder collected from the reaction solutions confirms the formation of anatase titanium dioxide.
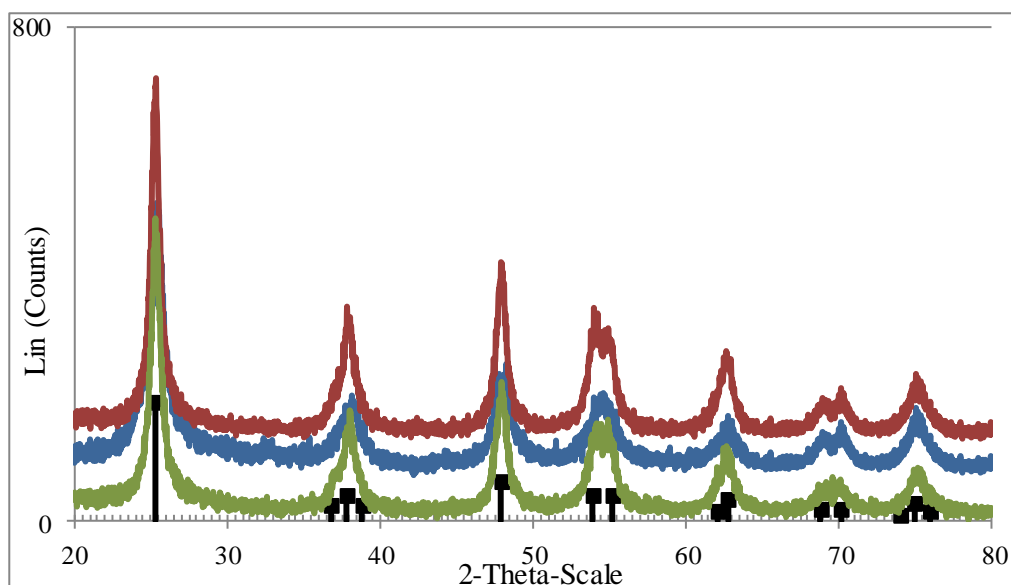
Figure 3-3: XRD Pattern of SMS039 B (red), SMS039 A (green), SMS035 (blue).

IR spectral analysis reveals the presence of an O–H bending absorption at *ca.* 1650 cm^{-1}. Peaks attributable to the presence of SO_4^{2-} were observed between 1,000 and 1,200 cm^{-1}, due to the fact that residual sulphuric acid (H_2SO_4) is difficult to remove completely by simply washing with water. The band corresponding to the Ti–O–Ti bond, generally appearing at *ca.* 600–400 cm^{-1}, could not be observed. [163]
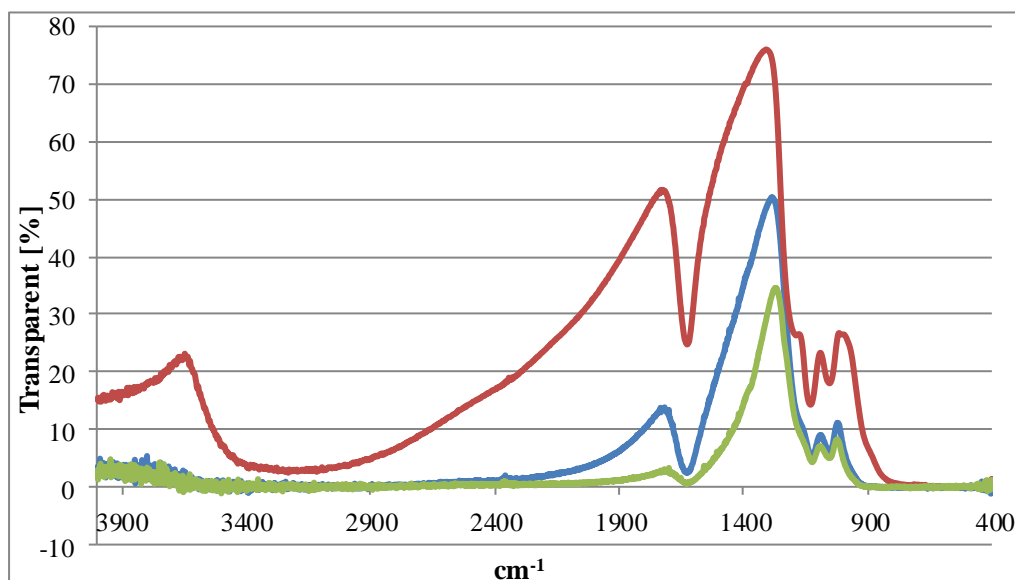
Figure 3-4: FT-IR spectra of samples SMS040 (red), SMS039A (blue), SMS03 B (green).

The BET surface area determined for SMS035 & SMS039B are 55.58 and 126.99 m^2g^{-1} respectively.

The stability of the aqueous colloidal solutions of SMS039 B stabilised using 0.5% starch, 0.5% AVEBE, 0.5% Starch or 0.5% CMS at pH = 12 is better than that found for the corresponding solutions prepared using method one. It was found that adjusting the degree of acidity to pH = 2 can further improve the stability of these solutions. The nanoparticle aqueous colloidal solutions of CMC-stabilised titanium dioxide nanoparticles prepared in the presence of 0.5% CMC can be stable for more than one day, although the formation of a small amount of precipitate is still observed. However, these solutions can be stable for up to two weeks, without any observable precipitate formation, if the acidity of the solutions is adjusted to about pH = 2.

Figure 3-5: Aqueous colloidal suspension of CMC-stabilised SMS039 B, prepared in the presence of 0.5% CMC, at pH = 2.

The greater stability of the aqueous colloidal solution of the CMC-stabilised titanium dioxide nanoparticles is probably due to the increase of the viscosity of these solutions on the reduction of the pH. The stability for the corresponding solutions prepared using a reaction time of 5 hours and 12 hours is also same as that found using a 22 hours reaction time (SMS039 B).

Table 3-3: The stability over time of aqueous colloidal solutions of CMC-, AVEBE- and starch-stabilised titanium dioxide nanoparticles prepared using different concentrations of the cellulose derivatives at different pH values.

Time	SMS039B (5 mg) pH = 7 (10 mL)	SMS039B (5 mg) pH = 12 (10 mL)	SMS039B (10 mg) CMC 1.5% (10 mL)	SMS039B (10 mg) CMS 0.5% (10 mL)	SMS039B (10 mg) AVEBE 0.5% (10mL)	SMS039B (10 mg) Starch 0.5% (10 mL)	SMS039B (10 mg) pH = 2 (10 mL)
60 min.	colloid, precipitate	colloid, precipitate	milky white colloid	milky white colloid	milky white colloid, little precipitate	colloid, precipitate	colloid, precipitate
120 min.	top clear, middle colloid, precipitate	top clear, middle colloid, precipitate	colloid, precipitate	colloid, precipitate	colloid, precipitate	top little clear, precipitate	top very little clear, precipitate
180 min.	top clear, middle colloid, precipitate	top clear, middle colloid, precipitate	colloid, precipitate	colloid, precipitate	colloid, precipitate	top little clear, precipitate	top very little clear, precipitate
270 min.	top clear, middle colloid, precipitate	top clear, middle colloid, precipitate	colloid, precipitate	colloid, precipitate	colloid, precipitate	top little clear, precipitate	top little clear, precipitate
24 h	Near to clear solution, precipitate	Near to clear solution, precipitate	colloid, precipitate	top little clear, middle colloid, precipitate	top little clear, middle colloid, precipitate	top little clear, precipitate	top little clear, precipitate
2 days	clear solution, precipitate	Near to clear solution, precipitate	colloid, precipitate	top clear, middle colloid, precipitate	top clear, middle colloid, precipitate	top clear, middle colloid, precipitate	top clear, middle colloid, precipitate

SMS029 was made using $TiOSO_4.xH_2SO_4.xH_2O$ as an economic starting material. Unfortunately, because starting reagent contains an impurity, it was replaced with $TiOS.xH_2O$ and H_2SO_4 added to reaction separately in the preparation of SMS035.

The stability of the aqueous colloidal solution of SMS035 was found to be better than that of SMS029.

The surface area of titanium dioxide nanoparticles prepared using $TiOSO_4.xH_2O$ (method 2), e.g., for SMS039B, was much higher than that of SMS035 (method 1). It was found that the stability of the aqueous colloidal solutions of titanium dioxide nanoparticles prepared using method 2, containing nanocrystals with both a larger surface area and diameter, is much better than that of the corresponding solutions prepared using method 1.

The aqueous colloidal solutions of titanium dioxide nanoparticles prepared using both of the methods were used to deposit a partial coating of titanium dioxide nanoparticles on the surface of the cellulose fibres of test samples of commercial printing paper. Unfortunately, these paper samples were found to change colour from white to yellow after one month when left under natural conditions of ambient visible light at room temperature.

3.2.2 Titanium dioxide nanoparticles prepared using a seeded approach

This method differs from the previous methods in that sulphuric acid was slowly added to control the reaction process in order to prepare titanium dioxide nanoparticles with diameter of approximately 200 nm.

3.2.2.1 Analysis of titanium dioxide NPs using $TiOSO_4.xH_2SO_4. H_2O$ as starting material.

TEM images of the products prepared using this method reveal that small nanoparticles of titanium dioxide aggregate to form much larger secondary nanoparticle aggregates with a diameter, d, larger than *ca.* 190 nm as shown in Figure 3-7. The corresponding SEM images show that nanoparticles with a size of about 200 nm are aggregated to form even larger nanoparticles, as shown in Figure 3-6.
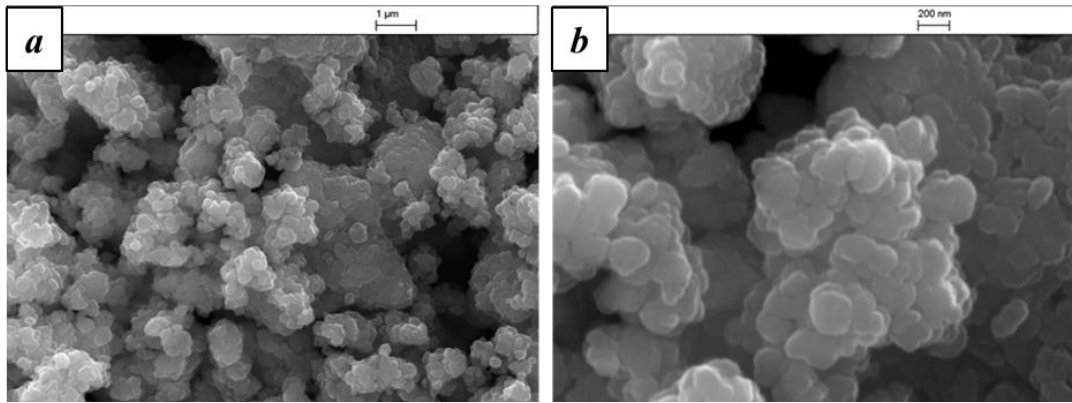
Figure 3-6: SEM image of titanium dioxide nanoparticles prepared from hydrolysis of TiOSO₄ with seed formation (SMS041).
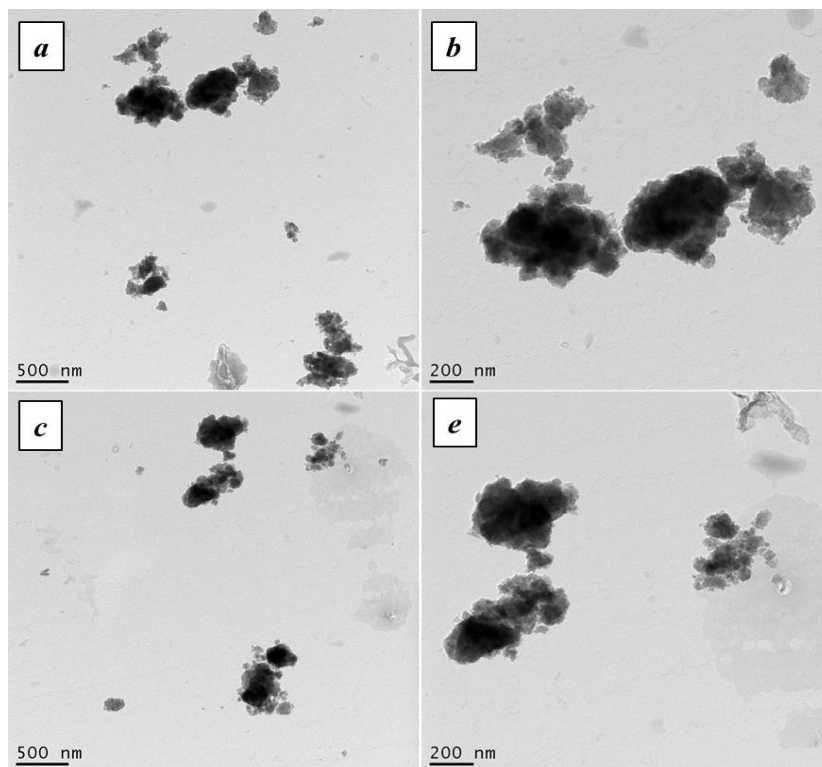
Figure 3-7: TEM images of titanium dioxide nanoparticles prepared from hydrolysis of TiOSO₄ with seed formation (SMS041).

Analysis using XRD indicates the formation of nanoparticles of anatase titanium dioxide with an average crystal size of d = 6.55 nm. These small nanoparticles aggregate to form much larger agglomerates with a diameter of *ca.* d = 200 nm.

The surface area established of these agglomerates, determined using BET analysis, is 52.5 m^2g^{-1}.

The stability of aqueous dispersions of the cellulose-stabilised titanium dioxide nanoparticles, prepared in this way in the presence of CMC, CMS, AVEBE and starch, was investigated by adding 10 mg of these solid products obtained from the reaction solutions to 10 mL of water, followed by sonication for 2 h, shaking by hand for about one minute and then setting the samples to stand for given length of time under regular, periodic observation.

Table 3-4: The stability over time of aqueous colloidal solutions of CMC-stabilised TiO$_2$ NPs prepared using different concentrations of CMC at different pH values.

Time	1% CMC	1% CMC @ pH = 5	1% CMC @ pH = 3-4	1% CMC @ pH = 2	0.5 % CMC @ pH = 2
60 min.	colloid	colloid, little precipitate	colloid, little precipitate	colloid	colloid
120 min.	colloid	colloid, little precipitate	colloid, precipitate	colloid	colloid
270 min.	colloid, little precipitate	colloid, precipitate	colloid, precipitate	colloid	colloid
Overnight (~12 hours)	colloid, little precipitate	top solution clear, precipitate	colloid, precipitate	colloid	top solution not very clear, colloid, no precipitate
2 days	colloid, little precipitate	milky clear solution, precipitate	colloid, precipitate	colloid	milky little clear, colloid, no precipitate

The stability of the aqueous colloidal solutions of cellulose-stabilised titanium dioxide nanoparticles formed in the presence of either 0.5% starch or 0.5% AVEBE is poor. After two hours clear solutions are formed at the top of the samples with a lot of precipitate formed in the bottom of the tubes. Adjusting the pH to a value of 2, can improve the stability, taking an additional hour for the same degradation to be observed.

The stability of the aqueous colloidal solutions of cellulose-stabilised titanium dioxide nanoparticles formed in the presence of either 0.5% CMS or 0.5% and 1% starch solutions is much better. The CMC-stabilised titanium dioxide nanoparticle colloidal solutions can be stable for more than 4 h, although a small amount of precipitate may be observed. The CMC-stabilised titanium dioxide colloidal solution can be stable for more than two weak without precipitate formation if the acidity of the solutions is adjusted to about pH = 2. The increased stability of the titanium dioxide colloid is probably due to the increase of the viscosity of the CMC solutions on the reduction of the pH.

Figure 3-8: SMS041 prepared with 0.5% CMC and pH = 2.

3.2.2.2 Titanium dioxide nanoparticles prepared using TiOSO$_4$.H$_2$O as a starting material

This reaction was carried out at different concentrations of sulphuric acid in the reactions, i.e., in some reactions only one concentration of acid was used and in others two different concentrations of the acid and using TiOSO$_4$.H$_2$O as a starting material.
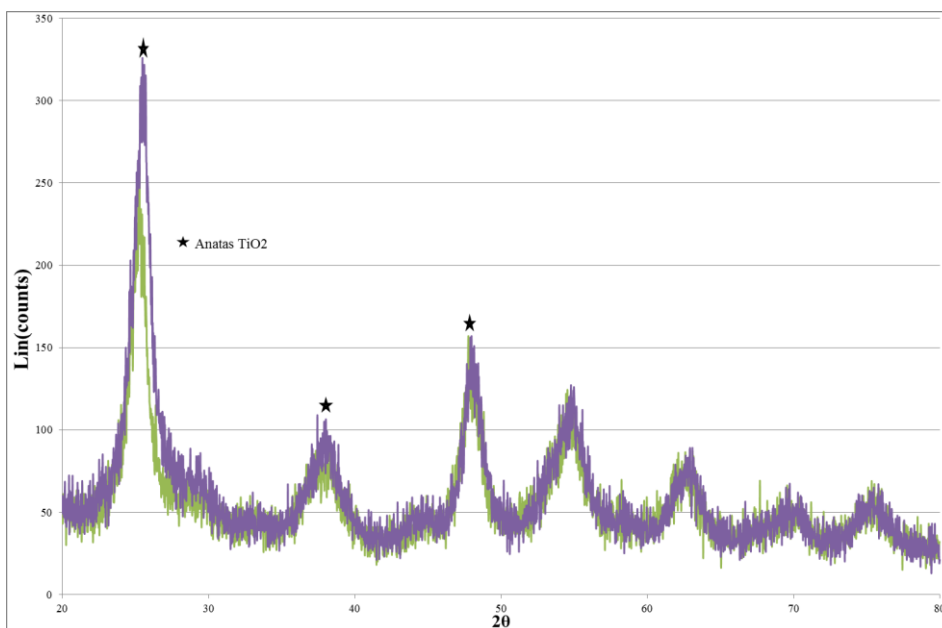
Figure 3-9: XRD Pattern of (purple) SMS062, (green) SMS061.

The XRD spectra of the samples SMS061 and SMS062 reveal that the intensity of peaks increases with increasing reaction time (Figure 3-9). The XRD of the white powder collected from the reaction solutions confirms the formation of the anatase polymorph of titanium dioxide with an average diameters for SMS061 and SMS062 of d = 8.3 nm and d = 6.1 nm, respectively.
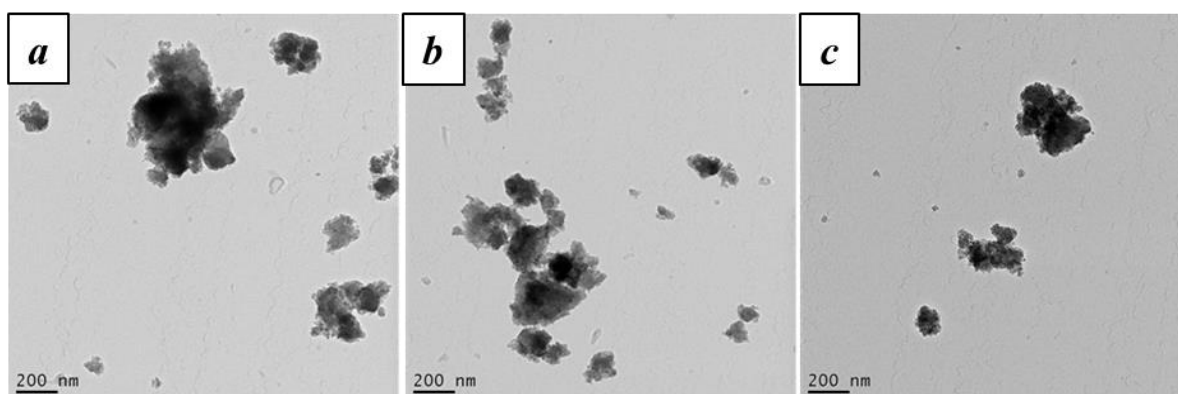
Figure 3-10: TEM images of the SMS036 sample of titanium dioxide nanoparticles prepared using $TiOSO_4 \cdot H_2O$ as the starting material.

The TEM images for SMS036 reveal that small nanoparticles aggregate to form larger secondary nanoparticle agglomerates with a diameter greater than d = 180 nm.
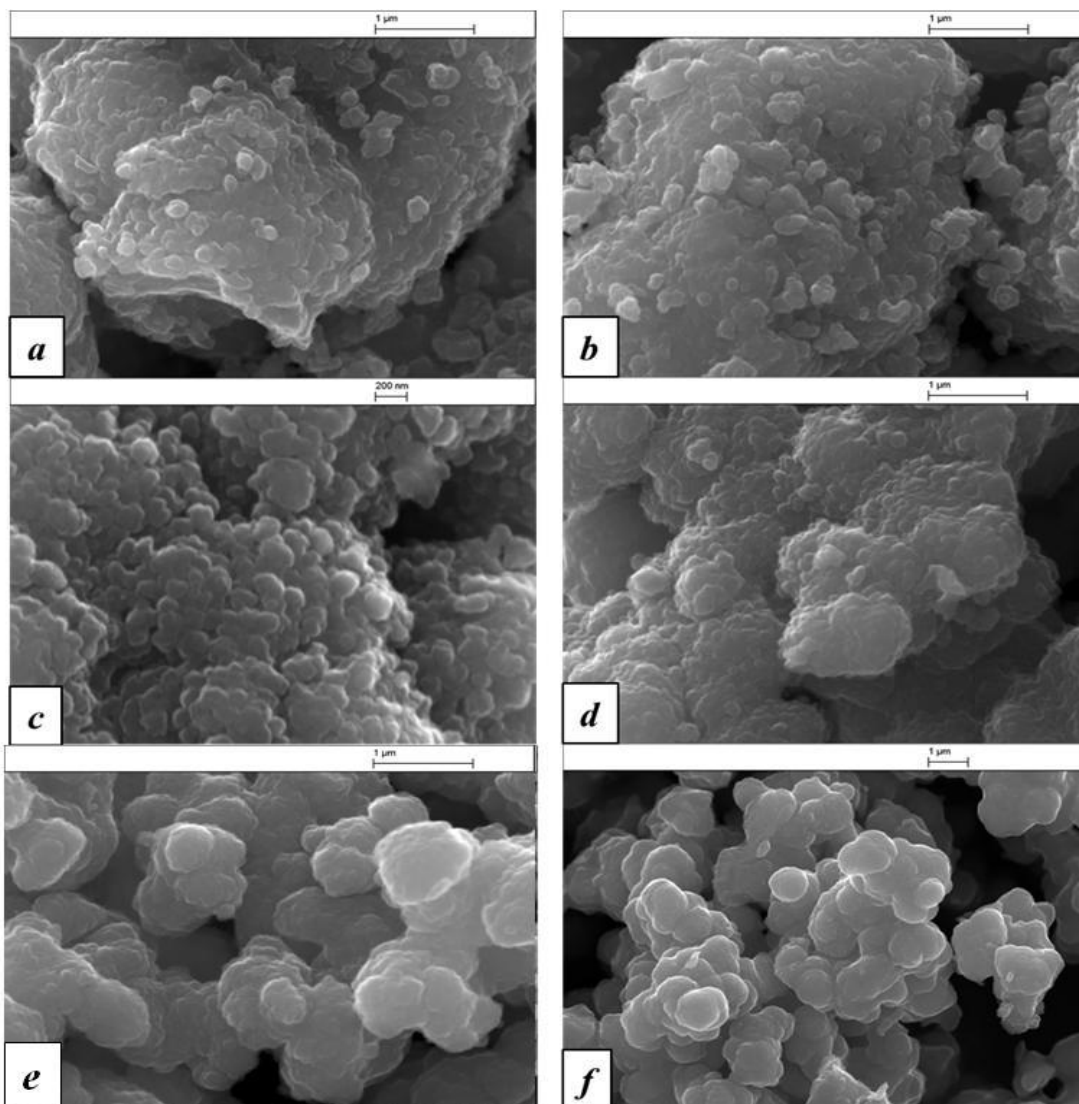
Figure 3-11: SEM of titanium dioxide nanoparticles using TiOSO4.H2O as starting agent of (a) SMS061, (b) SMS062, (c) SMS050, (d) SMS 063, (e) SMS047, (f) SMS036.

SEM images of SMS036 reveal that the nanoparticles with a diameter, d, larger than 500 nm are aggregated to form even larger nanoparticle agglomerates. The products SMS061, SMS062, SMS050, SMS063 and SMS047 contain titanium dioxide nanoparticles with an approximate diameter, d = 200 nm. Analysis shows that a BET surface area for the SMS036 sample is very low, i.e., 4.7 m^2g^{-1}. The XRD spectrum of the white powder collected from the reaction solution confirms the formation of the anatase polymorph of titanium dioxide and shows small nanoparticles aggregated together to form nanoparticles ca 200 nm size (Table 3-5).

Table 3-5: Crystal size of different titanium dioxide nanoparticles samples

Sample	SMS061	SMS062	SMS036	SMS047	SMS050	SMS063	SMS057
Crystallite size (nm)	8.34	6.12	10.87	2.54	2.93	7.22	4.08

Figure 3-12 shows the difference in the FT-IR of the products prepared by three different ways for preparation of the titanium dioxide nanoparticles. IR spectral analysis reveals the presence of an O–H bending absorption at *ca.* 1650 cm^{-1}. Peaks attributable to the presence of SO_4^{2-} were observed between 1,000 and 1,200 cm^{-1}, due to the fact that residual sulphuric acid (H_2SO_4) is difficult to remove completely by simply washing with water. The band corresponding to Ti–O–Ti bond, generally appearing at ca 600–400 cm^{-1}, could not be observed. [163]
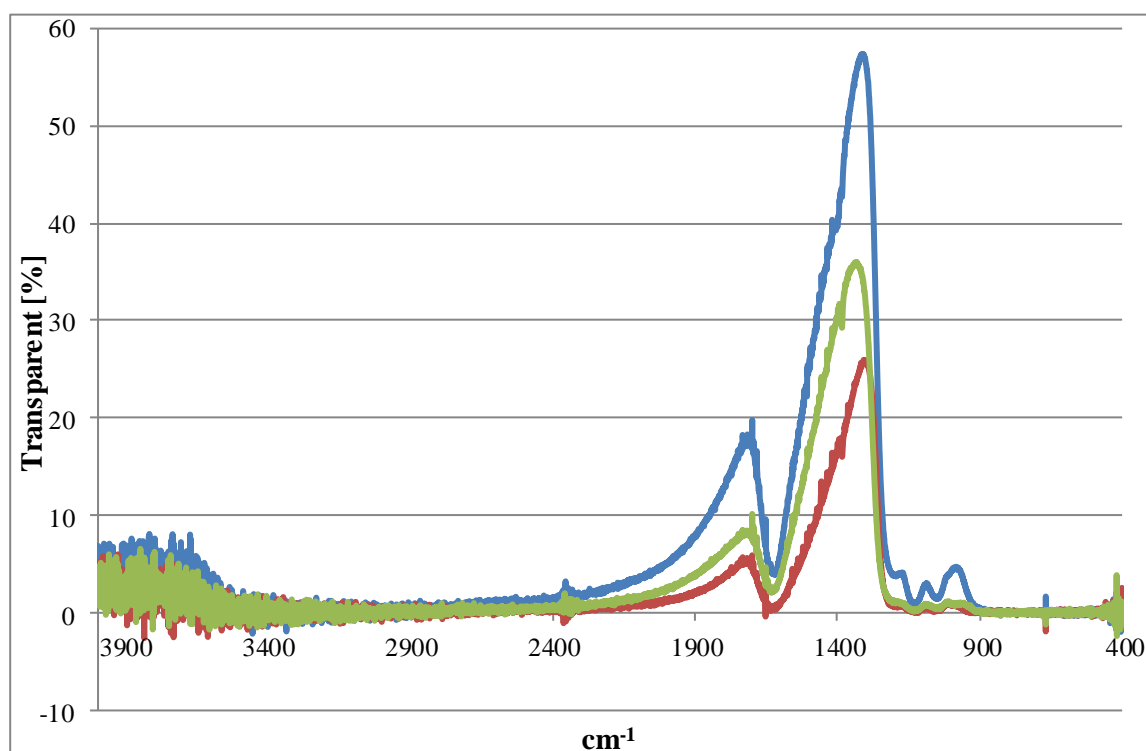
Figure 3-12: FT-IR spectra of the samples SMS035 (red), SMS036 (green) and SMS041 (blue).

Table 3-6: The stability over time of aqueous colloidal solutions of CMC-stabilised titanium dioxide nanoparticles prepared using different concentrations of CMC at different pH values.

Time	SMS036 20 mg 1% CMC @ pH = 2	SMS036 10 mg 1% CMC @ pH = 3-4	SMS036 10 mg 1% CMC @ pH = 2	SMS036 10 mg 0.5 % CMC @ pH = 2
60 min	colloid	colloid	colloid	colloid
120 min	colloid	colloid	colloid	colloid
180 min	colloid	colloid	colloid	colloid
270 min	colloid	colloid	colloid	colloid
overnight	colloid	colloid	colloid	colloid
2 days	colloid	colloid	colloid	colloid

The stability of aqueous colloidal solution of cellulose-stabilised titanium dioxide nanoparticles prepared in the presence of either CMC, CMS, AVEBE or starch is less than that observed for the corresponding solutions of SMS041 for the CMC, CMS, AVEBE and starch solutions except for the CMC solution stabilised at pH =2, which can be stable for a week without precipitates being observed.

$TiOSO_4.xH_2SO_4.H_2O$ is a cheaper starting reagent than the $TiOSO_4.xH_2O$ also used in the chapter to synthesise the titanium dioxide nanoparticles. SEM images of the powders isolated from the reactions solutions using both starting materials shows a similar size for the nanoparticles. However, the stability of the aqueous colloidal solutions prepared using the products prepared from $TiOSO_4.xH_2O$ are better than those of the samples prepared from $TiOSO_4.xH_2SO_4.H_2O$.

All of the titanium dioxide nanoparticles prepared using this seed–mediated method were used to deposit a coating of titanium dioxide nanoparticles on the surface of the cellulose fibres of test samples of commercial printing paper. Unfortunately, these paper samples were also found to change colour from white to yellow after one month, when left under natural conditions of ambient visible light at room temperature.

3.3   *In-situ* coating of titanium dioxide on paper

The results for the preparation of titanium dioxide nanoparticles with seed formation and without seed formation in previous parts of this thesis show that aqueous colloidal suspensions of non-cellulose-stabilised titanium dioxide nanoparticles are not stable over time.

3.3.1   Titanium dioxide prepared using $TiOSO_4 \cdot xH_2SO_4 \cdot H_2O$

Although it was found in the previous sections of this chapter that aqueous colloidal suspensions of CMC- and CMS-stabilised titanium dioxide nanoparticles exhibit sufficient stability over time to be used in tests of their ability to coat paper samples with titanium dioxide nanoparticles, it was found that titanium dioxide nanoparticles did not attach themselves to the surface of the constituent cellulose fibres making up the paper samples studied in this thesis. This failure may be due to the fact that the CMC- and CMS-stabilised titanium dioxide nanoparticles possess a negative charge and, since the surface of the cellulose-based paper also is negatively charged due to the presence of ionised hydroxyl-groups (OH^-), coulombic repulsion inhibits the fixation of the cellulose-stabilised nanoparticles on the cellulose surface. Therefore, in this part of research, a new method was investigated and used to prepare colloidal suspensions of titanium dioxide nanoparticles and then to use them *in situ* in the direct coating of paper, without isolating the nanoparticles beforehand.

The hydrolysis of titanium sulphate, the so-called sulphate process, is an important technique in the industrial production of titanium dioxide pigment for commercial applications. The hydrated titanium dioxide precipitates from the titanyl sulphate solution in sulphuric acid during the hydrolysis process.[87]

$$m\text{Ti}^{4+}(\text{aq}) \; + \; 4m\text{H}_2\text{O(l)} \; \longrightarrow \; m\text{Ti(OH)}_4(\text{aq}) \; + \; 4m\text{H}^+(\text{aq}) \quad (1)$$

$$m\text{Ti(OH)}_4(\text{aq}) \; \longrightarrow \; m\text{TiO}_2(\text{s}) \; + \; 2m\text{H}_2\text{O(aq)} \quad\quad\quad (2)$$

Table 3-7: Synthesis conditions for *in-situ* preparation of TiO₂/CP

Sample	TiOSO₄* (g)	H₂SO₄ solution (0.25 M) (mL)	Cellulosic paper (g)	Temperature (° C)	Time (min)	Particle size (nm)
SMS006	2.40	150	1.43	95	60	≥ 500
SMS021	0.80	50	0.70	110	20	≤ 200
SMS022A	1.67	50	0.78	110	20	∼ 200
SMS022B	3.30	50	0.70	110	20	≥ 200
SMS030	1.67	50	2.15	110	20	∼ 200

*TiOSO₄·xH₂SO₄·H₂O solution (15 wt%)

SMS006 was prepared at a lower temperature and with the longest reaction time. The rest of the series of experiments were carried out with a shorter reaction time, with increasing temperature, which is needed for the preparation of the colloid solution. SEM analysis shows that titanium dioxide nanoparticles with a diameter larger than 500 nm are deposited on the surface of CPs after hydrolysis reaction at 90 °C for 60 min. In order to obtain nanoparticles with size about 200 nm at a shorter reaction time, the temperature was increased to 110 °C.

The results from SEM analysis show that the particle size increases with increasing starting $TiOSO_4$ concentration. Homogenous titanium dioxide nanoparticles with a size of about 200 nm can be found on the surface of cellulose fibres prepared from 1.67 g of $TiOSO_4$ solution. Similar results can also be obtained when the weight of CPs was increased from 0.78 g to 2.15 g. All the samples which were prepared with this method have similar results for EDX analysis, which suggest that titanium dioxide ratios on the surfaces of treated CPs have the same properties to that of titanium dioxide powders.
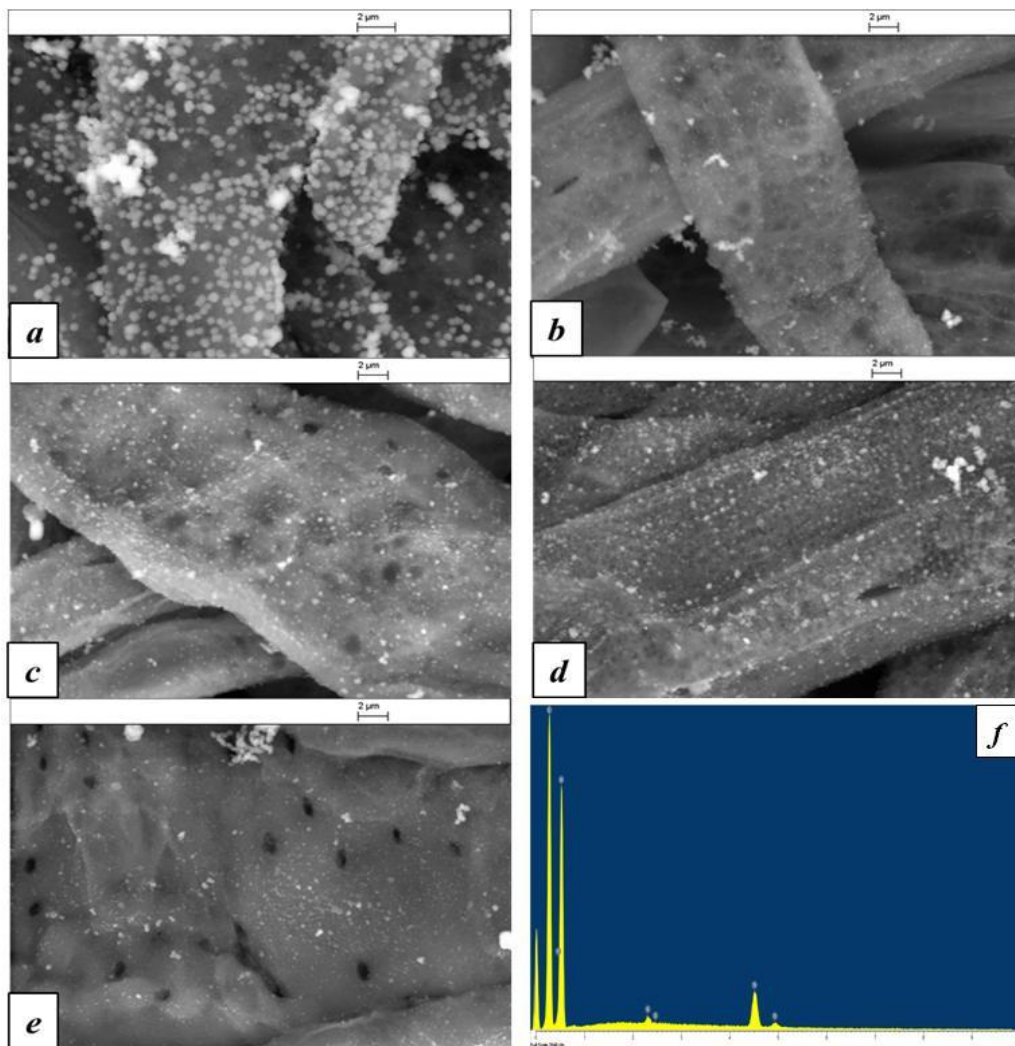
Figure 3-13: SEM of TiO_2/CPs prepared by in-situ hydrolysis $TiOSO_4.xH_2SO_4.H_2O$ (15 Wt%) of samples (a) SMS006, (b) SMS021, (c) SMS022A, (d) SMS022B, (e) SMS030. EDX Pattern of (f) SMS030.

Although no titanium dioxide peaks can be found in the XRD spectra of these coated CPs, due to the low concentration of titanium dioxide and very strong substrate cellulose peaks, XRD analysis of the white powder collected from the reaction solutions confirms the formation of anatase titanium dioxide. XRD results for other reactions with more cellulose-based paper products or a higher surface area are similar to the XRD results shown below. XRD spectra show crystallite sizes for SMS021, SMS022A and SMS022B of 6.61 nm, 6.59 nm and 6.08 nm, respectively. Although the crystal sizes for all three samples are similar, SEM images show that with increase of TiOSO$_4$ concentration, the titanium dioxide nanoparticles size increased. Increasing the titanium dioxide concentration didn't increase the crystals size, but did increase the aggregated nanoparticles size.
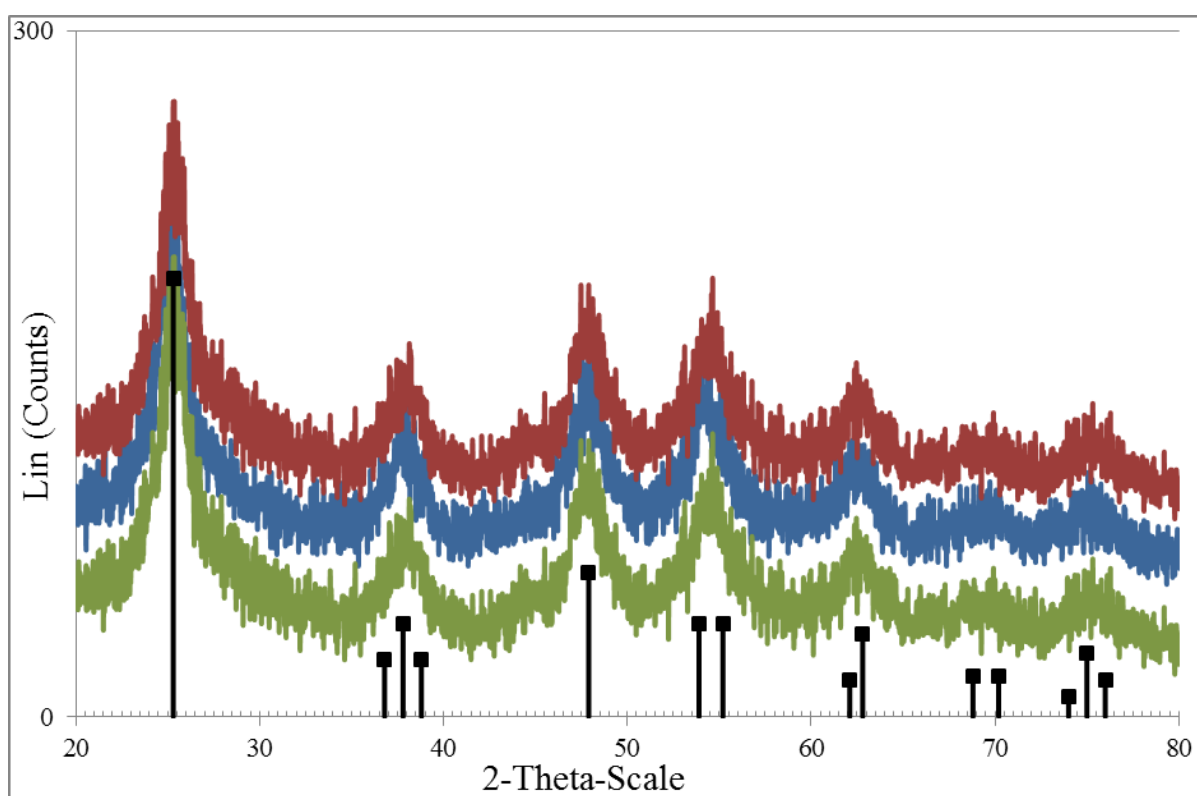
Figure 3-14: XRD pattern of titanium dioxide powders collected from in-situ hydrolysis solution samples of (blue) SMS021 B, (green) SMS22A and (red) SMS22B.

The ICP results for these reaction products show that the percentage of titanium and titanium dioxide grows with increasing concentration. The reactions with a greatest concentration of TiOSO$_4$.xH$_2$SO$_4$.H$_2$O solution (15 wt%), have a higher concentration of titanium dioxide.

Table 3-8: preparation of titanium dioxide with TiOSO₄.xH₂SO₄.H₂O (15 Wt%)

Sample	TiOSO$_4$.xH$_2$SO$_4$. H$_2$O (g)	Cellulosic paper (g)	Ti (%)	TiO$_2$ (%)
SMS021	0.80	0.70	0.69	1.16
SMS022A	1.67	0.70	0.73	1.22
SMS022B	3.30	0.70	0.77	1.29

3.3.2   Coating of titanium dioxide on cellulose-based paper using TiOSO₄. xH₂O

SEM analysis shows that titanium dioxide NPs with a diameter larger than 200 nm are present on the surface of CPs after a hydrolysis reaction at 110 °C for 20 min. The coverage is not homogeneous and in some parts of the sample small nanoparticles stick together and make bigger NPs with a diameter of at least 1000 nm. EDX analyses suggest that titanium dioxide ratios on the surfaces of treated CPs are close to that of titanium dioxide powders.
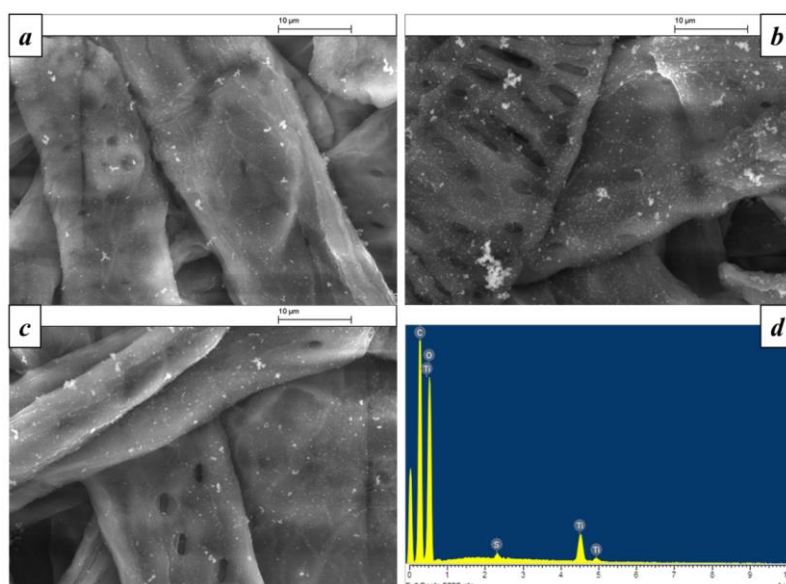
Figure 3-15: SEM of TiO₂/CPs prepared by in-situ hydrolysis TiOSO₄·xH₂O of samples (a) SMS079A, (b) SMS079B, (c) SMS079C. EDX Pattern of (d) SMS079B.

First it was decided to just to use $TiOSO_2.xH_2O$ in the reaction, because it is more economical than using the $TiOSO_2.xH_2SO_4.H_2O$ for practical applications and H_2SO_4 solution can added manually to the reaction but analysis of the results obtained for the reaction in the presence of other $TiOSO_2.xH_2SO_4.H_2O$ and $TiOSO_2.xH_2O$.
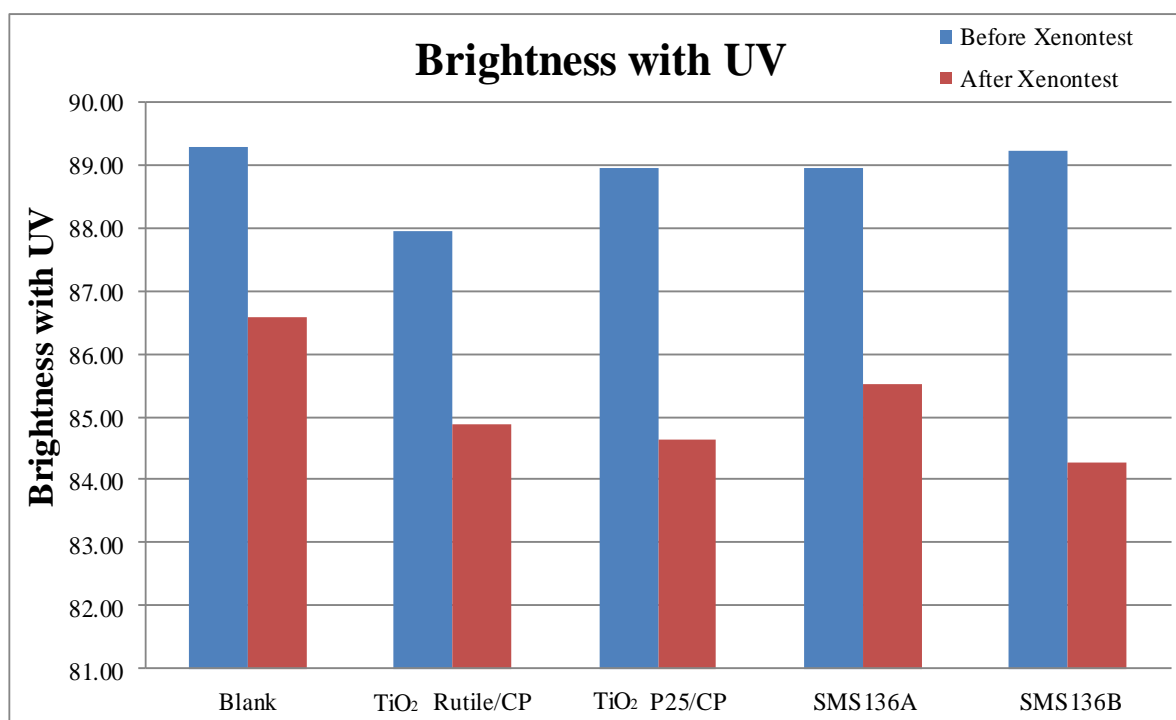
Figure 3-16: CIE whiteness of blank reference paper and the paper samples in-situ coated with titanium dioxide nanoparticles using $TiOSO_4.xH_2O$ (SMS136A) and $TiOSO_4.xH_2SO_4.H_2O$ (SMS136B) before and after the UV-stability test.

The ISO-brightness determined for the blank reference paper and the paper samples coated either with untreated TiO_2-P25 nanoparticles, TiO_2-RA nanoparticles, *in-situ* titanium dioxide nanoparticles using $TiOSO_4.xH_2O$ and $TiOSO_4.xH_2SO_4.H_2O$ before and after illumination with UV-light in the standard xenon UV-stability test. It can be seen that the brightness of the blank paper reference is sharply reduced after illumination with UV radiation in the standard xenon test. The reduction in brightness is even more significant for the paper samples coated with untreated TiO_2-P25nanoparticles, TiO_2-RA nanoparticles, In-situ coating titanium dioxide nanoparticles.
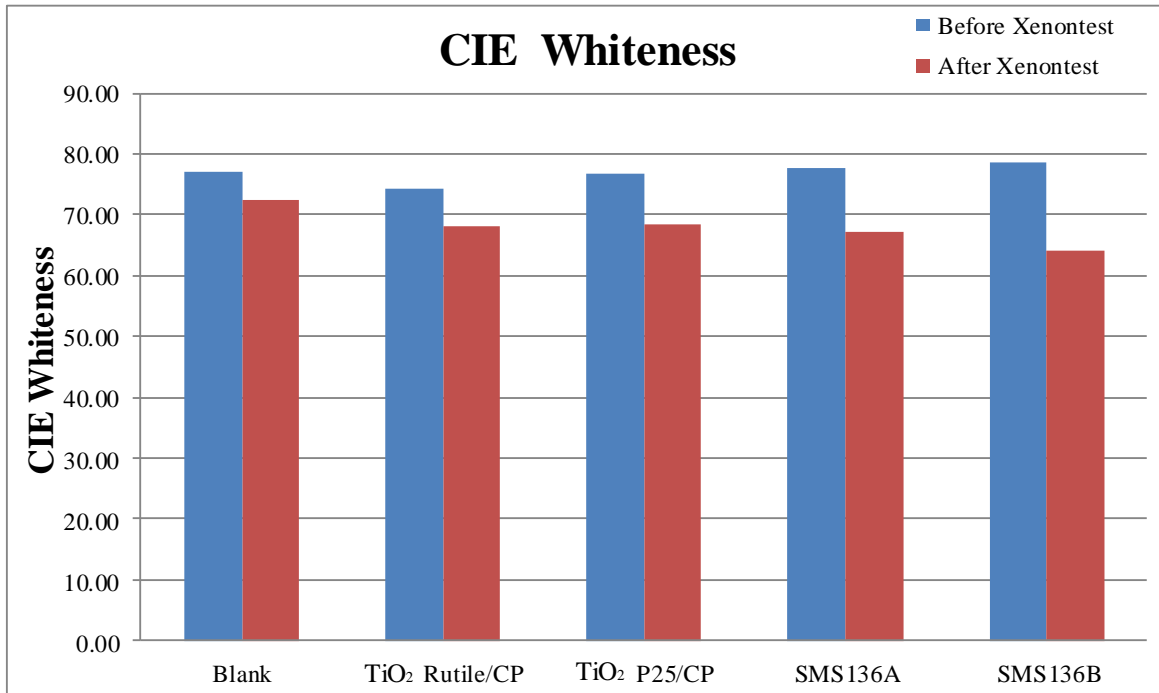
Figure 3-17: ISO brightness of blank reference paper and the paper samples in-situ coated with titanium dioxide nanoparticles using TiOSO$_4$.xH$_2$O (SMS136A) and TiOSO$_4$.xH$_2$SO$_4$.H$_2$O (SMS136B) before and after the UV-stability test.

The value for the CIE-whiteness of the cellulose-based paper products coated with untreated TiO$_2$-P25 nanoparticles, TiO$_2$-RA nanoparticles, *in-situ* titanium dioxide nanoparticles using TiOSO$_4$.xH$_2$O and TiOSO$_4$.xH$_2$SO$_4$.H$_2$O nanoparticles are slighter lower than the blank paper in contrast to the sharp reduction in the whiteness of the blank paper reference sample and another coating paper in *in-situ* method, after the standard xenon UV-stability tests.

3.4 Summary

The intention was try to find a new and economical way for making a titanium dioxide nanoparticle powder for transportation, storage and usage in an industrial setting. The stability of the colloidal solutions prepared on-site to form these titanium dioxide nano-powders is one of the most important parameters from a commercial or industrial standpoint.

Another important consideration for coating titanium dioxide nanoparticle on cellulose-based paper products is that the particle size should not be too small, which can reduce redox activity of titanium dioxide.

The reactions in this part of the work for this thesis can be divided into two main groups: preparation of the titanium dioxide nanoparticles *without* seed formation and, in contrast, preparation of titanium dioxide nanoparticles *with* seed formation and *in-situ* coating of titanium dioxide nanoparticles on the constituent fibres of cellulose making up commercial writing and printing paper.

Preparation of titanium dioxide nanoparticles without the formation of seeds

In the preparation of the titanium dioxide nanoparticles without seed formation, all the reactions were carried out using $TiOSO_4.xH_2SO_4.xH_2O$ or $TiOSO_4.xH_2O$ as sources of titanium dioxide. TEM images of these products show small nanoparticles aggregate together to form much larger secondary nanoparticles. The size of the secondary nanoparticles are about 120 nm and 50 nm for the products prepared from $TiOSO_4.xH_2SO_4.xH_2O$ and $TiOSO_4.xH_2O$, respectively. Unfortunately, due to the presence of an impurity in the $TiOSO_4.xH_2SO_4.xH_2O$, this starting material was not used anymore. Furthermore the products of the $TiOSO_4.xH_2O$ reactions were more stable than those prepared using $TiOSO_4.xH_2SO_4.xH_2O$ as a reagent.

Another method for the preparation of the titanium dioxide nanoparticles without seed formation was a precipitate water washing process, so that SiO_4^{2-} ions were completely removed from the system, as shown by a $BaCl_2$ monitoring method of analysis.

The XRD results show that with increasing reaction time, the crystalline particle size increases. The result of IR analysis shows the presence of O-H banding and possibly SO_4^{2-} ions. The nanoparticle diameter obtained from SEM images are ca 200 nm and the surface area for SMS035 is about 55.58 m^2g^{-1} and for SMS039B is 127 m^2g^{-1} based on BET analysis. The stability of colloidal solutions of titanium dioxide nanoparticles stabilised by the presence of 0.5% CMC and at a pH = 2 is two weeks without precipitation.

Preparation of titanium dioxide nanoparticle with the formation of seeds

In this approach a small amount of titanium dioxide seed solution was prepared and then they were mixed with $TiOSO_4$ solution at *ca.* 95 °C. Initially this reaction was performed with $TiOSO_4.xH_2SO_4.H_2O$ as a source of titanium dioxide. TEM images show nanoparticles sizes of larger than 190 nm. This is confirmed by SEM analysis with values of about 200 nm. Analysis by XRD shows the presence of anatase and BET analysis reveals an average surface area of 52.5 m^2g^{-1} for these nanoparticles. The CMC stabilised titanium dioxide colloidal solution can be stable for more than two weeks without precipitation if the pH is adjusted to a value of about 2. The increase in the stability of the titanium dioxide colloidal solutions is probably due to the increase of the viscosity of the CMC solutions on the reduction of the pH.

In another reaction on this method $TiOSO_4 \cdot H_2O$ was used as a starting reagent. This method was studied as a function of varies concentrations of H_2SO_4 in the reactions. TEM of SMS036 shows the nanoparticles diameter is 180 nm as confirmed in SEM images as about 200 nm. The XRD spectra of the white powder collected from the reaction solutions confirms the formation of anatase titanium dioxide. The BET surface area for the product SMS036 is 47.7 m^2g^{-1}. This solution is stable when stabilised by a CMC solution (pH = 2) for more than two weeks.

In-situ coating of titanium dioxide on cellulosic paper

The titanium dioxide nanoparticles were prepared using two different kinds of sources of titanium oxide, i.e., $TiOSO_4.xH_2SO_4.H_2O$ and $TiOSO_4.xH_2O$. The diameter of the nanoparticles produced by both reactions is about 200 nm and the nanoparticle size can be

changed by changing the concentration of $TiOSO_4$. Particle size increase with increasing concentration of $TiOSO_4$. EDX, XRD, SEM and ICP methods, suggests that titanium dioxide ratios on the surfaces of treated CPs are close to that of original sources of titanium dioxide. However for the titanium dioxide nanoparticles produced using $TiOSO_4.xH_2O$, SEM images show titanium dioxide nanoparticles are not homogeneous and in some parts of the sample, small nanoparticles aggregated together and make bigger nanoparticles with the size about 1000 nm.

4 Preparation of small titanium dioxide nanoparticles

4.1 Introduction

As the titanium dioxide nanoparticles that were synthesised as described in Chapter 3 exhibit poor stability in aqueous colloidal solutions, it was sought to create more stable colloidal solutions using smaller rutile-phase titanium dioxide nanoparticles. The interest in synthesising the rutile polymorph lies primary in the lower catalytic activity toward photo-degradation and higher reflective index *viz.* the rutile polymorph.[164]

4.2 Stable TiO$_2$-RP solution from TiOCl$_2$ at 50 ºC

4.2.1 TiO$_2$ rutile powder in water

4.2.1.1 Analysis

The XRD of white powders prepared from TiOCl$_2$-water solution with different reaction times are confirming the formation of rutile titanium dioxide. The sizes of the crystalline titanium dioxide NPs are *ca.* 5.5 nm for all samples based on the XRD analyses (Figure 4-1). Attempts to synthesise the rutile polymorph failed when the synthesis was attempted with a 0.53 M solution of TiOCl$_4$ in water with 0.5% starch and 1% urea, with XRD analysis of the product (SMS003) exhibiting peaks corresponding to the unwanted anatase polymorph.

Since the dispersed solutions of the dried titanium dioxide powder are not very stable, another experiment was attempted in which the titanium dioxide nanoparticles were prepared according to method 3. The precipitate formed during the reaction was isolated by centrifugation and washing, but was not dried. Instead, 50 mL ultrapure water was added the paste product and shaken to make an aqueous colloidal solution.

In order to investigate the effect of temperature on the structure and morphology, the rutile titanium dioxide powder was annealed at 500 °C for 3 hours. XRD spectra show that after heating at 500 °C for 3 h, the peaks characteristic crystalline rutile titanium dioxide increased greatly, see Figure 4-1.
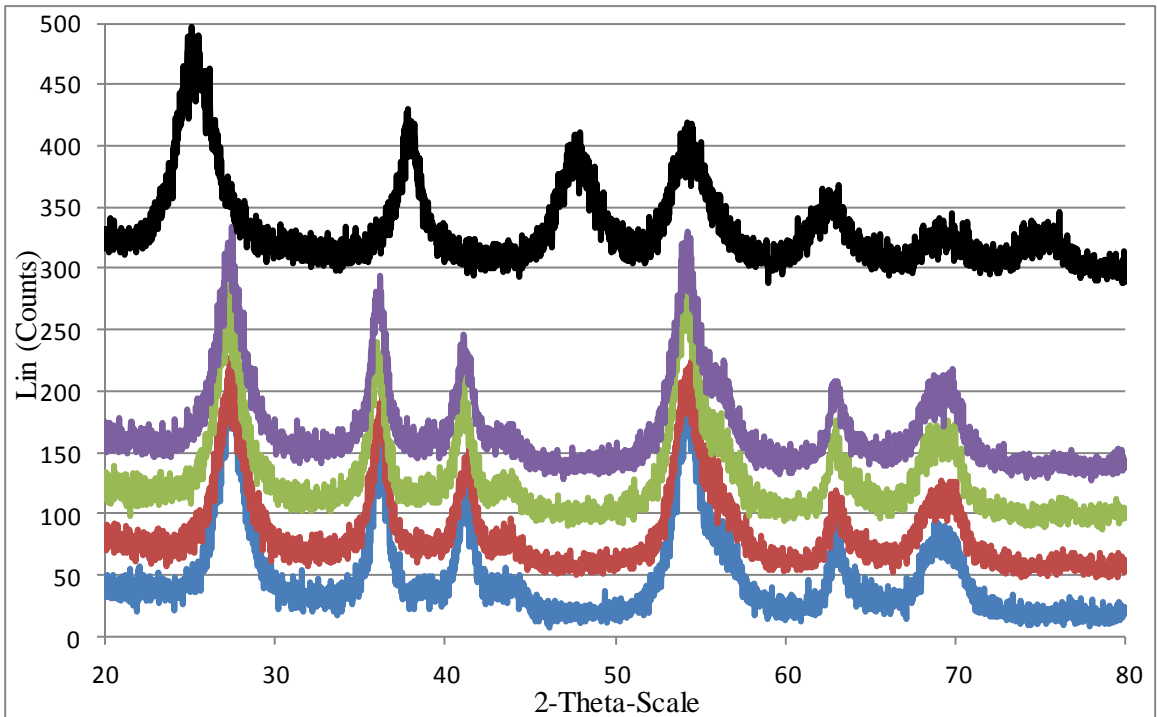
Figure 4-1: XRD patterns of TiO₂-RP formed by method 2 after 6 h heating at 50 °C: (blue), after heating for 12 h at 50 °C (red), after heating for 24 h at 50 °C (green), after heating for 48 h at 50 °C (purple) and SMS003 precipitate (black).
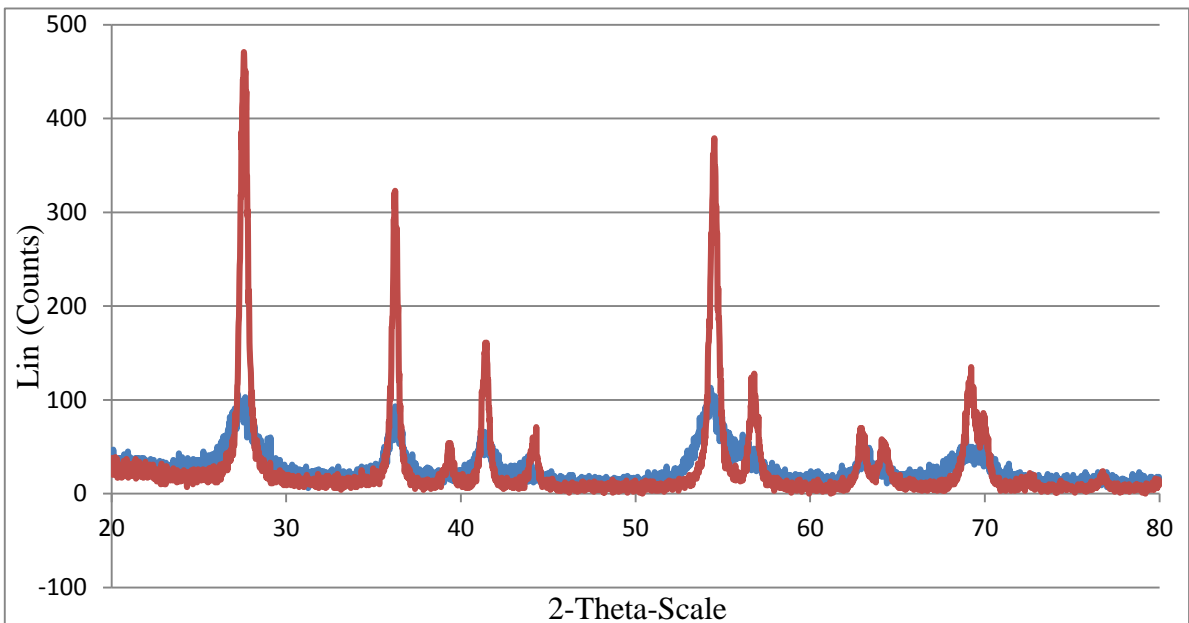
Figure 4-2: XRD patterns of TiO₂-RP samples generated by method 1 (SMS088C in blue) and by method 2 (SMS104C in red).

The SEM image of the TiO$_2$-RP powder prepared for 24 h shows the presence of titanium dioxide nanoparticles with a size of ca 100 nm. The diameter of the constituent nanoparticles of TiO$_2$-RP formed after heating at 500 °C is larger than 100 nm. Since rutile titanium dioxide has a higher refractive index (2.8) than anatase titanium dioxide (2.6) and a lower catalytic activity,[36] it is expected to be a better material to coat cellulose fibres in order to increase their UV stability, whiteness.
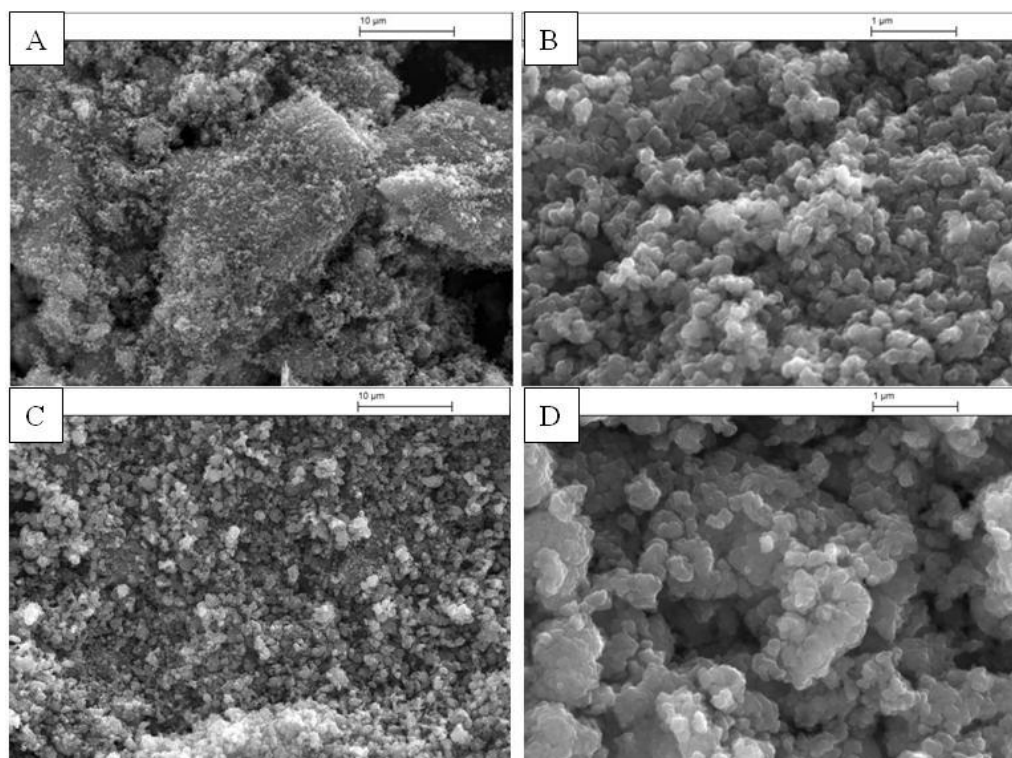
Figure 4-3: SEM images of TiO$_2$-RP synthesised using method 1 (A&B) and method 2 (C&D).

Different kinds of nanoparticles with completely different shapes are observed in the TEM images, i.e., for both the powder (generated by method 1) and the solution (generated by method 3). The TEM images show the presence of hair-like nanorods that aggregate to form bigger nanoparticles and nanorods with a size of *ca.* 20-100 nm. Nanorods can be observed in the TEM images of the TiO$_2$-RP sample. However, the nanorods disappear and nanoparticles with size about 35-100 nm are formed after heating the samples at 500 °C for 3 h.
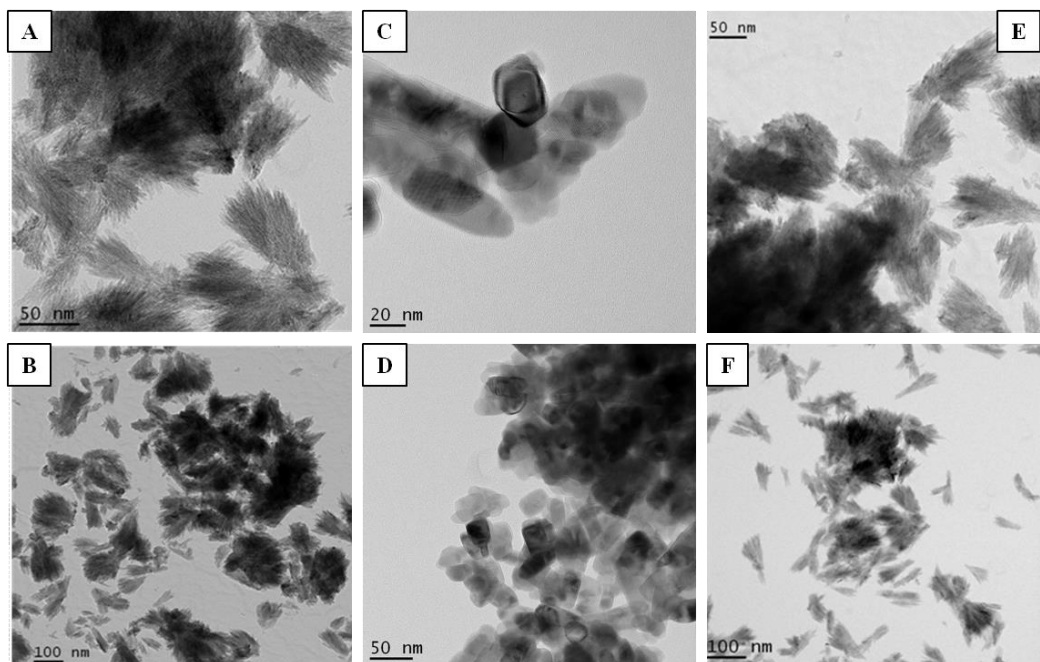
Figure 4-4: TEM images of NPs synthesised by method 1[SMS088C] (A&B), synthesised by method 2 [SMS104C] (C&D), and synthesised by method 3 [SMS091B] (E&F).

4.2.1.2 Stability

Figure 4-5: Stable aqueous colloidal solution of TiO₂ rutile after standing one month prepared by method 3.

Aqueous of colloidal dispersions TiO$_2$ rutile were prepared (method 1) followed by shaking by hand for about one min, which was then allowed to stand at room temperature in order to determine the stability over time of this aqueous nanoparticle colloidal solution. The colloidal solution with 1% CMC has the greatest stability, i.e., it is stable for more than two days as a stable aqueous colloidal solution.

Table 4-1. The stability of the titanium dioxide NP powders (method 1) in starch, CMC and CMS solutions.

Time	SMS088C 10 mg 1% Starch pH = 2 10 mL	SMS088C 10 mg 1% Starch water 10 mL	SMS088C 10 mg 1% CMC pH = 2 10 mL	SMS088C 10 mg 1% CMC water 10 mL	SMS088C 10 mg 1% CMS pH = 2 10 mL	SMS088C 10 mg 1% CMS water 10 mL
60 min	top milky	milky	milky	milky	milky	milky
40 hours	milky clear Middle colloidal suspension and precipitate	milky clear colloidal suspension no precipitate	milky clear colloidal suspension and precipitate	Clear solution and precipitate	milky clear, middle colloidal suspension and precipitate	Half clear with extensive precipitation
Two weeks	milky clear, middle colloidal suspension and precipitate	milky clear, middle colloidal suspension and precipitate	milky clear, middle colloidal suspension and precipitate	Clear solution and precipitate	milky clear, middle colloidal suspension and precipitate	Half clear with extensive precipitation
One month	clear solution, Precipitate	clear solution, Precipitate	milky clear, middle colloidal suspension and precipitate	Clear solution and precipitate	milky clear, middle colloidal suspension and precipitate	half clear with extensive precipitation

The aqueous colloidal solution of the rutile polymorph of titanium dioxide nanoparticles prepared using method 2 is not stable on standing at room temperature more than five minutes. The stability of the aqueous colloidal solutions of the rutile polymorph of titanium dioxide nanoparticles synthesised using method 3 is even lower than that of the corresponding solutions prepared using method 2.

Table 4-2: The stability of the aqueous colloidal solutions of the rutile polymorph of TiO$_2$ NPs prepared in method 3 stabilised by the addition of 1% starch, CMC or CMS.

Time	SMS091B 5 mL 1% starch 5 mL	SMS091B 5 mL 1% CMC 5 mL	SMS091B 5 mL 1% CMS 5 mL	SMS091B 5 mL water 5 mL
0 min.	Colloidal	milky (colloidal)	Jelly	milky (colloidal)
24 h	Near to clear, extensive precipitation	colloidal	jelly	colloidal
one week	clear solution, Precipitate	milky little clear, middle colloid, little precipitate	jelly	milky little clear, middle colloid, little precipitate
one month	clear solution, precipitate	milky little clear, middle colloid, little precipitate	jelly	milky little clear, middle colloid, little precipitate

In order to test the stability over time of in aqueous colloidal solutions of cellulose-stabilised titanium dioxide stabilised by the addition of either starch, CMC or CMS, 5 mL of the titanium dioxide aqueous colloidal solution was added to 5 mL of 1 wt% starch, CMC or CMS solutions. The stability of the aqueous colloidal solutions of the titanium dioxide nanoparticles in 1% CMC solution was similar to that in water and can be stable for more

than one month, although a small amount of precipitate on the bottom. However, the aqueous colloidal suspension of the titanium dioxide nanoparticles with 1% starch was not stable. A jelly-like solution formed when the titanium dioxide colloidal solution was added to the CMS solution.
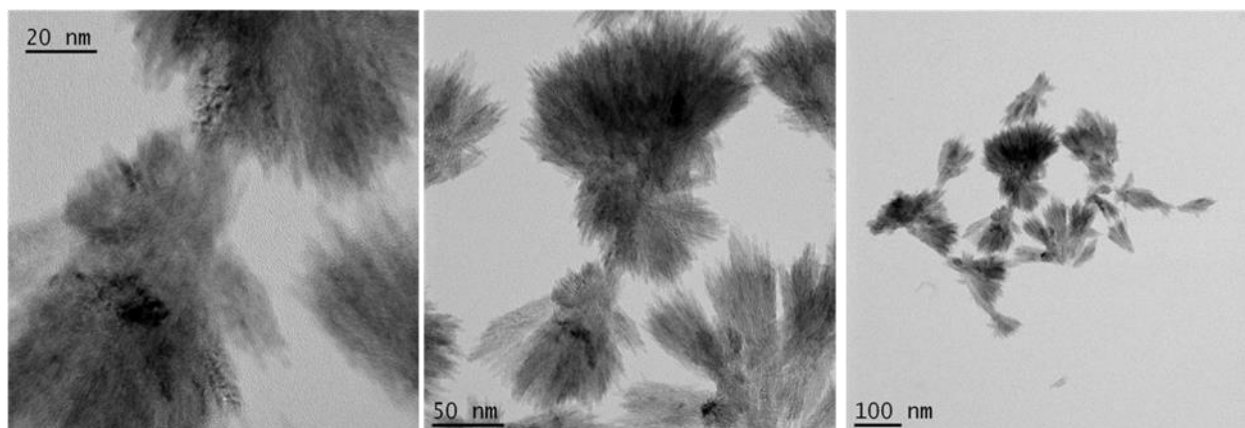
Figure 4-6: the TEM images of the product (SMS091B) after 5 mL of a 1% CMC solution was added to 5 mL of a stable aqueous solution of TiO$_2$-RP nanoparticles prepared according to method 3.

TEM images show that there are no significant differences in size and shape of the titanium dioxide nanoparticles before and after the addition of a 1% CMC solution to the aqueous colloidal suspension of titanium dioxide nanoparticles prepared according method 3.

The titanium dioxide nanoparticle size distribution in the colloidal solution is relatively narrow and the average particle size for the colloidal solution of rutile titanium dioxide (Figure 4-7A) is 90 nm according to nanoparticle tracking analysis by LM10 NanoSight, UK. The solution contains 17.0 gL^{-1} of titanium dioxide nanoparticles and can be stable for more than two months, although a small amount of precipitate is observed. The Nano Sight results show that the nanoparticle size increases in solution over time. Figure 4-7D shows the results of mixing the titanium dioxide nanoparticles with 1% CMC in aqueous solution.

stable rutile TiO$_2$ colloid solution
Heating time 24h / It was tested after 1 day

stable rutile TiO$_2$ colloid solution
Heating time 24h / It was tested after 3 weeks

stable rutile TiO$_2$ colloid solution
Heating time 24h / It was tested after 2 mounts

It was tested after 2 mounts
5 mL SK091B + 5 mL CMC 1%
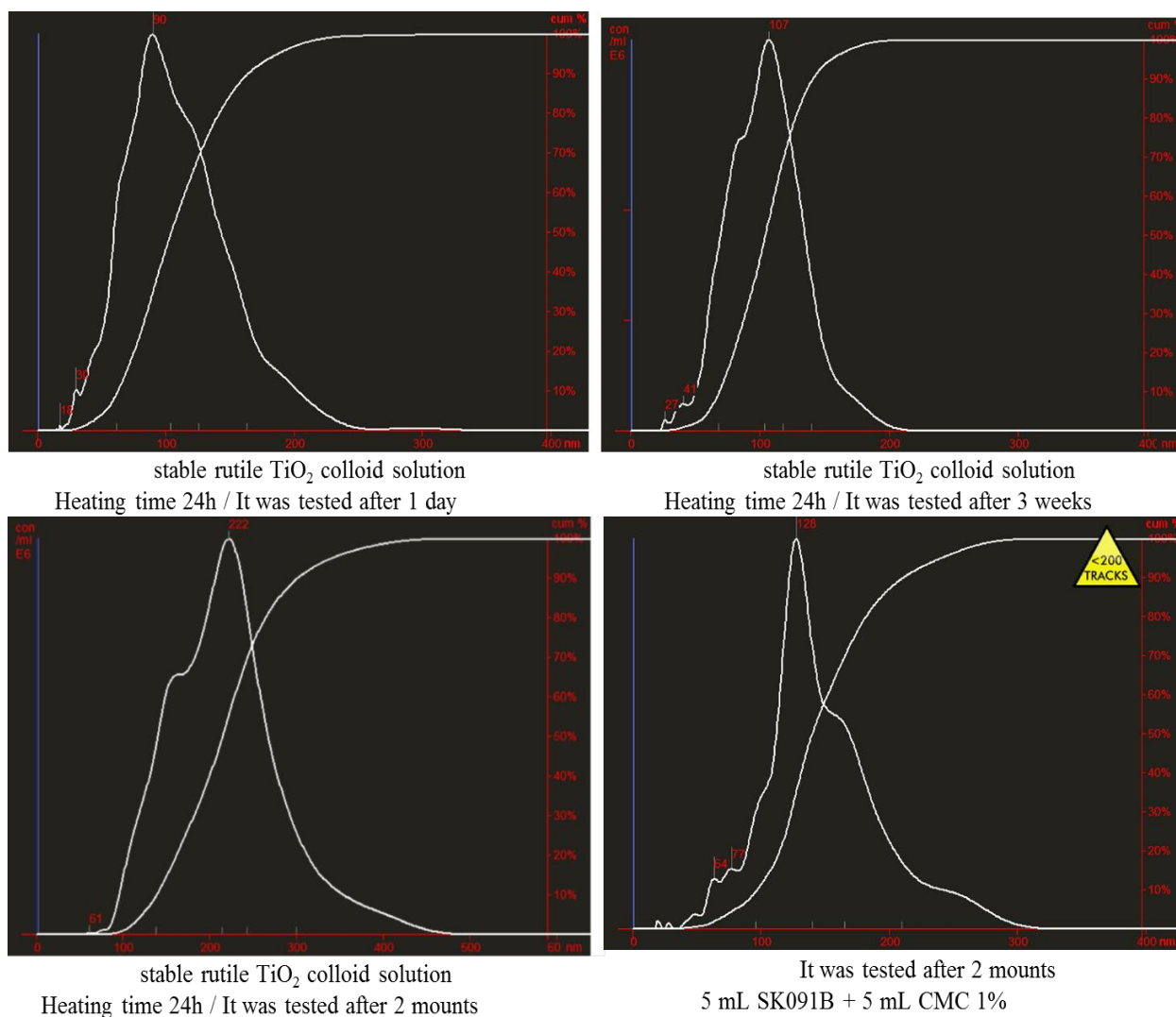
Figure 4-7: Nanoparticle Tracking Analysis for different samples of TiO$_2$-RP nanoparticles prepared according to method 3.

4.2.1.3 Coating

The refractivity measurements of the coated CPs after pressing at 7 tons (10 tons pressure used to compress KBr powder to make thin discs for IR analysis) shows that all of the paper sample coated with rutile titanium dioxide prepared using method 1 and 3 is the same. However, cellulose-based paper products coated by a mixture of rutile titanium dioxide and CMC have a higher refractivity.

87
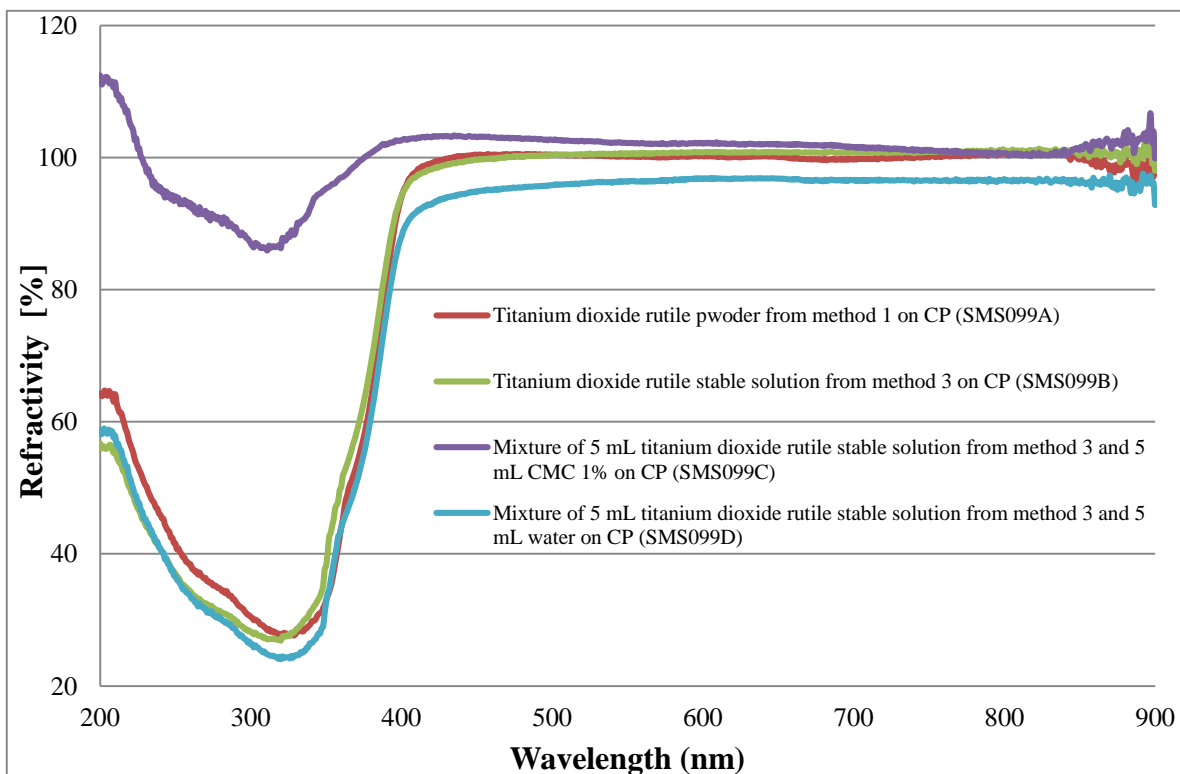
Figure 4-8: UV-Vis transmittance curves of TiO2-RP products after coating CPs and compressing them.

4.2.2 TiO₂ nanoparticles prepared in starch, CMC and CMS solutions

4.2.2.1 Analysis

Analysis using XRD shows that, like the reaction in water, the reaction in 1% starch or 1% CMS aqueous solution leads to the formation of the rutile polymorph of titanium dioxide nanoparticles with a crystalline nanoparticle size of d = 5.5 nm and d = 6.9 nm, respectively. However, anatase titanium dioxide with crystalline nanoparticle size of d = 4.6 nm was obtained when the reaction was carried out in 1% CMC solution.
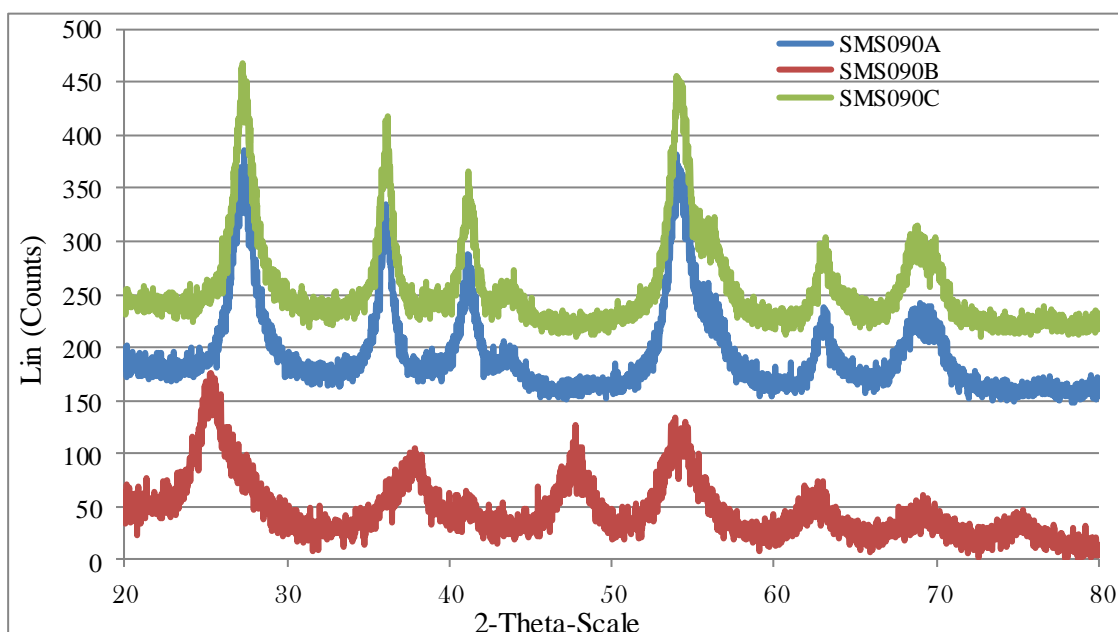
Figure 4-9: XRD pattern of materials obtained by method 4: titanium dioxide in starch (blue), CMC (red), CMS (green).

The SEM images of the TiO_2-RP powders are shown in Figure 4 10. Very large nanoparticle agglomerates with a diameter of about 1.40 μm alongside smaller nanoparticles with a diameter of ca d = 300 nm can be observed in the SEM image of the sample prepared in 1% starch solution. The SEM image of the sample prepared in 1% CMC solution shows the presence of very large nanoparticle aggregates consisting of nanoparticles with sizes of ca d = 300 nm. Nanoparticles with a diameter of ca d = 160 nm aggregate to form much larger nanoparticle aggregates in the sample prepared using a 1% CMS solution.
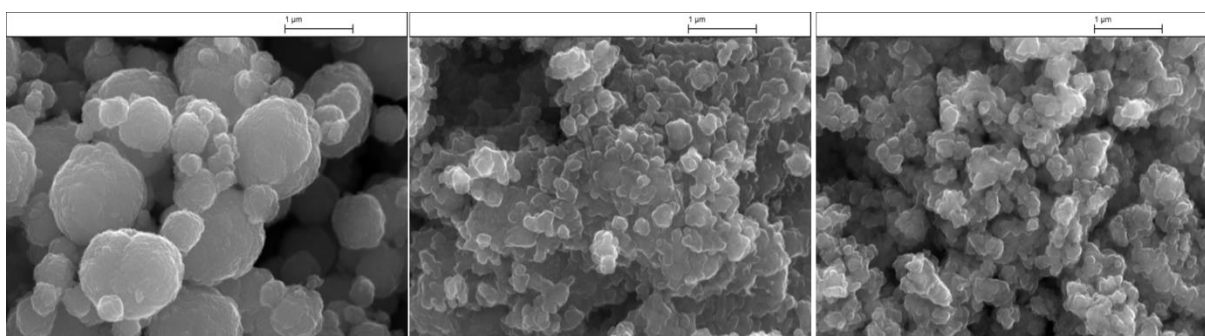
Figure 4-10: SEM images of the titanium dioxide nanoparticles prepared using method 4 in the absence of a cellulose stabiliser (left), CMC (middle) and CMS (right).
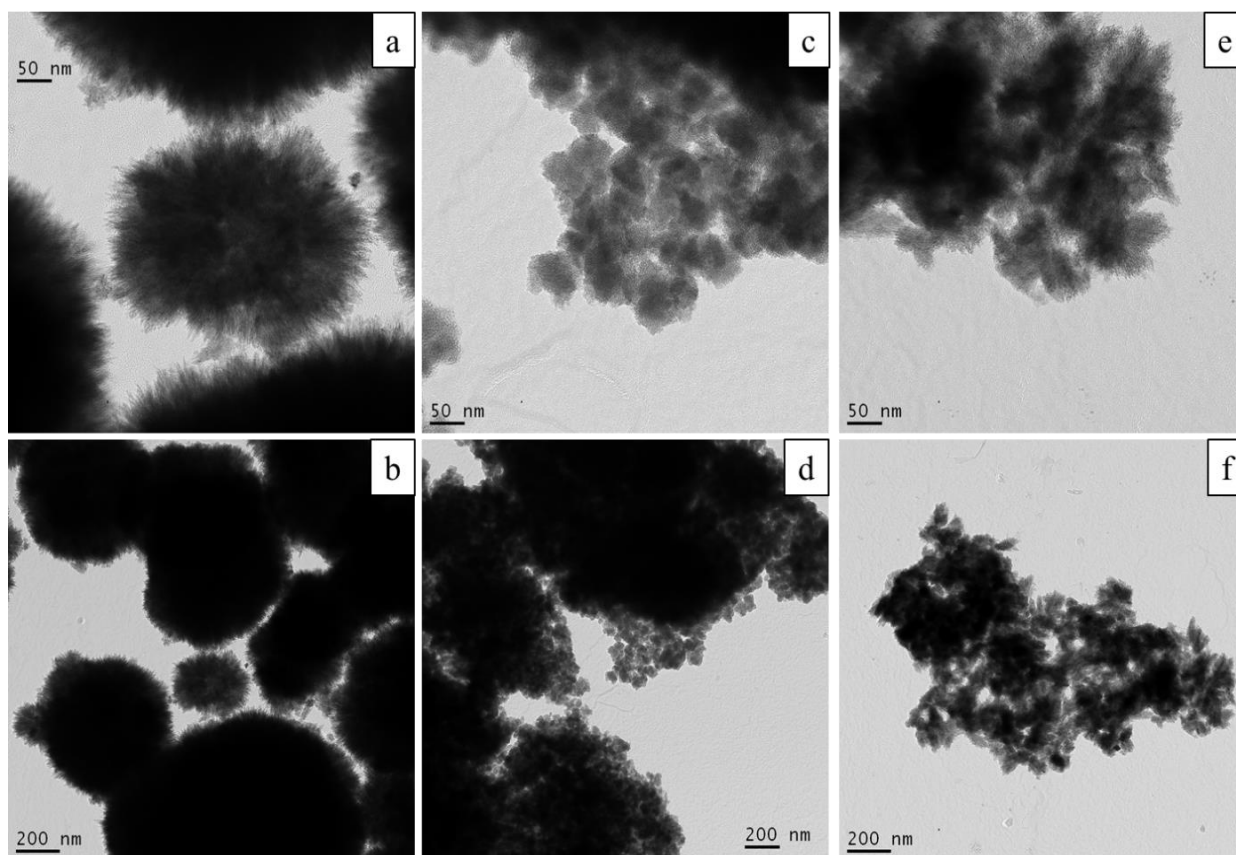
Figure 4-11: TEM images of method 4, titanium dioxide in water with 1%starch (a&b), or 1% CMC (c&d), or 1% CMS (e&f).

The TEM images show that different shapes and sizes of titanium dioxide nanoparticles are present in the three different powder products prepared using method 4. The starch-stabilised titanium dioxide nanoparticles are seen to form hair-like structures, which aggregate to form much larger nanoparticles with a diameter, d = 200-900 nm.

The CMS-stabilised titanium dioxide nanoparticles also have a hair-like nanorod shape, similar to that of the nanoparticles prepared using methods 1 and 3.

However, no hair-like nanorods were observed for the CMC-stabilised titanium dioxide nanoparticles, where the nanoparticle diameter, d, is found to be less than 50 nm.

4.2.2.2 Stability

The stability over time of aqueous colloidal dispersions prepared from the three products prepared using method 4 has been evaluated. The starch-stabilised titanium dioxide nanoparticles are more stable than the corresponding CMC- and CMS-stabilised titanium dioxide nanoparticles. The aqueous colloidal solutions of starch-stabilised titanium dioxide nanoparticles are stable on standing at room temperature for more than 15 hours. The aqueous colloidal dispersions of CMC-stabilised titanium dioxide nanoparticles are not stable for more than two hours, although the CMS-stabilised titanium dioxide nanoparticles suspensions are stable for *ca.* 10 hours.

After changing the value of the pH from 3.5 to 7, the stability of the starch-stabilised aqueous colloidal solutions does not change, but the stability of the aqueous colloidal solutions of CMC-stabilised titanium dioxide nanoparticles reduces to 5 min whereas that determined for the corresponding CMS-stabilised titanium dioxide nanoparticles increases to more than seven days.

However, the aqueous colloidal solutions of starch-stabilised titanium dioxide nanoparticles are not stable. After three days, a transparent colloidal solution was formed above significant amount of precipitates in the dispersion of TiO_2/CMC in 1% CMC solution. A stable jelly-like solution is formed after titanium dioxide -CMS was dispersed in 1% CMS solution.

Changing the pH does not improve the stability of these aqueous colloidal suspensions. It appears reasonable to conclude that method 5 is not a good way for coating cellulose-based paper products with titanium dioxide nanoparticles due to very poor stability of the colloidal suspensions.

4.2.2.3 Coating

Table 4-3: Different methods to prepare powder samples of titanium dioxide nanoparticles and stable aqueous collouidal solutions from them.

Sample	Additive	Extent of solution [mL]	Heating time [hours]	Crystallite size [nm]	Type of TiO$_2$	Product Type	Method
SMS088A	None	14	72	5.61	rutile	Powder	Method 1
SMS088B	None	14	48	5.49	rutile	Powder	Method 1
SMS088C	None	14	24	5.60	rutile	Powder	Method 1
SMS088D	None	14	6	5.67	rutile	Powder	Method 1
SMS104C	None	14	24	5.57	rutile	Powder	Method 2
SMS091B	None	14	24	-----	rutile	Solution	Method 3
SMS090A	Starch 1%	25	24	5.49	rutile	Powder	Method 4
SMS090B	CMC 1%	25	24	4.59	anatase	Powder	Method 4
SMS090C	CMS 1%	25	24	6.95	rutile	Powder	Method 4
SMS125A	Starch 1%	25	24	-----	rutile	Solution	Method 5
SMS125B	CMC 1%	25	24	-----	anatase	Solution	Method 5
SMS125C	CMS 1%	25	24	-----	rutile	Solution	Method 5
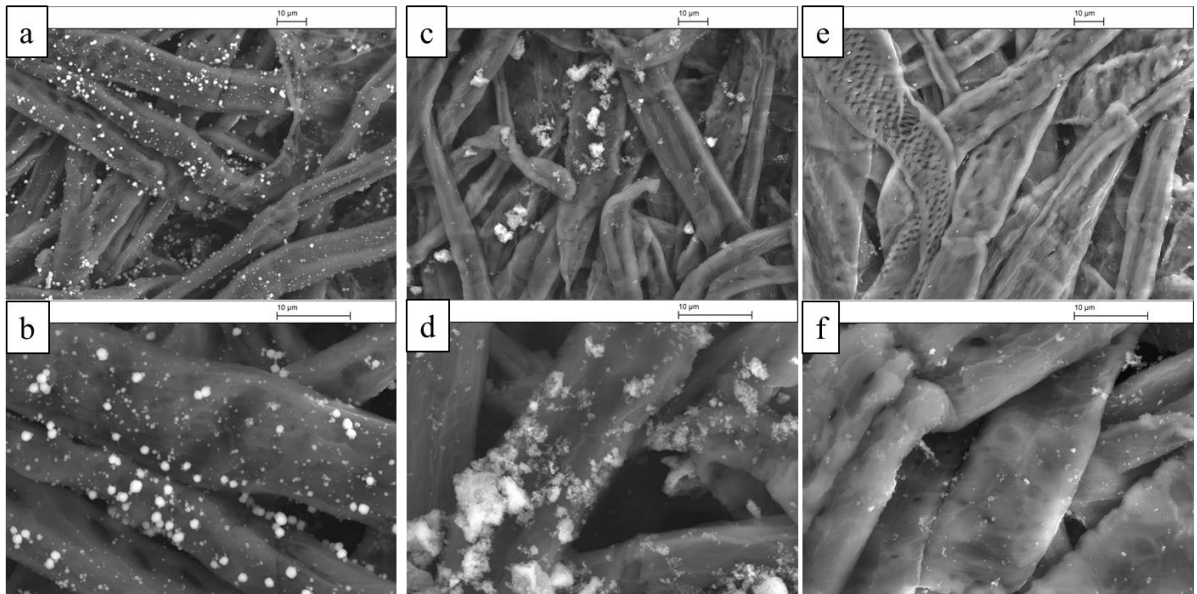
Figure 4-12: SEM images of TiO₂ prepared with method 4, SMS090A (a&b), SMS090B (c&d) and SMS090C (e&f) after coated on CP.

on surface of the constituent cellulose fibres of paper was relatively homogeneous but that the nanoparticles are large with a diameter, *ca.* d = 200 nm - 1 μm. Unfortunately the SEM images also reveal that coating of the surface of the constituent cellulose fibres of paper with CMC- and CMS-stabilised titanium dioxide nanoparticles was not good as the aqueous suspensions of the CMC- and CMS stabilised titanium dioxide nanoparticles were jelly-like after dissolving them in water.
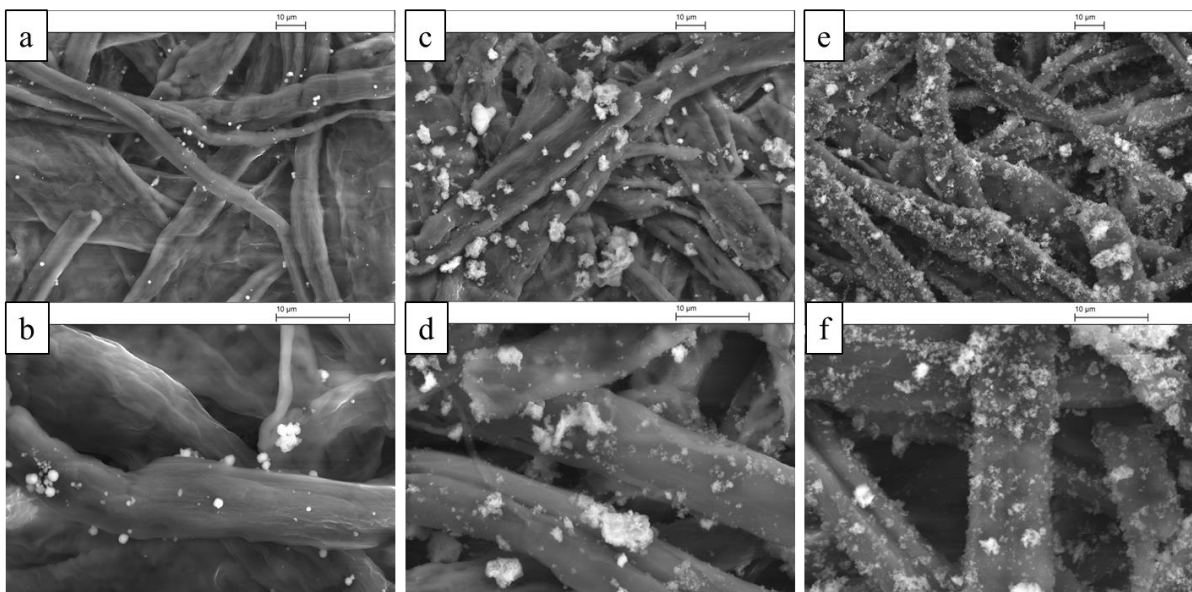
Figure 4-13: SEM images of TiO₂ prepared with method 4, SMS090A (a&b), SMS090B (c&d) and SMS090C (e&f) after LBL coated on CP.

In this part SEM images show the deposition of starch-stabilised titanium nanoparticles on the surface of LBL-treated CP was not effective in comparison with that observed coating the same nanoparticles on untreated CP samples. The coating of CMC-stabilised titanium nanoparticles on LBL CP surface is much more homogeneous, although the nanoparticles with a diameter of $d = 200 - 500$ nm aggregate to form much bigger nanoparticles with a diameter $d = ca$ 5 μm. The coating of CMS-stabilised titanium nanoparticles on surface of LBL-treated CP is the most homogeneous and extensive with the presence of a mixture of relatively small nanoparticles, $d = 200$-500 nm and larger nanoparticle agglomerates of $d = ca$ 2 μm present on the LBL-treated CP surface.
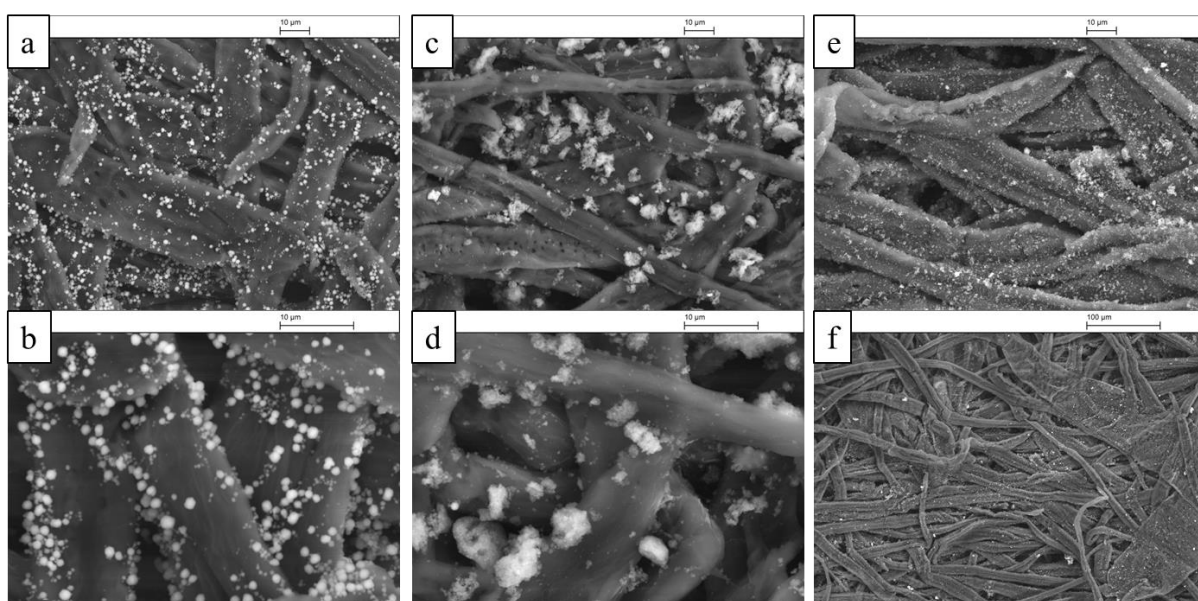
Figure 4-14: SEM images of TiO₂ prepared with method 4, SMS090A (a&b), SMS090B (c&d) and SMS090C (e&f) after change the pH and LBL coated on CP.

The SEM images shown in Figure 69 show the coating of nanoparticles on the surface of LBL-treated CP after changing the pH of the coating solution from acidic, i.e., pH = 3.5, to neutral, i.e., pH = 7. The coating of starch-stabilised titanium dioxide nanoparticles is more homogeneous than that observed for either the samples of blank or LBL-treated CP before changing the pH to neutral. However, the nanoparticle size is similar. The nature and quality of the coating of CMC-stabilised titanium dioxide nanoparticles is very similar to that observed for either the samples of blank or LBL-treated CP before changing the pH to neutral.

The coating of CMS-stabilised titanium dioxide nanoparticles is more homogeneous than that observed for either the samples of blank or LBL-treated CP before changing the pH to neutral. However, the nanoparticles size, d, is ca 100 – 500 nm.

The quality of the coating appears to depend on two factors, i.e., coating on LBL-treated paper is better than on blank CP and coating at pH to 7 is much better than coating in an acidic medium.

4.3   Preparation of titanium dioxide colloidal solutions

Another way for the preparation of nanoparticles is to make the nanoparticle solutions directly. It was hoped that the titanium dioxide nanoparticle colloidal solution prepared by this way would be stable for more than two weeks.

4.3.1   Stable aqueous colloidal titanium dioxide solution from $TiOCl_2$ at 95 °C

The TEM images for the solution show that titanium dioxide nanoparticles with hair-like shape are formed. The XRD of white powder confirms the formation of anatase titanium dioxide with a diameter, d =4.59 nm size. These aqueous colloidal solutions were found to be stable for more than twelve months. ICP results show a concentration of Ti = 2.75% in the stable solution.
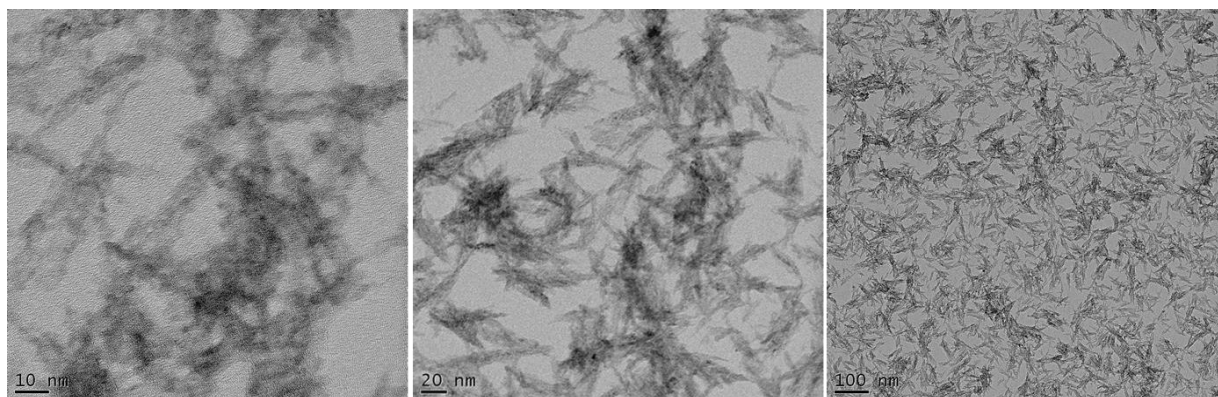
Figure 4-15: TEM images of titanium dioxide solution **of sample SMS003.**
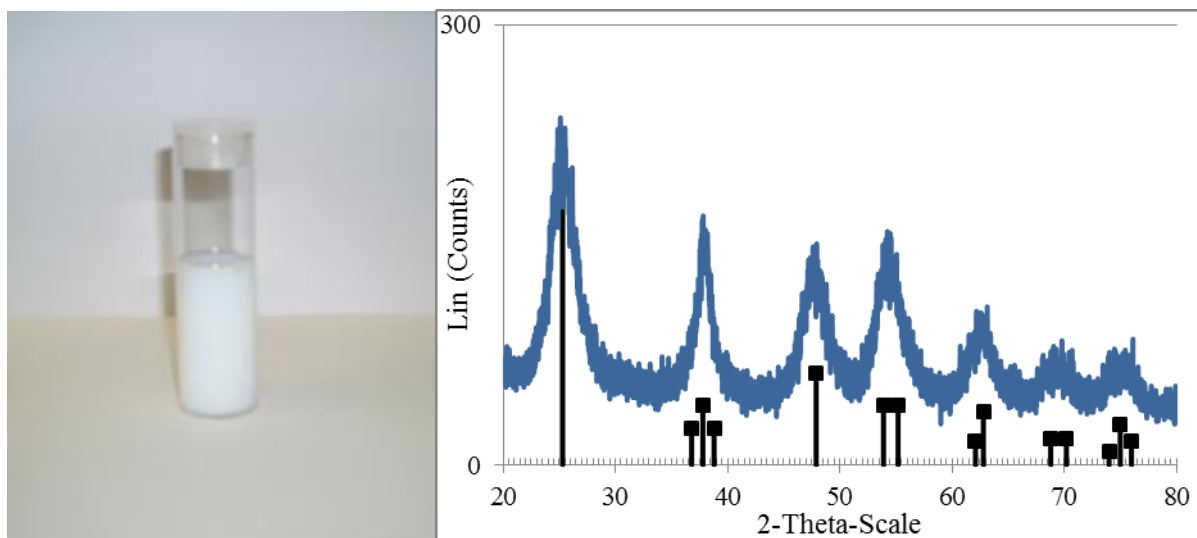
Figure 4-16: titanium dioxide solution **of sample SMS003 picture of stable solution after 9 months(left) and a XRD pattern of precipitate(right).**

4.3.1.1 Coating on paper samples

EDX of the titanium dioxide coated CP clearly shows the presence of titanium dioxide. The SEM images show that titanium dioxide nanoparticles were present between the fibres, but did not coat the surface of the fibres, as hoped.
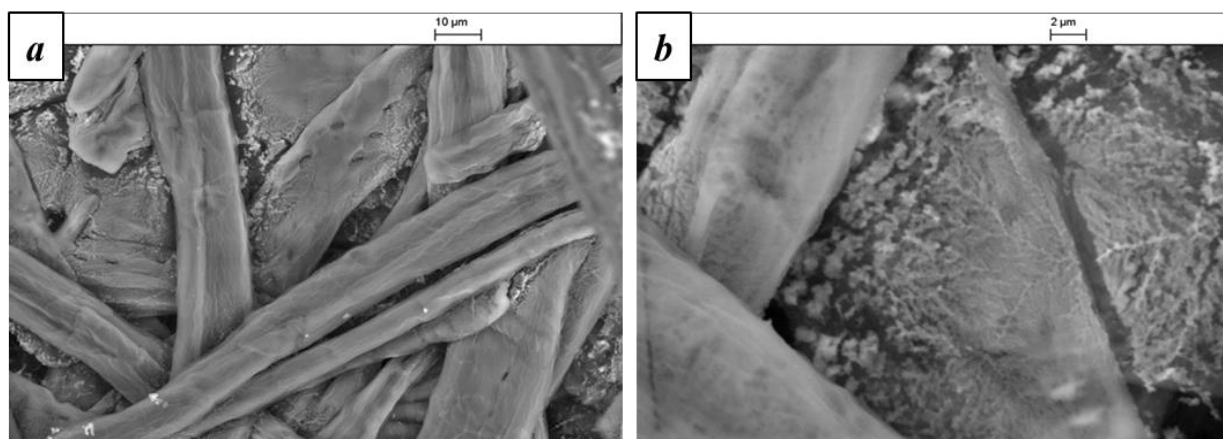
Figure 4-17: SEM images of coating TiO$_2$ solution (SMS003) on CP.

4.4 Summary

The first part of this chapter reports the preparation of TiO_2-RP nanoparticle from $TiOCl_2$ in water. Methods one and two are about making a TiO_2-RP nanoparticle powders after drying the resultant precipitate. Two kinds of rutile nanoparticle powders were prepared from $TiOCl_2$ at different temperatures. The first one is comprised of hair-like rutile titanium dioxide nanorods prepared at 50 °C. After heating at 500 °C for 3 h, the nanorods disappear and nanoparticles with a diameter, d = 30-100 nm, is formed. This is confirmed by SEM analysis with values of about 100 nm. XRD shows the presence of rutile phase with peaks for the low temperature prepared titanium dioxide. After heating these samples at 500 °C, the rutile titanium dioxide crystalline peaks increase significantly.

The titanium dioxide colloidal solutions of starch, CMC and CMS of the hair-like titanium dioxide nanorods can be stable for two weeks with little precipitation if the pH is adjusted to about 2. It is also stable for more than 2 days in water but titanium dioxide powder with 500 °C heating cannot be stable in water more than 5 min.

Method 3 is about making the TiO_2-RP nanoparticle stable solution from $TiOCl_2$ directly without dry precipitate. The particle size distribution of the colloid solution is relative narrow and the average particle size for TiO_2-RP solution is 90 nm. The titanium dioxide solution can be stable for more than nine months although small amount of precipitate can be observed. The content of the elemental titanium in the solution is 2.75%. The TEM images show the presence titanium dioxide nanoparticles are hair-like nanorods and homogeneously on the cellulose fibres.

In second part of this chapter two methods were used make the titanium dioxide nanoparticle powders from mixture of $TiOCl_2$ in starch, CMC and CMS after drying the precipitate. In the preparation of the titanium dioxide nanoparticles in 1% starch, CMC and CMS solution, all the reactions were carried out using TiO_2-RP as the source of titanium dioxide nanoparticles. The XRD and TEM images of these products show completely different phases and nanoparticle sizes. For TiO_2/starch, the nanoparticles are hair-like nanorods which aggregate to form bigger nanoparticles with a size 200-900 nm. TiO_2/CMS is also hair-like nanorod but the nanorod can be observed for TiO_2/CMC, the nanoparticles size is d < 50 nm.

The XRD results show that hydrolysis of $TiOCl_2$ in starch or CMS solution leads to the formation of the rutile polymorph of titanium dioxide with a crystalline nanoparticle size, d = 5.5 and d = 6.9 nm respectively. However, anatase titanium dioxide with crystalline nanoparticle size of d = 4.6 nm was obtained when the reaction was carried out in the presence of CMC. The SEM images reveal that the nanoparticle diameter is large and disperse, i.e., d = 300- 1400 nm, ca 300 nm and about 160 nm for starch-, CMC- and CMS-stabilised titanium dioxide nanoparticles, respectively.

The SEM images reveal that a homogeneous coating of titanium dioxide nanoparticles on CP can be obtained using samples of LBL-treated paper.

Aqueous colloidal suspensions of starch-stabilised TiO_2-RP nanoparticles can be stable for more than fifteen hours. The corresponding aqueous colloidal suspensions of CMC-stabilised TiO_2-RP nanoparticles are not stable for more than two hours, the corresponding suspensions of CMS-stabilised TiO_2-RP nanoparticles are stable for about ten hours. After changing the pH from pH = 3.5 to pH = 7, the stability of the aqueous colloidal suspensions of starch-stabilised TiO_2-RP nanoparticles does not change, but that of the suspensions of the CMC stabilised TiO_2-RP nanoparticles reduced to five minutes and that of CMS-stabilised TiO_2-RA nanoparticle solutions increased to more than seven days.

The second method described in this chapter yields stable aqueous colloidal suspensions of cellulose-stabilised TiO_2-RP nanoparticles prepared from $TiOCl_2$ in the presence of starch, CMC and CMS. Unfortunately, the results of stability teats show these solutions are not stable for more than a few minutes whatever the pH value.

5 Cellulosic paper and core/shell TiO$_2$/SiO$_2$ nanocomposites

5.1 Introduction

In paper industrial TiO$_2$ is adding to cellulose paper to increase whiteness and brightness on CP surface. The most important factor in titanium dioxide powder property is excellent pigmentary and whiteness. But high redox activity of TiO$_2$ can photodegrade organic support and break cellulose chains. It would be interesting to devise nano-particles capable of enhancing the brightness and whiteness of paper without catalysing the degradation of the cellulose chains.

The combination of a very large, active surface area and a high redox activity of small titanium dioxide nanoparticles often results in photo-degradation of organic supports under illumination with sunlight or other sources of UV-radiation thereby severely limiting or inhibiting their use in a range of commercial applications. In order to inhibit or totally suppress this photocatalytic effect, titanium dioxide nanoparticles are usually passivated with an inert shell, such as silica (SiO$_2$) or polymers, to avoid direct contact with the surface of the organic supports. However, there are a number of limitations to current approaches to this process.

There are several reports of the preparation of silica-coated titanium dioxide nanoparticles with hydrophilic and insulating properties. Of particular note in the literature is the use of TiO$_2$/SiO$_2$ core/shell nanoparticles, which are deemed to be simple and cost-effective to synthesise. The synthetic conditions are typically mild and occasionally environmentally friendly.[165] The presence of an ultra-thin layer of silica on the outside of a TiO$_2$ nanoparticle typically leads to a higher degree of hydrophilicity for the TiO$_2$/SiO$_2$ core/shell nanoparticles as compared to titanium dioxide nanoparticles. The greater degree of hydrophilicity typically improves the clarity of films coated with the TiO$_2$/SiO$_2$ core/shell nanoparticles, by preventing the formation of water droplets on the surface of the film that give rise to optical distortions.[84, 166, 167] However, if the active sites of the titanium dioxide nanoparticles are incompletely shielded by the silica shell, some residual photocatalytic activity can be observed.[168]

This chapter describes an integrated green chemistry approach to protect products comprised of cellulosic fibres against photodegradation, for example celluloid films, writing or printing paper. In the case of paper, an increase in whiteness and brightness is also observed, by coating their constituent cellulosic fibers with a fine layer of TiO_2/SiO_2 core/shell nanoparticles to create improved organic/inorganic nanocomposite products. This simple approach could, for example, facilitate the mass manufacture of lighter sheets of paper, such as A4 writing or printing paper, which would represent a significant saving in the enormous amounts of pulp used in paper manufacture, be much more energy efficient and produce much less contaminated waste water, which is very expensive to decontaminate to re-attain its original level of purity.

In this chapter, four kinds of titanium dioxide nanoparticles, i.e., two commercial products (TiO_2-P25 nanoparticles from Evonik and rutile titanium dioxide (TiO_2-RA) nanoparticles from Aldrich) and two novel products prepared as part of the work for this thesis(nanorod TiO_2-RP and spherical rutile TiO_2-RP500 nanoparticles). The novel nanoparticles were synthesised using water as both the solvent and a reagent. These four nanoparticles have been chosen as the core of our four different TiO_2/SiO_2 core/shell nanoparticles (TiO_2-P25/SiO_2, TiO_2-RA/SiO_2, TiO_2-RP/SiO_2 and TiO_2-RP500/SiO_2). These silica coated nanoparticles were used to modify the surface of samples of CP, using two related Layer-by-Layer (LBL) deposition methods, in order to improve their optical properties, without significantly impacting the mechanical properties of the paper.

The four uncoated titanium dioxide nanoparticles (TiO_2-P25, TiO_2-RA, TiO_2-RP and TiO_2-RP500) are coated with a thin layer of silica by an optimised sol-gel process, using a water/ethanol mixture as the solvent, to yield four novel TiO_2/SiO_2 core/shell nanoparticles (TiO_2-P25/SiO_2, TiO_2-RA/SiO_2, TiO_2-RP/SiO_2 and TiO_2-RP500/SiO_2). In order to suppress the photoactive properties of the titanium dioxide (core) nanoparticles it is essential to create an inert, very thin, but dense, robust and mechanically stable, silica coating (shell) on them.

A thin coating of the UV-absorbing silica coated nanoparticles was deposited on and then fixed to the surface of CP. This could be achieved by two different polyelectrolytic layer-by-layer (LBL) approaches, both using water as the reaction solvent. The first LBL approach involves the deposition of a fine layer of PDDA/PSS/PDDA-coated TiO_2/SiO_2 core/shell nanoparticles onto the surface of the fibres CP samples from aqueous solution. The second

LBL approach involves the deposition of a fine layer of TiO_2/SiO_2 core/shell nanoparticles onto the surface of the PDDA/PSS/PDDA-coated fibres of the CP samples, again from aqueous solution. The relative drawbacks and advantages of these two approaches are then identified and evaluated. These particles were envisioned to be capable of inhibiting the photo-degradation of paper, and the effect of these particles on the rate of paper degradation was evaluated.

The efficacy of the four different kinds of silica coated TiO_2/SiO_2 core/shell nanoparticles (TiO_2-P25/SiO_2, TiO_2-RA/SiO_2, TiO_2-RP/SiO_2 and TiO_2-RP500/SiO_2) in protecting paper samples from photochemical degradation by UV-light was then determined and rationalised. The ability of the four different coatings to improve the whiteness and brightness of the paper samples compared to the untreated reference samples was then determined.

5.2 TiO$_2$-P25/SiO$_2$ and TiO$_2$-RA/SiO$_2$ core/shell nanoparticles

5.2.1 Analysis of TiO$_2$-P25/SiO$_2$ and TiO$_2$-RA/SiO$_2$ core/shell nanoparticles

Figure 5-1 shows the IR spectra of the uncoated TiO$_2$-P25 nanoparticles and the coated TiO$_2$-P25/SiO$_2$ nanoparticles. The silica-coated TiO$_2$-P25/SiO$_2$ shows a new peak at 1068 cm^{-1}, which can be ascribed to the asymmetric stretching vibration of v_{as}(Si-O-Si).
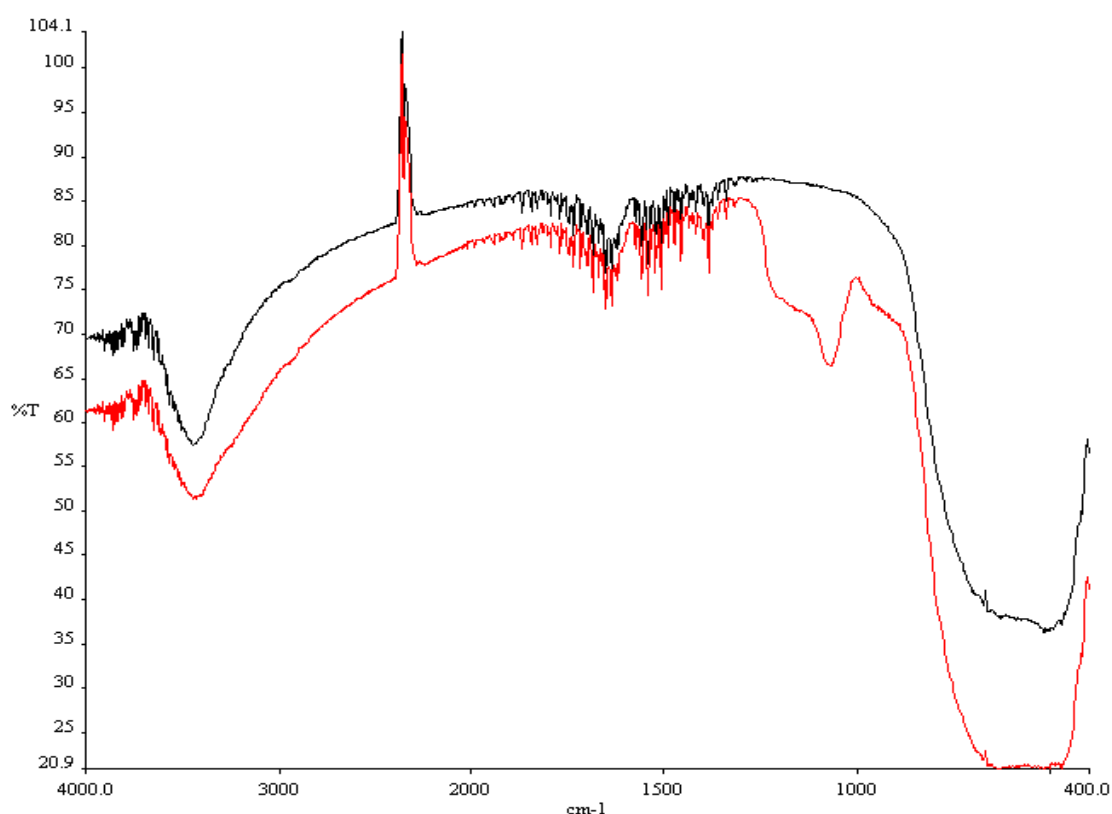
Figure 5-1: IR spectra of TiO$_2$-P25 NPs (black) and TiO$_2$-P25/SiO$_2$ core/shell NPs (red)

Figure 5-2 shows TEM images of the silica-coated TiO$_2$-RA/SiO$_2$ and TiO$_2$-P25/SiO$_2$ core/shell nanoparticles. It can be seen that TiO$_2$-RA/SiO$_2$ core/shell nanoparticles have been successfully prepared with a silica shell with a thickness of approximately 3 nm. Analysis of the Energy-dispersive X-ray spectroscopy (EDX) spectrum of the TiO$_2$-RA/SiO$_2$ core/shell nanoparticles suggests that the Si/Ti ratios at the top right and the edge of the nanoparticles

shown in Figure 5-2b are 0.03 and 0.22, respectively. In the case of the TiO_2-P25/SiO_2 core/shell nanoparticles, the thickness of the silica shell cannot be clearly determined as the nanoparticles are too small to be clearly observed. However, the Si/Ti ratio at the centre (0.04) is lower than that at edge (0.09), suggesting that silica has successfully coated the titanium dioxide cores.
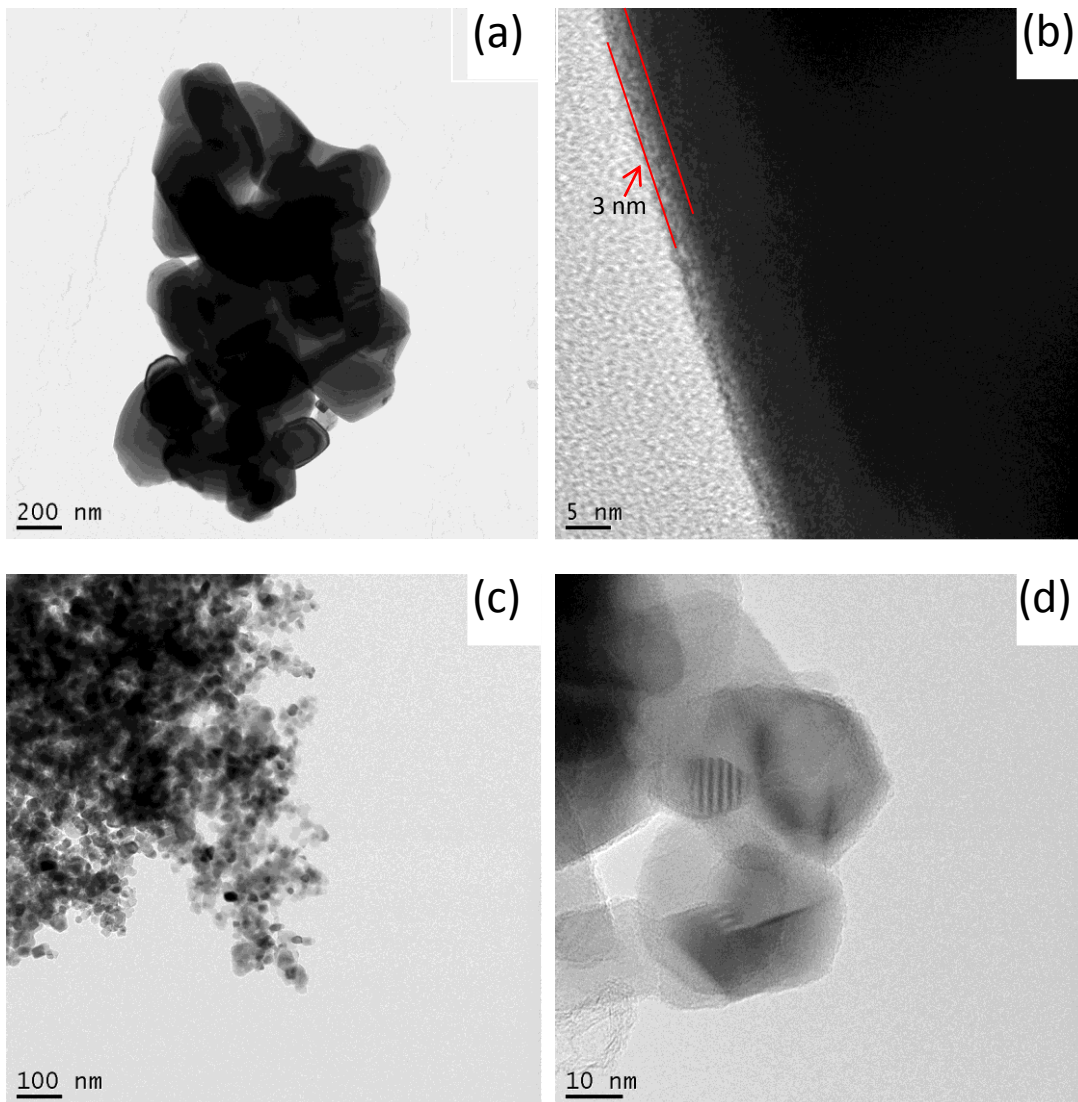
Figure 5-2: Transmission electron microscopy (TEM) images of the TiO_2-RA/SiO_2 nanoparticles (a & b) and TiO_2-P25/SiO_2 core/shell nanoparticles (c & d).
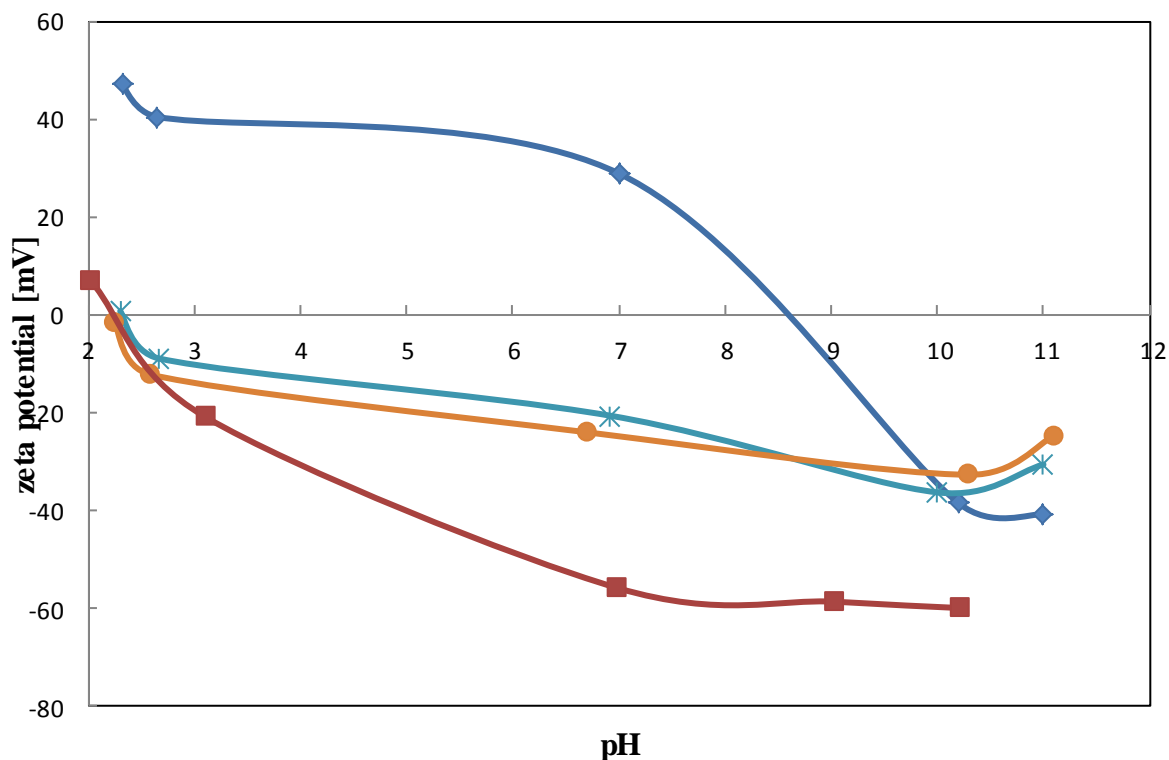
Figure 5-3: The value of the zeta potential at different pH values for the uncoated TiO₂-P25 NPs (dark blue), silica-coated TiO₂-RA/SiO₂ core/shell NPs (light blue), silica-coated TiO₂-P25/SiO₂ core/shell NPs (orange) and silica NPs(red).

The variations in the values of the zeta potential with varying pH values for the titanium dioxide nanoparticles and TiO₂/SiO₂ core/shell nanoparticles were determined in order to investigate the effect of the surface coating on the dispersion of the nanoparticles and their surface characteristics. The zeta potential is positive below the isoelectric point IEP and negative above the IEP. The isoelectric points (IEP) of coated TiO₂-P25 nanoparticles and commercial TiO₂-RA with core/shell method are found to occur at pH = 2.2. The graph above appears to show TiO₂-P25 crossing the Zeta potential at pH = 8.5 The IEP of the silica nanoparticles is also found to be occur at approximately pH = 2.2. The zeta potential is also negative above pH = 2.2. Lin *et al.* had reported that incomplete coating, such as nucleation coating, does not modify the titanium nanoparticles effectively, therefore the zeta potential *vs* pH curve and IEP of ineffectively coated titanium particles are similar to those of pure titanium nanoparticles.

It can be seen from Figure 5-3 that the zeta-potential *vs* pH curves of the silica-coated titanium dioxide core/shell nanoparticles are very different from that observed for the pure titanium dioxide nanoparticles and are similar to those of pure silica nanoparticles. As a result, it appears that the silica sol did not self-nucleate to form silica particles *via* a homogeneous nucleation process. Instead, it seems to have formed a dense layer on the TiO_2-P25 nanoparticles and thereby fully coated the surface of the TiO_2-P25.

5.2.2   Deposition of TiO_2-P25/SiO_2 and TiO_2-RA/SiO_2 core/shell nanoparticles on CP samples using the layer-by-layer (LBL) process

It was decided to evaluate the ability to prepare TiO_2/SiO_2 coated CP nanocomposites by two variants of the layer-by-layer (LBL) deposition technique, which was of interest for reasons of simplicity, scalability and use of green solvents.

Cellulose fibres are normally negatively charged over a wide pH range, due to the presence of ionisable moieties, such as carboxyl or hydroxyl groups, on the surface of the fibres. Additionally, the surfaces of TiO_2/SiO_2 core/shell nanoparticles in neutral aqueous solutions are also typically negatively charged, hence a Coulombic barrier to the deposition of these particles onto cellulose fibres arises. Therefore, in order to be able to efficiently deposit the TiO_2/SiO_2 core/shell nanoparticles onto the surface of the fibres of the CP samples, either the polarity of the surface of the TiO_2/SiO_2 core/shell nanoparticles or the cellulose fibres themselves may be changed from negatively to positively charge.

Therefore it was decided to investigate the efficacy of two LBL procedures, the first involved the deposition from solution of a fine layer of positively charged PDDA/PSS/PDDA-coated TiO_2/SiO_2 core/shell nanoparticles onto the negatively charged surface of the cellulosic paper samples and the second (inverse) approach involved the deposition from solution of a fine layer of negatively charged TiO_2/SiO_2 core/shell nanoparticles onto the surface of the positively charged PDDA/PSS/PDDA-coated cellulosic paper samples (see the Experimental section).[169]

5.2.2.1 Solution-deposition of LBL-modified TiO2-P25/SiO₂ core/shell nanoparticles on cellulosic paper samples

Although there were no significant differences between the IR spectrum of untreated TiO_2/SiO_2 core/shell nanoparticles and that of the coated $TiO_2/SiO_2/PDDA$ core/shell/outer-shell nanoparticles, absorption peaks attributable to PSS can be observed in the IR spectra of the $TiO_2/SiO_2/PDDA/PSS$ and $TiO_2/SiO_2/PDDA/PSS/PDDA$ core/shell nanoparticles. In addition to a strong peak attributable to cellulose at $2\theta = 23.1º$, weak peaks characteristic of the anatase polymorph of titanium dioxide originating from the TiO_2-P25 nanoparticles can be observed in the XRD spectrum of the treated samples of CP. 80% of the titanium dioxide present in commercial TiO_2-P25 nanoparticles is present in the anatase polymorph. Therefore, it is reasonable to assume that the rutile peak for the remaining 20% of the titanium dioxide is very weak in comparison with that observed for the anatase polymorph in the TiO_2-P25 nanoparticles and therefore cannot be observed in Figure 5-4.
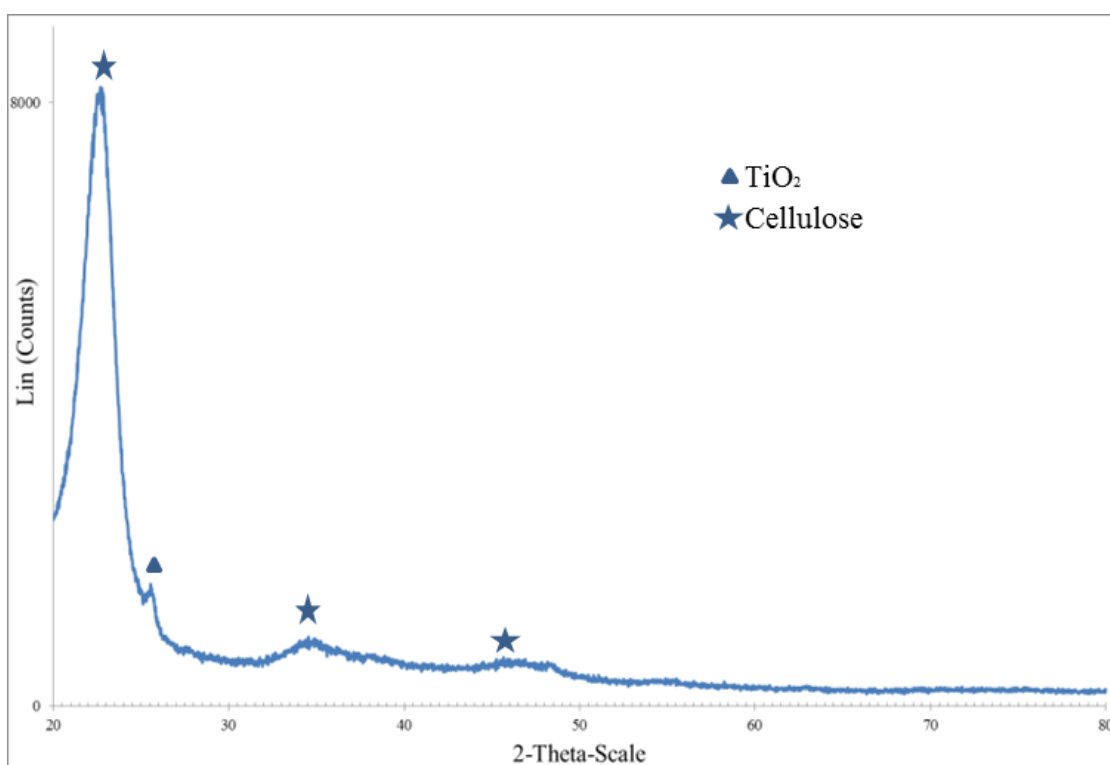
Figure 5-4: XRD pattern for a TiO₂-P25/SiO₂ core/shell nanoparticle coated CP sample produced by the LBL approach

The SEM-EDX images of a TiO-P25/SiO$_2$ core/shell nanoparticle coated CP sample produced by the LBL approach are shown in Figure 5-5.

The SEM images show that the surfaces of the cellulose fibres are partially coated with TiO-P25/SiO$_2$ core/shell nanoparticles with a size of approximately 250 nm, although not homogeneously. Analysis by ICP shows that the Si/Ti concentration (w/w %) is 1.76. Analysis by EDX of the product of coating CP, by LBL technique, clearly shows the presence of titanium and silicon.
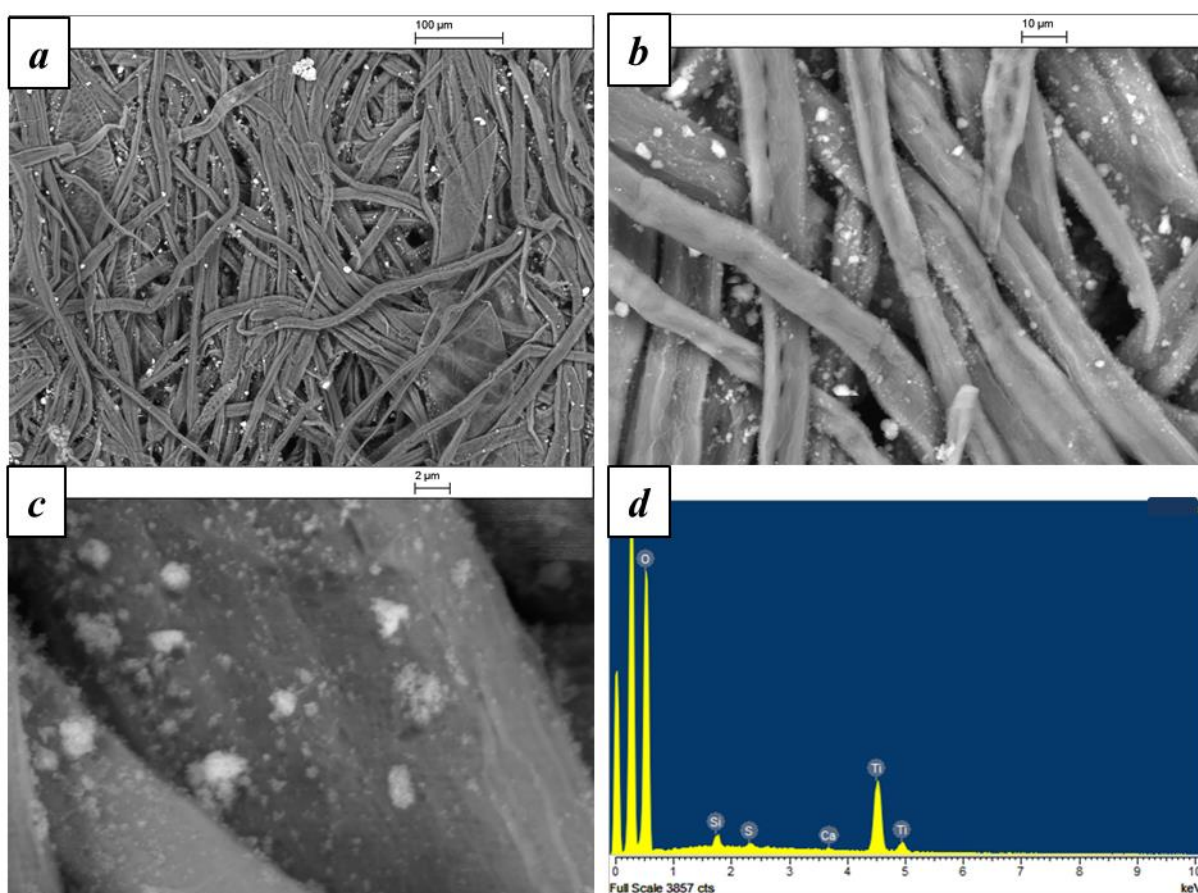
Figure 5-5: SEMs of the nanocomposite CP samples coated with TiO$_2$-P25/SiO$_2$ core/shell nanoparticles by the LBL approach for sample SMS020 (a – c). The EDX pattern for sample SMS020C (d).

5.2.2.2 Solution-deposition of TiO₂-P25/SiO₂ and TiO₂-RA/SiO₂ core/shell nanoparticles on LBL-modified cellulosic paper samples

In this method samples of CP, whose constituent fibres had first been covered by a composite layer of PDDA/PSS/PDDA, were coated with a fine layer of core/shell TiO_2/SiO_2 nanoparticles by immersing the paper samples in a colloidal solution of core/shell TiO_2/SiO_2 nanoparticles followed by sonication of the resultant mixture. The XRD analyses of the nanocomposite CP samples coated with TiO_2-P25/SiO_2 core/shell nanoparticles by this LBL approach are shown in Figure 5-6. The XRD spectrum contains weak peaks attributable to the presence of P25 titanium dioxide nanoparticles and a strong peak characteristic of cellulose at $2\theta = 23^o$. These peaks were found in all of the spectra of the TiO_2/SiO_2 coated cellulosic papers prepared either by using sonication of the paper samples or just by immersion of the paper samples in the colloidal solutions of the TiO_2/SiO_2 core/shell nanoparticles without sonication. However, the intensity of titanium dioxide peaks of the sonicated CP samples is greater than that of the immersed (non-sonicated) CP samples, which suggests a greater degree of coating for the former compared to that of the latter. Hence, sonication is thought to lead to greater deposition of TiO_2/SiO_2 core/shell nanoparticles on the PDDA/PSS/PDDA coated paper than simple immersion does.
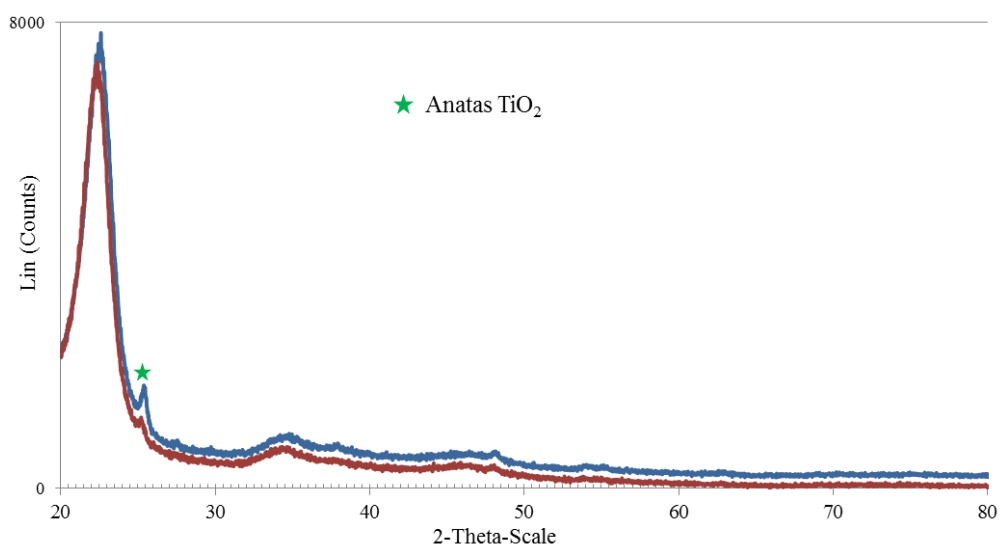
Figure 5-6: XRD spectra of the two TiO₂/SiO₂ coated CP samples prepared from PDDA/PSS/PDDA coated CP. (blue): papers that were sonicated in the TiO₂/SiO₂ colloidal solution, (red): papers that were immersed in the TiO₂/SiO₂ colloidal solution.

Analysis using SEM shows that TiO_2/SiO_2 core/shell nanoparticles are homogeneously coated on the sonicated CPs. Although TiO_2/SiO_2 core/shell nanoparticles are also observed on the surface of the immersed (non-sonicated) CP samples, the covering is not very homogenous. EDX analyses suggest that TiO_2/SiO_2 ratios on the surfaces of both treated CPs are close to that of the original TiO_2/SiO_2 core/shell nanoparticles as expected.
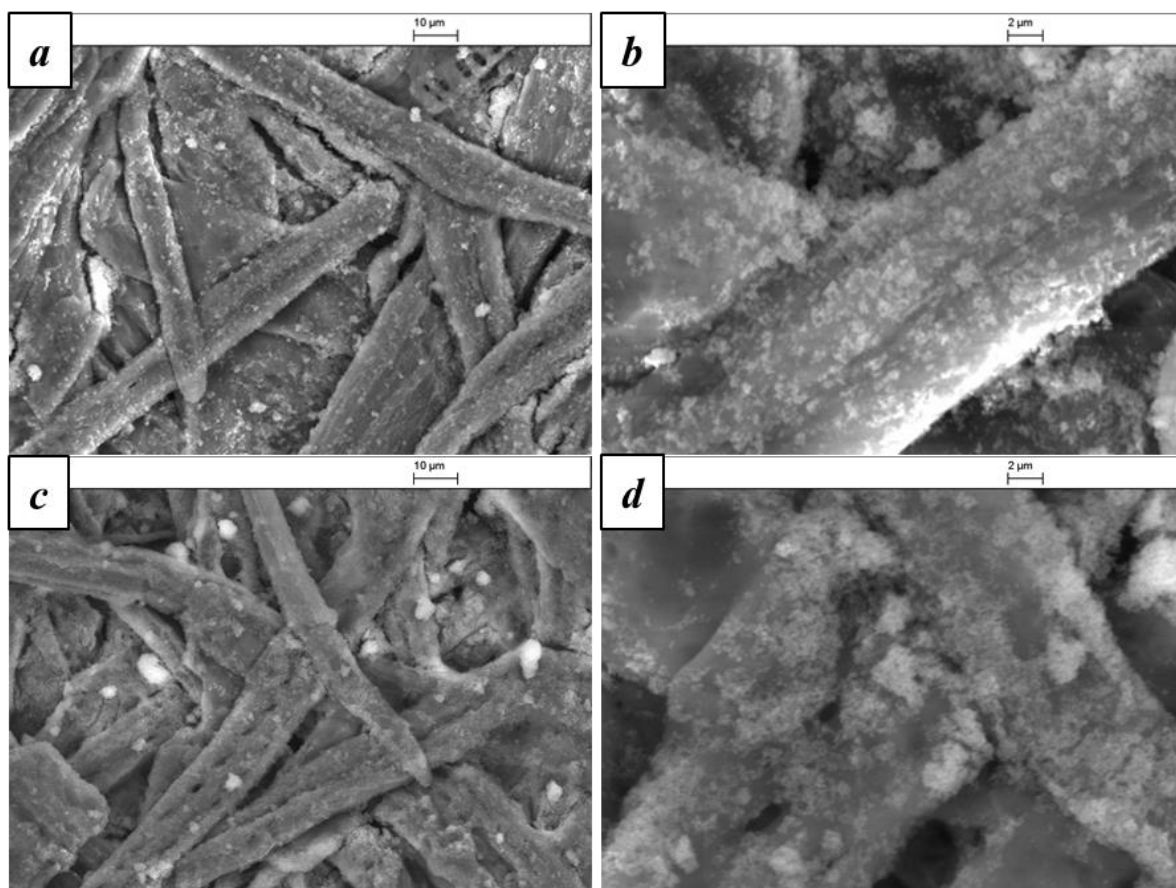
Figure 5-7: SEM image of TiO_2 P25/SiO_2/cellulosic nanocomposites by LBL coating of cellulosic paper samples of (a & b) SMS025A, (c & d) SMS025B.

ICP analyses of the TiO_2/SiO_2/cellulosic nanocomposites paper shows that the TiO_2-RA/SiO_2 for coating prepared using the sonication method is 11.1%, which represents a similar value to that found from the ICP analysis of the original rutile TiO_2/SiO_2 core/shell nanoparticles.

Table 5-1: Concentration (wt%) of titanium and silicon found on the surface of treated CPs, analysed using EDX, and of TiO$_2$/SiO$_2$ core/shell NPs, analysed using ICP.

	Ti (wt %)	Si (wt %)	TiO$_2$ (%)	SiO$_2$ (%)	TiO$_2$/SiO$_2$
Sonicated CP	4.39	0.310	7.32	0.660	11.1
Immersed CP	4.99	0.450	8.29	0.962	8.62
TiO$_2$/SiO$_2$ powder	56.67	4,02	94.54	8.60	11.0

TiO$_2$-RA/SiO$_2$ core/shell nanoparticles were deposited on the PDDA/PSS/PDDA-modified surface of the constituent fibres of cellulose. However, the nanoparticle coating of the fibres is seen to be neither continuous nor homogeneous. It is surmised that the poor quality of nanoparticle coating is probably due to the low stability of the colloidal solutions of TiO$_2$-RA/SiO$_2$ core/shell nanoparticles in water. Hence, an alternative to TiO$_2$-RA/SiO$_2$ core/shell nanoparticles was sought.

5.2.3 TiO2-RP/SiO$_2$ and TiO2-RP500/SiO$_2$ core/shell nanoparticles

5.2.3.1 Analysis

Given the low stability of aqueous colloidal suspensions of TiO$_2$-RA/SiO$_2$ core/shell nanoparticles, it was thought that changing the core of the nanoparticles could increase the stability of the colloidal solution. Therefore TiO$_2$-RP and TiO$_2$-RP500 nanoparticles were synthesised using a sol-gel reaction between TESO and commercial rutile-type titanium dioxide (RP), as described in the experimental section. The IR spectra of the newly generated TiO$_2$-RP and TiO$_2$-RP500 nanoparticles were collected. Comparison of the IR spectra suggest that TiO$_2$-RP500 has lost significantly more surface hydroxyl groups during synthesis than TiO$_2$-RP as the bands at *ca*. 1650 and 3300 cm^{-1} are of lower intensity for TiO$_2$-RP500 than TiO$_2$-RP. This loss of surface hydroxyl groups presumably arises during the heating period (500 °C for 3 hours).

The newly generated TiO_2-RP and TiO_2-RP500 nanoparticles were coated with SiO_2 as described in chapter 3. To yield the new core/shell nanoparticles TiO_2-RP/SiO_2 and TiO_2-RP500/SiO_2. The IR spectra of the TiO_2-RP/SiO_2 and TiO_2-RP500/SiO_2 core/shell nanoparticles were collected. TiO_2-RP/SiO_2 exhibits a new band at 1068 cm^{-1} compared to the IR spectra of TiO_2-RP, which can be ascribed to the asymmetric stretching vibration of v_{as}(Si-O-Si), indicative that SiO_2 has been incorporated into our nanoparticles. Additionally, TiO_2-RP/SiO_2 exhibits new bands centred at 1380, 1238 and 1154 cm^{-1} in the IR spectrum as compared with the core TiO_2-RP IR spectrum. It is known that the O–Si asymmetric stretching vibration of amorphous silica leads to the absorption bands at about 1080 and 1220 cm^{-1}. The new peaks at 1238 and 1154 cm^{-1} that appear in the spectrum of TiO_2-RP/SiO_2 can be ascribed to the same asymmetric stretch. Although the vibration frequency has shifted to a slightly higher frequency of 1154 cm^{-1} from 1080 cm^{-1}, this is probably due to the chemical reaction between the coated hydrous silica and the surface of titanium dioxide nanoparticles that brakes the symmetry of Si–O tetrahedron and led to the formation of a new absorption band. The IR spectrum of TiO_2-RP500/SiO_2 exhibits bands at 1080 and 1228 cm^{-1} that correspond to the v_{as}(Si-O-Si) stretch, indicating that SiO_2 has been incorporated into our nanoparticles.
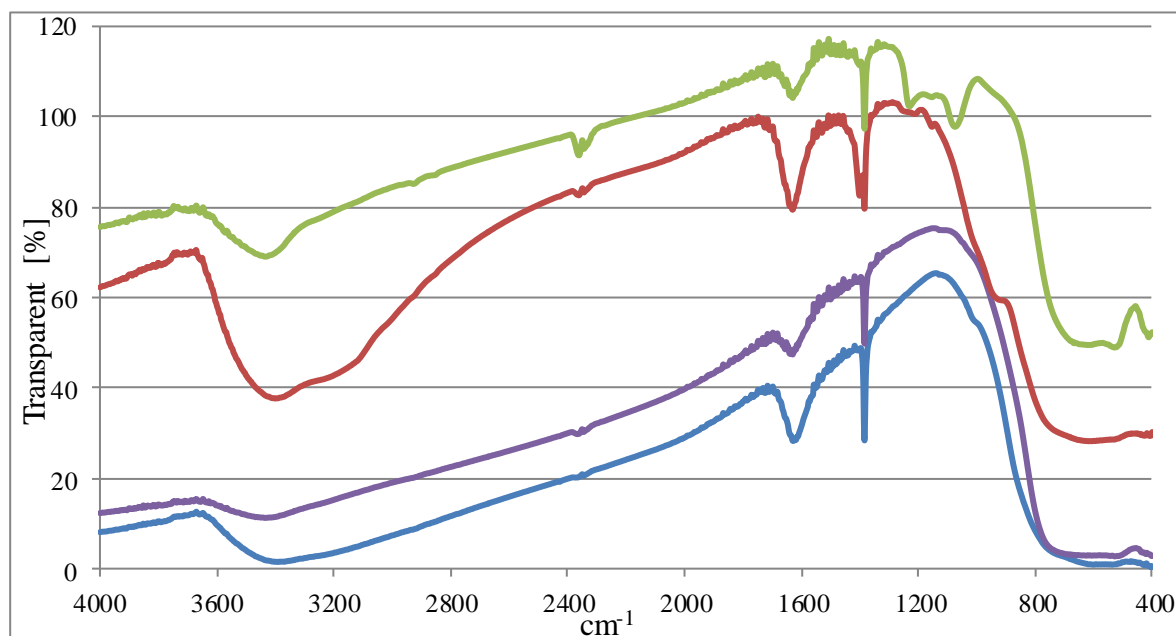
Figure 5-8: IR spectra of (blue) (SMS102) TiO_2-RP, (red) (SMS104A) TiO_2-RP/SiO_2, (purple) (SMS104C) TiO_2-RP500 and (green) (SMS104B)TiO_2-RP500/SiO_2.

111
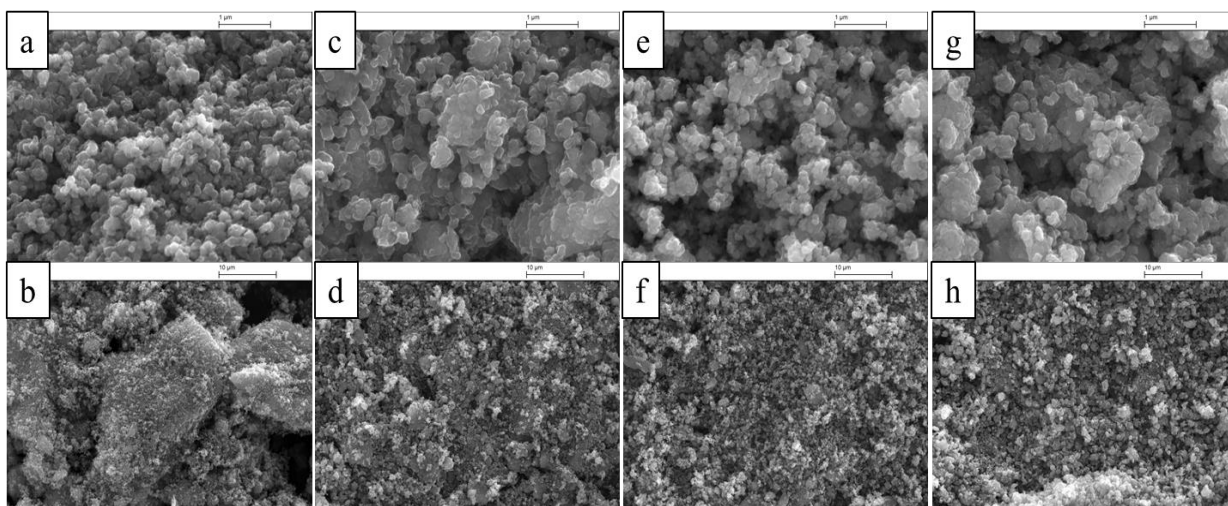
Figure 5-9: SEMs of TiO₂-RP(a & b), TiO₂-RP/SiO₂ (c & d), TiO₂-RP500 (e & f) and TiO₂-RP500/SiO₂ (g & h).

Comparison of the images obtained by SEM conducted on the nanoparticles cores (TiO$_2$-RP and TiO$_2$-RP500) and those of the silica-coated nanoparticles (TiO$_2$-RP/SiO$_2$ and TiO$_2$-RP500/SiO$_2$) exhibit no marked difference in particle shape from coating the particles in silica.

The BET surface areas determined for TiO$_2$-RP/SiO$_2$ and TiO$_2$-RP500/SiO$_2$ are 100.9 and 33.4 m^2/g respectively, very similar to those of TiO$_2$-RP (105.3 m^2/g) and TiO$_2$-RP500 (31.7 m^2/g). The average pore diameters were decreased from 20.0 nm (TiO$_2$-RP) and 22.0 nm (TiO$_2$-RP500) to 12.8 nm (TiO$_2$-RP/SiO$_2$) and 18.4 nm (TiO$_2$-RP500/SiO$_2$) respectively. This further supports the formation of coatings of SiO$_2$ ca the titanium dioxide nanoparticles.

TEM of TiO$_2$-RP/SiO$_2$ and TiO$_2$-RP500/SiO$_2$ are shown in Figure 5-10 compared with the TEM images of TiO$_2$-RP and TiO$_2$-RP500 Figure 5 11, no big differences can be observed after coating with SiO$_2$. Since the nanoparticles were very small, it was not possible to use EDX to indentify the Si/Ti ratio difference at different area of the nanoparticles.

112
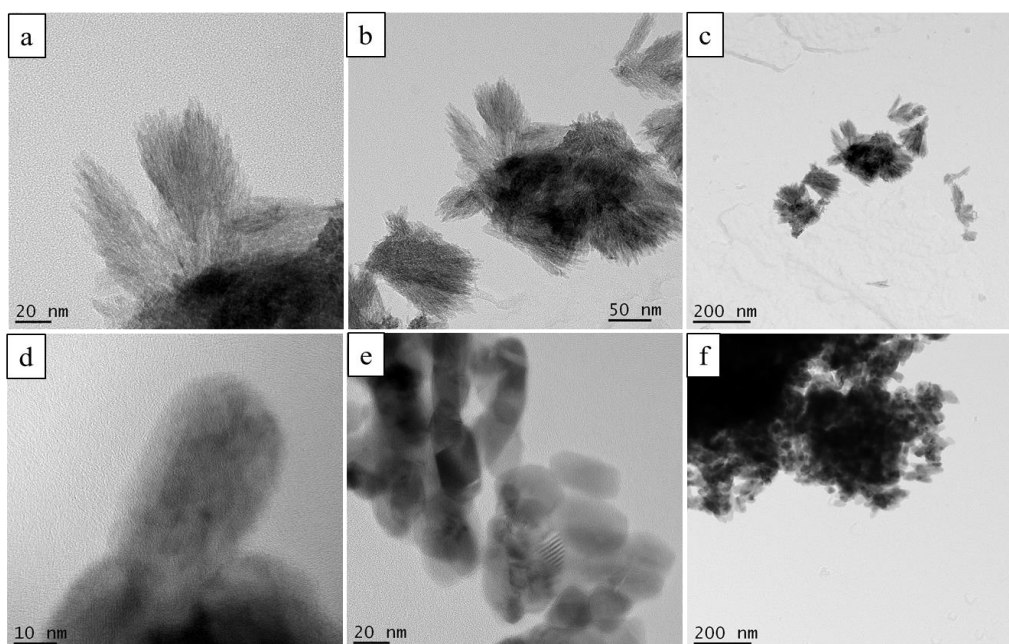
Figure 5-10: TEM images of nanoparticles synthesised by TiO₂-RP/SiO₂ (a-c) and TiO₂-RP500/SiO₂ (d-f).
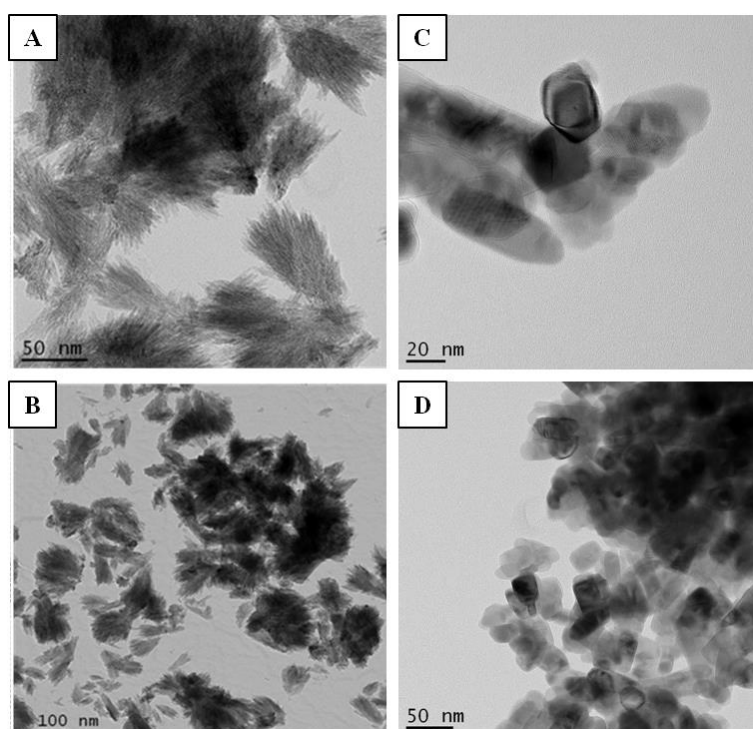
Figure 5-11: TEM images of nanoparticles synthesised by TiO₂-RP (A&B), synthesised by method TiO₂-RP500 (C&D).
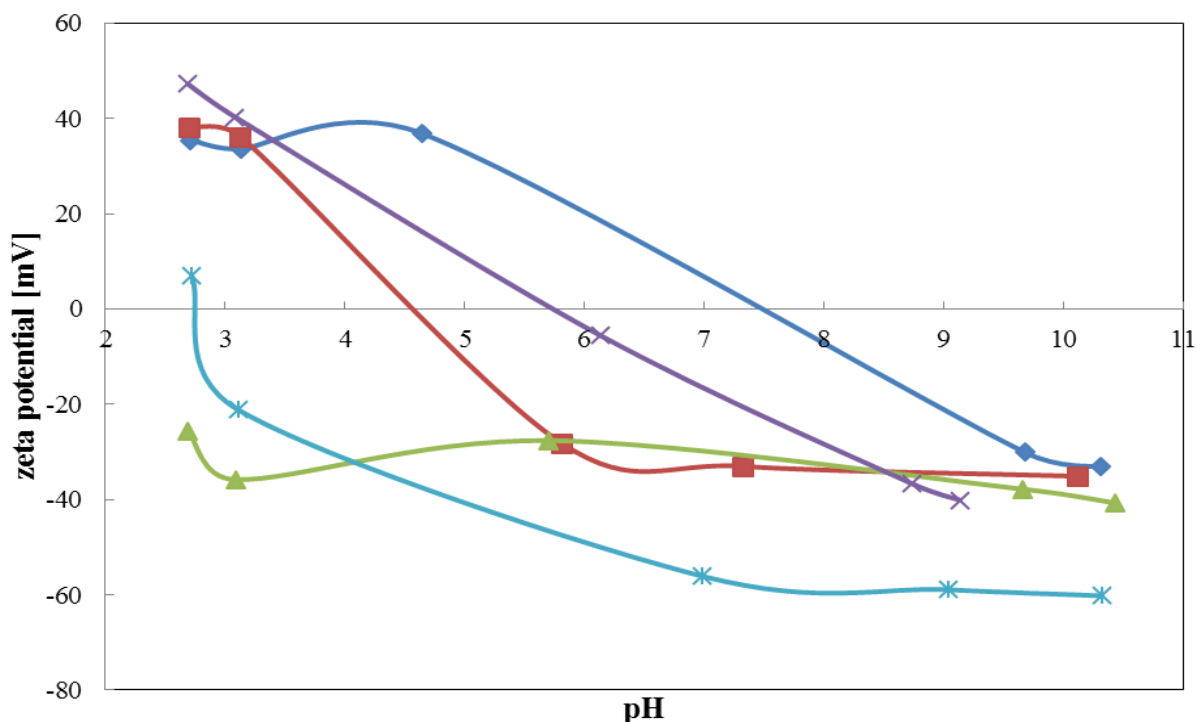
Figure 5-12: Zeta potential at different pH for SiO₂ (light blue), TiO₂-RP (SMS102A) (dark blue), TiO₂-RP/SiO₂ (SMS104A) (red), TiO₂-RP500 (SMS104B) (green), TiO₂-RP500/SiO₂ (SMS104C) (purple).

The variations of zeta potential with pH for TiO_2-RP and TiO_2-RP/SiO_2 core/shell nanoparticles were measured to check the surface coating effect on the dispersion of the core/shell nanoparticles and their surface characteristics. The isoelectric points (IEPs) of the (non-silica-coated) TiO_2-RP and TiO_2-RP500 nanoparticles are ca pH = 7.5 and pH = 5.8, respectively.

Lin *et al.* had reported that incomplete coating, such as nucleation coating, of titanium dioxide nanoparticles, with silica, did not modify their physical properties in an effective way, so, for example, the zeta-potential *vs* pH curve and IEP of the TiO_2/SiO_2 core/shell nanoparticles prepared in this way were found to be similar to those of the original titanium dioxide nanoparticles used to form the TiO_2/SiO_2 core/shell nanoparticles in the first place. [95]

It can be seen from Figure 5-12, that the zeta-potential *vs* pH curves of the silica-coated nanoparticles, TiO_2-RP/SiO_2 and TiO_2-RP500/SiO_2, are very different from those of non-silica-coated nanoparticles, TiO_2-RP and TiO_2-RP500, resemble more closely that of silica

nanoparticles (SiO_2). Therefore, it seems reasonable to conclude that the silica sol has not self-nucleated to form silica nanoparticles *via* homogeneous nucleation, i.e., the samples are not a mixture of silica and titanium dioxide nanoparticles, but rather a layer of silica (shell) on the TiO_2-RP and TiO_2-RP500 titanium dioxide nanoparticle cores. This shell of silica then effectively shields the surface of the titanium dioxide nanoparticles to yield stable silica/titanium dioxide (TiO_2-RP/SiO_2 and TiO_2-RP500/SiO_2) core/shell nanoparticles. [84, 170]

5.2.3.2 Stability

Compare the stability of different methods of preparation TiO_2 shows TiO_2-RP, TiO_2-RP/SiO_2 and TiO_2-RP500/SiO_2 were stable for more than 2400 minutes but TiO_2-RP500 wasn't stable for long time.

Table 5-2: Compare stablity of collouidal solutions from different methods for prepare rutile TiO_2 nanoparticles powder stable aqueous.

Time	SMS102A (70 mg) Water (20 mL)	SMS104A (70 mg) Water (20 mL)	SMS104B (70 mg) Water (20 mL)	SMS104C (70 mg) Water (20 mL)
5 min	milky white colloid	milky white colloid	milky white colloid	colloid, precipitate
60 min	colloid	milky white colloid	Colloid	near to clear, precipitate
1200 min	very little clear, middle colloid and precipitate	milky white colloid	milky very little clear, middle colloid and precipitate	clear solution, Precipitate
After five days	top clear, middle colloid and precipitate	top clear, middle colloid and precipitate	top clear, middle colloid and precipitate	clear solution, Precipitate

115

5.2.4 Deposition of TiO$_2$-RP/SiO$_2$ and TiO$_2$-RP500/SiO$_2$ core/shell nanoparticles on CP samples using the LBL process

The addition of the silica coated nanoparticles, TiO$_2$-RP/SiO$_2$ and TiO$_2$-RP500/SiO$_2$, onto CP by the LBL process was investigated. For these test, the CP (standard commercial printing paper) was initially coated with a layer of PDDA, then PSS and then PDDA again. Subsequent to this, the CP was treated with a colloidal, aqueous solution of the silica coated nanoparticles (either TiO$_2$-RP/SiO$_2$ or TiO$_2$-RP500/SiO$_2$). Treating cellulosic paper with the corresponding silica coated nanoparticles under the same conditions, but without the PDDA/PSS/PDDA pre-treatment of the paper, was investigated by SEM. The SEM images of these tests exhibited zero evidence of the nanoparticles absorbing onto the cellulose fibres (Figure 5 15).

The effect of immersing the PDDA/PSS/PDDA pre-treated paper in an aqueous solution of either TiO$_2$-RP/SiO$_2$ or TiO$_2$-RP500/SiO$_2$ silica coated nanoparticles was shown by SEM to be the partial coating of the cellulose fibres with nanoparticles (Figure 5-15), although some aggregates can also be observed. The nature and quality of the layer of TiO$_2$-RP/SiO$_2$ and TiO$_2$-RP500/SiO$_2$ core/shell nanoparticles attached to the surface of the LBL modified cellulosic papers appear to be very similar to those of the comparable test samples of paper coated with TiO$_2$-P25/SiO$_2$ core/shell nanoparticles and it shows nanoparticles absorbed onto the CP.

Figure 5-13: Coating process for LBL paper with PDDA, PSS and then PDDA.

EDX analysis reveals that the ratio of SiO_2/TiO_2 present on the modified CPs coated with either TiO_2-RP/SiO_2 or TiO_2-RP500/SiO_2 core/shell nanoparticles was 0.067 and 0.047, respectively. ICP analysis shows that the ratios of SiO_2 to TiO_2 in the TiO_2-P25/SiO_2, TiO_2-RP/SiO_2 and TiO_2-RP500/SiO_2 core/shell nanoparticles are 0.091, 0.066 and 0.050 respectively, which is very near to EDX results.
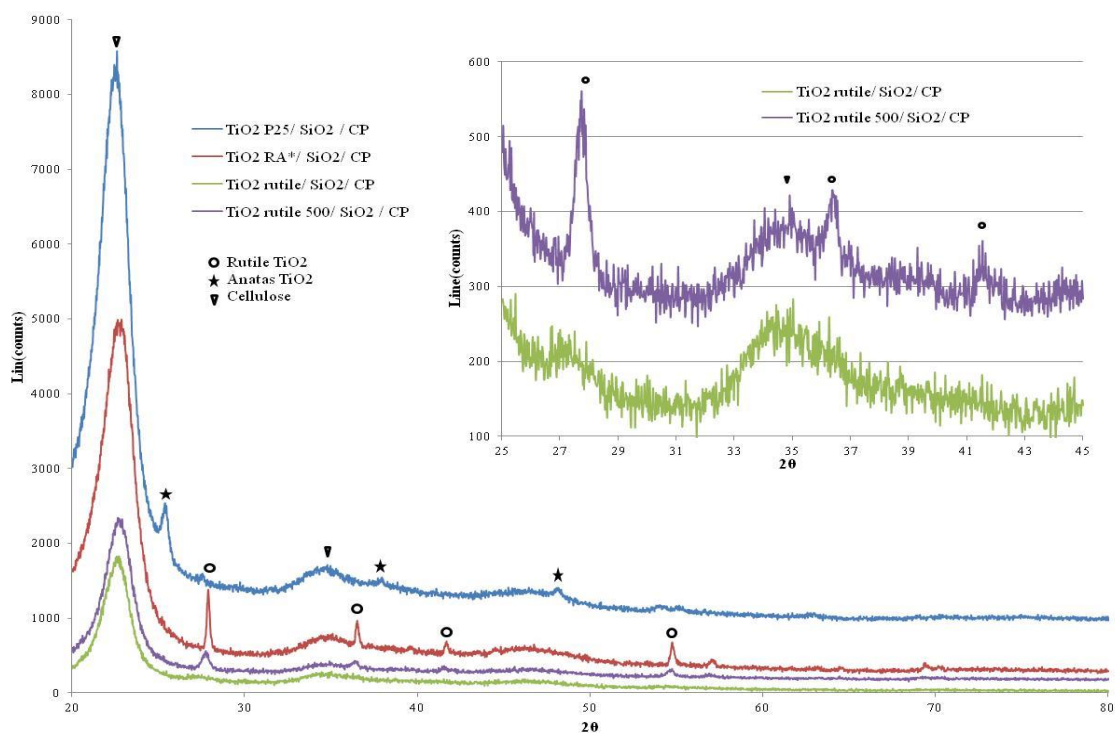
Figure 5-14: XRD pattern of the paper samples coated with TiO_2 P25/SiO_2 (blue), TiO_2 RA/SiO_2 (red), TiO_2 rutile/SiO_2 (green), TiO_2 rutile/SiO_2 (purple),

XRD pattern of the paper samples coated with TiO_2-P25/SiO_2 shows that beside a strong peak of cellulose at $2\theta = 23^o$, weak anatase titanium dioxide peaks from TiO_2-P25 can also been observed, but the rutile peaks are too weak to be observed. The XRD pattern of the paper samples coated with TiO_2-RA/SiO_2 core/shell nanoparticles (which is commercial rutile titanium dioxide from sigma Aldrich company for compare with titanium dioxides made in this research from different methods) clearly shows rutile titanium dioxide peaks. Weak rutile titanium dioxide peaks can also be observed in the XRD pattern of the paper samples coated with TiO_2-RP500/SiO_2 core/shell nanoparticles, but cannot be observed in the

117

pattern of the paper samples coated with TiO$_2$-RP/SiO$_2$/CP, although a very weak peak at about $2\theta = 27$ ° can be seen.
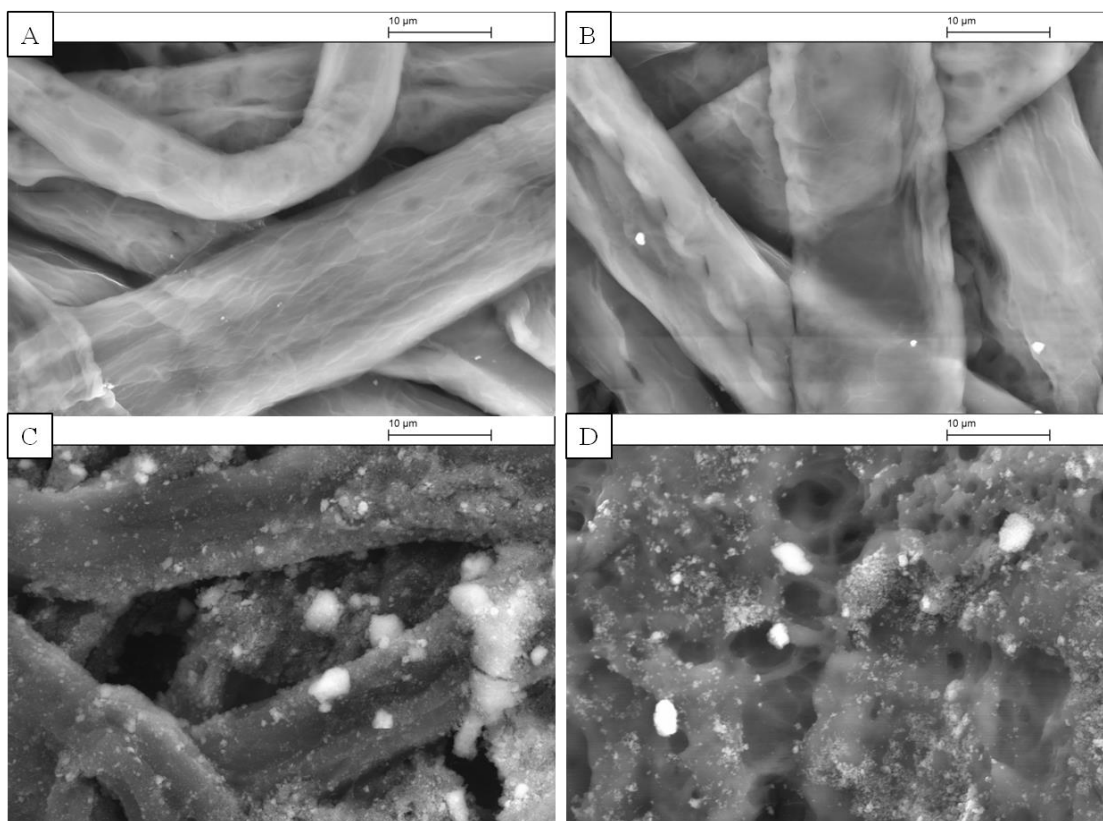
Figure 5-15: SEM images of TiO$_2$/SiO$_2$/CP (A), TiO$_2$-RP500/CP (B), TiO$_2$/SiO$_2$/LBL CP (C), TiO$_2$-RP500/LBL CP (D).

5.2.5 Brightness and whiteness of nanoparticle treated cellulosic paper

Figure 5-16 shows the ISO-brightness for the blank reference paper and the paper samples coated either with uncoated nanoparticles (TiO$_2$-P25, TiO$_2$-RP or TiO$_2$-RP500) or silica coated nanoparticles (core/shell TiO$_2$-P25/SiO$_2$, TiO$_2$-RP/SiO$_2$ or TiO$_2$-RP500/SiO$_2$), both before and after illumination with UV-light in a standard xenon UV-stability test. It can be seen that the brightness of the blank paper reference is sharply reduced after illumination with UV radiation in the standard xenon test, which is ascribed to photo-degradation. The reduction in brightness is greater for paper samples treated with uncoated TiO$_2$-P25

118

nanoparticles or TiO$_2$-Rp nanoparticles, demonstrating that uncoated TiO$_2$ nanoparticles accelerate the photo-degradation process.
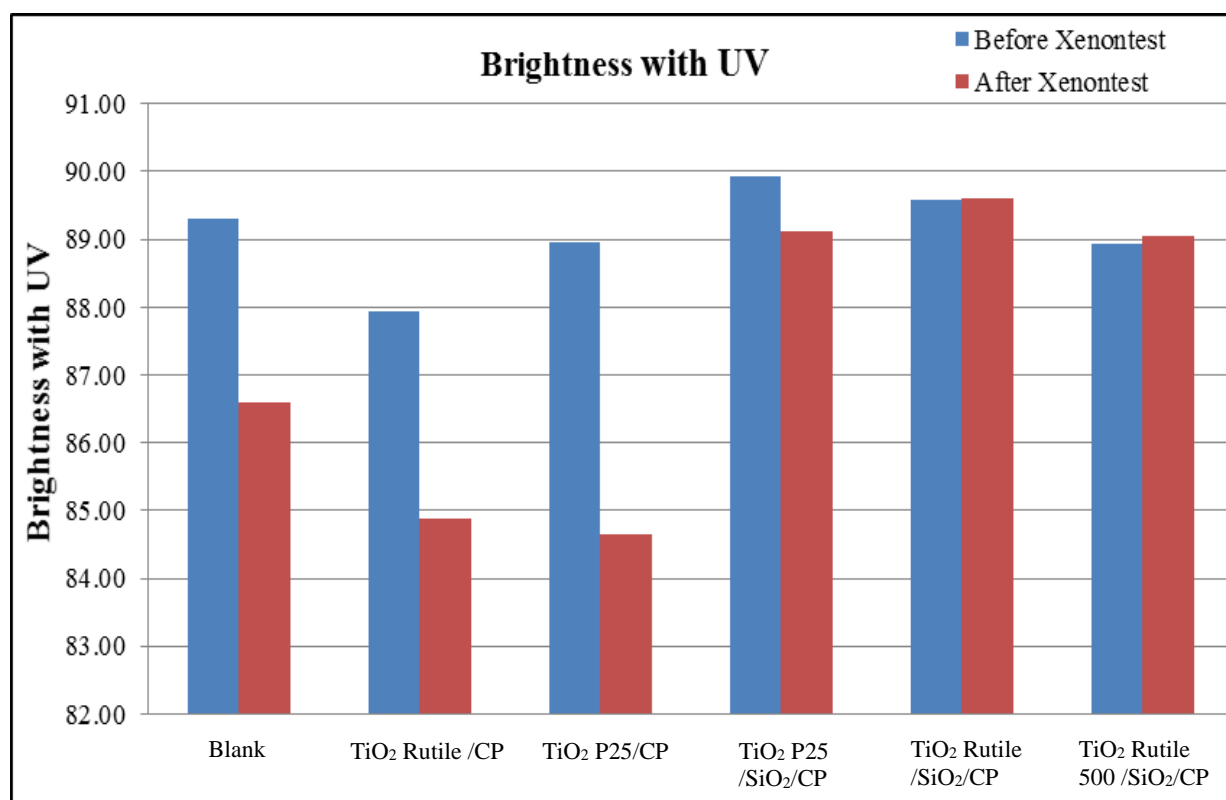
Figure 5-16: ISO brightness of blank reference paper and the paper samples coated either with uncoated TiO$_2$-RP nanoparticles or silica coated TiO$_2$-RP/SiO$_2$ core/shell nanoparticles before (blue) and after the UV-stability test (red).

In contrast, there is only a marginal reduction in the brightness of the paper samples treated with the silica-coated nanoparticles (TiO$_2$-P25/SiO$_2$, TiO$_2$-RP/SiO$_2$ or TiO$_2$-RP500/SiO$_2$). That the degradation of the paper is lesser than that of the reference paper is especially note-worthy, as the treatment of the paper with silica-coated nanoparticles increases the stability of the paper to photo-degradation. It seems reasonable to assume that the small reduction in the brightness of the paper samples coated with TiO$_2$-P25/SiO$_2$, TiO$_2$-RP/SiO$_2$ and TiO$_2$-RP500/SiO$_2$ core/shell nanoparticles, after the xenon UV-test, is attributable to the fact that the photo-catalytically active titania nanoparticles present in commercial paper have been coated effectively with a thin, inert layer of silica, which passivates the surface of the

titanium dioxide nanoparticles and thereby inhibits their inherent high degree of photo-catalytic activity.
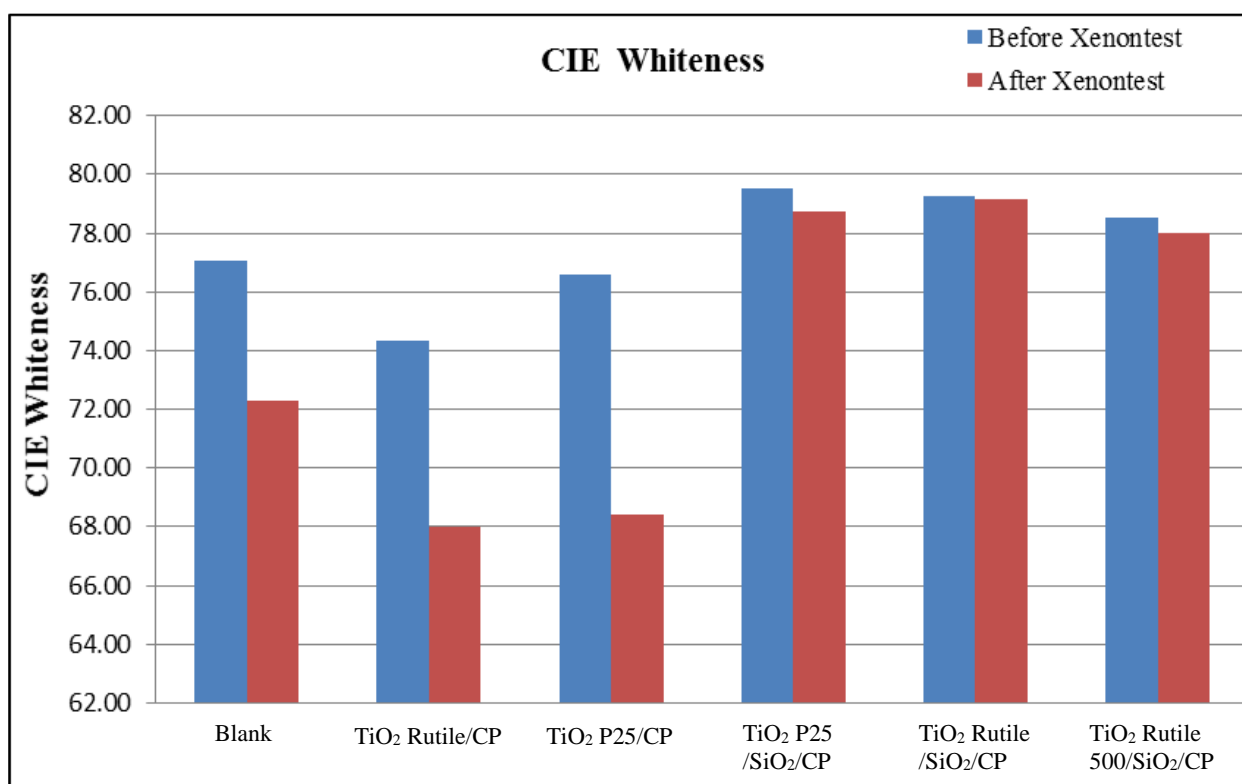
Figure 5-17: CIE whiteness of blank reference paper and the paper samples treated with uncoated TiO$_2$-RP nanoparticles or silica-coated TiO$_2$-RP/SiO$_2$ core/shell nanoparticles, both before (blue) and after the UV-stability test (red).

The values for the CIE-whiteness of the CP coated with the silica-passivated TiO$_2$-P25/SiO$_2$, TiO$_2$-RP/SiO$_2$ and TiO$_2$-RP500/SiO$_2$ core/shell nanoparticles are slighter higher than those of either the blank paper reference and that of the paper sample coated with either (non-silica-passivated) TiO$_2$-P25 nanoparticles or the TiO$_2$-RP nanoparticles. In contrast to the sharp reduction in the whiteness of the blank paper reference sample and the paper samples coated with the (non-silica-passivated) TiO$_2$-P25 and TiO$_2$-RP nanoparticles, no reduction in whiteness can be observed for the paper samples coated with the silica-passivated TiO$_2$-P25/SiO$_2$, TiO$_2$-RP/SiO$_2$ and TiO$_2$-RP500/SiO$_2$ core/shell nanoparticles, after the standard xenon UV-stability test.

5.3 Summary

In order to protect and passivate the surface of titanium dioxide nanoparticles, several new approaches were evaluated, whereby the surface of the titanium dioxide nanoparticles was successfully coated, using a sol-gel approach, with a stable, uniform, thin layer of chemically and photo-chemically inert silica to create stable TiO_2/SiO_2 core/shell nanoparticles.

The surface of samples of commercial paper, consisting of cellulose fibres, were partially coated with these silica-coated TiO_2/SiO_2 core/shell nanoparticles using two related layer-by-layer approaches utilising stable, aqueous, colloidal solutions of the nanoparticles.

In first method, TiO_2-$P25/SiO_2$ core/shell nanoparticles were first coated with PDDA, PSS and PDDA using a layer-by-layer method. The presence of PDDA and PSS was confirmed by analysis of the IR spectra of the reaction intermediates. SEM images show that TiO_2-$P25/SiO_2$ core/shell nanoparticles, with diameter of about 250 nm, are present on the surface of the coated CP, but the surface coverage with nanoparticles is not homogeneous.

In the second method, samples of CP were first coated with PDDA, PSS and PDDA, respectively, using a similar stepwise layer-by-layer method followed by coating with a thin, uniform layer of TiO_2-$P25/SiO_2$ core/shell nanoparticles. Analysis of the XRD spectra of these nanocomposite materials suggests that immersing LBL-modified CP in TiO_2/SiO_2 colloidal solution under sonication results in a greater coverage of the paper surface than that observed for similar paper samples coated by immersing them in the colloidal solutions of the TiO_2-$P25/SiO_2$ core/shell nanoparticles, but without subsequent sonication.

SEM images of the CP/TiO_2-$P25/SiO_2$ core/shell nanocomposites prepared using the sonication show that the surface coverage was more homogeneously coated than that found on the paper samples coated with TiO_2-$P25/SiO_2$ core/shell nanoparticles by immersing the CP in the aqueous nanoparticle colloidal solutions without sonication. EDX analysis suggests that the TiO_2/SiO_2 ratios on the surfaces of both treated CPs are close to that of original TiO_2-$P25/SiO_2$ core/shell nanoparticles.

The value for the ISO-brightness and CIE-whiteness of the CP after coating with TiO_2-$P25/SiO_2$ core/shell nanoparticles shows a significant improvement, as does the UV stability, compared to the values observed for the untreated reference paper samples.

Commercially available (Aldrich) TiO_2-RA/SiO_2 core/shell nanoparticles, with a diameter ranging from 2.0 μm to 4.5 μm, were also deposited on the modified surface of the constituent fibres of cellulose making up the PDDA/PSS/PDDA-modified paper samples. However, the nanoparticle coating of the fibres is seen to be neither continuous nor homogeneous. It is surmised that the poor quality of nanoparticle coating is probably due to the low stability of the colloidal solutions of TiO_2-RA/SiO_2 core/shell nanoparticles in water.

The rutile polymorph of titanium dioxide nanoparticles (TiO_2-RP), prepared from $TiOCl_2$ as part of the work for this thesis, was also coated with a thin layer of silica by the sol-gel approach. Samples of CP coated with TiO_2-RP/SiO_2 and TiO_2-RP500/SiO_2 core/shell nanoparticles were also prepared first by a LBL coating CP with PDDA, PSS and PDDA, followed the deposition of the TiO_2-P25/SiO_2 core/shell nanoparticles from solution as described above.

The SEM of CP nanocomposites reveals a homogeneous coating of TiO_2-RP/SiO_2 and TiO_2-RP500/SiO_2 core/shell nanoparticles can be observed on the LBL-modified CP surfaces. The BET surface area of the TiO_2-RP/SiO_2 and TiO_2-RP500/SiO_2 core/shell nanoparticles are 100.9 and 33.4 m^2/g respectively, very similar to those of the original TiO_2-RP (105.3 m^2/g) and TiO_2-RP500 (31.7 m^2/g) nanoparticles used to prepare the silica-coated titanium dioxide core/shell nanoparticles. The TEM images of the cellulose nanocomposites are similar to those of the TiO_2-RP and TiO_2-RP500 core/shell nanoparticles. The values for the ISO-brightness, CIE-whiteness and stability to UV-illumination are also very similar to those observed for the analogous paper nanocomposites coated with TiO_2-P25/SiO_2 core/shell nanoparticles.

An alternative summary: A range of TiO_2 nanoparticles were coated with a layer of silica using an aqueous sol-gel method. These silica-coated TiO_2 nanoparticles were analysed by a range of techniques, including IR, SEM, EDX and zero potential determination, and were shown to be fully coated with a layer of silica of sufficient depth to change its chemical behaviour. The capacity of these silica-coated TiO_2 nanoparticles to adsorb onto CP was evaluated, and it was determined that it was necessary to either coat the cellulose or the nanoparticles in functional groups that bear positive charge at neutral pH. This was achieved by two different layer-by-layer techniques that coat either the cellulose in PDDA/PSS/PDDA layers or coat the nanoparticles in PDDA/PSS/PDDA layers. The modified cellulose was

found to be capable of absorbing silica-coated nano-particles and cellulose was found to be capable of absorbing PDDA/PSS/PDDA-coated core/shell TiO_2/SiO_2 nanoparticles. It was determined that silica-coated TiO_2 nanoparticles adsorbed onto cellulose increased the resistance of the material to photo-degradation, as determined by both the brightness and whiteness of the CP.

6 APTES-modified-titanium dioxide/CP nanocomposites

6.1 Introduction

In this chapter, commercial titanium dioxide nanoparticles (TiO_2-P25) and rutile titanium dioxide nanorods (TiO_2-RP), prepared as part of the work for this thesis, were chosen to be deposited onto the surface of CP in attempts to improve the optical properties of the paper without compromising its mechanical properties, based on the results of previous studies, see Chapters 4 and 5.

The surface of the titania nanoparticles (TiO_2-P25 and TiO_2-RP) were first modified with a surface-treatment of 3-aminopropyltriethoxysilane (APTES). These APTES-modified titanium dioxide nanoparticles were then deposited and fixed on surface of CP *via* a simple and cost-effective approach, i.e., immersion of the paper samples in an aqueous, colloidal solution of the APTES-modified titanium dioxide nanoparticles.

APTES is a cross-linking organic compound due to the presence of two different kinds of functional group, i.e., three ethoxy-chains and an amino-group, at opposite ends of its molecular structure $[(C_2H_5O)_3Si(CH_2)_3NH_2]$. The surface of the titanium dioxide nanoparticles are coated with a monolayer of APTES through the silanisation of the nanoparticle surface, by reaction of the surface nanoparticle hydroxyl-groups with the APTES ethoxy-groups, to form a series of covalent Ti-O-Si bonds.

The amino-group of the APTES moeity act as a coupling agent by interacting with the negatively charged surface of the cellulose substrate. Thus, the cellulose fibres coated with APTES modified titanium dioxide nanoparticles will have a thin layer silicon oxide between the surface of fibre and titanium dioxide, which may suppress the photo-catalytic activity and protect the cellulose surfaces.

This is first time, to the author's knowledge, that APTES-modified titanium dioxide nanoparticles have been fixed on the surface of CP to improve the whiteness, brightness and stability to UV-bleaching of the paper.

6.2 TiO₂-P25-APTES NPs in HCl solution

6.2.1 Preparation

The XRD spectrum of white powder, isolated from the reaction solutions of TiO_2-P25 nanoparticles and APTES, shows the presence of anatase and rutile polymorphs of titanium dioxide.
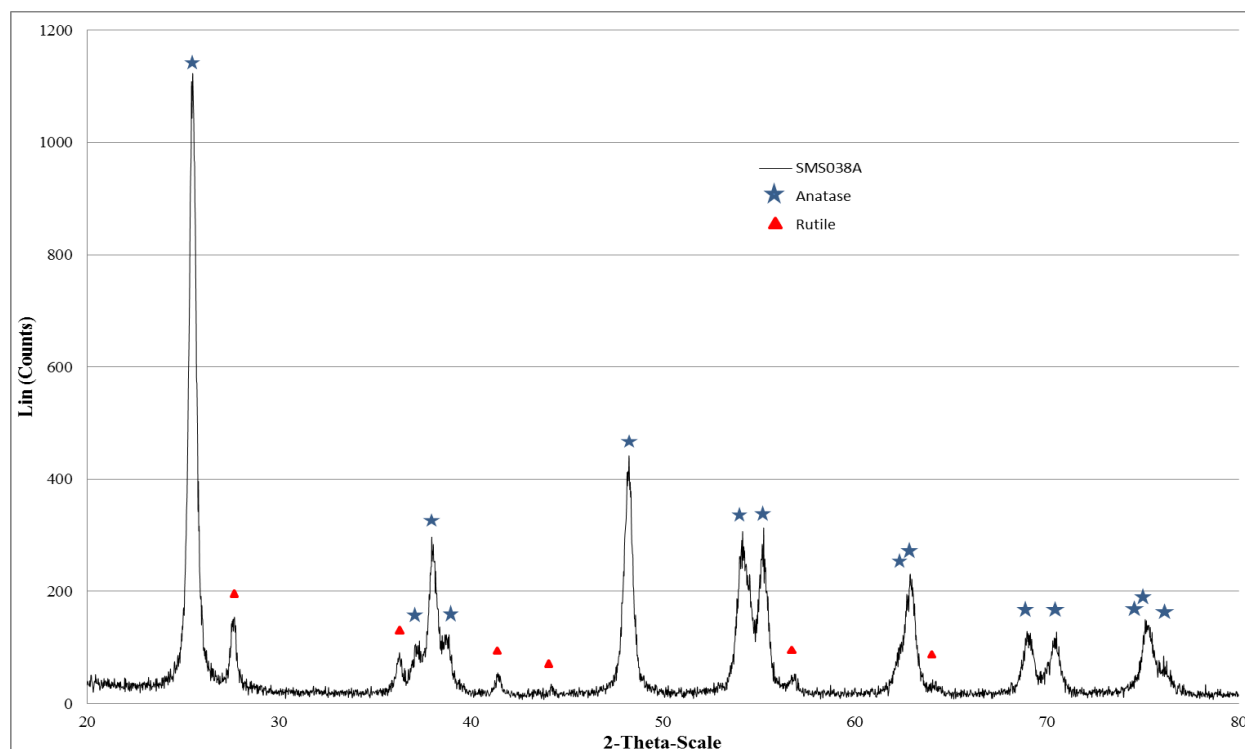
Figure 6-1: XRD pattern of sample SMS038 A- heated at 110 °C for 6 hours.

The IR spectrum of the APTES treated TiO_2-P25 nanoparticles confirm the presence of amino groups, i.e., the N–H bending vibration of primary amines is observed at *ca.* 1650 cm⁻¹, see Figure 6-2 and a characteristic weak, broad band appears at *ca.* 1500 cm⁻¹. Furthermore, a peak at *ca.* 940 cm⁻¹, assigned to the stretch vibration band of Ti–O–Si, indicates that the condensation reaction between the APTES silanol groups and the hydroxyl groups on the surface of the titanium dioxide nanoparticles has indeed occurred.[171]
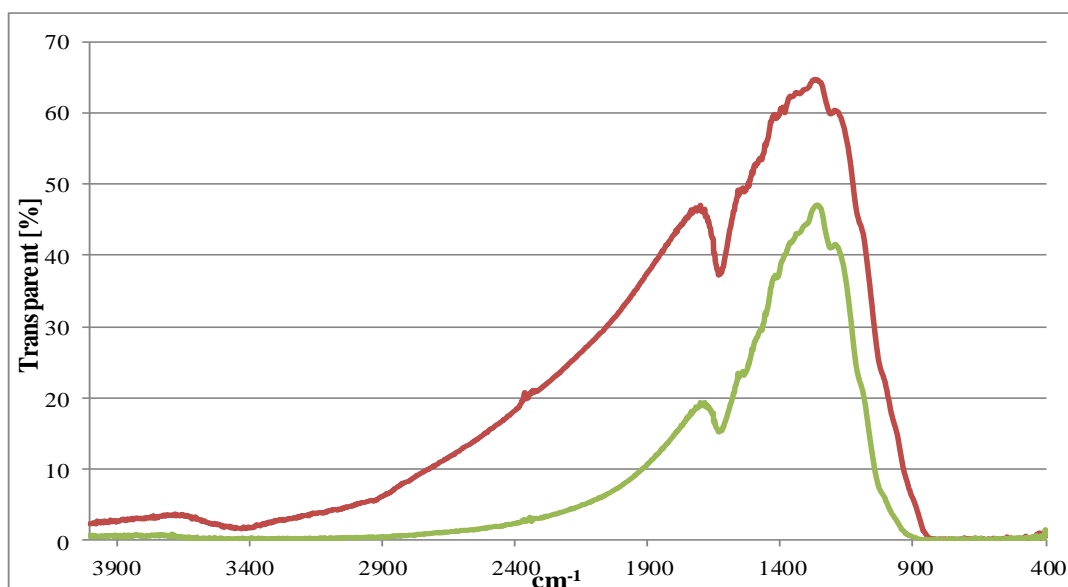
Figure 6-2: Infrared spectra of samples SMS038A-heated at 110 ºC for 6 hours (a), SMS038B- after heating at 110 ºC for 22 hours (b).
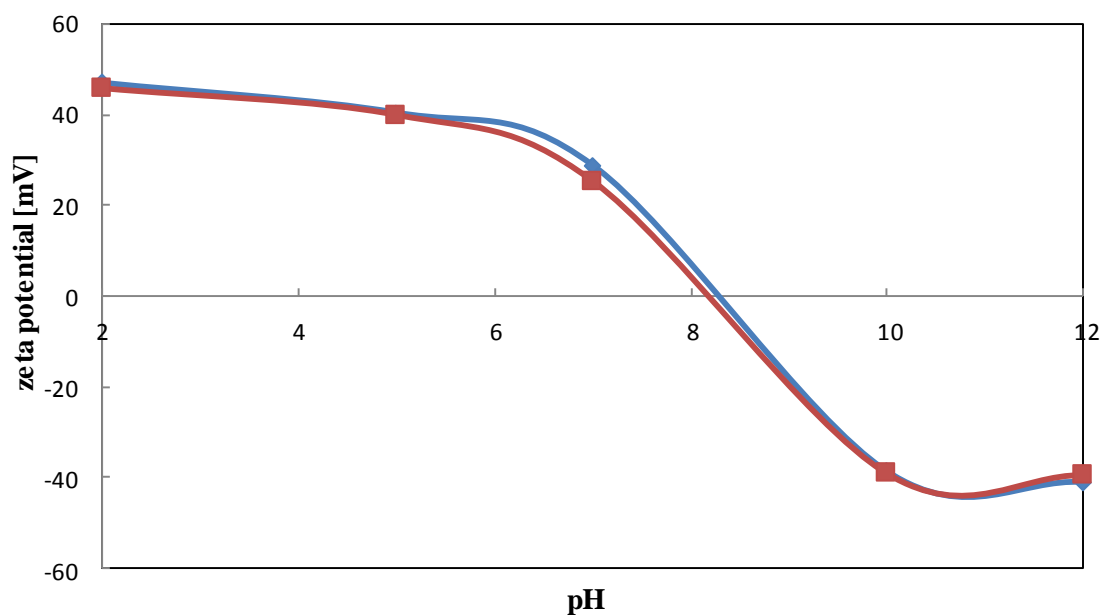
Figure 6-3: Zeta potential at different pH for non-functionalized (TiO$_2$-P25), amine-functionalized (TiO$_2$-P25-APTES).

Electrophoresis measurements were used to obtain the electrophoretic mobility and isoelectric point (IEP) of the TiO$_2$-P25-APTES nanoparticles. Figure 6-3 shows the variations of zeta potentials with pH values for the titanium dioxide nanoparticles and APTES-treated

TiO$_2$-P25 nanoparticles. The variations give an IEP at pH = 8.15 for the titanium dioxide nanoparticles and pH = 8.1 for the APTES-treated TiO$_2$-P25 nanoparticles. This behaviour shows a similar trend with that reported in the literature.[74] It is possible that the presence of the 3-aminopropylsilane groups coating the surface of the titanium dioxide nanoparticles has increased the electrophoretic mobility and shifted the IEP to a similar value to that observed for bulk titanium dioxide.

6.2.2 Stability of APTES-treated TiO$_2$ Nanoparticles

The stability of the TiO$_2$-P25 nanoparticles in aqueous sodium hydroxide solutions with pH = 12 was determined as not exceeding one hour.

Table 6-1: The stability of titanium dioxide nanoparticles in CMC colloidal solutions.

Time (min.)	SMS038A 20 mg 1% CMC PH=3-4	SMS038A 20 mg 1% CMC PH=2	SMS038B 10 mg 1% CMC PH 3-4	SMS038B 10 mg 1% CMC PH=2
60	Colloid Precipitate	Colloid precipitate	Colloid precipitate	Colloid precipitate
120	milky clear, middle colloid and precipitate	clear solution Precipitate	milky clear, middle colloid and precipitate	clear solution Precipitate
270	milky clear, middle colloid and precipitate	clear solution Precipitate	milky clear, middle colloid and precipitate	clear solution Precipitate
1500	clear solution Precipitate	clear solution Precipitate	clear solution Precipitate	clear solution Precipitate

6.2.3 Coating

The SEM images show that the APTES-treated TiO_2-P25 -modified CP nanocomposites are coated homogeneously with TiO_2-P25-APTES nanoparticles when using the sonication method, as seen in Chapter 4 and 5. The diameter of the TiO_2-P25-APTES nanoparticles on the surface of the fibres of the CP is more than 200 nm. EDX analyses suggest that TiO_2-P25 ratios on the surface of treated CPs are close to that of titanium dioxide colloidal solutions used to coat the paper, as expected.
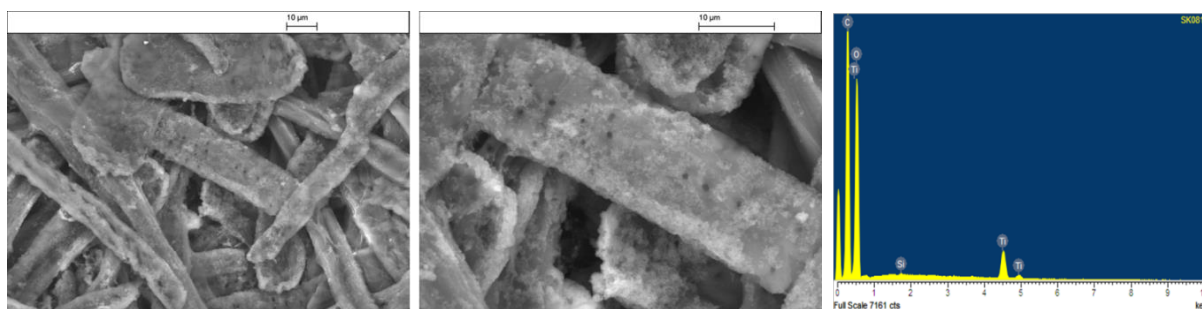
Figure 6-4: Image left: SEM image of the TiO2-APTES nanoparticles deposited in aqueous HCl solution on the paper sample SMS081B. Image right: EDX pattern of the paper sample SMS081B.

6.3   Preparation of TiO₂-P25-APTES in xylene solution

6.3.1   Preparation

Six reactions, carried out using xylene as the solvent and six different concentrations of 3-aminopropyltriethoxysilane (APTES), used as a surface modifier.

The TiO_2-P25-APTES nanoparticles prepared were investigated using FTIR analysis, as shown in Figure 6-5. The weak bands observed at 2927 and 2872 cm^{-1} can be assigned to the presence of alkyl groups [–$(CH_2)_n$–] in APTES. No obvious N–H bending vibration could be observed at *ca.* 1560 cm^{-1}, when the amount of APTES used was 0.04 mL or 0.1 mL. With increasing concentration of APTES, the intensity of the absorption band observed at 1610 cm^{-}

[1] reduces and the intensity of the absorption band observed at 1560 cm^{-1} increases. In addition, the broad absorption band observed at ca 1116 cm^{-1} is probably attributable to the Si–O–Si stretch vibration due to the condensation reaction between silanol and hydroxyl groups.
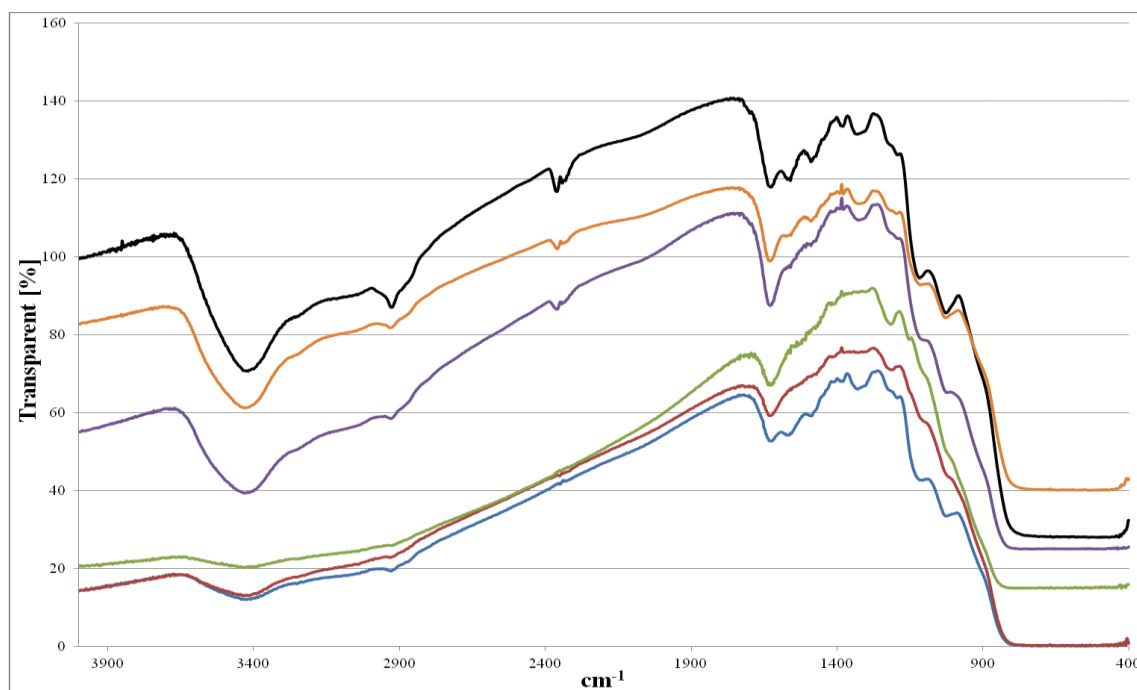
Figure 6-5: Infrared spectra of samples (orange) SMS080, (black) SMS071, (purple) SMS046B, (red) SMS055, (blue) SMS043A, (green) SMS053A.

The APTES molecules are attached onto the titanium dioxide surface through Si-O-Ti bonds, so the absorption peak observed at ca 1024 cm^{-1} can be assigned to the stretch vibration of Ti–O–Si bonds formed by the condensation reaction between silanol groups of APTES and titanium dioxide surface hydroxyl groups.[171] Although, another absorption band corresponding to Ti–O–Ti bonds generally appears ca 600–400 cm^{-1}, this peak could not be observed because these spectra (Figure 6-5) were obtained by subtraction of the IR spectrum of the original TiO_2-P25 nanoparticles.[163] The absorption band observed at 1600 cm^{-1} can be attributed to the presence of free, unreacted hydroxyl groups (OH^{-}) anions on the surface of titanium dioxide nanoparticles.

The TEM images of the TiO_2-P25-APTES nanoparticles indicate a diameter of between 10 to 50 nm similar to that of untreated TiO_2-P25 nanoparticles, as expected.
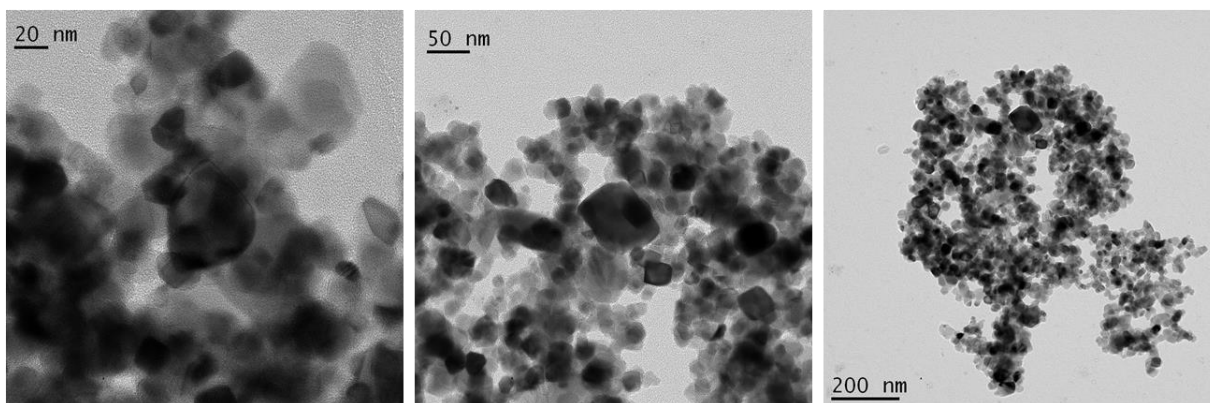
Figure 6-6: TEM image of TiO₂-P25 – APTES 3 mL (SMS080)

ethoxy-groups in APTES have been hydrolyzed and that the aminopropyl-groups are present on the titanium dioxide surface. However, the value of the BET surface area does not a show regular variation with increasing concentration of APTES in the reaction mixture. The values of the BET surface area are very similar to that ($50 \text{ m}^2\text{g}^{-1}$) determined for the untreated TiO₂-P25 nanoparticles, suggesting the APTES layer coating the TiO₂-P25 nanoparticles is very thin, e.g., a monolayer, as expected.
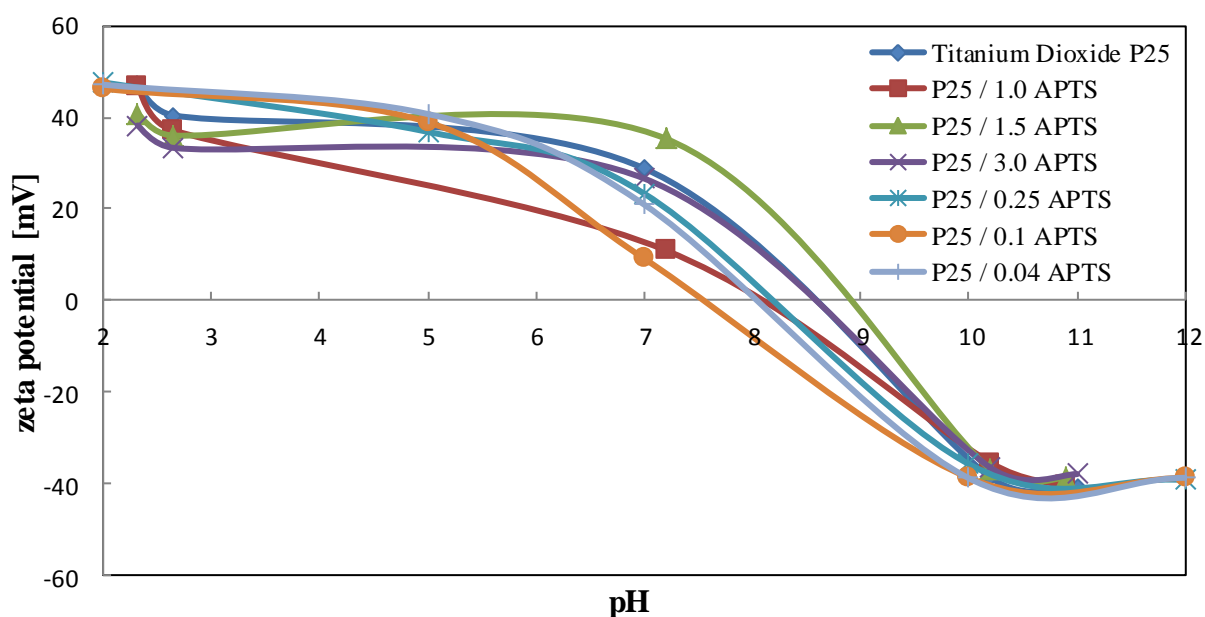
Figure 6-7: Plot of Zeta-potential *vs* pH after coating the titanium dioxide nanoparticles with different concentration of APTES.

Figure 6-7 shows the changes in the zeta potential at different pH values for the untreated titanium dioxide nanoparticles and the surface-modified TiO_2-P25-APTES nanoparticles. The variations give an IEP at pH = 8.6 for the titanium dioxide nanoparticles. After treatment with APTES, the IEP shifts, but not regularly with the increasing amounts of APTES concentration, which suggests the reaction of the hydroxyl groups present on the surface of the titanium dioxide nanoparticles may occur with either amino- or hydroxyl-groups of the APTES molecules, as shown in Figure 6-9.

The XPS spectra of the surface-modified TiO_2-P25-APTES product using the TiO_2-P25 nanoparticles and APTES (1.5 mL) are shown in Figure 6-8. Comparison with the standard spectrum of TiO_2-P25 nanoparticles (Figure 6-8A), the new peaks of N 1s and Si 2p observed in the spectrum of TiO_2-P25-APTES nanoparticles clearly indicate that APTES molecules have been grafted onto the titanium dioxide surface.

Figure 6-8B – Figure 6-8F show the high-resolution spectra of C 1s, O 1s, Si 2p, N 1s and Ti 2p. The three peaks at 284.41, 286.04 and 288.15 in the C 1s spectrum of TiO_2-P25 are from CHx, C–O and C=O bonds respectively, indicating the presence of hydrocarbon contamination on the titanium oxide surface.[172] After APTES modification, there are also three peaks at 284.84, 286.20 and 288.16 in the C 1s spectrum of the APTES-modified titanium dioxide nanoparticles, which can be attributed to CHx + C–C + C–Si, C–N + C–O and C=O respectively, although the peak positions are similar to those observed for the original, unreacted TiO_2-P25 nanoparticles. A new peak at 532.13 eV, ascribed to O-Si-R, is observed in the O 1s spectrum after APTES modification.

The presence of a sharp peak at 102.13 eV in the Si 2p clearly indicates the attachment of APTES on the titanium dioxide surface. Since the silicon is present in APTES, it can be seen that from the relative atomic percentage of silicon to titanium, 17.2 % of elemental silicon is present in the APTES-modified TiO_2-P25 nanoparticles.

After APTES modification, three peaks are observed in the N 1s spectra at 339.18, 400.61 and 401.61 eV. The peak at 339.18 can be assigned to free terminal NH_2 groups on APTES, whereas the peaks at 400.61 and 401.61 are possibly indicative of the presence of hydrogen bonded amino-groups or protonated amines, such as $–NH_3^+$.
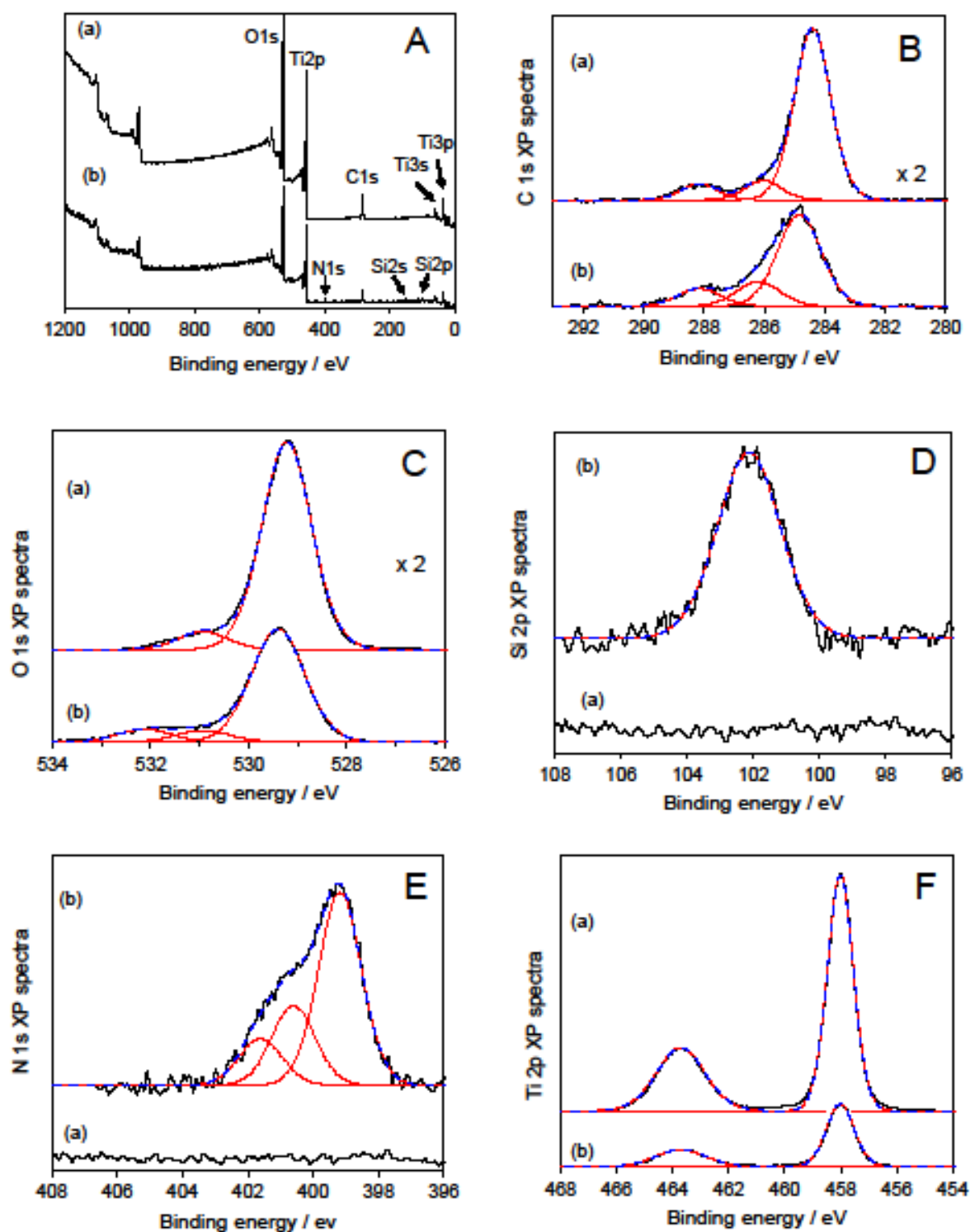
Figure 6-8: (A) XPS survey spectra and (B) C 1s, (C) O 1s, (D) Si 2p, (E) N 1s and (F) Ti 2p high-resolution spectra of (a) commercially available, untreated TiO$_2$-P25 nanoparticles and (b) APTES-modified TiO$_2$-P25 nanoparticles.

Table 6-2: XPS surface analysis of TiO₂-P25 and APTES (1.5 mL) modified titanium dioxide nanoparticles.

	titanium dioxide		titanium dioxide APTES	
	Binding energy/eV	%	Binding energy/eV	%
Ti 2p	458.00		458.00	
O 1s	529.23	92.01	529.40	82.03
	530.94	7.99	530.93	8.63
			532.13	9.34
C 1s	284.41	82.70	284.84	68.33
	286.04	9.44	286.20	18.51
	288.15	7.86	288.16	13.17
N 1s			399.18	60.42
			400.61	24.92
			401.61	14.67
Si 2p			102.13	

The possible interactions of APTES with the titanium dioxide nanoparticle surface are shown in Figure 6-9.[173, 174] If the silane groups react with the hydroxyl groups on the titanium dioxide surface to form a silanized surface, as shown in Figure 6-9 (a-d), the free terminal amino-groups which is away from the titanium dioxide surface can be observed at 399.18 eV (normal attachment). One the other hand, if amino-groups are attached to the surface of the titanium dioxide nanoparticles through hydrogen bonding or by coulombic interaction between the hydroxyl groups and protonated amines, such as $-NH_3^+$, as shown in Figure 6-9 (e) and (f), the N 1s peak will appear at higher energy ($\sim$ 400.9 eV) (reverse attachment).

Since the contribution of the peak at 399.18 eV is 60.42 % and is much higher than that of the peaks at 400.61 eV (24.92 %) and 401.61 (14.67 %), it seems reasonable to conclude that APTES is mainly attached by silanized bonding with the free terminal NH_2. The Si:N ratio is 0.9, close to 1:1 ratio of Si:N present in ATPES molecules.

Table 6-3: XPS surface elemental analysis for APTES-modified TiO₂-P25 nanoparticles.

Sample	Atomic %							
Elements	Ti 2p	O 1s	C 1s	N 1s	Si 2p	C:Si	Si:N	O:Ti
TiO₂ P25	23.34	55.32	21.34					2.37
SMS043A	15.42	54.34	23.26	3.54	3.43	6.78	1	3.52
SMS046B	19.89	55.32	17.71	3.54	3.53	5.02	1	2.78
SMS053A	23.33	57.08	14.28	2.59	2.72	5.25	1.1	2.45
SMS055	22.26	57.75	14.41	2.81	2.77	5.2	1	2.59
SMS071	18.88	51.14	23.16	3.56	3.25	7.13	0.9	2.71
SMS143	19.16	51.69	20.33	5.04	3.77	5.39	0.7	2.7

The C:Si ratio of APTES molecule is 9:1. If all the ethoxy groups had been hydrolysed, the C:Si ratio should be 3:1. However, the C:Si ratio of the APTES-modified titanium dioxide nanoparticles is 7:1, indicating that some ethoxy groups on the Si-O tails are still retained on the surface-grafted APTES. Thus, most of the silane coupling reactions between APTES and titanium dioxide should form monodentate and bidentate bonds, see Figure 6-9 (a&b), which is similar to the behaviour reported previously.[101, 172, 175]

Figure 6-9: Possible surface interactions and potential modes of chemical bonding between the hydroxyl-moieties present on the surface of titanium dioxide nanoparticle and APTES molecules.

6.3.2   Preparation sample for UV/Vis evaluation.

The photo-catalytic activity of the TiO_2-P25 nanoparticles and that of the APTES-modified TiO_2-P25 nanoparticles was tested by adding samples of the untreated and treated-P25 titanium dioxide nanoparticles to a Rhodamine solution followed by UV-irradiation of the resultant solutions at 365 nm for 30 min.

Figure 6-10: UV/Vis spectra for different concentrations of Rhodamine B in 20 mL of water, (green) 0.125 mL, (blue) 0.1 mL, (red) 0.075 mL, (yellow) 0.05 mL, (dark green) 0.02 mL, (pink) 0.01 mL.

The concentration of the Rhodamine B in solution is 20 mg/L. Different volumes of the Rhodamine B solution were dissolved in 2 mL of water and then their UV absorption determined, see Figure 6-10. The concentration of Rhodamine B was then calculated as shown in Figure 6 10.

$$\text{Rhodamine B concentration} = \frac{(mL) \text{ Rhodamine B solution} \times 10^{-3} \times 20 \frac{mg}{L}}{(2 \text{ mL water} + \text{ mL Rhodamine B solution}) \times 10^{-3}}$$

Figure 6-10 indicates that the standard curve is good enough for analysis. Figure 6-11A is the UV-vis spectra of the Rhodamine B solutions after being treated with TiO_2-P25-APTES nanoparticles under UV-illumination.

Table 6-4: The concentration of Rhodamine B *vs* the UV/Vis absorbance in Figure 6-11B as determined from Figure 6-11A.

Rhodamine B [μL]	Rhodamine B concentrate in Cuvette X [mg/L]	Absorbance Y [A°]
0	0	-
10 (0.01 mL)	0.099	0.167
20 (0.02 mL)	0.195	0.282
50 (0.05 mL)	0.488	0.629
75 (0.075 mL)	0.723	0.915
100 (0.1 mL)	0.963	1.212
125 (0.125 mL)	1.176	1.528
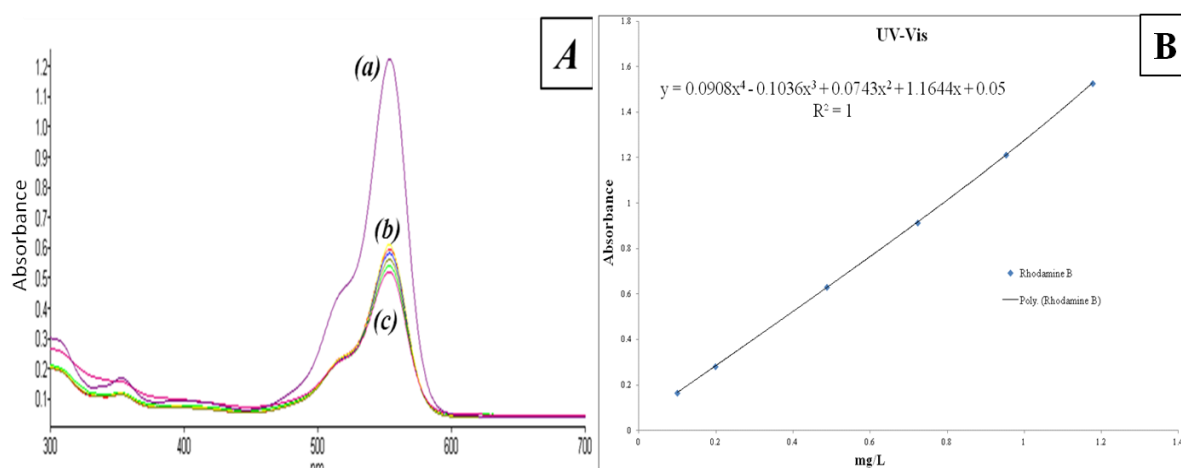
Figure 6-11: Left; UV-vis transmittance curve of (a) original Rhodamine B, (b&c) mixture of Rhodamine B with different sample of TiO₂/APTES. (b) SMS080, (c) TiO₂-P25. Right; diagram of UV/Vis of original Rhodamine B with different concentration.

The degree of degradation of Rhodamine B treated with TiO2/APTES after UV-illumination calculated from Figure 6-11A and Figure 6-11B is shown in Table 6-5 and Figure 6-13.

Table 6-5: The concentration of solutions prepared for UV/Vis spectra calculated from Figure 6 11 and Figure 6-13.

UV/Vis solutions	Absorbance Y	X Which was put in equation and be found from Figure 6-11B [mg/L]	Concentration of samples [(0.963-X)/0.963]	Percent of Rhodamine B degraded
SMS080	0.6009	0.4649	0.5173	51.73
SMS071	0.5980	0.4625	0.5198	51.98
SMS043A	0.5854	0.4521	0.5306	53.06
SMS055	0.5629	0.4333	0.5501	55.01
SMS053A	0.5423	0.4161	0.5679	56.79
P25	0.5230	0.3999	0.5846	58.46

Table 6-5 and Figure 6-13 show that 58.5% of the Rhodamine had been degraded in contact with TiO_2-P25 nanoparticles for 30 min of UV-irradiation. The percent of Rhodamine B degraded decreases with increasing concentration of APTES. The reduction of photocatalytic activity with increasing in amount of APTES further supports the assumption of the formation of a monolayer of APTES on the surface of the TiO_2-P25 nanoparticles.

Figure 6-12: mixture of TiO$_2$/APTES and Rhodamine B samples observed under illumination with UV light.
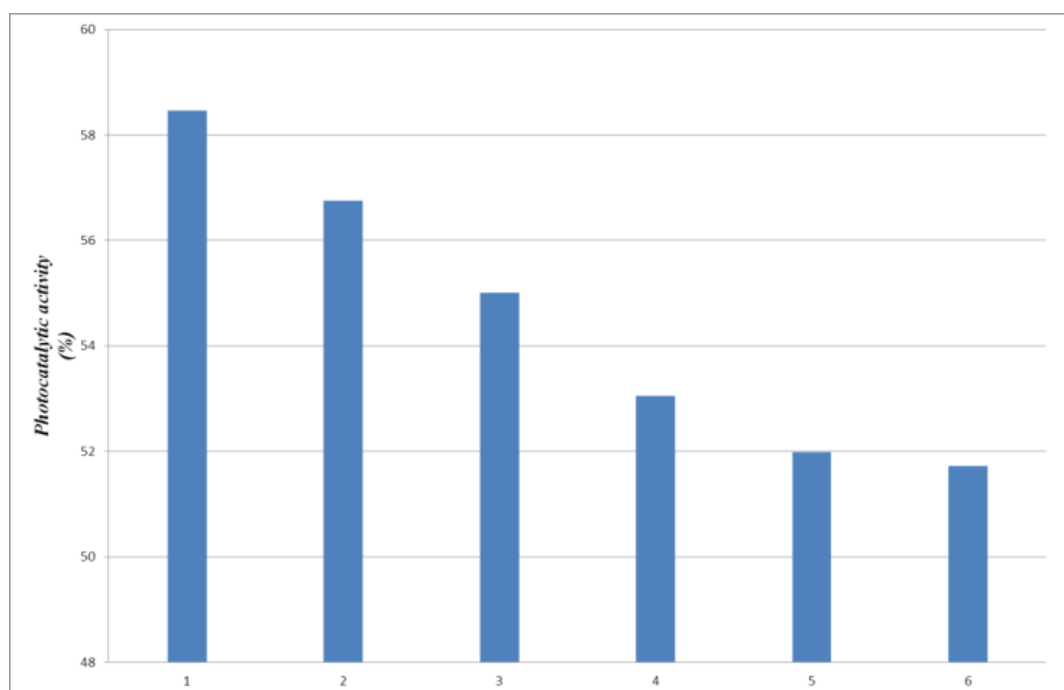
Figure 6-13: Distribution of concentration [mol/L] of samples (1) TiO$_2$-P25, (2) SMS053A, (3) SMS055, (4) SMS043A, (5) SMS071, (6) SMS080.

6.3.3 Coating

Surface modification of commercially available TiO_2-P25 nanoparticles with APTES was also carried out in *o*-xylene. [173] Besides the reaction between the silane groups of APTES and the hydroxyl groups on the surface of the titanium dioxide nanoparticles, the amino-groups of APTES also interact with the free hydroxyl-groups present on the titanium dioxide surface, which results in a higher number of surface-functional groups (N_R).

A simple dip-coating procedure has been successfully applied to attach APTES-modified, commercially available TiO_2-P25 nanoparticles onto the surface of standard, commercial uncoated paper samples. The presence of free terminal amino-groups and hydrolysable silane groups in the TiO_2-P25-APTES nanoparticles contributes to the attachment of titanium dioxide onto the negatively charged surface of the constituent cellulosic fibres of the test paper samples. The presence of the APTES monolayer-coating between the titania nanoparticles and the organic (readily oxidised) surface of the cellulose fibres effectively inhibits the strong UV-catalysed photo-catalytic degradation effect of the titania nanoparticles.

The XRD of the white powder samples of CP/TiO_2-P25-APTES nanocomposites isolated from all the solutions prepared using this method are similar to those prepared using *para*-xylene, see previous section. A strong cellulose peak at $2\theta = 23°$ and weak peaks characteristic of TiO_2-P25 nanoparticles can be observed in the XRD pattern after coating the CP samples with the APTES-modified titanium dioxide nanoparticles. The XRD results confirm the presence of the TiO_2-P25 nanoparticles on the surface of the CP samples, although typical peaks for the rutile phase of titanium dioxide could not be observed in the XRD spectrum.
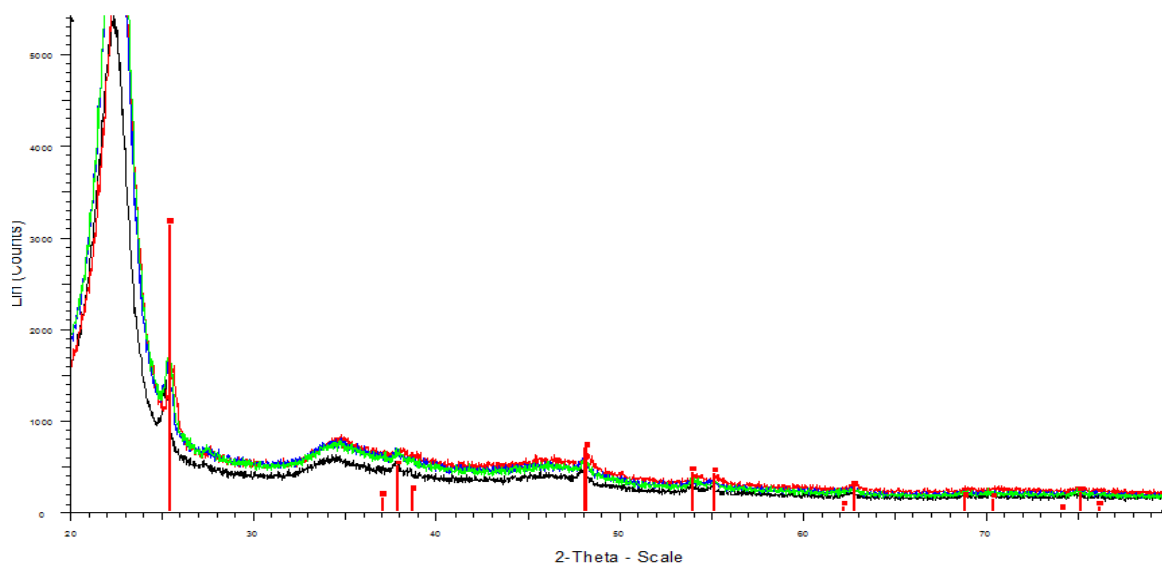
Figure 6-14. XRD pattern of SMS076A (black), SMS076B (red), SMS072A (green), SMS072B (blue) samples.
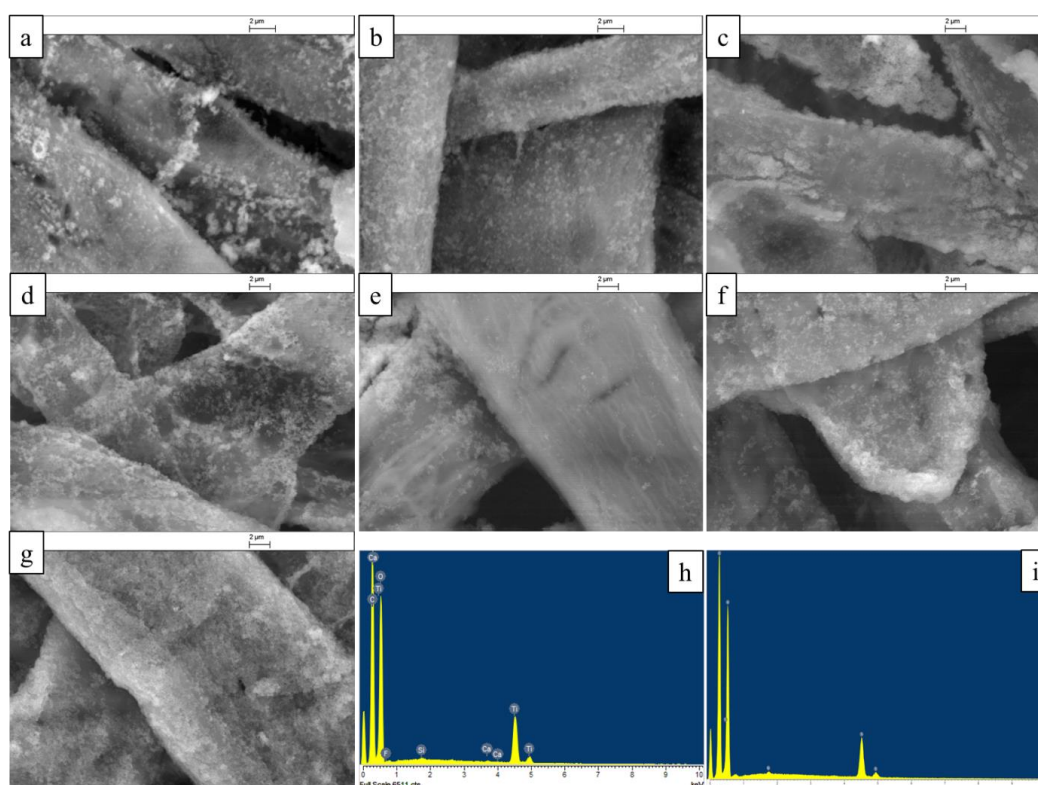
Figure 6-15: SEM of coating TiO2-P25-APTES nanoparticles in xylene solution samples of (a) SMS072A, (b) SMS072B, (c) SMS86B, (e) SMS86C, (e) SMS86D, (f) SMS86E, (g) SMS86H and EDX pattern of sample (h) SMS86B and (i) SMS072A.

The SEM images show that the surfaces of the cellulose fibres are covered with titanium dioxide particle with a diameter of about 200 nm. The nanoparticles diameter for the samples with a long heating time is larger than that after sonication of the paper samples in the colloidal solutions of nanoparticles without heating. The surface coating of the paper samples treated with additional sonication is more homogeneous than that observed for the paper samples prepared under the heating without sonication. Unfortunately, the coating on the surface of the sample prepared using 3.0 mL APTES is very thick and not very homogenous. . However, a very thin, uniform film of TiO$_2$-P25-APTES nanoparticles can be observed on the surface of fibres of cellulose coated with the colloidal solutions of TiO$_2$-P25-APTES nanoparticles prepared using 0.1 mL solutions of APTES.
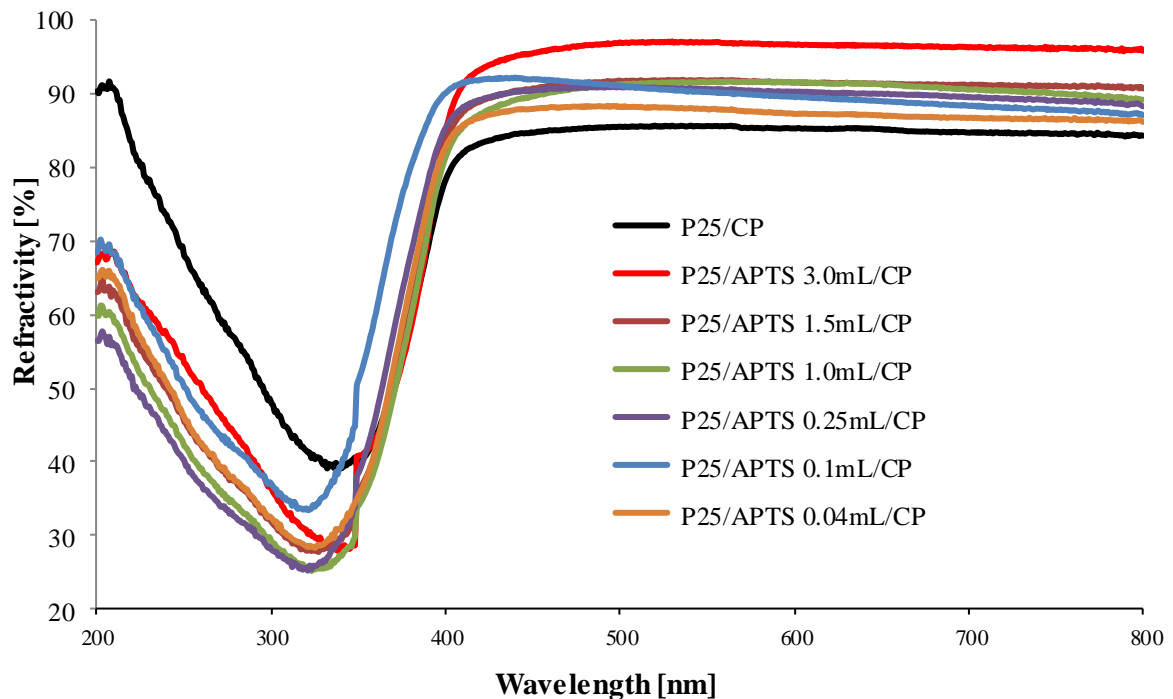
Figure 6-16: UV-Vis transmittance curves of the original TiO$_2$-P25 nanoparticles and samples modified with APTES after press coated cellulosic papers.

The UV-vis transmittance curves of TiO_2-P25 and APTES-modified-TiO_2-P25 nanoparticles are shown in Figure 6.16. In order to reduce the effect of the rough surface and thickness of the paper sample, all the samples were compressed at 10 tons of pressure for 5 min before the UV-test. The results show that TiO_2-P25-APTES is more refractive than TiO_2-P25 and that, with an increase in the APTES concentration in the reaction, the refractivity of the TiO_2-P25-APTES sample increases.

Table 6-6: TiO₂/APTES nanoparticles results.

Sample	APTES [mL]	Concentration [mol/L]	BET Surface Area [m²/g]	CHN C/N (%)	pH which have IEP	ICP Si/Ti Powder	ICP Si/Ti coating CP
SMS053A	0.04	0.0034	46.60	4.4	8.3	0.12	0.18
SMS055	0.1	0.0086	46.70	3.6	7.6	0.18	0.22
SMS046B	0.25	0.0215	48.08	2.4	8.2	0.17	0.22
SMS043A	1.0	0.0860	45.49	2.2	8.1	0.19	0.23
SMS071	1.5	0.1291	47.50	2.1	8.9	0.19	0.24
SMS080	3.0	0.2582	47.97	3.3	8.6	0.21	0.25

The ICP results confirm the concentration of elemental Si/Ti, after coating nanoparticles on CP surface, is not very different from that of the TiO_2-P25-APTES nanoparticles, as expected. The molar ratio of carbon to nitrogen (C/N) varies from 2.1 to 4.4, suggesting most of the

ethoxy-groups in the hydrolysed APTES and the aminopropyl-groups remain on the titanium dioxide surface. However, the BET surface area does not show regular changes with increases in the concentration of APTES as explained above.
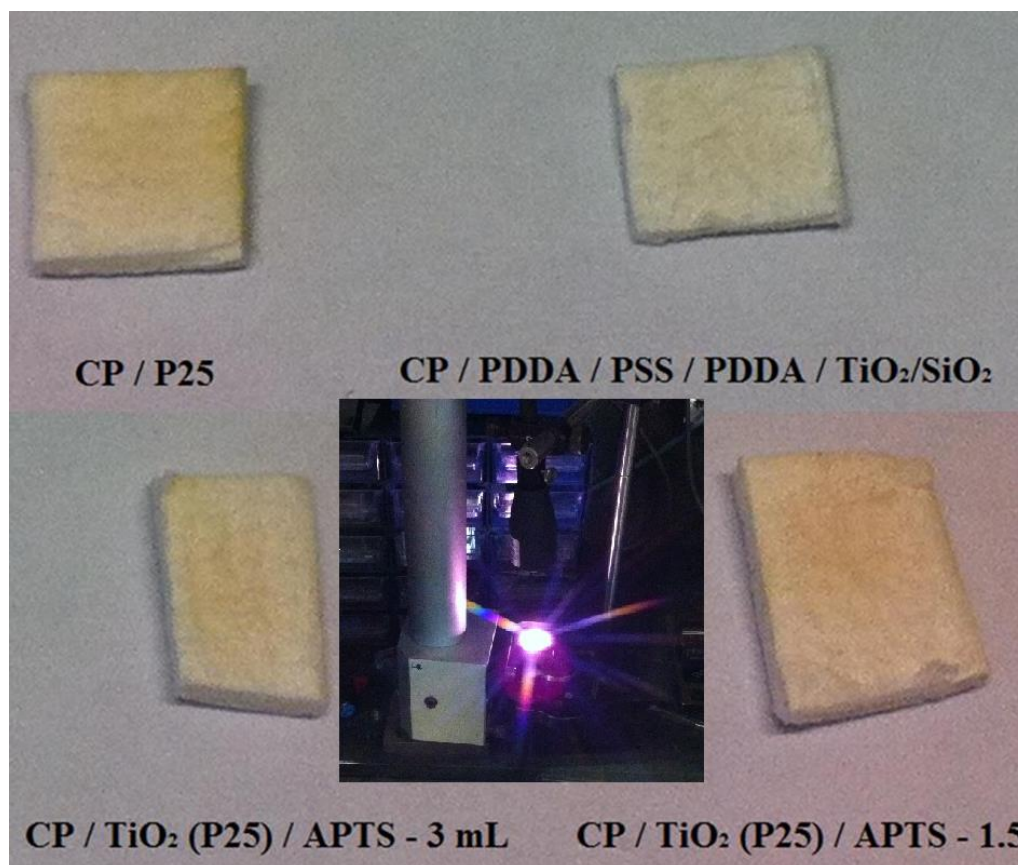
Figure 6-17: Photo-catalytic stability of different coating CP under UV light.

In order to compare the degree of photochemical stability of the TiO_2-P25-APTES nanoparticle/ CP nanocomposites were exposed to UV-light using an Omni Cure series 1000 instrument for 30 min. The results illustrate the fact that CP coated with TiO_2-P25-APTES nanoparticles is more stable than those coated TiO_2-P25 nanoparticles or the reference blank paper. Furthermore, the degree of photo-degradation appears to decreases with the increasing of the concentration of APTES used to coat the highly photo-chemically active, commercial TiO_2-P25-APTES nanoparticles.

6.3.4 Brightness and whiteness of cellulosic paper
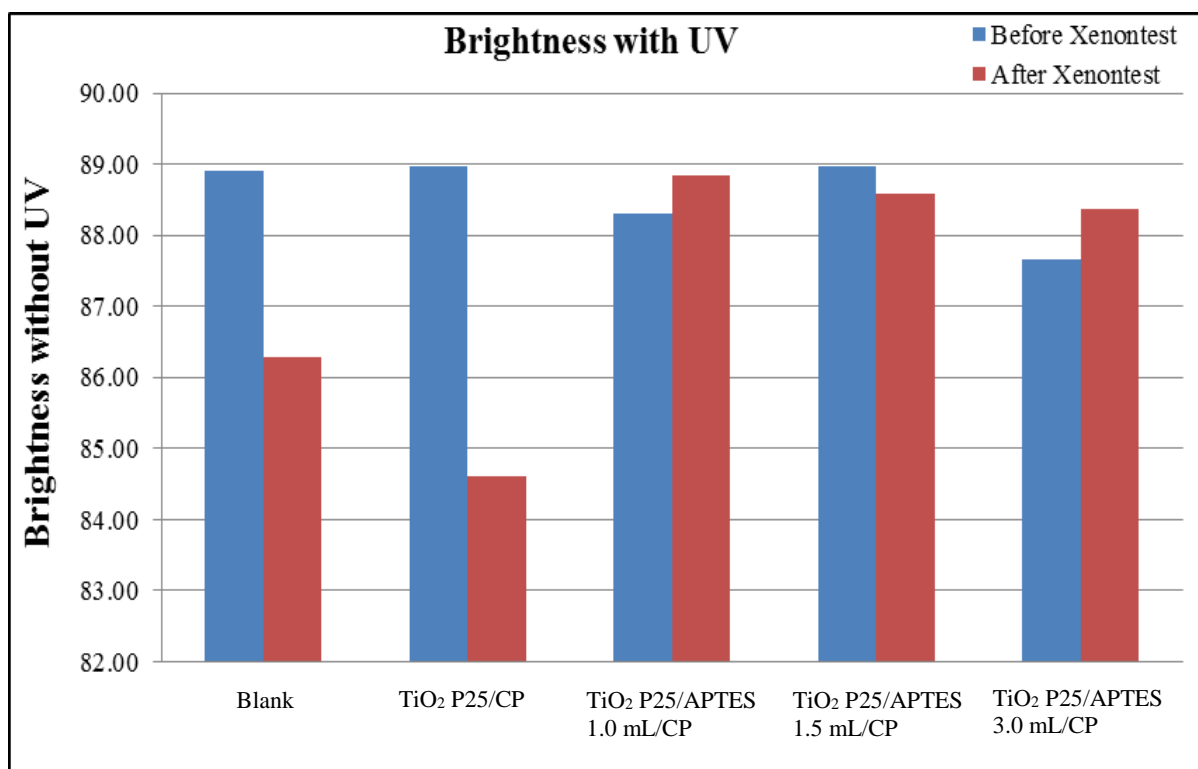
Figure 6-18: ISO-brightness of blank reference paper and the paper samples coated either with untreated TiO₂-P25 nanoparticles or APTES-modified TiO₂-P25 nanoparticles before and after the UV-stability test.

Figure 6-18 shows the ISO-brightness determined for the blank reference paper and the paper samples coated either with untreated TiO$_2$-P25 nanoparticles or APTES-modified-TiO$_2$-P25 nanoparticles, before and after illumination with UV-light in the standard xenon UV-stability test. It can be seen that the brightness of the blank paper reference is sharply reduced after illumination with UV radiation in the standard xenon test. The reduction in brightness is even more significant for the paper samples coated with untreated TiO$_2$-P25 nanoparticles. In contrast, there is only a marginal reduction in the brightness of the paper samples coated with the TiO$_2$-P25-APTES-nanoparticles. It seems reasonable to assume that the small reduction in the brightness of the TiO$_2$-P25-APTES-nanoparticle coated paper sample after the xenon UV-test is attributable to the fact that the photo-catalytically active TiO$_2$-P25 nanoparticles have

been coated effectively with a thin, inert layer of APTES, which passivates their surface and thereby inhibits their inherent photo-catalytic activity.
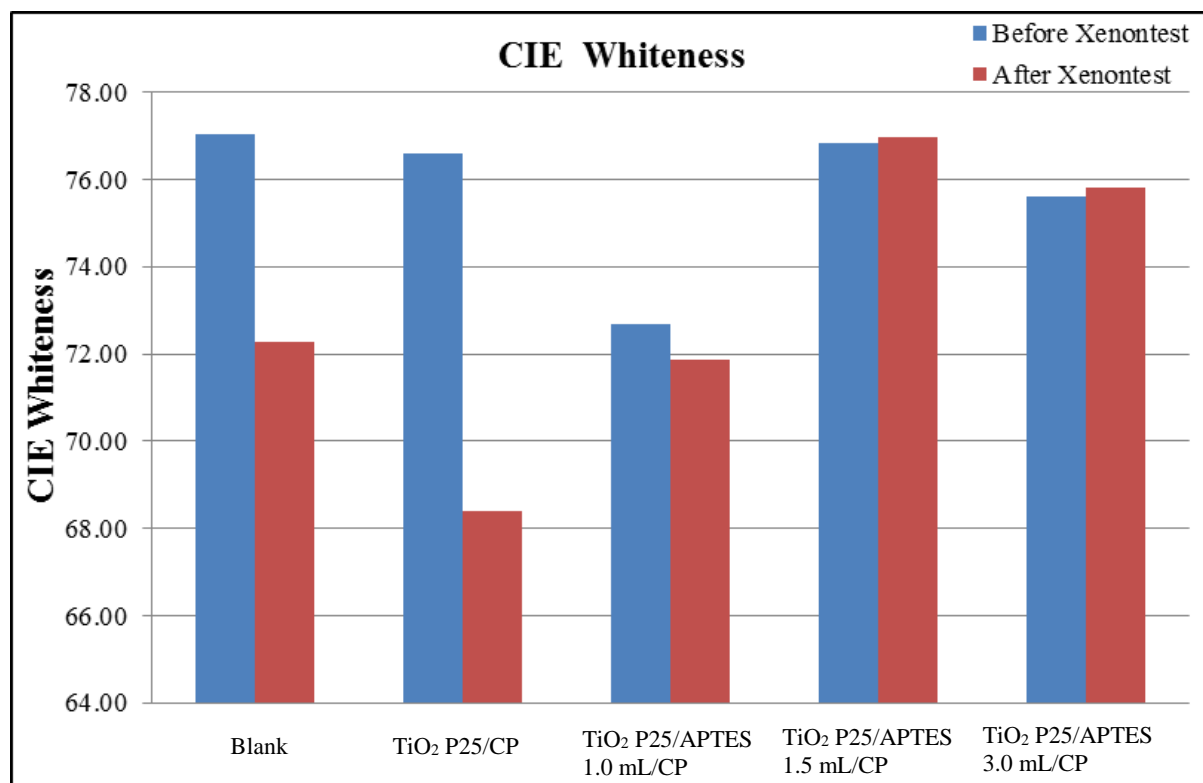
Figure 6-19: CIE whiteness of blank reference paper and the paper samples coated either with untreated TiO₂-P25 nanoparticles or APTES-modified-TiO₂-P25 nanoparticles before and after the UV-stability test.

The value for the CIE-whiteness of the CP coated with APTES-modified-TiO₂-P25 nanoparticles is slighter higher than that of either the blank paper reference and that of the TiO₂-P25-nanoparticle-coated paper sample. In contrast to the sharp reduction in the whiteness of the blank paper reference sample and the-P25 titanium dioxide nanoparticle coated paper sample, no reduction in whiteness can be observed for the paper coated with the APTES-modified-TiO₂-P25 nanoparticles, after the standard xenon UV-stability test.

6.4 TiO₂-RP-APTES nanoparticles

6.4.1 Analysis
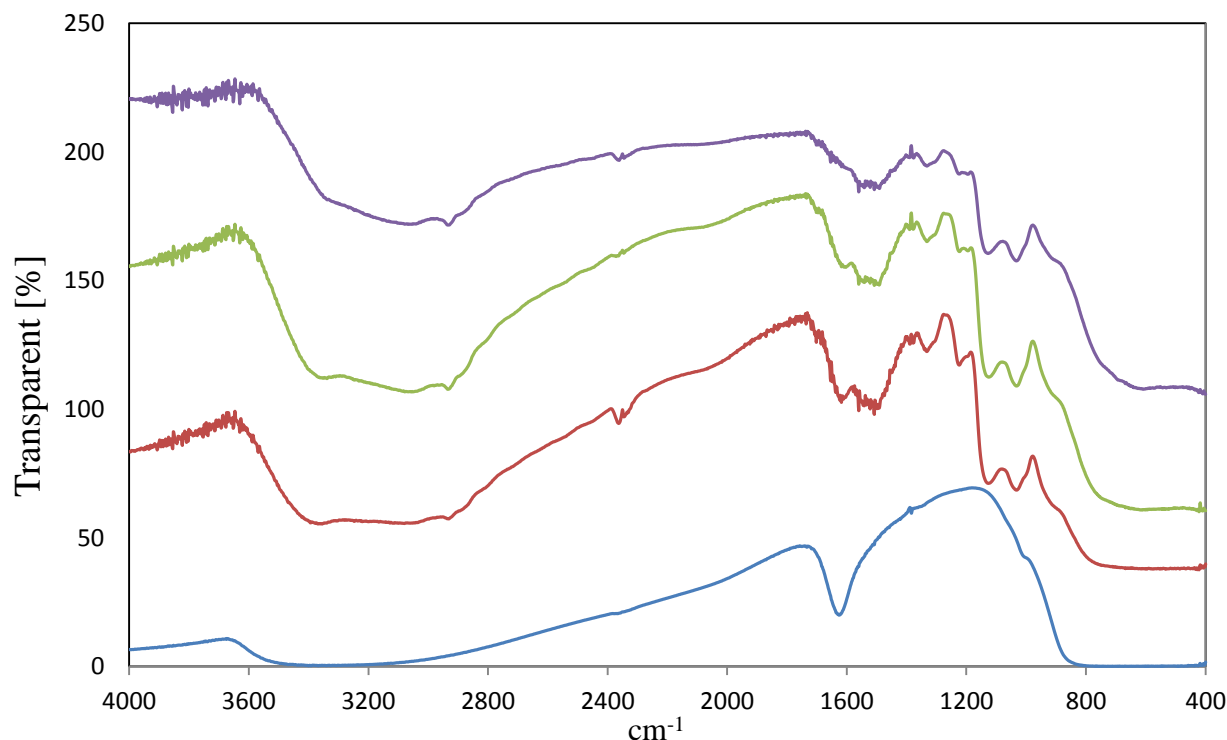
Figure 6-20: Infrared spectra of samples titanium dioxide (blue), TiO₂-RP-APTES 1mL (red),TiO₂-RP-APTES 1.5mL (green), TiO₂-RP-APTES 3mL (purple).

The TiO$_2$-RP-APTES nanoparticles, prepared using this method, see experimental part, were investigated using FT-IR analysis. The IR spectra of the TiO$_2$-RP-APTES nanoparticles are shown in Figure 6-20. The weak bands at 2927 and 2872 cm^{-1} can be assigned to alkyl groups [–(CH$_2$)$_n$–] present in the APTES monolayer coating.

The amino-groups are ionized in water and separated by the compensating negative charge of ionised hydroxyl-groups (OH$^-$) and by the presence of a cloud of screening water molecules. The band at 1600 cm^{-1} is attributable to ionised hydroxyl-groups present on the surface of the titanium dioxide nanoparticles. The concentration of ionised hydroxyl-groups groups in TiO$_2$-RP-APTES nanoparticles is less than that present in the titanium dioxide powder. The CP

surface also has ionised hydroxyl-groups bonds to which the TiO_2-RP-APTES nanoparticles can bond.

The amino-groups of APTES also appear to have chemically interacted with the titanium dioxide surface, which results in a higher number of surface functional groups (N_R) and so an N–H bending vibration could also be observed at ca 1510 cm^{-1}.

With increasing concentration of APTES, the intensity of the absorption band at 1610 cm^{-1} decreases and the intensity of the band at 1510 cm^{-1} increases. The APTES molecules are attached to the titanium dioxide surface through Si-O-Ti bonds, so the peak at *ca.* 1050 cm^{-1} can be assigned to the stretch vibration of Ti–O–Si[171] formed by the condensation reaction between the silanol groups of APTES molecules and titanium dioxide surface hydroxyl-groups. In addition, the broad band at *ca.* 1150 cm^{-1} is probably attributable to the stretch vibration of Si–O–Si bonds resulting from the condensation reaction between adjacent silanol groups.

Although the band corresponding to the Ti–O–Ti bond generally appears *ca.* 600–400 cm^{-1}, this peak could not be observed, because these spectra were obtained by subtraction of the original rutile titanium dioxide spectrum.[163,173]

All these facts suggest that APTES is attached to the titanium dioxide surface especially when higher amounts, such as 3.0 mL, were used. The BET surface area of the titanium dioxide nanoparticles is lower after they were modified with APTES, suggesting the presence of a monolayer of APTES on the titanium dioxide surface.
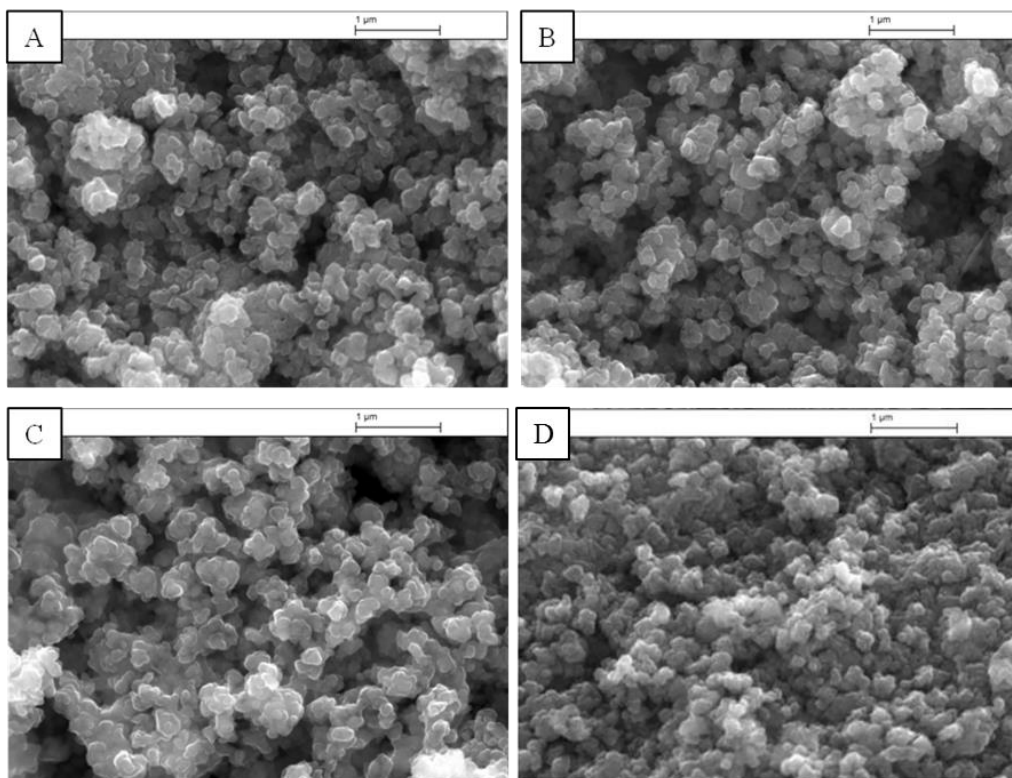
Figure 6-21: SEM images of TiO$_2$-RP-APTES nanoparticles (a) 1 mL APTES, (b) 1.5 mL APTES, (c) 3 mL APTES and (d) TiO$_2$-RP nanoparticles.
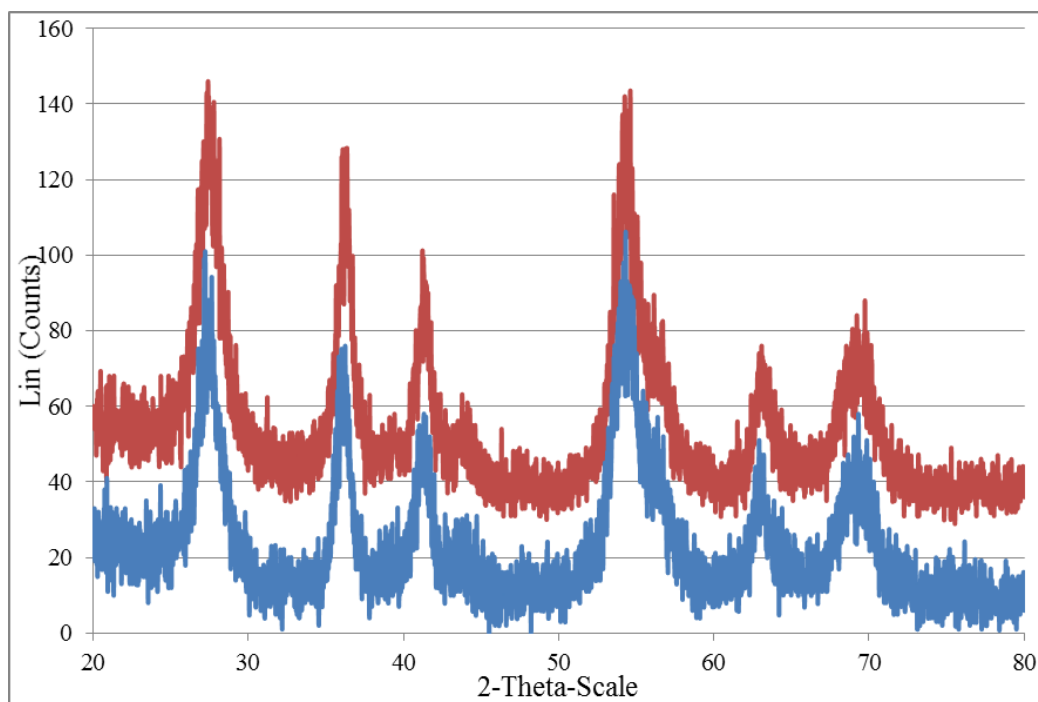
Figure 6-22: XRD pattern of (blue) TiO$_2$-RP, (red) TiO$_2$-RP/1mL APTES.

The XRD pattern of the white powders consisting of TiO$_2$-RP-APTES nanoparticles is the same as that of rutile titanium dioxide, as expected. No peaks characteristic of silica can be observed in the XRD spectra, also as expected.
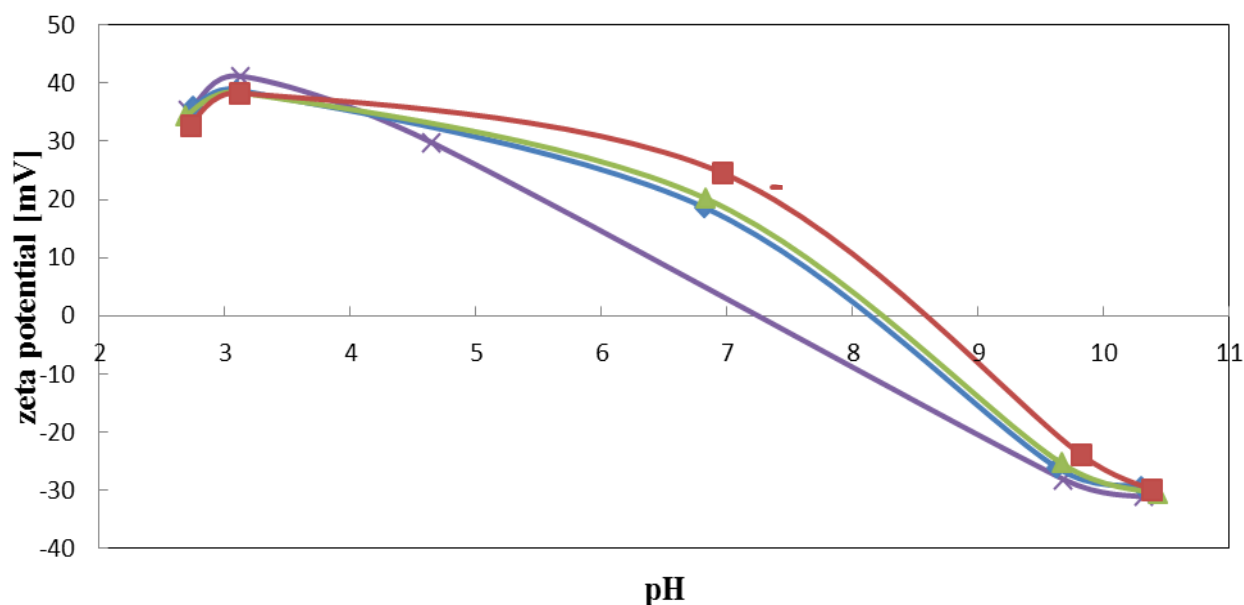
Figure 6-23: Zeta potential at different pH for TiO$_2$-RP-APTES (purple), TiO$_2$-RP, APTES 1 mL (blue), APTES 1.5 mL (green), APTES 3 mL (red).

Electrophoresis measurements were used to obtain the electrophoretic mobility and isoelectric point (IEP) of the prepared nanoparticles. Figure 6-23 shows the variations of the zeta potentials with pH values for the uncoated TiO$_2$-RP nanoparticles and the modified TiO$_2$-RP-APTES nanoparticles. The Zeta-potential analysis indicates that, compared with TiO$_2$-RP, the isoelectric points (IEP) of the TiO$_2$-RP-APES nanoparticles have shifted to a higher value, indicating the presence of free amino-groups on the nanoparticle surface. This behaviour shows a similar trend to that reported in the literature.[74] It is clear that the presence of the APTES coating on the titanium dioxide nanoparticles has increased the electrophoretic mobility and shifted the IEP to similar values to those observed for the bulk, rutile TiO$_2$-RP nanopowders.
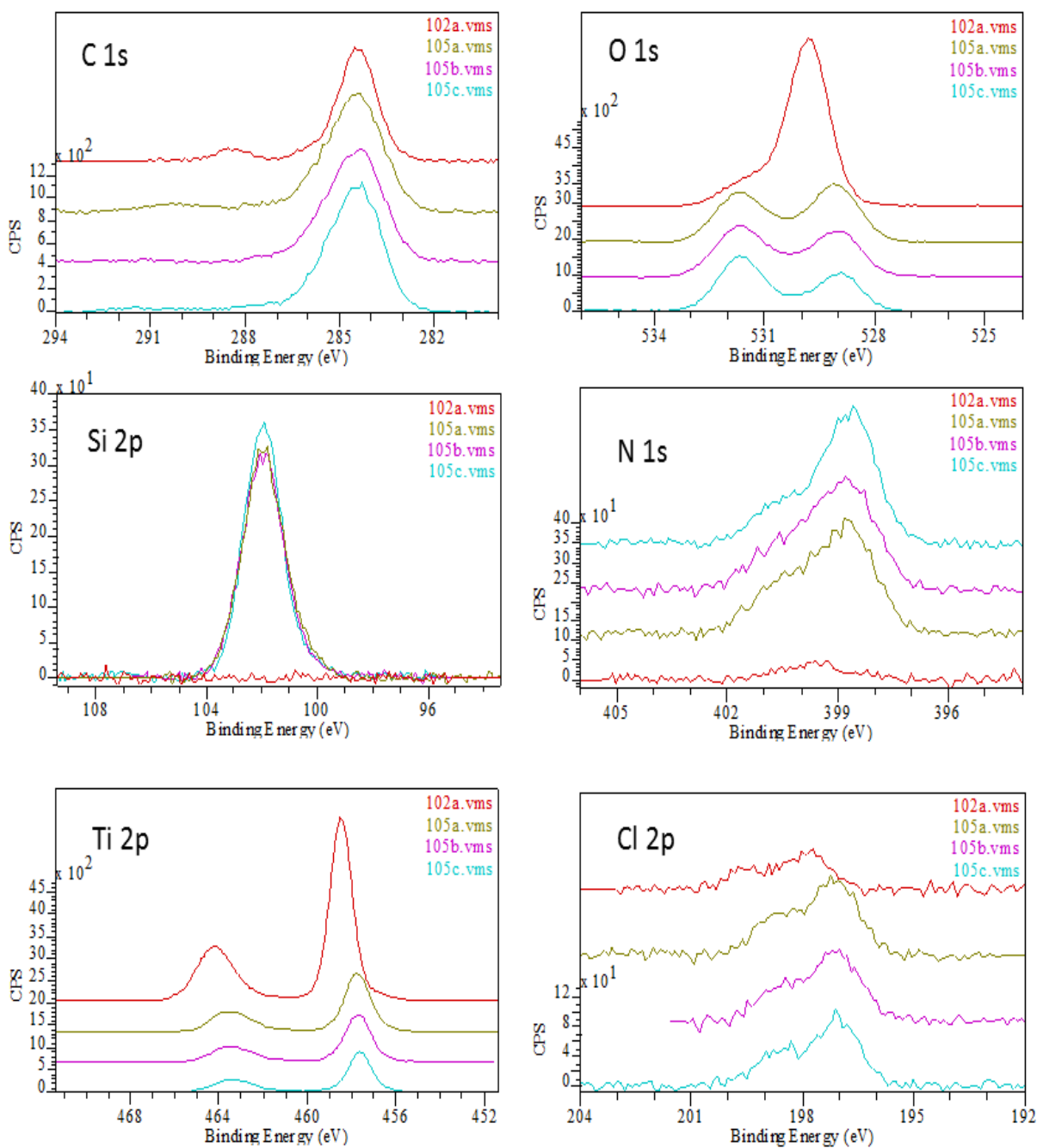
Figure 6-24: XPS survey spectra of (A) C 1s, (B) O 1s, (C) Si 2p, (D) N 1s, (E) Ti 2p, (F) Cl 2p high-resolution spectra of TiO$_2$-RP nanoparticles (red) and 1.0 mL APTES-modified TiO$_2$-RP nanoparticles (green), 1.5 mL APTES-modified TiO$_2$-RP nanoparticles (purple) and 3.0 mL APTES-modified TiO$_2$-RP nanoparticles (blue).

The XPS spectra of the TiO_2-RP and the TiO_2-RP/APTES nanoparticles are shown in Figure 6-24. The two peaks observed at 284.30 and 288.30 in the C 1s spectrum of SMS102A (TiO_2-RP) are from alkyl (CH_x) and carbonyl (C=O) moieties, respectively, indicating the presence of hydrocarbon contamination on the titanium oxide nanoparticle surface.[172]

After APTES modification of the TiO_2-RP nanoparticles, only one peak is observed at 284.30 in the C 1s spectrum of the resultant TiO_2-RP-APTES nanoparticles, which can be attributed to the presence of moieties of $CH_x + C - C + C - Si$.

In the O 1s spectrum, after APTES modification, the peak at 529.80 eV from rutile titanium dioxide disappears and two new peaks at 529.00 and 531.70 eV can be observed. The new peak at 531.70 eV can be ascribed to the presence of O-Si-R groups.

The presence of a sharp peak at 103.00 eV in the Si 2p clearly indicates the attachment of APTES onto the titanium dioxide surface. For the N 1s spectra, after APTES modification, a main peak at 398.80 with a shoulder between 400.01 and 401.60 eV can be observed. The peak at 398.80 can be assigned to free terminal amino-groups of APTES molecules bound to the nanoparticle surface by silanol bonds, whereas the peaks between 400.01 and 401.60 eV are possibly attributable to hydrogen-bonded amino-groups or protonated amines, such as ammonium moieties ($-NH_3^+$).[105]

APTES has two functional groups: hydrolysable silane groups and NH_2 group. If the silane groups react with the free hydroxyl-groups present on the titanium dioxide surface to form a silanized surface, then the free terminal amino-groups should be observed at 398.80 eV (normal attachment). On the other hand, if the amino-groups are attached to the nanoparticle surface through hydrogen bonding or coulombic attraction to protonated amines, such as ammonium groups ($-NH_3^+$) or ionic bonding with other hydroxy-groups, then the N 1s peak should appear at higher energy (reverse attachment). From the N 1s spectra, it can be seen that APTES is mainly attached by silanized bonding with free terminal amino-groups in this system.

It should be noted that for all the rutile titanium dioxide and APTES-modified titanium dioxide nanoparticles studied in this section, that weak peaks can be observed in the Cl 2p spectra. The XPS surface analysis shows that 0.91 % of chlorine is present in the rutile

titanium dioxide nanoparticles and about 1.3 % of chlorine present in the APTES-modified titanium dioxide nanoparticles. The presence of chlorine is probably a residue from the $TiOCl_2$ starting material used for the preparation of the rutile titanium dioxide nanoparticles, although the reaction product is carefully washed, to remove impurities, such as chlorine derivatives, before being dried.

Table 6-7: XPS surface elemental analysis for TiO₂-RP-APTES nanoparticles.

Sample	Atomic %							
Elements	Ti 2p	O 1s	C 1s	N 1s	Si 2p	Cl 2P	Si:N	C:N
TiO₂-RP	25.75	60.44	11.68	1.22		0.91		9.57
SMS105A	7.24	29.44	45.08	7.68	9.23	1.33	1.20	5.87
SMS105B	6.39	30.13	43.79	8.17	10.2	1.33	1.25	5.36
SMS105C	4.94	26.82	47.64	8.45	10.92	1.33	1.29	5.64

6.4.2 Stability

Aqueous colloidal solutions of TiO_2-RP-APTES nanoparticles are stable for more than one day and, as such, they are more stable than the corresponding colloidal solutions of TiO_2-P25-APTES nanoparticles.

Table 6-8: Compare stability of different TiO_2 P25 and TiO_2-RP, before and after protect with APTES.

Time	TiO_2 rutile 70 mg Water 20 mL	TiO_2-P25 70 mg Water 20 mL	SMS105A 70 mg Water 20 mL	SMS105B 70 mg Water 20 mL	SMS105C 70 mg Water 20 mL	SMS043A 70 mg Water 20 mL	SMS080 70 mg Water 20 mL
30 min.	milky white colloid	Milky white colloid	milky white colloid	milky white colloid	colloid	milky white colloid	milky white colloid
60 min.	colloid	colloid	colloid	colloid	colloid precipitate	colloid	colloid
120 min.	colloid	colloid	colloid	colloid	colloid precipitate	milky little clear, middle colloid precipitate	milky little clear, middle colloid precipitate
1200 min.	milky very little clear, middle colloid precipitate	colloid	milky little clear, middle colloid precipitate	milky little clear, middle colloid precipitate	Near to clear precipitate	Near to clear precipitate	Near to clear precipitate
2400 min.	milky little clear, middle colloid precipitate	milky very little clear, middle colloid precipitate	Near to clear precipitate	Near to clear precipitate	Clear solution Precipitate	Near to clear precipitate	Near to clear precipitate

154

6.4.3 Preparation of samples for UV/Vis analysis

The Rhodamine B concentration in solution is 20 mg/L. In Figure 6-10 different amounts of Rhodamine B solution were added to 2 mL of water and the resultant solutions were put in the Civet instrument for UV measurement. The concentration of Rhodamine B in the cuvette is shown in Table 6-9.

$$\text{Rhodamine B concentrate in Cuvette} = \frac{(mL)\ Rhodamine\ B\ solution \times 10^{-3} \times 20\frac{mg}{L}}{(2\ mL\ water +\ mL\ Rhodamine\ B\ solution) \times 10^{-3}}$$

Table 6-9: Concentration of Rhodamine B, calculated from Figure 6-25.

Rhodamine B [µL]	Rhodamine B concentrate in Cuvette X [mg/L]	Absorbance Y [A°]
0	0	-
10 (0.01 mL)	0.099	0.16688
20 (0.02 mL)	0.195	0.28207
50 (0.05 mL)	0.488	0.62975
75 (0.075 mL)	0.723	0.91514
100 (0.1 mL)	0.963	1.212
125 (0.125 mL)	1.176	1.5277
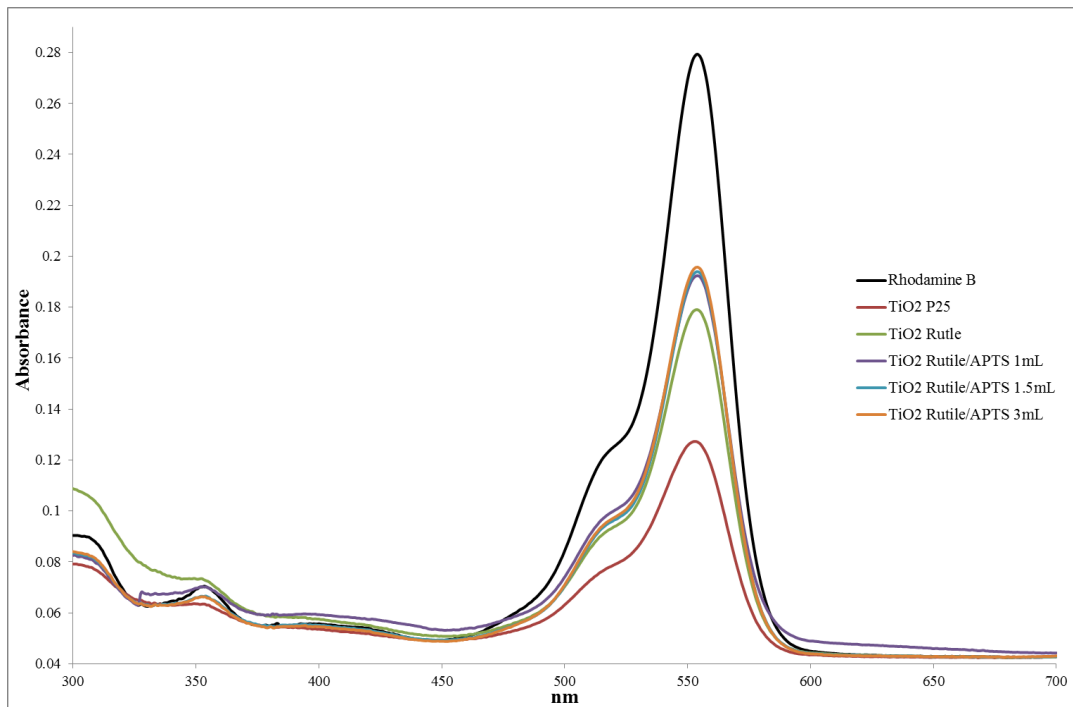
Figure 6-25: UV-vis transmittance curve of (from top to bottom) original Rhodamine B, SMS105C, SMS105B, SMS105A, SMS097 and TiO₂-P25.
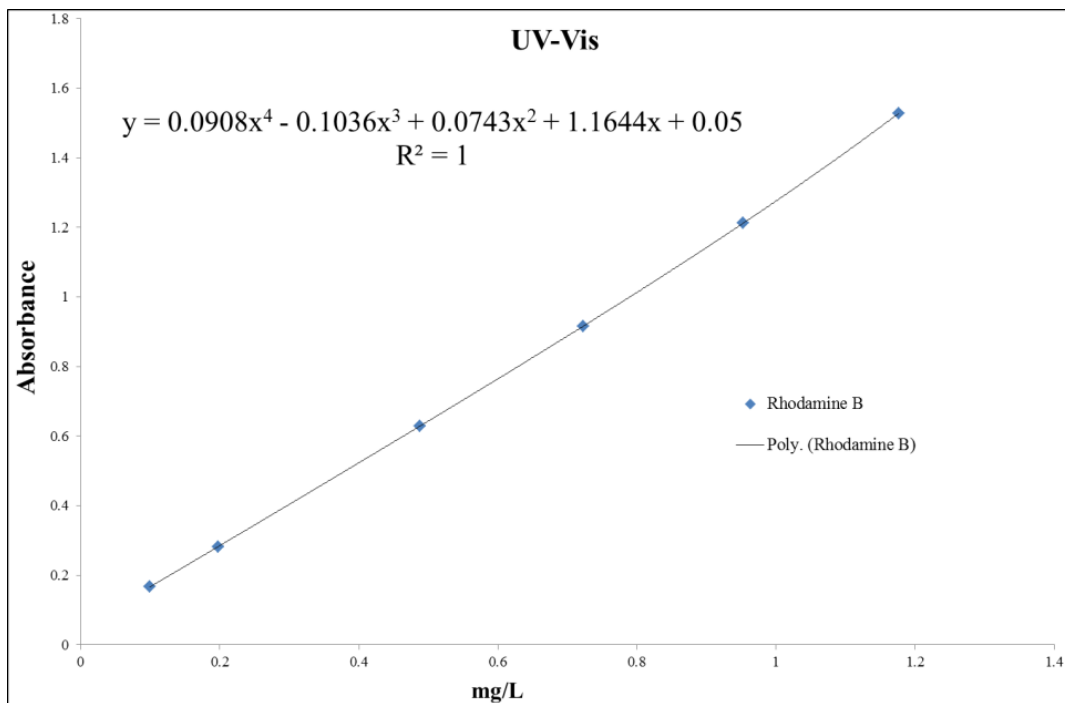
Figure 6-26: diagram of UV/Vis of original Rhodamine B with different concentrations.

Figure 6-26 was drawn using the data collated in Table 6-9. When mixture of TiO$_2$-RP-APTES and Rhodamine B solution peak is near to Rhodamine B solution, it mean is the UV light was absorbed by Rhodamine B not with TiO$_2$-RP-APTES nanoparticles. The result explains that nanoparticles UV absorption was reduced.

Figure 6 25 shows that with increasing APTES concentration the peak is stronger and more like that of the Rhodamin B solution. The UV/Vis diagram Figure 6-26 was drawn with different concentrations of Rhodamine B. In order to determine the concentration of each sample they were measured in Figure 6-25. Each mixture of TiO$_2$-RP-APTES and Rhodamine B samples absorbance was put in equation and found from Figure 6-26. In order to measure the sample 0.1 mL a mixture of TiO$_2$-RP-APTES and Rhodamine B solution was added in 20 mL water in a cuvette.
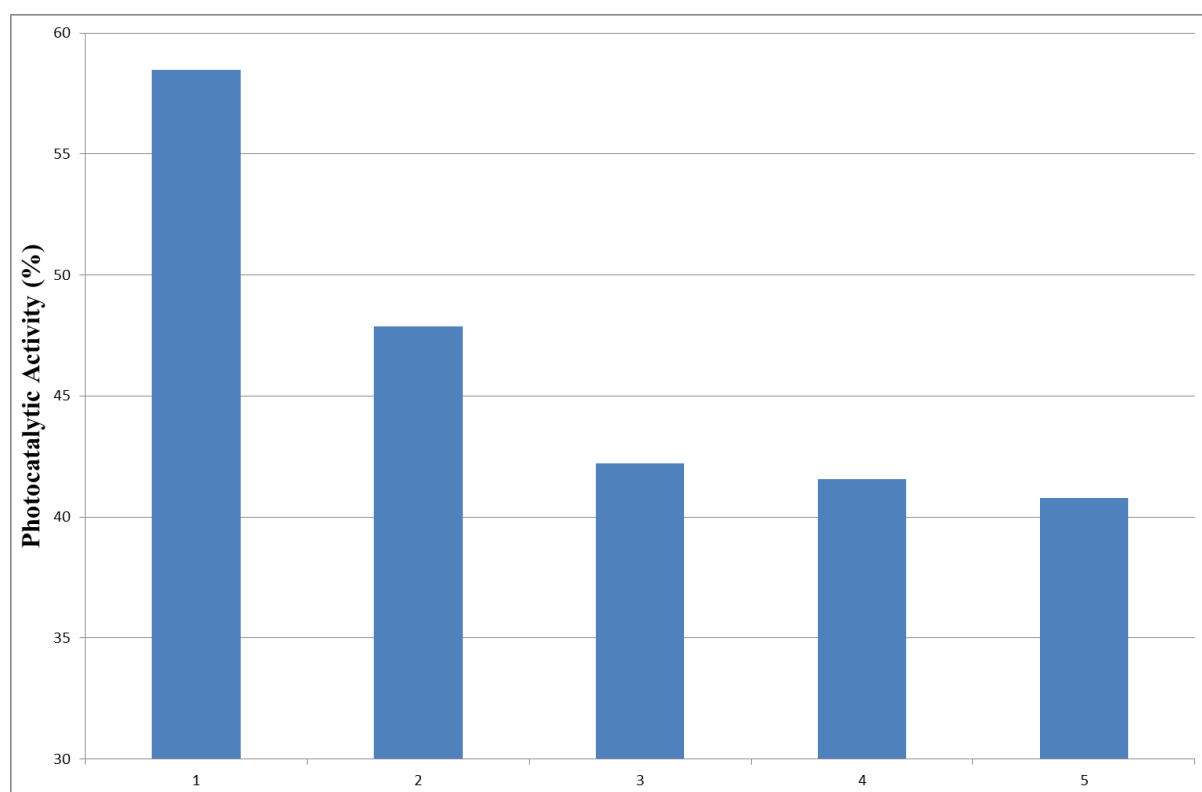
Figure 6-27. Distribution of concentration [mol/L] of samples (left to right) TiO$_2$-P25, TiO$_2$-RP, SMS105A, SMS105B, SMS105C.

157

Figure 6-27 shows that for rutile titanium dioxide, 47.8% of Rhodamine was degraded after 30 min UV-irradiation. The photo-catalytic activity decreases with increasing concentration of the APTES, which further supports the supposition of the formation of a monolayer of APTES on the surface of the TiO_2-RP-APTES nanoparticles. The results for show that, compared with non-coated TiO_2-RP-APTES nanoparticles, the TiO_2-RP-APTES nanoparticles have a much lower photo-catalytic activity as desired.

Table 6-10. Concentration of solutions for UV/Vis analysis

UV/Vis solutions	samples Absorbance Y	X Which was put in equation and be find from Figure 6-26 [mg/L]	Concentration of samples [(0.963X)/0.963]	Percent of concentrations
SMS088C	0.18	0.501897665	0.479	47.9
SMS093A	0.19	0.556544907	0.422	42.2
SMS093B	0.19	0.562734397	0.416	41.6
SMS093C	0.19	0.570184464	0.408	40.8
P25	0.13	0.290534734	0.698	69.8

6.4.4 Coating

Only cellulose peaks can be observed on the XRD pattern. Probably this because the TiO_2-RP-APTES layer on CP is very thin, i.e., a chemically bonded monolayer, as expected.
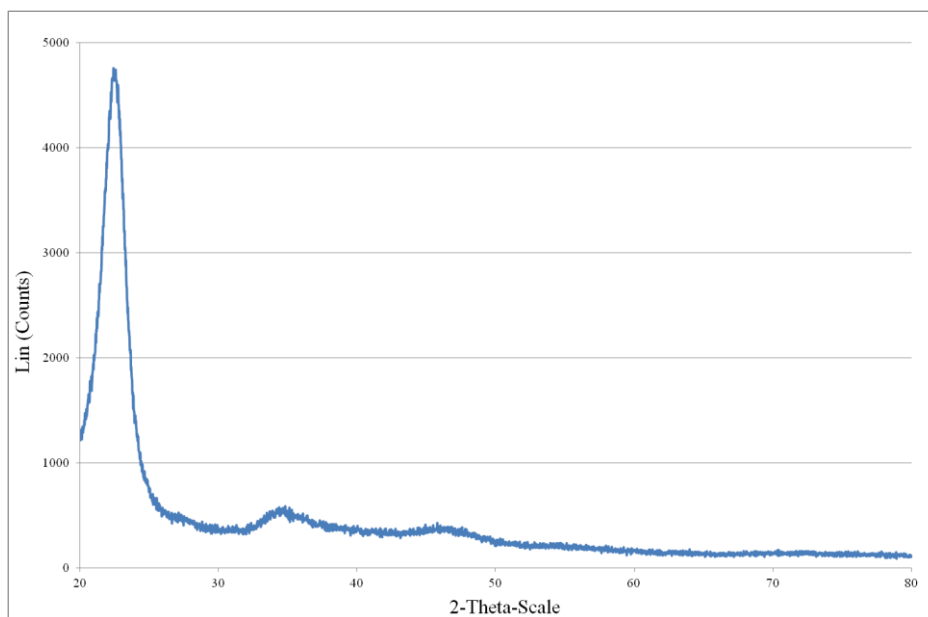
Figure 6-28: XRD pattern of cellulosic paper after coating with TiO₂-RP-APTES.
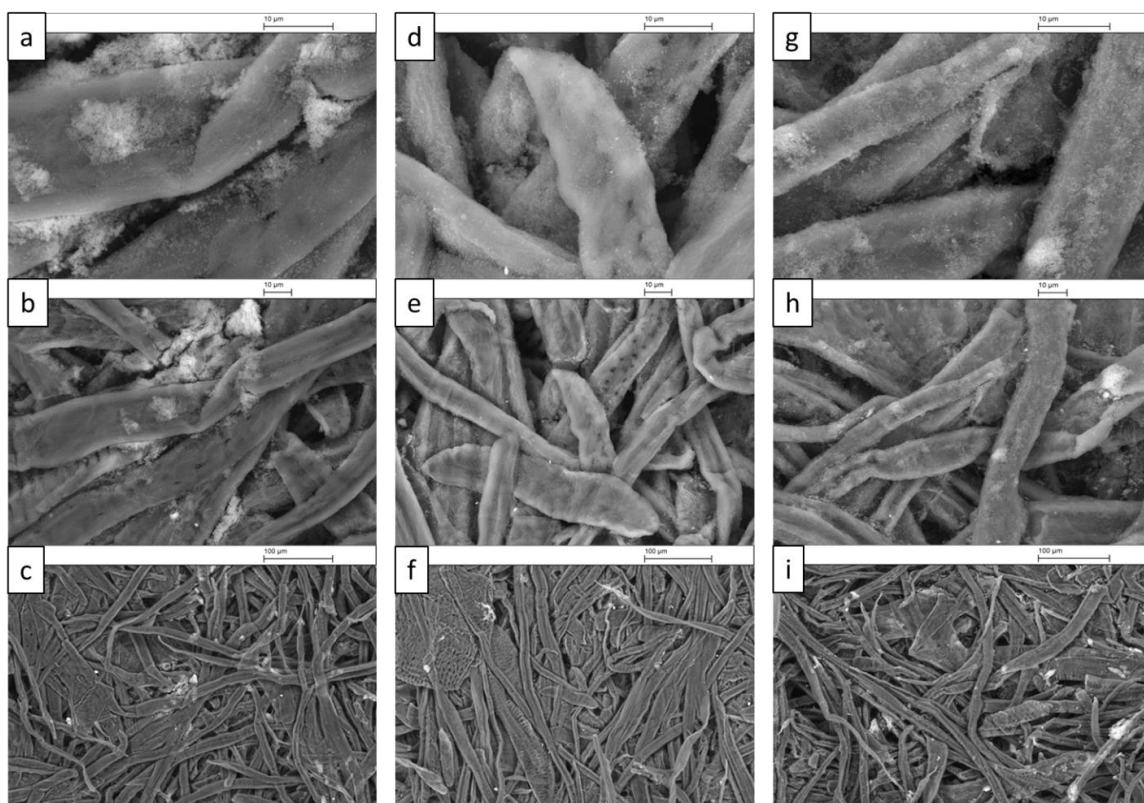
Figure 6-29: SEM images of Mondi CP coated with TiO₂-RP-APTES (a-c) SMS106A, 1 mL APTES, (d - f) SMS106B 1.5 mL APTES and (g - i) SMS106C 3 mL APTES.

The SEM images show that for APTES 1.5 and 3.0, generally titanium dioxide nanoparticles are homogenously distributed on the surface of the cellulose fibres, although there are some white aggregates in some areas. It can be seen from the visible region of the UV-Vis spectra that the refractivity of the CPs coated with TiO_2-RP-APTES nanoparticles is higher than that of the CP samples coated with non-coated TiO_2-RP nanoparticles. Also, the reflectivity of CPs coated with TiO_2-RP-APTES nanoparticles increases with increasing concentration of APTES used in the preparation of TiO_2-RP-APTES nanoparticles, see Figure 6-30.
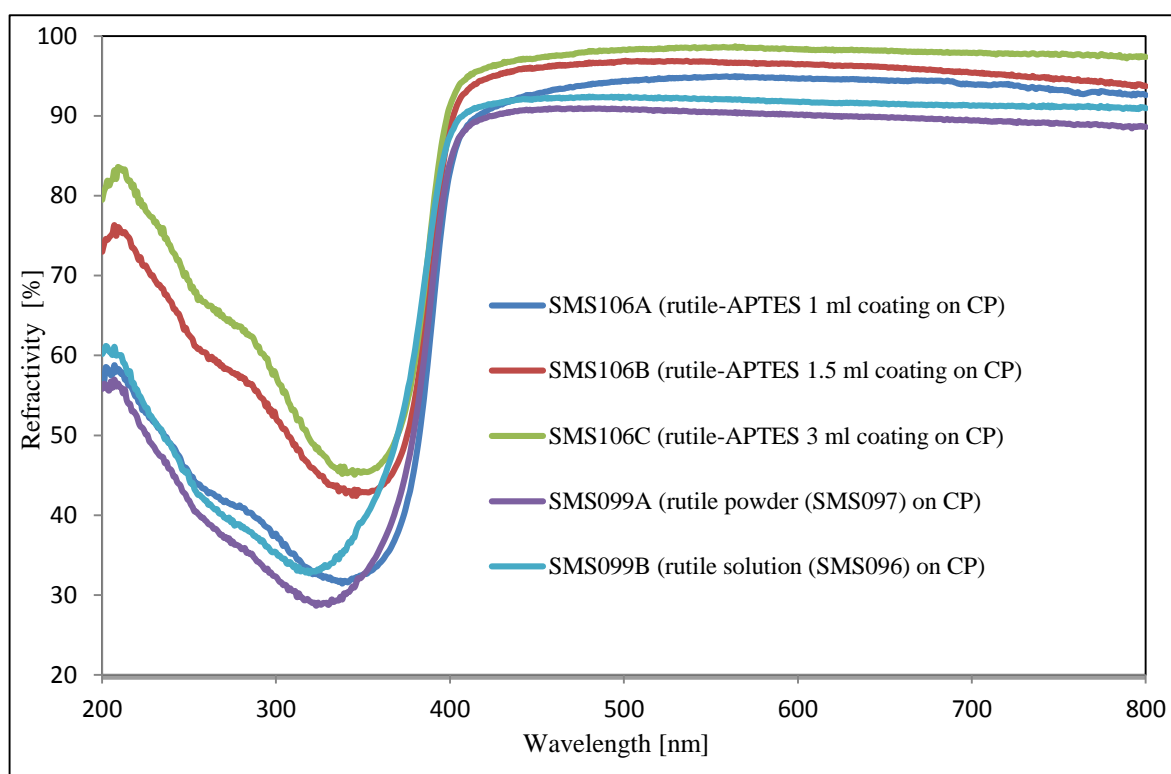
Figure 6-30: UV-vis transmittance curves of TiO₂-RP and TiO₂-RP-APTES NPs.

The refractivity of coated CP after compression shows that APTES can increase the refractivity, i.e., the refractivity of the TiO_2-RP-APTES-coated CP samples increases with increasing APTES concentration used in the coating of the TiO_2-RP nanoparticles.

Table 6-11: Comparison of the results of TiO₂-RP-APTES nanoparticles.

	APTES [mL]	Concentration [mole/L]	BET surface area [m²/g]	CHN analysisC /N (%)	pH which have IEP	ICP Si/Ti	ICP coating Si/Ti
SMS102	---	---	91.36	---	7.2	---	---
SMS105A	1.0	0.086	15.07	3.44	8.1	0.11	0.17
SMS105B	1.5	0.129	17.07	4.89	8.2	0.14	0.21
SMS105C	3.0	0.258	17.48	2.32	8.6	0.15	0.22

The molar ratio of carbon to nitrogen (C/N) varies from 2.32 to 4.89, suggesting that most of the ethoxy-groups in APTES have been hydrolyzed and that residual, unreacted amino propyl groups are present on the titanium dioxide nanoparticle surface. The BET surface area reduces after the TiO₂-RP nanoparticles have been modified with APTES. However, the BET surface area does not show regular changes with the increasing concentration of APTES. The ICP results show that the concentration of Si/Ti after depositing the TiO₂-RP-APTES nanoparticles on the CP surface is not very different from that of the original TiO₂-RP-APTES nanoparticles before deposition, as expected
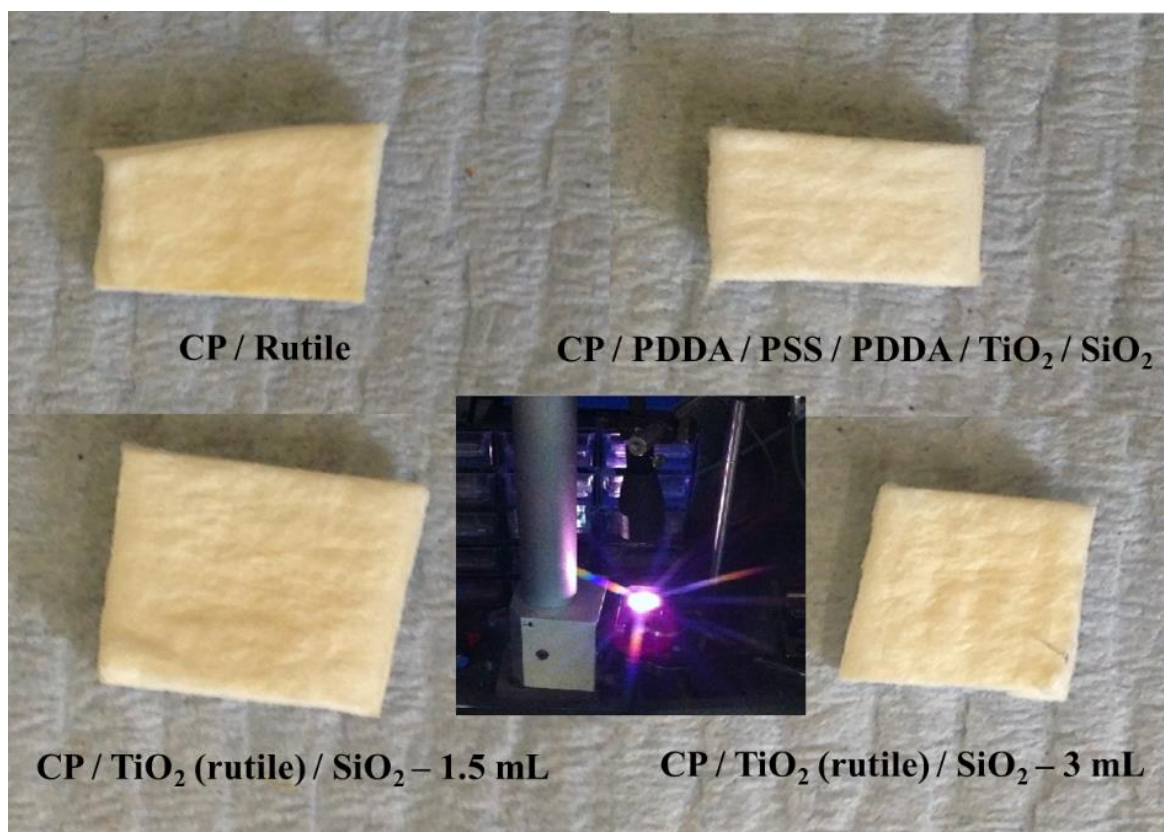
Figure 6-31: Compare photocatalytic stability of different coating CP under UV light.

In order to compare photo-catalytic stability, coated CPs were illuminated in an UV light Omni Cure series 1000 instrument. The images illustrate that CP coated using the LBL method is more stable compared to the other samples. Furthermore, in the case of using APTES, an increase in the concentration of APTES results in a reduction of the photo-catalytic activity. However, the main problem for this result is that the photo-catalytic activity could not be measured and also UV light Omni Cure series 1000 was very powerful to examine the coated CP. Therefore, this image just shows the fact that silica compounds can protect titanium dioxide on CP surface.

6.4.5 Brightness and whiteness of cellulosic paper
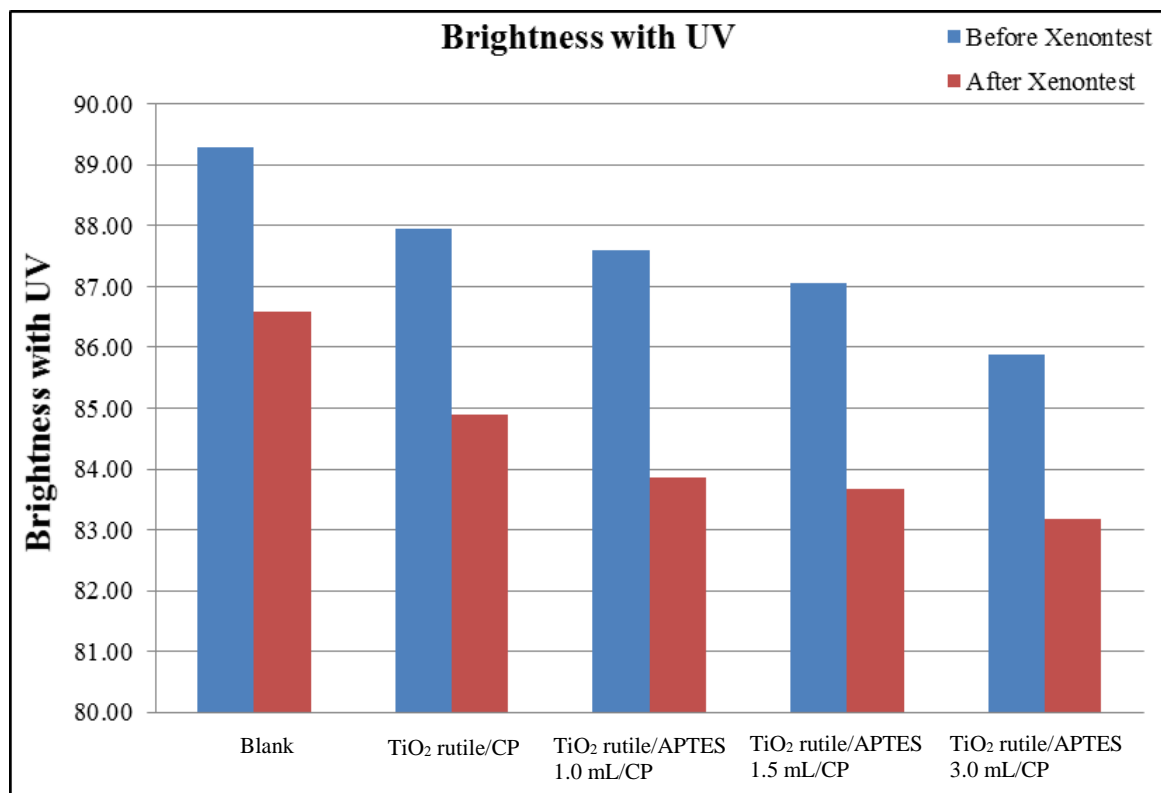
Figure 6-32: ISO brightness of blank reference paper and the paper samples coated either with untreated TiO₂-RP nanoparticles or APTES-modified TiO₂-RP nanoparticles before and after the UV-stability test.

Figure 6-32 shows the ISO-brightness determined for the blank reference paper and the paper samples coated either with untreated TiO_2-RP nanoparticles, or APTES-modified-TiO_2-RP nanoparticles, before and after illumination with UV-light in the standard xenon UV-stability test. It can be seen that for both before and after UV test, the brightness of the TiO_2-RP or rutile TiO_2/APTES coated paper is lower than of blank paper. The decrease in brightness is even more significant for the paper samples coated with APTES-treated TiO_2-RP nanoparticles.

The whiteness for the paper samples coated with TiO_2-RP-APTES nanoparticles also is lower than that of the blank paper reference. One possible reason for this phenomenon is the presence of chlorine in the TiO_2-RP nanoparticles, before and after APTES treatment, as shown in XPS result, which may reduce the brightness and whiteness of the coated paper by reaction with the paper.
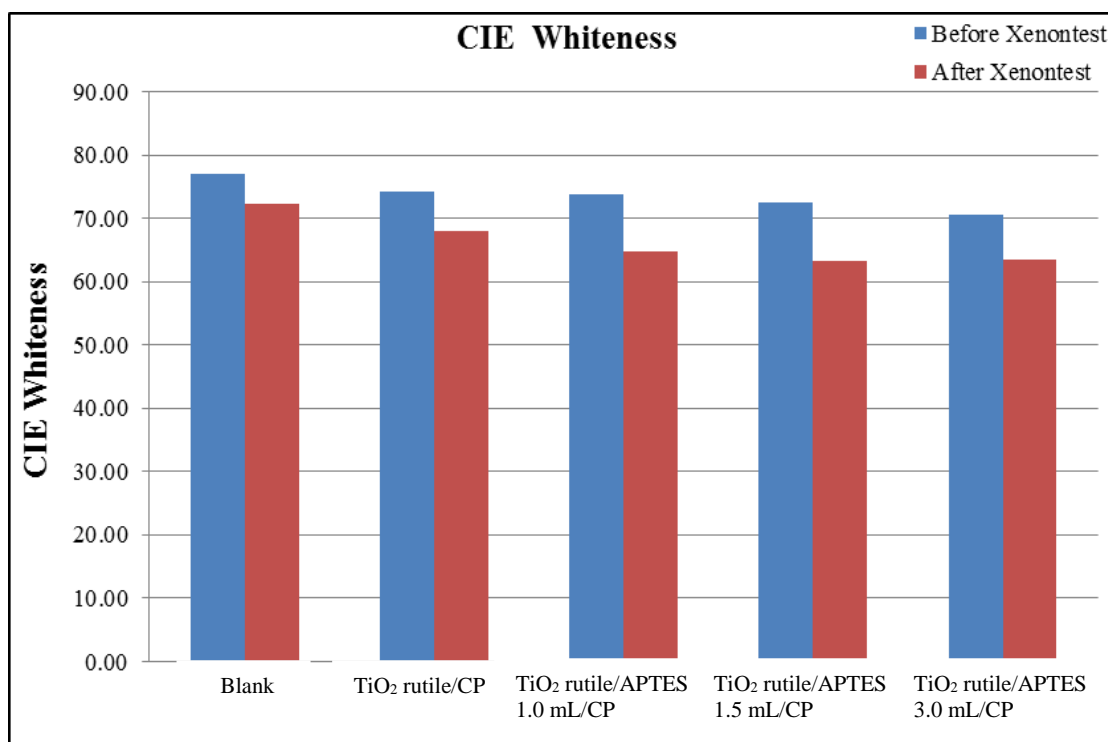
Figure 6-33: CIE whiteness of blank reference paper and the paper samples coated either with untreated TiO_2-RP nanoparticles or APTES-modified-TiO_2-RP nanoparticles before and after the UV-stability test.

Another possible reason is that the nanoparticles obtained are not as crystalline as the TiO_2-P25-APTES nanoparticles. The TiO_2-RP nanoparticles were heated at 500 ℃ in an attempt to produce more crystalline titanium dioxide nanoparticles. However, the heat-treated products did not form stable colloidal solutions and, as a result, a good surface coating on paper samples could not be obtained.

6.5 Summary

In this method, the surface of commercially available P25-TiO$_2$ nanoparticles and rutile TiO$_2$-RP nanoparticles, prepared as part of the work for this thesis, was successfully modified with 3-aminopropyltrimethoxysilane (APTES). These surface-modified P25-TiO$_2$-APTES and TiO$_2$-RP-APTES nanoparticles were then deposited on CP by deposition from solution.

Treating TiO$_2$-P25 with APTES was shown to successfully coat the nanoparticles, as shown by XRD analyses. It was shown that treating TiO$_2$-P25 nanoparticles with APTES did not significantly alter the size or shape of the nanoparticles. Therefore, any changes in brightness/reactivity as ascribable to a change in surface chemistry rather than a change in shape or plasmon resonance. The ATPES modified TiO$_2$-P25 nanoparticles were shown to have significantly lower photo-catalytic activity on CP than untreated TiO$_2$-P25 nanoparticles. CP treated with ATPES modified TiO$_2$-P25 nanoparticles was found to resist photo-degradation more than paper treated with TiO$_2$-P25 nanoparticles, as well as exhibit higher reflectivity.[173]

Part 2. Silicon Diimide Gel as a Stationary Phase for

Chromatography

7   Silicon Diimide Gel as a Stationary Phase for Chromatography

7.1   Introduction

Microporous and mesoporous inorganic filters and membranes with small pore sizes and high effective surface areas have been investigated over the last two decades for use as gas sensors and separation technology because of their thermal and chemical stabilities, good reliability, high sensitivity and low cost.[176, 177] The synthesis and fabrication of novel nano-porous inorganic membranes with controlled chemical and physical properties is very important for the development of new applications of nano-porous nanocomposites.[178-180] Silicon nitride and its precursors, such as silicon diimide gel, offer potential advantages as a novel membranes and filters because of oxidation resistance and the unique combination of superior high-temperature mechanical properties of silicon nitride, for example, especially in chemically harsh conditions and high temperature separation processes.[181-183]

A variety of methods have already been reported for the synthesis of dense silicon nitride, including pyrolysis of silicon-based materials such as polycarbosilanes and polysilazanes.[177, 184] However, there is not an extensive knowledge of the properties and preparation of microporous and in particular mesoporous silicon diimide and silicon nitride ceramic materials. Microporous silicon imidonitrides were prepared for the first time by the pyrolysis reactions of polysilazanes.[185-187]

Liquid-phase chromatography and purification currently uses stationary phases based on two different types of porous silica gel, SiO_2, either non-modified (normal phase) silica gel, such as DAVISIL®, or silica gel functionalised with long hydrocarbon chains (reverse phase).[188, 189] Silica gel has a high surface area (usually *ca.* 800 $m^2 g^{-1}$) and is intrinsically acidic, which can lead to the degradation of acid-sensitive compounds, especially when using it as a stationary phase during column chromatography. Organic compounds incorporating common protective groups, such as those with acetal, thioacetal, ether or silane functional groups, are especially labile and prone to decomposition on silica gel columns. Basic alumina (pH ~ 7-10) is an alternative to using silica gel. Unfortunately, it is hygroscopic, also decomposes a

large range of organic compounds, often requires an aqueous pre-treatment to control compound specific activity and affinity and generally exhibits a low surface area, e.g., 200 m^2 g^{-1}. [190] [191] Porous zirconia may allow the treatment of acid-sensitive compounds, but it also exhibits significant drawbacks in terms of cost, ease of use and reusability. [192]

Silicon diimide gel, Si(NH)$_2$, is an isoelectronic alternative to silica in chromatography. It is neutral of weakly basic (pH ~ 7-10) in nature, mesoporous, e.g., pore size ~3.6 nm, exhibits a narrow pore size dispersity, possesses a large surface area, e.g., 600 m^2 g^{-1}, and its surface is covered with residual amine groups. The interactions with an analyte in chromatographic applications would involve surface nitrogen atoms and amine groups, strong electron donor interactions, as well as a good dispersive component, coming mostly from acid-base exchanges and hydrogen bonding. As such, it should be possible to control the retention times of analytes. Silicon diimide gel behaves like a soft base and should tolerate a wider range of functional organic groups than basic alumina and silica gel.[193] [194, 195]

It would be highly advantageous to coat aluminium, plastic substrates and especially paper with silicon diimide gel to produce a new approach to thin film chromatography using an intrinsically weakly basic solid phase. Many synthetic pharmaceutical products and protein-based medicaments are acid stable and the development of a simple cost-effective solid substrate for the analysis of these compounds by thin layer chromotography and purification by column chromatography would be highly desirable.

7.1.1   Thin Layer Chromatography (TLC)

It has been reported that thin layer chromatography (TLC) was first discovered at the Institute of Pharmacy of the State University of Kharkove, Ukraine, by Schraiber and Izmailov in 1938 and standardized later by Stahl. It was used for analysis of drop-chromatography and its application in pharmacy was reported in the same year in Moscow by Farmatzija.[196]

TLC is one of the most effective techniques for the identification, isolation and quantitative analysis of a very wide range of organic compounds.[197] TLC offers several advantages, such as wide choice of mobile phases, minimal sample clean-up, high sample loading capacity, flexibility in sample detection, easy accessibility, low solvent consumption, open and

disposable nature of TLC plates, comparatively low operational cost and relatively little need for modern laboratory facilities.[198]

Chromatography is a well-developed technique for analysing compounds by separation mixtures of substances into their components. All different forms of chromatography have a mobile phase (a gas or a liquid) and a stationary phase (a solid, or a liquid supported on a solid).
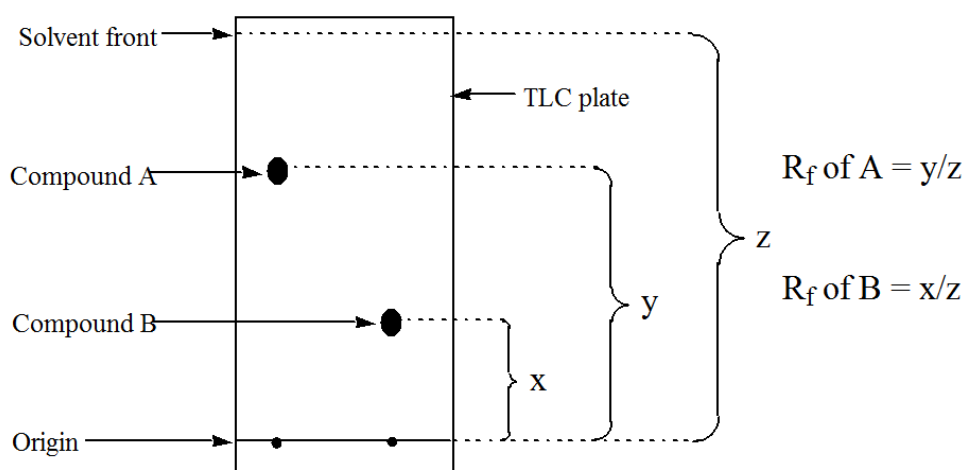
Figure 7-1: TLC plate

TLC is a simple, convenient, quick, and inexpensive procedure that gives the chemist a quick answer as to how many components are in a mixture and, in many instances, can be used to identify the components as well. TLC is also used to support the identity of a compound in a mixture when the Retention Value (R_f) of a compound is compared with the R_f of a known compound (preferably both run on the same TLC plate).

$$R_f \text{ Value} = \frac{\text{Distance from Baseline travelled by Solute}}{\text{Distance from Baseline travelled by Solvent (Solvent Front)}}$$

The mobile phase is a suitable liquid solvent or mixture of solvents. To carry the components of the mixture with the mobile phase, it flows through the stationary phase and different

169

components travel at different level. In most cases, the stationary phase (adsorbent) is very polar and the mobile phase (eluent) is fairly non-polar. Molecules that are more polar stick to the polar stationary phase more than fairly non-polar molecules which are carried along in the mobile phase. Other common polar adsorbents include alumina, charcoal and Florisil. Non-polar adsorbents may also be used with relatively polar solvent systems, this is known as "reverse phase" chromatography because the nature of the stationary and mobile phases is inverted. Drug purification frequently employs this technique.

Figure 7-2: (A) Common mobile phases listed by increasing polarity, (B) Elution order for some common functional groups from silica or alumina.

If the compounds are coloured, visualization is straightforward and if the compounds are not coloured, a UV lamp is used to visualize the plates. Thin layer chromatography (TLC) is a thin uniform layer of alumina or silica gel coated onto a piece of metal, glass or rigid plastic. The stationary phase (silica gel or the alumina) for TLC plate often contains a substance which fluoresces in UV light. TLC can be used to help determine the identity of compounds, the purity of a compound, the number of components in a mixture and also monitor the progress of a reaction by observing the disappearance of a reactant or the appearance of a product. TLC is a sensitive technique for analyse of microgram (0.000001 g) quantities and it takes about 5-10 minutes for an analysis.

170

In 1949 in order to separate organic ions Mainhard and Hall used a starch binder to give some firmness to the stationary phase of TLC plates. Further advances were made by Kirchner el al in 1951 and Reitsema separated several mixtures in one run in 1954.[199] Hence, TLC became a widely applied analytical method, especially to monitor the progress and state of reactions in organic chemistry, in the 1950s.[200]
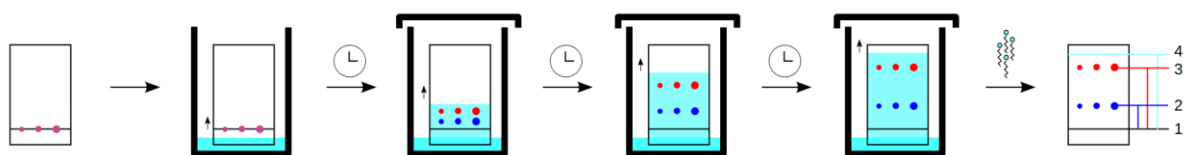
Figure 7-3: Development of a TLC plate, a purple spot separates into a red and blue spot.

In 1960 the significance of inorganic, as opposed to organic, TLC became apparent when Seiler succeeded in the separation of inorganic products using thin layer chromatographic techniques.[201] The TLC analysis of metal ions received the greatest amount of attention after the publication of this work. The most important fields of applications are currently the analysis of samples of rocks, food, industrial, bioinorganic compounds, soil, pharmaceutical agents, water and industrial waste-water.[202-204] An exhaustive review describing the principles, historical background and the mechanisms involved in chromatography was published in 1967.[205] Thereafter, extensive studies of the use of TLC to analyse inorganic compounds were published by Brinkman et al,[206] Mohammad et al (1979), Fenimore and Davis (1981), Borman (1982), Maugh (1982), Coddens et al (1983), Costanzo (1984), Jork and Wimmer (1986), Geiss (1987), Sherma (1991) and Berezkin (1995).[207-209]

Silica gel is usually prepared by the processes of polymerization and subsequent dehydration of aqueous silicic acid, which is generated by adding a mineral acid to a solution of sodium silicate (Szepesi and Nyiredy 1996).[210] The advantages and disadvantages of the various approaches and developmental methods of TLC were reviewed in detail by Cserhati and Forgacs in 1996.[211] Masami also reviewed progress in inorganic TLC, the developing devices, reporting the processing details related to TLC plates, detection and quantification in 1999.[212-214]

The University of Hull has pioneered, developed and optimised the synthesis of mesoporous silicon diimide gel, with a very well controlled and defined physical property spectrum, using a cost-effective, non-aqueous sol-gel process using *tris*(dimethylamino)aminosilane, [(CH₃)₂N]₃Siamino- , prepared from *tris*(dimethylamino)silyl chloride as the starting material.[215, 216] The University of Hull team reported the preparation of various mesoporous Si-M imide gels *via* a non-aqueous sol–gel route in 2002 using silicon diimide gels.[217] In 2004 they also reported novel mesoporous filters for selective gas absorption[181, 216] and in 2005 they published a general method for the preparation of mesoporous M/Si₃N₄ nano-composites *via* a non-aqueous sol-gel route.[218, 219] In 2006 they prepared and characterized a supported, Si₃N₄ membrane *via* a non-aqueous sol-gel process and then also prepared Pd/Si₃N₄ nano-composites as heterogeneous catalysts *via* three different chemical routes. Consequently, they reported the synthesis of a number of liquid crystals using Suzuki–Miyaura aryl-aryl coupling reactions catalysed using mesoporous, ligand-free Pd/Si₃N₄ catalysts in aqueous media.[220, 221]

We have now optimised a novel non-aqueous sol–gel technique for the preparation of a cost-effective, high-surface-area, porous silicon diimide gel by the acid-catalyzed ammonolysis of *tris*(dimethylamino)silyl amine [(CH₃)₂N]₃Siamino-, TDSA as previously reported.[215, 216] The mesoporous silicon diimide gel prepared in this way is stable in contact with water and air and can be regenerated after use by washing with a THF/NH₃ mixture. It has been studied as the inert support in membranes for the selective filtration of gas mixtures at elevated temperatures, e.g., 400-600 ºC, and in heterogeneous catalysts in various organic solvents and solvent mixtures including ethanol and water. [222]

The present research reports the proof of principle for the use of mesoporous silicon diimide gel as the stationary phase in thin film for acid-sensitive compounds. The silicon diimide gel was cast onto a glass to create a Layer Chromatography TLC) plate. A sol– gel process in an amino system was reported by Jansen and co-workers as part of a method to prepare polymeric boron-, titano, and tantalo-silazanes by controlled co-ammonolysis of the respective metal alkyamides.[223]

7.2 Preparation and application of silicon diimide thin film

7.2.1 Preparation of tris(dimethylamino)aminosilane, $(Me_2N)_3SiNH_2$ (TDSA)

All procedures were performed under an anhydrous nitrogen atmosphere using standard Schlenk techniques or in a nitrogen-filled glove bag. Tetrahydrofuran (THF), was freshly distilled from sodium/benzophenone prior to use.

All procedures for preparation of TDSA performed under an anhydrous nitrogen atmosphere using standard Schlenk techniques or in a nitrogen- filled glove box. Tetrahydrofuran (THF) 99.8% extra Dry was freshly distilled from sodium/benzophenone before use. Diethyl ether also flowed from alumina (Al_2O_3) and kept with silica gel for dry better. The silicon diimide gel used in this work was prepared as previously reported with Rovai and Lehmann at 1999 and also Cheng and Clark at 2004. 20 g Tris(dimethylamino)chlorosilane was added to 500 mL diethyl ether in a 3-neck round bottom flask. After stirred a few minutes, ammonia gas was bubbled in to the solution for 2 hour with the speed of 6 L.h^{-1} gas pressure under nitrogen protection. The white aluminium chloride was removed by filtration and the filtrate was distilled on 50 °C under nitrogen to remove ether.
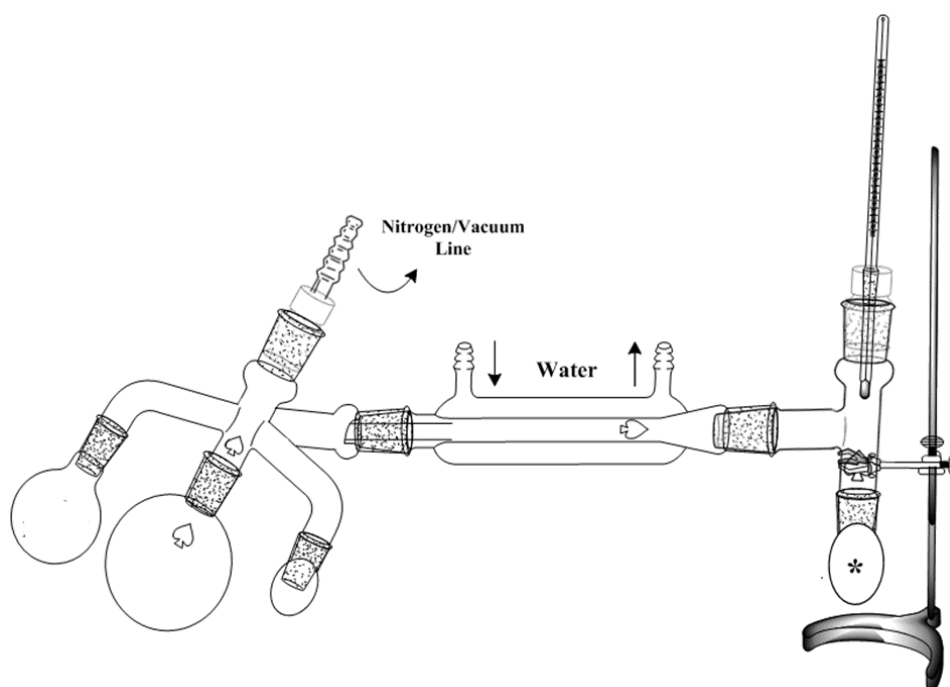
Figure 7-4: Purification of TDSA at 80 °C and 75 cm Hg pressure.

First, small amounts of diethyl ether was removed under 75 cm Hg at 40 °C. After removal of the diethylether, the temperature was raised to 80 °C in order to distil off the TDSA.

7.2.2 Preparation of silicon diimide gel

The silicon diimide gel was prepared by a modification of the previously reported method.[215] 1 mL Trifluoromethanesulfonic acid was added to the mixture of TDSA (15.97 g,) and THF (100 mL) in a round-bottom three-necked flask. After heating at 50°C for 16 h, the solution was allowed to cool to room temperature. For next step, a solution of ammonia (0.47 g, 27.8 mmol) in 10 mL of cold THF was prepared with bubble ammonia gas for 1 hour in the THF. The cold solution of ammonia in THF is then quickly transferred to previous three-necked flask. The resulting solution was softly shaken and left to react for 4 hours. The solution should stay translucid in this step.

In the last step of making gel, ammonia gas was bubbled through for 1 hour to saturate it. The resulting mixture was left standing at room temperature for another 18 h to give a rigid gel filling the original volume of the reaction mixture. Evaporation of the solvent and evolved dimethylamine in a stream of nitrogen followed by drying under reduced pressure at 50°C for 10 h yielded a translucent white solid (7.13 g).

7.2.3 Preparation of silicon nitride

Pyrolysis of the gels was conducted in a tube furnace. About 0.5 g of the gels was placed in an Al_2O_3 boat, which was then introduced into a quartz tube in a glove box. The tube was then connected with NH_3 flow. The gels were heated to 200°C and held for 2 h, and then heated to the 1000 °C and held for 2 h. The heating ramp rate was 5 °C.min^{-1} for pyrolysis under NH_3 flow.

7.2.4 Coating silicon diimide gel on the glass surface

0.2 g silicon diimide gel and 0.02 g plaster (Calcium sulphate, GYPSUM) were mixed with 1 ml of distilled water and stirred for 5 min to make a homogeneous paste.

We coated silicon diimide gel on glass slides by mixing the ground silicon dimide gel in water or ethanol to make a paste and then coating the paste on to the glass slide. After slowly evaporation of water or ethanol, homogenous silicon diimide films can be obtained. However, the silicon diimide films were very brittle and showed poor adhesion to the glass slides. In order to increase binding to the glass slide, calcium sulphate was used as a binder. 10 % weight/weight of Calcium Sulphate was mixed with the silicon diimide gel, the coating of silicon diimide on glass slide was strong enough to carry out successful Thin Layer Chromatography. In order to facilitate the coating of the glass surface with the stationary phase, two parallel strips of adhesive tape about 2 or 3 mm wide (50 μm thickness) were stuck on the edges of the glass plate (1 cm wide and 5 cm long). The mixture of silicon diimide gel and Calcium Suplhate as a paste was then deposited on the area between the two parallel strips of tape. The paste was applied homogeneously across the plate using a rigid squeegee, such as a microscope slide. This process was repeated several times to create a homogenous layer, which was left to dry at room temperature for 72 hours. The resulting solid stationary phase appeared quite uniform in thickness with no apparent cracks in the surface or bulk of the silicon diimide gel/Calcium Sulphate composite layer.

7.3 Result and discussion

7.3.1 Preparation and application of silicon diimide thin film

TDSA yield after purification was 80-90%. Chemical and analysing of NMR and FTIR, confirmed the formation of TDSA. Elemental analysis calcd: C 36.6, H 9.90, N 32.0, Si 21.3; found: C 36.9, H 9.86, N 32.0, Si 21.3; found ^{1}H NMR (300 MHz, CDCl$_3$): δ = 2.50 (s, 12H, Si[N(CH$_3$)$_2$]$_3$), 0.0 (br s, 3H, SiNH); ^{13}C NMR (75 MHz, CDCl$_3$): δ = 37.06 (s, Si[N(CH$_3$)$_2$]$_2$); ^{29}Si NMR (79.5 MHz, CDCl$_3$): δ = -31.5 (s, Si[N(CH$_3$)$_2$]; IR (KBr): υ = 3392 (m), (υ(NH)), 2971 (s), 2865 (s, sh), 2855 (s, sh), 2834 (s), 2786 (s; 5× υ(CH$_3$)), 1171 (s), 987 cm^{-1} (s).

TDSA was prepared by a procedure same as previous reported method. [224, 225] Silicon diimide gel was prepared by two steps process, as showed in equation (1) and (2).[216] In the first step, $(Me_2N)_3SiNH_2$ is converted to a cycle trimer $[(Me_2N)_2SiNH]_3$ by an acid-catalyzed self-condensation process (Equ. 1). The trimer was then ammonolysized at room temperature to form a semirigid translucent gel. In order to avoid fast precipitation during the ammonolysis and polycondensation, dilute ammonia solution in cold THF should be added to the trimer solution. After being left at room temperature for about 18 h to get a slight opalescent solution, pure ammonia gas can be bubbled through the opalescent solution and left for 18 h at room temperature to get a semirigid gel.

$$3(Me_2N)_3SiNH_2 \xrightarrow[50\,^{\circ}C]{CF_3SO_3H} [(Me_2N)_2SiNH]_3 + 3HNMe_2 \quad (1)$$

$$n[(Me_2N)_2SiNH]_3 + 6nNH_3 \xrightarrow{r.t.} 3[Si(NH)(NH_2)_2]_n + 6nHNMe_2 \quad (2)$$
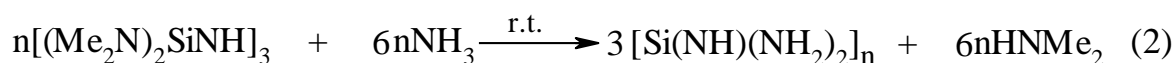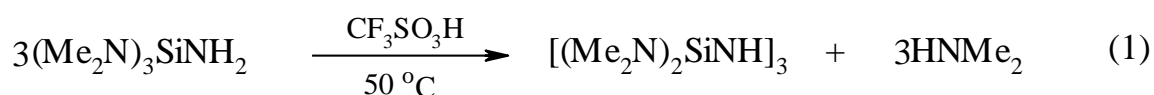
TEM images showed that many nano porous were present in the silicon diimide gel.
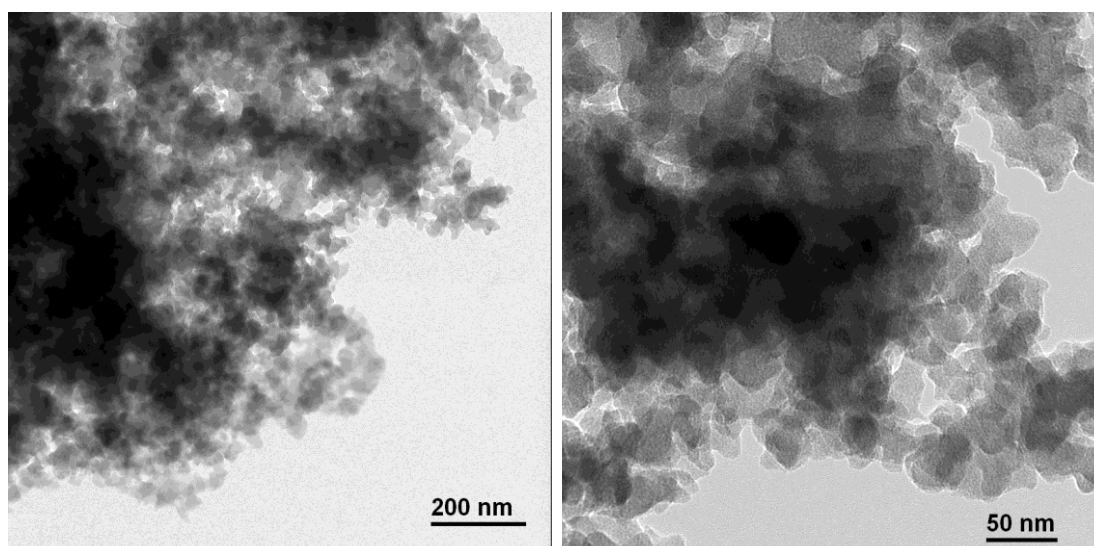
Figure 7-5: TEM image of silicon diimide gel nano porous.

176

The peak at 3400 cm^{-1} ascribed to n(NH) indicated the presence of NH or/and NH$_2$ groups. The strong band around 1000 cm^{-1} is primarily attributed to n(Si-N) in the silicon diimide gel. Compared with other reference for prepare silicon diimide gel, the dimethylamine Me$_2$N-groups have been completely removed because more ammonia has been added during the ammonolysis and polycondensation.
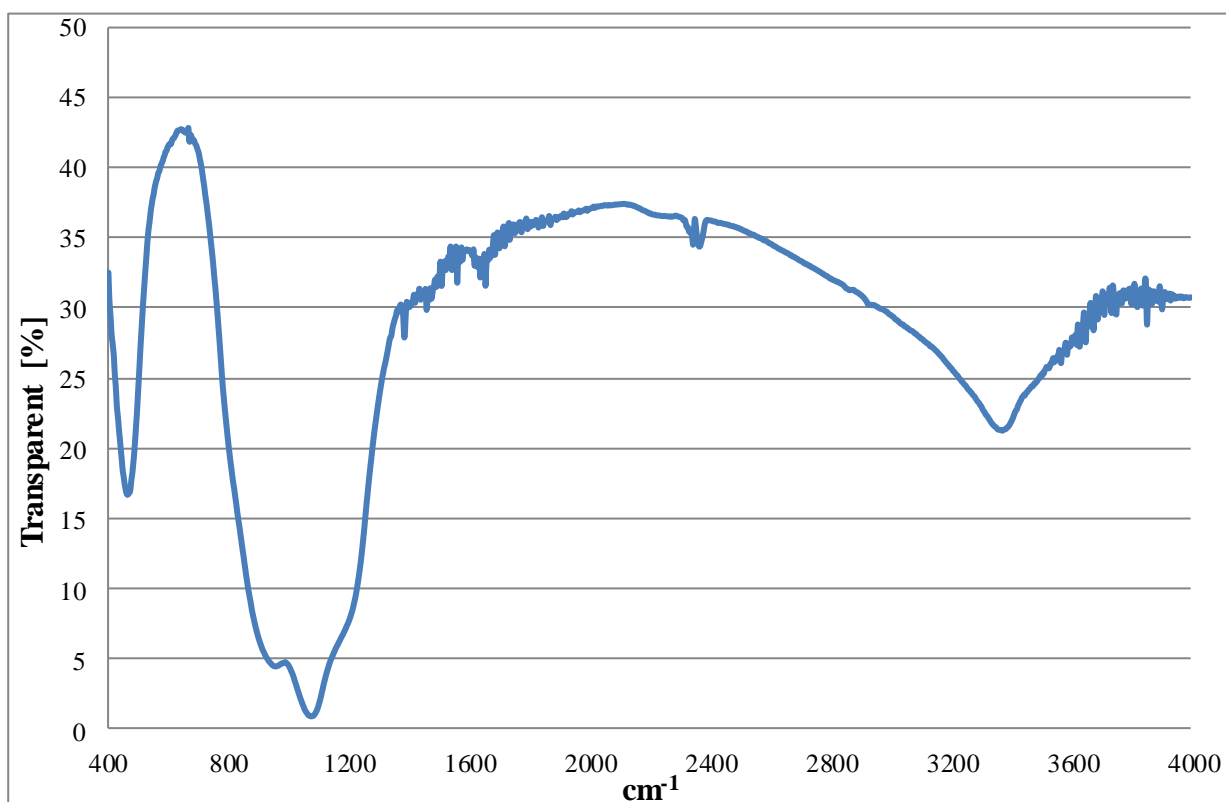
Figure 7-6: FT-IR spectrum of prepared silicon diimide gel (KBr method).

SEM results shows Aldrich commercial silica nanoparticles size is ca 40 μm and the powder is homogenise with similar nanoparticles size, but prepared silicon diimide size is not homogenise and its ca 10-40 μm. After pyrolysis of the silicon diimide gel under NH$_3$ flow at 1000 ºC some of the nanoparticles broken to smaller nanoparticles but still they are not homogenise. The silicon diimide cannot use for chromatography columns because nanoparticles size is different but it can use as thin layer chromatography plate.
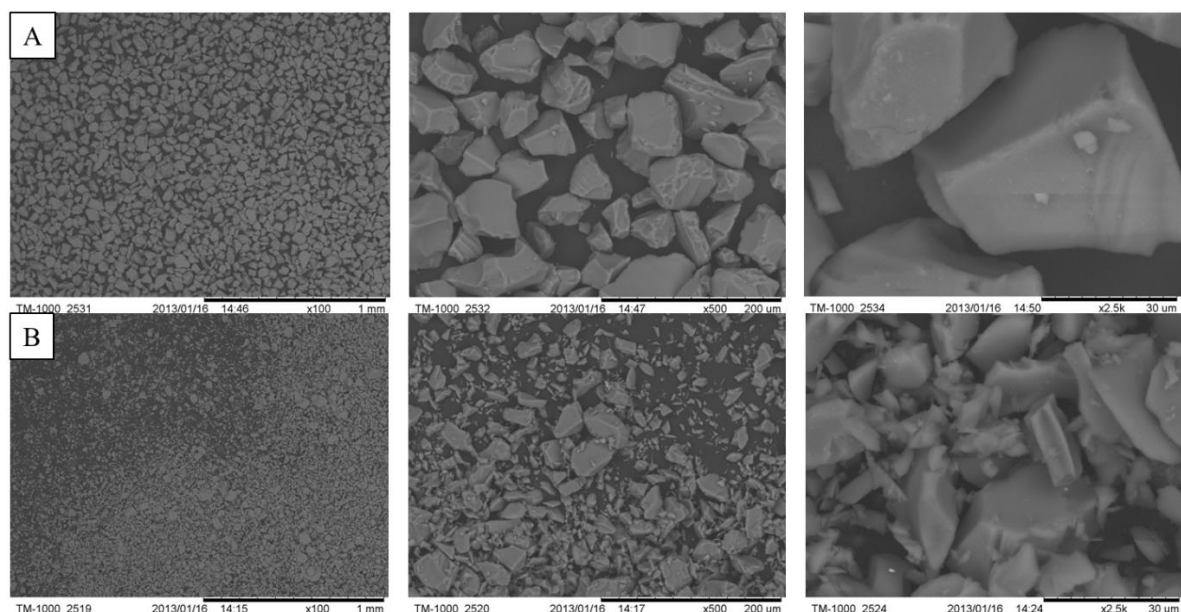
Figure 7-7: SEM images of (A) Aldrich commercial silica, (B) silicon diimide gel.

The silicon diimide gel has mesoporous with a specific surface area of 700 $m^2\ g^{-1}$). These value is higher than that of the standard silica (DAVISIL® supplied by Sigma Aldrich, 540 $m^2\ g^{-1}$) used as a reference solid phase in this study.

7.3.2 Test silicon diimide thin film

TLC analysis of a single compound

2-Phenoxytetrahydropyran was synthesized from 0.70 g of 3,4-dihydropyran and 0.75 g phenol in presence of sulfuric acid as a catalyst in 0.5 M dichloromethane (DCM).

After removal of the solvent from product under vacuum, analysis of the reaction mixture by ^{1}H-NMR spectroscopy revealed the presence of a mixture of unreacted phenol and tetrahydropyran alongside 2-phenoxytetrahydropyran, as expected for such an equilibrium-based reaction.

The reaction in Figure 7-8 was chosen as 2-phenoxytetrahydropyran is acid sensitive and often decomposes on silica gel to form phenol and tetrahydropyran. When silica diimide gel was used to separate the reaction mixture using column chromatography there was no evidence of product decomposition.
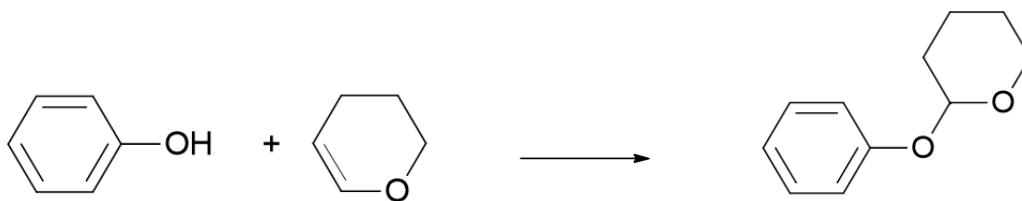
Figure 7-8: Scheme of phenol and tetrahydropyran reaction to make a 2-phenoxytetrahydropyran.

Three spots are applied to the base line of the silicon diimide gel TLC plate. The first spot (A) is the starting phenol, the second spot (B) is a combination of 0.01 g phenol and 0.01 g of reaction mixture, a co-spot, and the third spot (C) is reaction mixture in DCM solution.

Each TLC plate was run in the usual way in a glass TLC tank with an eluent mixture of 5% DCM and 95% hexane to near the top of the silicon diimide gel TLC plate and the commercial silica gel aluminium backed TLC plate used as a reference. A clear chromatographic effect is seen for the silicon diimide gel TLC plate, which is comparable with that observed for the reference silica gel TLC plate. The phenol remains at the origin on both plates and the product rises up both plates to a similar degree. The R_f values are approximately the same on both plates, but are difficult to measure with any real degree of accuracy.

Figure 7-9: Comparison of the chromatographic separation for (top) the silicon diimide gel TLC plate and (bottom) the reference silica gel TLC plate.

179

TLC analysis of a mixture of compounds

A mixture of 4.0 g 2,2-bithiophene (0.0137 mol), 1.0 g 2,7-dibromo-9,9-dioctylfluorene, DMF, 0.63 g K$_2$CO$_3$ (0.005 mol), 0.1 g PiOH (0.0009 mol) and 0.02 g Pd(OAc)$_2$ was heated at 80 °C for 4 hr.

Three spots (A-C) were applied to the baseline of both the silicon diimide gel and commercial silica gel aluminium backed TLC plates. The first spot (A) is the 2,2-bithiophene, the second spot (B) is 2,7-dibromo-9,9-dioctylfluorene and the third spot (C) is reaction mixture. Each TLC plate was run in the usual way in a glass TLC tank with an eluent mixture of 5% DCM and 95% hexane to near the top of the silicon diimide gel TLC plate and the commercial TLC plate used as a reference. After separation with the eluent the reaction mixture spot (C) separated into four spots: the first spot (1) on the baseline is an impurity caused by cross polymerisation of the 2,2-bithiophene, the second spot (2) is the desired product, the third spot (3) is the starting material 2,2-bithiophene and the last spot (4) is the other starting material,2,7-dibromo-9,9-dioctylfluorene.

Although there is a difference in colour contrast of the spots between the silica diimide and silica gel plates. The R$_f$ values are very similar and the plates clearly show a clear chromatographic effect for a more complex palladium catalysed direct hetero-arylation cross-coupling reaction than that used in Figure 7-8.
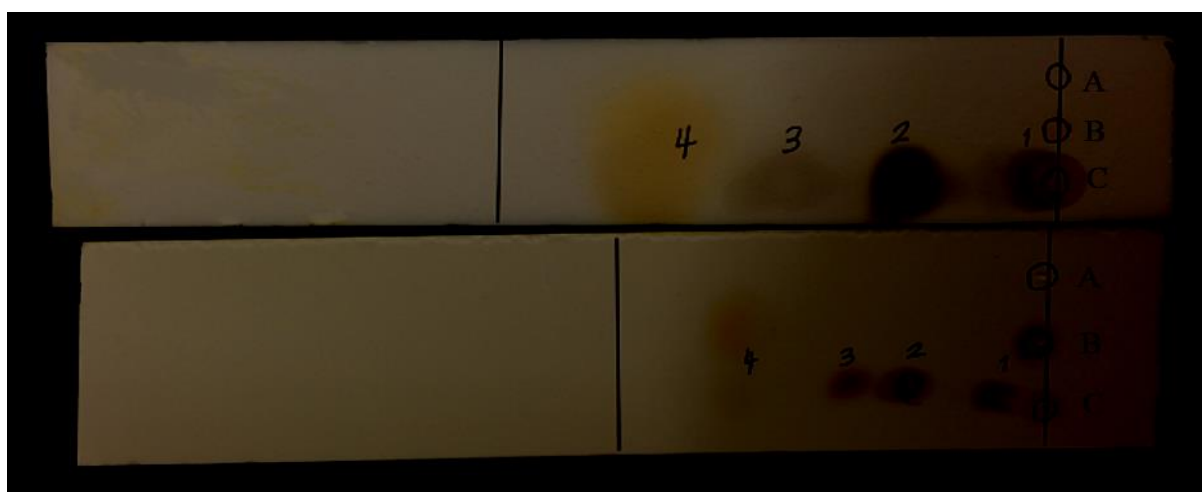
Figure 7-10: Comparison of the results of separation for (top) silicon diimide gel TLC plate and (bottom) the reference silica gel TLC plate.

7.4   Conclusion

Mesoporous silicon diimide gel, $Si(NH)_x(NH_2)_y(NMe_2)_z$, is a stable stationary phase for thin layer and column chromatography. It separates organic compounds chromatographically without altering acid-sensitive functions or bonds. It provides an alternative to either basic alumina or base-doped silica gel for use as a chromatographic stationary phase in the identification and purification of acid-labile chemical compounds, such as pharmaceutical intermediates or final products. Coating with silicon diimide gel on glass surface in compare with commercial TLC plate produced better and clearer results in separation of compounds. This new, highly stable and basic chromatographic stationary phase may also have considerable potential use in GLC, GPC and HPLC applications.

8 Conclusions

The preparation of titanium dioxide nanoparticles was investigated and a deeper understanding of the coating of CP by different methods was gained from this study. A series of different methods were investigated: preparation of titanium dioxide nanoparticles with the formation of seed, *in-situ* coating of titanium dioxide on CP, preparation of TiO_2-RP nanoparticle powder from $TiCl_4$, preparation of titanium dioxide colloidal solutions, coating CP with core/shell TiO_2/SiO_2 nanoparticles and APTES protected titanium dioxide nanoparticles.

Large titanium dioxide nanoparticles with sizes of approximately 200 nm have been successfully prepared. These large titanium dioxide nanoparticles are less catalytically active in comparison with smaller titanium dioxide nanoparticles, which have been used as UV absorbers in commercial cosmetic products. However, results shows titanium dioxide nanoparticles with a diameter of *ca.* 200 nm are not particularly soluble in standard organic solvents and water. Consequently is has proved difficult to make stable colloidal solutions for coating CP surfaces. We tried to make stable colloidal solutions of large titanium dioxide nanoparticles by using reagents such as AVBE, starch, CMC and CMS to modify the surface of the titanium dioxide nanoparticles and thereby increase colloid stability. Unfortunately, the colour of the titanium dioxide nanoparticle powders isolated from the reaction mixtures changed from white to yellow after a few months, which is indicative of a reduced UV stability of the surface-modified titanium dioxide nanoparticles.

I*n-situ* coating was another method investigated to deposit titanium dioxide nanoparticles directly onto the surface of paper using a simple heating whilst stirring process, without the requirement to make stable solutions for the coating process. The most significant issue encountered using this approach was that most of the paper was destroyed during the heating and stirring. Unfortunately, the CP coated with titanium dioxide nanoparticles did not exhibit good UV stability as was expected.

We then prepared titanium dioxide nanoparticles with a diameter less than 200 nm. The main problem for coating CP with smaller titanium dioxide nanoparticle is these smaler

nanoparticles possess a higher photo-catalytic activity than those of a larger size. However, the stability of aqueous colloidal solutions of these smaller titanium dioxide nanoparticles dispersed in water is greater. One of the most important parameters from a commercial or industrial standpoint is the stability of the colloidal solutions prepared on-site form these titanium dioxide nano-powders. Since $TiCl_4$ is sensitive to air-moisture, it is generally converted to $TiOCl_2$ by diluting with ice-cold distilled water. $TiOCl_2$ used as a starter material for prepare TiO_2-RP. But TiO_2-RP and commercial TiO_2-P25 nanoparticles size are less than 200 nm.

In order to reduce the photo-catalytic activity of these nanoparticles, coating TiO_2 nanoparticles with silica or reacting with APTES were investigated. A lot of publications have used silica as shell to reduce titanium dioxide photo-catalytic activity, but to our knowledge, we report the first protective coating of TiO_2 with APTES. For both kinds of titanium dioxide that were used in this research, whiteness and brightness of nano-particle treated CP was improved if the nanoparticles were coated with silica. TiO_2/SiO_2 coated CP was shown to have a higher reflectivity than standard titanium dioxide coated CP. But for the nanoparticles protected with APTES, it just has good whiteness, brightness and reflectivity results for TiO_2-P25 with lower photo-catalytic activity.

The second part of this research shows that silicon diimide gel can be deposited onto a glass substrate to make a TLC plate analogous to standard, commercial silica- gel TLC plate. The silicon diimide gel TLC plate shows a comparable chromatographic effect to that of commercial silica gel TLC plates. This property of silicon diimide gel TLC plate is very important to make column chromatography with silicon diimide gel as a basic stationary phase to better efficiency for separation of acid-sensitive organic compounds.

References

1.   M. Abdelmouleh, S. Boufi, M. N. Belgacem, A. Dufresne and A. Gandini, Journal of Applied Polymer Science, 2005, 98, 974-984.

2.   M. C. B. Salon, M. Abdelmouleh, S. Boufi, M. N. Belgacem and A. Gandini, Journal of Colloid and Interface Science, 2005, 289, 249-261.

3.   M. N. Belgacem and A. Gandini, Compos Interface, 2005, 12, 41-75.

4.   V. R. Botaro, A. Gandini and M. N. Belgacem, J Thermoplast Compos, 2005, 18, 107-117.

5.   A. Gandini and M. N. Belgacem, Macromol. Symp., 2005, 221, 257-270.

6.   E. Lasseuguette, A. Gandini, M. N. Belgacem and H. J. Timpe, Polymer, 2005, 46, 5476-5483.

7.   L. B. Kiss, J. Soderlund, G. A. Niklasson and C. G. Granqvist, Nanotechnology, 1999, 10, 25-28.

8.   F. Alam, S. A. Ansari, W. Khan, M. E. Khan and A. H. Naqvi, Funct Mater Lett, 2012, 5.

9.   V. Sharma, K. Park and M. Srinivasarao, Mat Sci Eng R, 2009, 65, 1-38.

10.   M. Faraday, Phil. Trans. Roy. Soc., 1857, 147, 145-181.

11.   P. Speiser, Acta Pharm Suec, 1976, 13, 35-35.

12.   K. E. Drexler, P Natl Acad Sci USA, 1981, 78, 5275-5278.

13.   D. Pissuwan, T. Niidome and M. B. Cortie, Journal of Controlled Release, 2011, 149, 65-71.

14.   C. Yu and J. Park, Journal of Solid State Chemistry, 2010, 183, 2268-2273.

15.   T. Tsuzuki, Int J Nanotechnol, 2009, 6, 567-578.

16.   J. Kreuter, Int J Pharm, 2007, 331, 1-10.

17.   M. A. El-Sayad, P. K. Jain, X. Huang and I. H. El-Sayed, Plasmonics, 2007, 2, 107-118.

18.   B. S. Kim, J. Y. Song and H. K. Jang, Process Biochem, 2009, 44, 1133-1138.

19.   A. J. Hurd and C. J. Brinker, Mater Res Soc Symp P, 1990, 180, 575-581.

20.   L. C. Klein, ed., Kluwer Academic Publishers, Boston, 1994.

21. W. L. WARREN, P. M. LENAHAN, C. J. BRINKER, C. S. ASHLEY AND S. T. REED, J ELECTRON MATER, 1990, 19, 425-428.

22. C. J. BRINKER, A. J. HURD, G. C. FRYE, K. J. WARD AND C. S. ASHLEY, J NON-CRYST SOLIDS, 1990, 121, 294-302.

23. V. R. CHAUDHARI, S. K. HARAM AND S. K. KULSHRESHTHA, COLLOIDS AND SURFACES 2007, 301, 475-480.

24. K.-M. LEE, S.-T. PARK AND D.-J. LEE, JOURNAL OF ALLOYS AND COMPOUNDS, 2005, 390, 297-300.

25. M. M. OLIVEIRA, D. C. SCHNITZLER AND A. J. G. ZARBIN, CHEMISTRY OF MATERIALS, 2003, 15, 1903-1909.

26. A. J. KOIVISTO, J. LYYRANEN, A. AUVINEN, E. VANHALA, K. HAMERI, T. TUOMI AND J. JOKINIEMI, INHAL TOXICOL, 2012, 24, 839-849.

27. N. BARKA, S. QOURZAL, A. ASSABBANE, A. NOUNAH AND Y. AIT-ICHOU, ARAB J CHEM, 2010, 3, 279-283.

28. L. G. PHILLIPS AND D. M. BARBANO, JOURNAL OF DAIRY SCIENCE, 1997, 80, 2726-2731.

29. E. V. BOROVIK AND O. M. MERKUSHEV, RUSS J APPL CHEM+, 1996, 69, 181-184.

30. G. A. SMOOK, J CHEM TECHNOL BIOT, 1989, 45, 15-27.

31. A. M. BALLO, D. BJOORN, M. ASTRAND, A. PALMQUIST, J. LAUSMAA AND P. THOMSEN, CLIN ORAL IMPLAN RES, 2013, 24, 1009-1017.

32. K. D. YUNL, S. W. PARK, K. M. LEE, H. S. KIM, M. S. VANGL, H. S. YANG, J. T. KOH, S. S. KANG, G. J. OH, G. H. KIM, M. K. JI, G. W. HWANG AND H. P. LIM, J NANOSCI NANOTECHNO, 2013, 13, 3864-3867.

33. S. A. KUKHARENKO, A. E. SHILO, P. P. ITSENKO AND A. N. KUTSAI, J SUPERHARD MATER+, 2010, 32, 396-405.

34. Y. I. BELYI AND N. A. MINAKOVA, GLASS CERAM+, 2005, 62, 337-340.

35. H. J. CHEN, L. WANG AND W. Y. CHIU, MATERIALS CHEMISTRY AND PHYSICS, 2007, 101, 12-19.

36. U. GESENHUES, CHEM. ENG. TECHNOL., 2001, 24, 685-694.

37. M. FERNANDEZ-GARCIA, A. MARTINEZ-ARIAS, J. C. HANSON AND J. A. RODRIGUEZ, CHEMICAL REVIEWS, 2004, 104, 4063-4104.

38. M. M. GODNEVA, D. L. MOTOV AND R. F. OKHRIMENKO, ZH NEORG KHIM+, 1987, 32, 1843-1847.

39. V. Samuel, R. Pasricha and V. Ravi, Ceramics International, 2005, 31, 555-557.

40. R. Pelton, X. L. Geng and M. Brook, Advances in Colloid and Interface Science, 2006, 127, 43-53.

41. A. Wold, Chemistry of Materials, 1993, 5, 280-283.

42. V. Ravi, S. R. Dhage, V. Samuel and R. Pasricha, Ceramics International, 2006, 32, 939-941.

43. Z.-G. Mei, Y. Wang, S.-L. Shang and Z.-K. Liu, Inorganic Chemistry, 2011, 50, 6996-7003.

44. X. Z. Ding, X. H. Liu and Y. Z. He, Journal of Materials Science Letters, 1996, 15, 1789-1791.

45. D. Hanaor and C. Sorrell, Journal of Materials Science, 2011, 46, 855-874.

46. L. M. Sharygin and S. M. Vovk, Zh Neorg Khim+, 1987, 32, 2285-2288.

47. J. A. Gamboa and D. M. Pasquevich, Journal of the American Ceramic Society, 1992, 75, 2934-2938.

48. T. Reztsova, C. H. Chang, J. Koresh and H. Idriss, Journal of Catalysis, 1999, 185, 223-235.

49. A. P. Alivisatos, J Phys Chem-Us, 1996, 100, 13226-13239.

50. A. P. Alivisatos, Science, 1996, 271, 933-937.

51. C. Burda, X. B. Chen, R. Narayanan and M. A. El-Sayed, Chemical Reviews, 2005, 105, 1025-1102.

52. C. B. Murray, C. R. Kagan and M. G. Bawendi, Annu Rev Mater Sci, 2000, 30, 545-610.

53. Y. Yin and A. P. Alivisatos, Nature, 2005, 437, 664-670.

54. A. Fujishima and K. Honda, Nature, 1972, 238, 37-38.

55. A. Fujishima, T. N. Rao and D. A. Tryk, Electrochim Acta, 2000, 45, 4683-4690.

56. A. L. Linsebigler, G. Q. Lu and J. T. Yates, Chemical Reviews, 1995, 95, 735-758.

57. M. R. Hoffmann, S. T. Martin, W. Y. Choi and D. W. Bahnemann, Chemical Reviews, 1995, 95, 69-96.

58. U. Gesenhues, Journal of Photochemistry and Photobiology a-Chemistry, 2001, 139, 243-251.

59. G. A. Somorjai, Science, 1978, 201, 489-497.

60. S. L. STOVER AND H. E. ZEIGER, JR., ARCHIVES OF PHYSICAL MEDICINE AND REHABILITATION, 1976, 57, 201-205.

61. H. O. FINKLEA, SEMICONDUCTOR ELECTRODES, ELSEVIER, AMSTERDAM ; NEW YORK, 1988.

62. W. P. MAKSYMOWYCH, S. TAO, M. LUONG, M. SUAREZ-ALMAZOR, R. NELSON, F. PAZDERKA AND A. S. RUSSELL, TISSUE ANTIGENS, 1995, 46, 136-139.

63. P. C. MANESS, S. SMOLINSKI, D. M. BLAKE, Z. HUANG, E. J. WOLFRUM AND W. A. JACOBY, APPLIED AND ENVIRONMENTAL MICROBIOLOGY, 1999, 65, 4094-4098.

64. D. AVNIR, J. J. CARBERRY, O. CITRI, D. FARIN, M. GRATZEL AND A. J. MCEVOY, CHAOS, 1991, 1, 397-410.

65. K. R. RAJESWARI, M. SATYANARAYANA, P. V. NARAYAN AND S. SUBRAHMANYAM, INDIAN JOURNAL OF EXPERIMENTAL BIOLOGY, 1985, 23, 194-197.

66. G. GONCALVES, P. MARQUES, R. J. B. PINTO, T. TRINDADE AND C. P. NETO, COMPOSITES SCIENCE AND TECHNOLOGY, 2009, 69, 1051-1056.

67. Y. HABIBI, L. A. LUCIA AND O. J. ROJAS, CHEMICAL REVIEWS, 2010, 110, 3479-3500.

68. W. A. DAOUD AND J. H. XIN, JOURNAL OF SOL-GEL SCIENCE AND TECHNOLOGY, 2004, 29, 25-29.

69. C. GIORDANO, CARYOLOGIA, 1999, 52, 65-73.

70. G. GAO, Y. G. ZHAI, Q. ZHANG AND F. Q. LIU, MATERIALS LETTERS, 2008, 62, 4563-4565.

71. S. R. DHAGE, V. D. CHOUBE, V. SAMUEL AND V. RAVI, MATERIALS LETTERS, 2004, 58, 2310-2313.

72. A. TESTINO, I. R. BELLOBONO, V. BUSCAGLIA, C. CANEVALI, M. D'ARIENZO, S. POLIZZI, R. SCOTTI AND F. MORAZZONI, J AM CHEM SOC, 2007, 129, 3564-3575.

73. H. F. SHURVELL, J MOL SPECTROSC, 1971, 38, 431.

74. H. H. CHOI, J. PARK AND R. K. SINGH, APPLIED SURFACE SCIENCE, 2005, 240, 7-12.

75. F. CHENG, S. J. ARCHIBALD, S. CLARK, B. TOURY, S. M. KELLY, J. S. BRADLEY AND F. LEFEBVRE, CHEMISTRY OF MATERIALS, 2003, 15, 4651-4657.

76. F. CHENG, C. N. HOPE, S. J. ARCHIBALD, J. S. BRADLEY, S. CLARK, M. G. FRANCESCONI, S. M. KELLY, N. A. YOUNG AND F. LEFEBVRE, INTERNATIONAL JOURNAL OF APPLIED CERAMIC TECHNOLOGY, 2011, 8, 467-481.

77. D. JIANG, AUSTRALIA, 2004.

78.   N. S. Allen, M. Edge, A. Ortega, G. Sandoval, C. M. Liauw, J. Verran, J. Stratton and R. B. McIntyre, Polymer Degradation and Stability, 2004, 85, 927-946.

79.   M. J. Uddin, F. Cesano, F. Bonino, S. Bordiga, G. Spoto, D. Scarano and A. Zecchina, Journal of Photochemistry and Photobiology a-Chemistry, 2007, 189, 286-294.

80.   J. H. He, T. Kunitake and A. Nakao, Chemistry of Materials, 2003, 15, 4401-4406.

81.   K. L. Xie, Y. H. Yu and Y. Q. Shi, Carbohydrate Polymers, 2009, 78, 799-805.

82.   X. P. Zhao and X. Duan, Journal of Colloid and Interface Science, 2002, 251, 376-380.

83.   H. A. Monreal, J. G. Chacon-Nava, U. Arce-Colunga, C. A. Martinez, P. G. Casillas and A. Martinez-Villafane, Micro & Nano Letters, 2009, 4, 187-191.

84.   T. Furusawa, K. Honda, E. Ukaji, M. Sato and N. Suzuki, Materials Research Bulletin, 2008, 43, 946-957.

85.   X. Chen and S. S. Mao, Chemical Reviews, 2007, 107, 2891-2959.

86.   W. A. Daoud and J. H. Xin, Journal of the American Ceramic Society, 2004, 87, 953-955.

87.   R. T. Wu, Y. Wei and Y. F. Zhang, Materials Research Bulletin, 1999, 34, 2131-2135.

88.   D. V. Bavykin, V. P. Dubovitskaya, A. V. Vorontsov and V. N. Parmon, Research on Chemical Intermediates, 2007, 33, 449-464.

89.   H. B. Yin, Y. Wada, T. Kitamura, S. Kambe, S. Murasawa, H. Mori, T. Sakata and S. Yanagida, Journal of Materials Chemistry, 2001, 11, 1694-1703.

90.   F. K. Urakaev, L. S. Bazarov, I. N. Meshcheryakov, V. V. Feklistov, T. N. Drebushchak, Y. P. Savintsev, V. I. Gordeeva and V. S. Shevchenko, Journal of Crystal Growth, 1999, 205, 223-232.

91.   B. U. Grzmil, D. Grela and B. Kic, Chemical Papers, 2008, 62, 18-25.

92.   S. Sathyamoorthy, G. D. Moggridge and M. J. Hounslow, Crystal Growth & Design, 2001, 1, 123-129.

93.   S. J. Kim, S. D. Park, Y. H. Jeong and S. Park, Journal of the American Ceramic Society, 1999, 82, 927-932.

94. Y. G. Zhai, Q. Zhang, F. Q. Liu and G. Gao, Materials Letters, 2008, 62, 4563-4565.

95. Y. L. Lin, T. J. Wang and Y. Jin, Powder Technol., 2002, 123, 194-198.

96. S. Ikeda, H. Kobayashi, Y. Ikoma, T. Harada, T. Torimoto, B. Ohtani and M. Matsumura, Phys. Chem. Chem. Phys., 2007, 9, 6319-6326.

97. S. Ikeda, Y. Ikoma, H. Kobayashi, T. Harada, T. Torimoto, B. Ohtani and M. Matsumura, Chem Commun, 2007, DOI: 10.1039/b704468b, 3753-3755.

98. S. Wang, T. Wang, W. X. Chen and T. R. Hori, Chem Commun, 2008, DOI: 10.1039/b802127a, 3756-3758.

99. Y. A. Ren, M. Chen, Y. Zhang and L. M. Wu, Langmuir, 2010, 26, 11391-11396.

100. J. Kim, J. Cho, P. M. Seidler, N. E. Kurland and V. K. Yadavalli, Langmuir, 2010, 26, 2599-2608.

101. R. M. Pasternack, S. R. Amy and Y. J. Chabal, Langmuir, 2008, 24, 12963-12971.

102. G. Balasundaram, M. Sato and T. J. Webster, Biomaterials, 2006, 27, 2798-2805.

103. P. Filippini, C. Rainaldi, A. Ferrante, B. Mecheri, G. Gabrielli, M. Bombace, P. L. Indovina and M. T. Santini, Journal of Biomedical Materials Research, 2001, 55, 338-349.

104. A. Andrzejewska, A. Krysztafkiewicz and T. Jesionowski, Dyes and Pigments, 2004, 62, 121-130.

105. Y.-Y. Song, H. Hildebrand and P. Schmuki, Surface Science, 2010, 604, 346-353.

106. A. Natarajan, C. Chun, J. J. Hickman and P. Molnar, Journal of biomaterials science. Polymer edition, 2008, 19, 1319-1331.

107. P. Fardim, T. Moreno and B. Holmbom, J Colloid Interface Sci, 2005, 290, 383-391.

108. S. Di Risio and N. Yan, J Colloid Interface Sci, 2009, 338, 410-419.

109. D. Roy, M. Semsarilar, J. T. Guthrie and S. Perrier, Chem Soc Rev, 2009, 38, 2046-2064.

110. C. W. Young and V. Raymond, Cancer treatment reports, 1986, 70, 51-63.

111. H. T. Sahin and M. B. Arslan, Int J Mol Sci, 2008, 9, 78-88.

112. G. Muralikrishna and M. V. Rao, Crit Rev Food Sci Nutr, 2007, 47, 599-610.

113. J. Sjoberg, A. Potthast, T. Rosenau, P. Kosma and H. Sixta, Biomacromolecules, 2005, 6, 3146-3151.

114. R. Boeva-Spiridonova, E. Petkova, N. Georgieva, L. Yotova and I. Spiridonov, Bioresources, 2007, 2, 34-40.

115. J. Pere, M. Siikaaho, J. Buchert and L. Viikari, Tappi J, 1995, 78, 71-78.

116. R. E. Cameron and K. L. Kato, Journal of Applied Polymer Science, 1999, 74, 1465-1477.

117. D. A. Sukhov, A. N. Zhilkin, P. M. Valov and O. A. Terentiev, Tappi J, 1991, 74, 201-204.

118. M. Gara and P. Lengyel, Zellst Pap, 1972, 21, 16.

119. J. Kim, S. K. Mahadeva and S. W. Lee, Acta Mater, 2008, 56, 1868-1875.

120. P. Cerruti, V. Ambrogi, A. Postiglione, J. Rychly, L. Matisova-Rychla and C. Carfagna, Biomacromolecules, 2008, 9, 3004-3013.

121. D. Klemm, B. Heublein, H. P. Fink and A. Bohn, Angewandte Chemie-International Edition, 2005, 44, 3358-3393.

122. R. J. B. Pinto, P. Marques, A. M. Barros-Timmons, T. Trindade and C. P. Neto, Composites Science and Technology, 2008, 68, 1088-1093.

123. X. Li, S. Y. Chen, W. L. Hu, S. K. Shi, W. Shen, X. Zhang and H. P. Wang, Carbohydrate Polymers, 2009, 76, 509-512.

124. Y. Iguchi, H. Ichiura, T. Kitaoka and H. Tanaka, Chemosphere, 2003, 53, 1193-1199.

125. B. Mahltig, H. Haufe and H. Bottcher, Journal of Materials Chemistry, 2005, 15, 4385-4398.

126. H. Matsubara, M. Takada, S. Koyama, K. Hashimoto and A. Fujishima, Chem Lett, 1995, 24, 767-768.

127. M. J. Simon and H. C. Salzberg, Am J Clin Hypn, 1981, 24, 14-21.

128. Y. H. Ngo, D. Li, G. P. Simon and G. Garnier, Ad. Colloid and Interface Sci., 2011, 163, 23-38.

129. S. Vaswani, J. Koskinen and D. W. Hess, Surf Coat Tech, 2005, 195, 121-129.

130. M. Afsharpour, F.T.Rad and H. Malekian, J. Cultural Heritage, 2011, 1-4.

131. M. S. Reis and P. M. Saraiva, Comput-Aided Chem En, 2006, 21, 1173-1178.

132. P. SAMYN, J. VAN ERPS, H. THIENPONT AND G. SCHOUKENS, APPLIED SURFACE SCIENCE, 2011, 257, 5613-5625.

133. C. DEUMIE, R. RICHIER, P. DUMAS AND C. AMRA, APPL OPTICS, 1996, 35, 5583-5594.

134. P. SAMYNA, M. DECONINCKA, G. SCHOUKENSA, D. STANSSENSB, L. VONCKB AND H. V. ABBEELEB, PROGRESS IN ORGANIC COATINGS, 2010, 69, 442-454.

135. N. ABIDI, L. CABRALES AND E. HEQUET, ACS APPLIED MATERIALS & INTERFACES, 2009, 1, 2141-2146.

136. K. H. QI, W. A. DAOUD, J. H. XIN, C. L. MAK, W. Z. TANG AND W. P. CHEUNG, JOURNAL OF MATERIALS CHEMISTRY, 2006, 16, 4567-4574.

137. N. S., PHOTOCATALYTIC PULP COMPOSITION, FOAM, MOULDED PULP, AS WELLAS PROCESSES AND APPARATUS FOR THEIR PREPARATION. APPLICATION, 2001.

138. L. Z. MENG, C. Q. DU, Y. Y. CHEN AND Y. B. HE, JOURNAL OF APPLIED POLYMER SCIENCE, 2002, 84, 61-66.

139. P. MARQUES, T. TRINDADE AND C. P. NETO, COMPOSITES SCIENCE AND TECHNOLOGY, 2006, 66, 1038-1044.

140. H. KOGA, T. KITAOKA AND A. ISOGAI, J. MATER. CHEM, 2011, 21, 9356-9360.

141. Y. ATOU, H. SUZUKI, Y. KIMURA, T. SATO, T. TANIGAKI, Y. SAITO AND C. KAITO, PHYSICA E, 2003, 16, 179-189.

142. M. POLAT, K. SATO, T. NAGAOKA AND K. WATARI, JOURNAL OF COLLOID AND INTERFACE SCIENCE, 2006, 304, 378-387.

143. Q. CHEN AND N. L. YAKOVLEV, APPLIED SURFACE SCIENCE, 2010, 257, 1395-1400.

144. J.-W. LEE, S. KONG, W.-S. KIM AND J. KIM, MATERIALS CHEMISTRY AND PHYSICS, 2007, 106, 39-44.

145. D. B. WILLIAMS AND C. B. CARTER, IN TRANSMISSION ELECTRON MICROSCOPY, SPRINGER US, 2009, DOI: 10.1007/978-0-387-76501-3_1, PP. 3-22.

146. E. SUZUKI, JOURNAL OF MICROSCOPY, 2002, 208, 153-157.

147. G. BALESTRINO, S. LAGOMARSINO, L. MASTROGIACOMO, F. SCARINCI AND A. TUCCIARONE, THIN SOLID FILMS, 1981, 78, 327-334.

148. L. SOOVÄLI, E.-I. RÕÕM, A. KÜTT, I. KALJURAND AND I. LEITO, ACCREDITATION AND QUALITY ASSURANCE: JOURNAL FOR QUALITY, COMPARABILITY AND RELIABILITY IN CHEMICAL MEASUREMENT, 2006, 11, 246-255.

149. B. CARR, LASER FOCUS WORLD, 2008, 44, 83-86.

150. B. CARR AND A. MAHOY, AM LAB, 2008, 40, 8-11.

151. R. W. O'BRIEN, D. W. CANNON AND W. N. ROWLANDS, JOURNAL OF COLLOID AND INTERFACE SCIENCE, 1995, 173, 406-418.

152. J. F. DUNCAN AND R. G. RICHARDS, NEW ZEAL J SCI, 1976, 19, 179-183.

153. E. A. BARRINGER AND H. K. BOWEN, LANGMUIR, 1985, 1, 420-428.

154. K. KUDAKA, K. IIZUMI AND K. SASAKI, AM CERAM SOC BULL, 1982, 61, 1236-1236.

155. M. M. A. SEKAR AND K. C. PATIL, JOURNAL OF MATERIALS CHEMISTRY, 1992, 2, 739-743.

156. M. T. HARRIS, O. A. BASARAN AND C. H. BYERS, MATER RES SOC SYMP P, 1992, 271, 291-296.

157. A. M. AZAD, S. A. AKBAR, S. G. MHAISALKAR, L. D. BIRKEFELD AND K. S. GOTO, J ELECTROCHEM SOC, 1992, 139, 3690-3704.

158. J. CASTRO, B. MACK, A. CRUZ, J. C. GONZALEZ, C. MARTIN, G. PESCADOR, L. F. RODRIGUEZ, V. SANCHEZ, N. SOSA AND M. WILLIAMS, P SOC PHOTO-OPT INS, 1994, 2199, 1141-1153.

159. L. D. BIRKEFELD, A. M. AZAD AND S. A. AKBAR, JOURNAL OF THE AMERICAN CERAMIC SOCIETY, 1992, 75, 2964-2968.

160. C. C. CHENG, Q. DONG, D. F. LIU, Y. L. LUO, L. F. LIU, A. Y. CHEN, C. YU, N. SAVARAJ AND T. C. CHOU, J MED CHEM, 1993, 36, 4108-4112.

161. R. BIRRINGER, J. KARCH AND H. GLEITER, JOM-J MIN MET MAT S, 1987, 39, A6-A6.

162. J. KARCH, R. BIRRINGER AND H. GLEITER, NATURE, 1987, 330, 556-558.

163. N. SUZUKI, E. UKAJI, T. FURUSAWA AND M. SATO, APPLIED SURFACE SCIENCE, 2007, 254, 563-569.

164. R. J. NUSSBAUMER, W. R. CASERI, P. SMITH AND T. TERVOORT, MACROMOL MATER ENG, 2003, 288, 44-49.

165. R. S. HERBST, Y. SUN, W. E. E. EBERHARDT, P. GERMONPRE, N. SAIJO, C. C. ZHOU, J. WANG, L. Y. LI, F. KABBINAVAR, Y. ICHINOSE, S. K. QIN, L. ZHANG, B. BIESMA, J. V. HEYMACH, P. LANGMUIR, S. J. KENNEDY, H. TADA AND B. E. JOHNSON, LANCET ONCOL, 2010, 11, 619-626.

166. E. LATASTE, C. LEGEIN, M. BODY, J. Y. BUZARE, A. TRESSAUD AND A. DEMOURGUES, JOURNAL OF PHYSICAL CHEMISTRY C, 2009, 113, 18652-18660.

167.   A. DEMOURGUES, N. PERLIN, E. DURAND, F. WEILL, D. DAMBOURNET, N. VIADERE AND A. TRESSAUD, CHEMISTRY OF MATERIALS, 2009, 21, 1275-1283.

168.   I. A. SIDDIQUEY, T. FURUSAWA, M. SATO, K. HONDA AND N. SUZUKI, DYES AND PIGMENTS, 2008, 76, 754-759.

169.   C. P. NETO, R. J. B. PINTO, P. A. A. P. MARQUES, A. M. BARROS-TIMMONS AND T. TRINDADE, COMPOSITES SCIENCE AND TECHNOLOGY, 2008, 68, 1088-1093.

170.   S. F. WANG, Y. F. HSU, T. C. K. YANG, C. M. CHANG, Y. CHEN, C. Y. HUANG AND F. S. YEN, MAT SCI ENG A-STRUCT, 2005, 395, 148-152.

171.   Z. LI, X. Y. CHEN AND D. LIU, J BASIC MED TRADITIONAL CHIN MED, 2005, 11, 149-150.

172.   A. ARRANZ, C. PALACIO, D. GARCIA-FRESNADILLO, G. ORELLANA, A. NAVARRO AND E. MUNOZ, LANGMUIR, 2008, 24, 8667-8671.

173.   E. UKAJI, T. FURUSAWA, M. SATO AND N. SUZUKI, APPLIED SURFACE SCIENCE, 2007, 254, 563-569.

174.   R. G. ACRES, A. V. ELLIS, J. ALVINO, C. E. LENAHAN, D. A. KHODAKOV, G. F. METHA AND G. G. ANDERSSON, JOURNAL OF PHYSICAL CHEMISTRY C, 2012, 116, 6289-6297.

175.   E. T. VANDENBERG, L. BERTILSSON, B. LIEDBERG, K. UVDAL, R. ERLANDSSON, H. ELWING AND I. LUNDSTROM, JOURNAL OF COLLOID AND INTERFACE SCIENCE, 1991, 147, 103-118.

176.   H. U. BLASER, A. BAIKER AND R. PRINS, HETEROGENEOUS CATALYSIS AND FINE CHEMICALS IV : PROCEEDINGS OF THE 4TH INTERNATIONAL SYMPOSIUM ON HETEROGENEOUS CATALYSIS AND FINE CHEMICALS, BASEL, SWITZERLAND, SEPTEMBER 8-12, 1996, ELSEVIER, AMSTERDAM ; NEW YORK, 1997.

177.   D. FARRUSSENG, K. SCHLICHTE, B. SPLIETHOFF, A. WINGEN, S. KASKEL, J. S. BRADLEY AND F. SCHUTH, ANGEWANDTE CHEMIE-INTERNATIONAL EDITION, 2001, 40, 4204-4207.

178.   Y. L. LI, E. KROKE, A. KLONCZYNSKI AND R. RIEDEL, ADV MATER, 2000, 12, 956-+.

179.   B. A. MCCOOL, N. HILL, J. DICARLO AND W. J. DESISTO, J MEMBRANE SCI, 2003, 218, 55-67.

180.   Y. IWAMOTO, K. SATO, T. KATO, T. INADA AND Y. KUBO, J EUR CERAM SOC, 2005, 25, 257-264.

181. M. BAUMBACH, A. SCHUTZE, F. CHENG, S. KELLY, H. DELPRAT, F. PARRET, P. MENINI, K. SOULANTICA, B. CHAUDRET AND A. MAISONNAT, IEEE SENSOR, 2004, DOI: DOI 10.1109/ICSENS.2004.1426326, 939-942.

182. H. D. TONG, H. V. JANSEN, V. J. GADGIL, C. G. BOSTAN, E. BERENSCHOT, C. J. M. VAN RIJN AND M. ELWENSPOEK, NANO LETT, 2004, 4, 283-287.

183. H. MORI, S. MASE, N. YOSHIMURA, T. HOTTA, K. AYAMA AND J. I. TSUBAKI, J MEMBRANE SCI, 1998, 147, 23-33.

184. E. KROKE, Y. L. LI, C. KONETSCHNY, E. LECOMTE, C. FASEL AND R. RIEDEL, MAT SCI ENG R, 2000, 26, 97-199.

185. R. H. BRADLEY AND I. I. MATHIESON, J COLLOID INTERFACE SCI, 1997, 194, 338-343.

186. J. S. BRADLEY, O. VOLLMER, R. ROVAI, U. SPECHT AND F. LEFEBVRE, ADV MATER, 1998, 10, 938-+.

187. O. VOLLMER, F. LEFEBVRE AND J. S. BRADLEY, J MOL CATAL A-CHEM, 1999, 146, 87-96.

188. L. F. GIRALDO, B. L. LOPEZ, L. PEREZ, S. URREGO, L. SIERRA AND M. MESA, MACROMOL. SYMP., 2007, 258, 129-141.

189. I. M. EL-NAHHAL AND N. M. EL-ASHGAR, J. ORGANOMET. CHEM., 2007, 692, 2861-2886.

190. J. J. KIRKLAND, J. CHROMATOGR. SCI., 1996, 34, 309-313.

191. Y. MAO AND B. M. FUNG, J. CHROMATOGR. A, 1997, 790, 9-15.

192. M. GRUN, A. A. KURGANOV, S. SCHACHT, F. SCHUTH AND K. K. UNGER, J. CHROMATOGR. A, 1996, 740, 1-9.

193. M. SCHWARZ, G. MIEHE, A. ZERR, E. KROKE, B. T. POE, H. FUESS AND R. RIEDEL, ADV MATER, 2000, 12, 883-887.

194. E. CHIBOWSKI, ABSTR. PAP. AM. CHEM. SOC., 1992, 203, 262-COLL.

195. W. WU, R. F. GIESE AND C. J. VANOSS, POWDER TECHNOL., 1996, 89, 129-132.

196. M. SAJEWICZ AND T. KOWALSKA, ACTA CHROMATOGR, 2010, 22, 499-513.

197. V. G. BEREZKIN AND K. V. SEDNEV, DOKL CHEM, 2008, 419, 65-68.

198. K. P. GUO AND Y. CHEN, ANAL METHODS-UK, 2010, 2, 1156-1159.

199. S. A. BHAWANI, O. SULAIMAN, R. HASHIM AND M. N. M. IBRAHIM, TENSIDE SURFACT DET, 2010, 47, 73-80.

200. C. MASTERSON, B. FRIED AND J. SHERMA, J LIQ CHROMATOGR, 1992, 15, 2967-2980.

201.   J. SHERMA, J AOAC INT, 2003, 86, 602-611.

202.   T. H. JUPILLE AND J. A. PERRY, CRC CR REV ANAL CHEM, 1977, 6, 325-359.

203.   J. SHERMA, J ENVIRON SCI HEAL B, 2009, 44, 193-203.

204.   J. SHERMA, J ENVIRON SCI HEAL B, 2011, 46, 557-568.

205.   R. BHUSHAN, V. K. MAHESH AND P. V. MALLIKHARJUN, BIOMED CHROMATOGR, 1989, 3, 95-104.

206.   J. MANN, NATURE, 1989, 338, 181-182.

207.   A. I. VOGEL, B. S. FURNISS AND A. I. VOGEL, VOGEL'S TEXTBOOK OF PRACTICAL ORGANIC CHEMISTRY, LONGMAN SCIENTIFIC & TECHNICAL ; WILEY, LONDON, NEW YORK, 5TH EDN., 1989.

208.   E. REICH AND A. SCHIBLI, HIGH-PERFORMANCE THIN-LAYER CHROMATOGRAPHY FOR THE ANALYSIS OF MEDICINAL PLANTS, THIEME, NEW YORK, 2007.

209.   S. C. PETROVIC, D. F. KING AND H. D. DEWALD, ELECTROANAL, 1998, 10, 393-398.

210.   D. CAPUTO, G. DE CESARE, C. MANETTI, A. NASCETTI AND R. SCIPINOTTI, LAB CHIP, 2007, 7, 978-980.

211.   M. P. VOLYNETS, J ANAL CHEM-USSR+, 1972, 27, 871.

212.   M. H. DOS SANTOS, J. MEGDA, P. B. M. CRUZ, F. T. MARTINS AND M. E. D. MOREIRA, QUIM NOVA, 2007, 30, 1747-1749.

213.   O. KAYNAR AND Y. BERKTAS, REV ANAL CHEM, 2010, 29, 129-147.

214.   J. SHERMA, J ENVIRON SCI HEAL B, 2013, 48, 417-430.

215.   R. ROVAI, C. W. LEHMANN AND J. S. BRADLEY, ANGEWANDTE CHEMIE-INTERNATIONAL EDITION, 1999, 38, 2036-2038.

216.   F. CHENG, S. CLARK, S. M. KELLY, J. S. BRADLEY AND F. LEFEBVRE, JOURNAL OF THE AMERICAN CERAMIC SOCIETY, 2004, 87, 1413-1417.

217.   F. CHENG, B. TOURY, R. SUPPLIT AND J. S. BRADLEY, MATER RES SOC SYMP P, 2002, 726, 255-260.

218.   F. CHENG, S. M. KELLY, S. CLARK, N. A. YOUNG, S. J. ARCHIBALD, J. S. BRADLEY AND F. LEFEBVRE, CHEMISTRY OF MATERIALS, 2005, 17, 5594-5602.

219.   F. CHENG, S. M. KELLY, N. A. YOUNG, S. CLARK, M. G. FRANCESCONI, F. LEFEBVRE AND J. S. BRADLEY, CHEM COMMUN, 2005, DOI: DOI 10.1039/B511790A, 5662-5664.

220. F. Cheng, S. M. Kelly, N. A. Young, C. N. Hope, K. Beverley, M. G. Francesconi, S. Clark, J. S. Bradley and F. Lefebvre, Chemistry of Materials, 2006, 18, 5996-6005.

221. S. P. Kitney, F. Cheng, S. Khan, C. N. Hope, W. Mcnab and S. M. Kelly, Liq Cryst, 2011, 38, 1027-1033.

222. F. Cheng, S. M. Kelly, S. Clark, J. S. Bradley, M. Baurnbachb and A. Schutze, J Membrane Sci, 2006, 280, 530-535.

223. J. Loffelholz, J. Engering and M. Jansen, Z Anorg Allg Chem, 2000, 626, 963-968.

224. F. Cheng, S. M. Kelly, F. Lefebvre, S. Clark, R. Supplit and J. S. Bradley, Journal of Materials Chemistry, 2005, 15, 772-777.

225. F. Cheng, S. M. Kelly, S. Clark, J. S. Bradley and F. Lefebvre, J. Organomet. Chem., 2007, 692, 3816-3822.